



**HAL**  
open science

# Phenomenological model of thermal effects on weld beads geometry produced by Wire and Arc Additive Manufacturing (WAAM)

Supasit Manokruang

► **To cite this version:**

Supasit Manokruang. Phenomenological model of thermal effects on weld beads geometry produced by Wire and Arc Additive Manufacturing (WAAM). Mechanics of materials [physics.class-ph]. Université Grenoble Alpes [2020-..], 2022. English. NNT : 2022GRALI058 . tel-03851334

**HAL Id: tel-03851334**

**<https://theses.hal.science/tel-03851334>**

Submitted on 14 Nov 2022

**HAL** is a multi-disciplinary open access archive for the deposit and dissemination of scientific research documents, whether they are published or not. The documents may come from teaching and research institutions in France or abroad, or from public or private research centers.

L'archive ouverte pluridisciplinaire **HAL**, est destinée au dépôt et à la diffusion de documents scientifiques de niveau recherche, publiés ou non, émanant des établissements d'enseignement et de recherche français ou étrangers, des laboratoires publics ou privés.

## THÈSE

Pour obtenir le grade de

### DOCTEUR DE L'UNIVERSITÉ GRENOBLE ALPES

Spécialité : GI : Génie Industriel : conception et production

Arrêté ministériel : 25 mai 2016

Présentée par

## Supasit MANOKRUANG

Thèse dirigée par **Frédéric VIGNAT**, Maître de Conférences HDR,  
Université Grenoble Alpes

et codirigée par **Matthieu MUSEAU**, Université Grenoble Alpes

et **Maxime LIMOUSIN**, Grenoble INP

et **Christelle GRANDVALLET**, Grenoble INP

préparée au sein du **Laboratoire des Sciences pour  
la Conception, l'Optimisation et la Production de Grenoble**  
dans **l'École Doctorale I - MEP2 - Ingénierie - Matériaux,  
Mécanique, Environnement, Énergétique, Procédés,  
Production**

### **Modèle phénoménologique de la forme du cordon en Fabrication Additive arcs fils (WAAM)**

### **Phenomenological model of thermal effects on weld beads geometry produced by Wire and Arc Additive Manufacturing (WAAM)**

Thèse soutenue publiquement le **29 août 2022**,  
devant le jury composé de :

**Monsieur Jérôme PAILHES**

PROFESSEUR DES UNIVERSITES, Arts et Métiers Institute of  
Technology, Université de Bordeaux, Rapporteur

**Monsieur Cyril BORDREUL**

PROFESSEUR DES UNIVERSITES, Laboratoire de Mécanique et  
Génie Civil (LMGC), Université de Montpellier, Rapporteur

**Monsieur Xavier FISCHER**

PROFESSEUR DES UNIVERSITES, ESTIA Institute of  
Technology, Université de Bordeaux, Examineur

**Monsieur François VILLENEUVE**

PROFESSEUR DES UNIVERSITES, Université Grenoble Alpes,  
Président

**Monsieur Nattapong KONGPRASERT**

PROFESSEUR ASSISTANT, Faculty of Engineering,  
Srinakharinwirot University, Examineur

**Monsieur Frédéric VIGNAT**

MAITRE DE CONFERENCES HDR, Université Grenoble Alpes,  
Directeur de thèse

**Monsieur Matthieu MUSEAU**

MAITRE DE CONFERENCES, Université Grenoble Alpes,  
Co-encadrants

**Monsieur Maxime LIMOUSIN**

Grenoble INP, Co-encadrants

**Madame Christelle GRANDVALLET**

Grenoble INP, Co-encadrants





# Acknowledgements

I would like to thank sincerely to my supervisors, Frédéric VIGNAT, as well as Matthieu MUSEAU, Maxime LIMOUSIN, and Christelle GRANDVALLET of the laboratories G-SCOP in Grenoble for their invaluable advice, continuous support, and patience during my PhD study. Their immense knowledge and great experience have encouraged me throughout my academic research and daily life.

I acknowledge the generous financial support from the Ministry of Education and Science Scholarships of Thailand. Moreover, I would also like to thank Tools and Die Engineering, Faculty of Engineering, Rajamangala University of Technology Lanna (RMUTL) Chiang Mai, Thailand, for the opportunity in my career path.

Thank you to my family: Nattaya, Udom, and Katchamart MANOKRUANG, for your endless support. You have always been the wind beneath my wings. Thank you so much for all of your love. Also thanks to Kornkanok who has been presented here for three years (with your encouragement). Thanks for going along with me until this present stage. (Your encouragement is speechless).

Many thanks to all of the members of additive manufacturing Team for their kind support during my PhD study. Special thanks to the teammates: Mansour, Pascal, Nicolas, Franck, Philippe, Rafael, Emilio, Vo Hang, Pierre Thomas and Camille.

Moreover, my doctoral student life would not be complete if there is no Cofi-Cofa band which brought amity and joy here. Thank you so much.

Finally, thank you again, Fred for always being so supportive and helping me in every step of the way.



# Remerciements

Mes remerciements s'adressent tout d'abord à mon Directeur de thèse, Frédéric VIGNAT, puis à tous mes co-encadrants : Matthieu MUSEAU, Maxime LIMOUSIN, et Christelle GRANDVALLET du laboratoire G-SCOP de Grenoble. Je vous remercie sincèrement pour vos précieux conseils, votre soutien, votre disponibilité, votre écoute, votre confiance et votre patience tout au long de mon doctorat.

Je remercie le ministre de l'Éducation et de la Science thaïlandais pour le soutien financier qu'il m'a apporté dans le cadre de mes études. Par ailleurs, je tiens également à remercier le département d'ingénierie « Tools and Die Engineering » de l'Université de Rajamangala Technology Lanna (RMUTL), Chiang Mai, Thaïlande pour cette merveilleuse opportunité pour ma carrière professionnelle. Merci à ma famille : Nattaya, Udom, et Katchamart MANOKRUANG pour votre soutien indéfectible.

Merci beaucoup pour l'amour inconditionnel que vous me portez. Également merci à Kornkanok qui m'a accompagné pendant trois ans et m'a encouragé jusqu'à l'accomplissement de ma thèse.

Par ailleurs, je tiens également à témoigner toute ma reconnaissance aux membres de l'équipe de la Fabrication Additive pour leur soutien constant pendant mes études doctorales. Je remercie plus spécialement mes collègues : Mansour, Pascal, Nicolas, Franck, Philippe, Rafael, Emilio, Vo Hang, Pierre Thomas et Camille.

Ma vie en tant que doctorant ne serait pas complète sans la bande Cofi-Cofa qui m'a entraîné l'amitié et la joie ici. Je tiens également à vous remercier.

Enfin, je renouvelle toute ma sympathie à Fred qui m'a toujours témoigné son soutien et son aide tout au long de ce travail de recherche.

*Remerciements*

---

*“You’ll Never Walk Alone”*

... YNWA

# Contents

<b>Acknowledgements</b>	<b>i</b>
<b>Remerciements</b>	<b>iii</b>
<b>Contents</b>	<b>v</b>
<b>List of Figures</b>	<b>vii</b>
<b>List of Tables</b>	<b>xiii</b>
<b>Introduction</b>	<b>1</b>
Context . . . . .	1
Problematic . . . . .	6
Scientific and technical issue . . . . .	10
<b>1 Literature review</b>	<b>11</b>
1.1 Influence of process parameters on the weld bead shape . . . . .	12
1.2 Weld beads modeling . . . . .	19
1.3 Thermal simulation . . . . .	23
<b>2 Design of Experiment and procedure</b>	<b>33</b>
2.1 Geometry of deposition surface . . . . .	34
2.2 Thermal simulation . . . . .	39
2.3 Experimental procedure . . . . .	48
<b>3 Geometrical identification</b>	<b>57</b>
3.1 Acquisition of numerical models of weld beads through 3D-scan correct	58
3.2 Cross-section profile measurement . . . . .	60
3.3 Weld bead cross-section modeling . . . . .	61
3.4 First discussions on weld bead shape evolutions . . . . .	65



<b>4</b>	<b>Interpolation &amp; Validation</b>	<b>83</b>
4.1	Data collection . . . . .	84
4.2	Artificial Neural Network (ANN) and Multi-Layers Perceptron (MLP) model creation . . . . .	86
4.3	Training & Learning process . . . . .	91
4.4	Interpolation analysis . . . . .	93
4.5	Validation . . . . .	97
	<b>Conclusion &amp; Perspectives</b>	<b>103</b>
	Conclusion . . . . .	103
	Perspectives . . . . .	105
	<b>Bibliography</b>	<b>109</b>
	<b>Appendix</b>	<b>127</b>
<b>A</b>	<b>The result of thermal simulation</b>	<b>129</b>
A.1	Exp.1: Single weld bead on substrate thermal simulation . . . . .	129
A.2	Exp.2: Single weld bead on cylinder substrate thermal simulation . .	133
A.3	Exp.3: Lateral overlap weld bead thermal simulation . . . . .	161
A.4	Exp.4: Vertical overlap weld bead thermal simulation . . . . .	176
<b>B</b>	<b>The result of experiment produce</b>	<b>197</b>
B.1	Design of experiment Exp.2: Single weld bead on cylinder substrate .	197
B.2	The result of Exp.2: Single weld bead on cylinder substrate at Tinit 25°C, 100°C, 200°C, 300°C and 400°C . . . . .	197
B.3	Design of experiment Exp.3: Lateral overlap weld beads . . . . .	200
B.4	Design of experiment Exp.4: Vertical overlap weld beads . . . . .	201
B.5	The result of Exp.4: Vertical overlap weld beads at Tinit 100°C, 200°C and 300°C . . . . .	202
<b>C</b>	<b>MLP Regression in Python</b>	<b>205</b>
C.1	Import library . . . . .	205
C.2	The MLP regression results of training and testing set . . . . .	208
C.3	Case study validation . . . . .	209

# List of Figures

0.1.1	Schematic diagram of Additive Manufacturing process . . . . .	1
0.1.2	Type of Additive Manufacturing process [86, 119] . . . . .	2
0.1.3	Schematic representation of the Wire and Arc Additive Manufacturing (WAAM) process [35] . . . . .	3
0.1.4	The principal phases in the CMT process: 1) Arc (re)-ignition 2) Short circuit phase 3) Inversion of wire feed direction [44] . . . . .	5
0.1.5	Overview of the CMT characteristic parameters, Wire feed rate (m/s), current ( $I$ ) and voltage ( $V$ ) curve during a CMT cycle-time [44] . . . . .	5
0.2.1	Typology of defects in WAAM process: (a) dimensional defect [19], (b) Undulatory defect [48], (c)&(d) distortion and residual stress defects Wu et al. [120], Rodrigues et al. [93], Jafari et al. [59], (e) cracking defect [134, 133, 29] and (f) Porosity formation defect [29] .	6
0.2.2	Wall weld bead problem [19] . . . . .	9
1.1.1	(a) Definition of welding parameters [121], (b) weld bead structure [89, 138, 137] . . . . .	13
1.1.2	Examples of strategies for trajectory planning in WAAM: (a) Raster, (b) Zig-Zag, (c) Contour, (d) Spiral, (e) Fractal space curves, (f) Continuous, and (g) Hybrid [116, 42] . . . . .	17
1.2.1	Overlapping weld bead models (a) Horizontal overlapping [104, 17, 123], (b) Vertical overlapping [75] . . . . .	20
1.3.1	Goldak double ellipsoidal heat source model [49] . . . . .	23
1.3.2	Heat accumulation of weld bead shape . . . . .	28
1.4.1	Thesis approach . . . . .	30
2.0.1	Research approach of design of experiment and procedure . . . . .	34
2.1.1	The conceptual design of WAAM process . . . . .	34

LIST OF FIGURES

---

2.1.2	Configuration of the weld bead deposition for design of experiment; a) Exp.1: Single weld bead on flat substrate, (b) Exp.2: Single weld bead on the cylinder substrate, (c) Exp.3: Lateral overlap weld bead and (d) Exp.4: Vertical overlap weld bead. . . . .	35
2.1.3	Design of experiment: (a) Single weld bead on flat substrate, (b) Single weld bead on cylinder substrate (c) Lateral overlap weld bead and (d) Vertical overlap weld bead . . . . .	36
2.1.4	Equipment set up: (a) robot wire and arc additive systems and (b) the heating device . . . . .	37
2.2.1	Surface deposition temperature ( $T_{dep}$ ) criterion [19] . . . . .	39
2.2.2	Illustration of the building process of the deposition temperature criteria graphics for Exp.1 at the initial temperature ( $T_{init}$ ) of 100°C, (a) $T_{dep}$ at start point, (b) $T_{dep}$ at 40 mm, (c) $T_{dep}$ at end point (endpoint) . . . . .	41
2.2.3	Thermal simulation results of Exp.1 at different initial temperatures ( $T_{init}$ ) of 25°C, 100°C, 200°C, 300°C and 400°C . . . . .	41
2.2.4	Evolution of $T_{dep}$ according to $T_{init}$ for the deposition of single weld beads on flat substrates. . . . .	42
2.2.5	Substrate area of temperature analysis: (a) cylinder area, (b) simu- lation area (rectangular) . . . . .	43
2.2.6	Thermal simulation result of Exp.2: Single weld bead on cylinder substrate at initial temperature ( $T_{init}$ ) at 400°C . . . . .	44
2.2.7	Evolution of $T_{dep}$ according to $T_{init}$ for the deposition of single weld bead on cylinder substrate. . . . .	45
2.2.8	Thermal simulation result of Exp.3: Lateral overlap weld bead at initial temperature ( $T_{init}$ ) at 400°C . . . . .	46
2.2.9	Evolution of $T_{dep}$ according to $T_{init}$ for the deposition of lateral over- lap weld bead. . . . .	46
2.2.10	Thermal simulation result of Exp.4: Vertical overlap weld bead at initial temperature ( $T_{init}$ ) at 400°C . . . . .	47
2.2.11	Evolution of $T_{dep}$ according to $T_{init}$ for the deposition of vertical overlap weld bead. . . . .	48
2.3.1	Design of experiment of single weld bead on a flat substrate . . . . .	49
2.3.2	The result of Exp.1: Single weld bead on flat substrate . . . . .	50
2.3.3	The result of Exp.4 at $T_{init}= 400^\circ\text{C}$ . . . . .	51
2.3.4	Trajectory of lateral overlap weld bead deposition . . . . .	52

2.3.5	The result of Exp.3: Lateral overlap weld beads at $T_{init} = 200^{\circ}\text{C}$ , 300 $^{\circ}\text{C}$ and 400 $^{\circ}\text{C}$ . . . . .	53
2.3.6	Trajectory of vertical overlap weld bead . . . . .	54
2.3.7	The result of Exp.4: Vertical overlap weld bead at $T_{init} = 400^{\circ}\text{C}$ . . .	54
3.0.1	Geometrical identification approach . . . . .	58
3.1.1	The experiment 3D scan process . . . . .	59
3.1.2	Examples of experiments and scanner results (processed at $WFS =$ 5m/min, $TS = 0.6$ m/min and $T_{init} = 300^{\circ}\text{C}$ . . . . .	60
3.2.1	Cross-sections extraction of experiment. . . . .	61
3.3.1	Algorithm of circle fitting model. . . . .	62
3.3.2	Illustration of the process of bead cross-section modelling . . . . .	63
3.3.3	Definition of weld bead dimensions . . . . .	64
3.3.4	Deviations of weld bead cross-section . . . . .	65
3.4.1	Wetting angles for each initial temperature ( $T_{init}$ ) . . . . .	66
3.4.2	Weld bead dimensions of each initial temperature ( $T_{init}$ ) . . . . .	67
3.4.3	Comparison cross-sectional of calculation ( $A_{th}$ ) and curve fitting area	67
3.4.4	Radius of weld bead deposited on cylinder substrates. . . . .	68
3.4.5	Width of weld bead deposited on cylinder substrates. . . . .	69
3.4.6	Wetting angle of weld beads deposited on cylinder substrates . . . . .	70
3.4.7	Wetting angle of weld beads related to substrate curvatures . . . . .	71
3.4.8	Heights of weld beads deposited on cylinder substrates . . . . .	71
3.4.9	Height of weld beads related to substrate curvatures . . . . .	72
3.4.10	Relation between wetting angles and heights of weld beads deposited on cylinder substrates (every conditions are shown) . . . . .	72
3.4.11	Cross section area of weld beads deposited on cylinder substrates . .	73
3.4.12	Heights of weld beads deposited in the lateral direction . . . . .	74
3.4.13	Cross-section area of weld beads deposited in the lateral direction . .	74
3.4.14	Radius of weld beads deposited in the lateral direction . . . . .	75
3.4.15	Widths of weld beads deposited in the lateral direction . . . . .	75
3.4.16	Wetting angle of weld beads deposited in the lateral direction . . . . .	76
3.4.17	Radius of the last layers of walls . . . . .	77
3.4.18	Walls heights . . . . .	78
3.4.19	Comparison of widths between data extracted from scans and circle models. . . . .	79
4.0.1	Interpolation & validation approach . . . . .	83

LIST OF FIGURES

---

4.2.1	Overview of Artificial Intelligence (AI) [64] . . . . .	88
4.2.2	Architecture of Multi-layers perceptron (MLPs) neural network [114]	89
4.2.3	How to choose an hidden layer activation function [14] . . . . .	90
4.2.4	The Rectified Linear Activation (ReLu) function [3] . . . . .	91
4.3.1	Multi-Layer Perceptron (MLP) architecture for interpolating weld bead shape . . . . .	92
4.3.2	Flowchart of the Machine Learning process [21] . . . . .	93
4.4.1	Comparison of radius experiment and predicted values in data set .	96
4.5.1	Trajectory deposition and case study part . . . . .	97
4.5.2	Thermal simulation of case study . . . . .	98
4.5.3	Case study of weld bead cross-sections . . . . .	99
4.5.4	Comparison between $T_{dep}$ prediction and case study dimension . . .	100
5.0.1	The future projects in my career path . . . . .	107
A.2.1	Exp.4 Single weld bead on cylinder substrate thermal simulation at initial temperature ( $T_{init}$ )= 200°C: (a) Cylinder substrate at Ø20 mm or 17 x 18 x 110 mm ( $a \times b \times l$ ), (b) At start point, (c) Weld bead position is 50 mm, (d) Weld bead position is 100 mm . . . . .	134
A.2.2	Thermal simulation result of Exp.2: Single weld bead on cylinder substrate at initial temperature ( $T_{init}$ ) of 25°C . . . . .	135
A.2.3	Thermal simulation result of Exp.2: Single weld bead on cylinder substrate at initial temperature ( $T_{init}$ ) of 100°C . . . . .	136
A.2.4	Thermal simulation result of Exp.2: Single weld bead on cylinder substrate at initial temperature ( $T_{init}$ ) of 200°C . . . . .	136
A.2.5	Thermal simulation result of Exp.2: Single weld bead on cylinder substrate at initial temperature ( $T_{init}$ ) of 300°C . . . . .	137
A.3.1	Thermal simulation of Exp.3 Lateral overlap weld bead (L4) at ini- tial temperature ( $T_{init}$ )= 200°C, (a) At start point, (b) Weld bead position is 40 mm and (c) Weld bead position is 80 mm (endpoint) .	162
A.3.2	Thermal simulation result of Exp.3: Single weld bead on cylinder substrate at initial temperature ( $T_{init}$ ) of 200°C . . . . .	162
A.3.3	Thermal simulation result of Exp.3: Single weld bead on cylinder substrate at initial temperature ( $T_{init}$ ) of 300°C . . . . .	163
A.4.1	Thermal simulation of Exp.2: Vertical overlap weld bead, (a) Num- ber of 5 <sup>th</sup> layer (L5) and (b) Number of 10 <sup>th</sup> layer . . . . .	177

A.4.2 Thermal simulation result of Exp.4: Vertical overlap weld bead at initial temperature ( $T_{init}$ ) at 100°C . . . . .	178
A.4.3 Thermal simulation result of Exp.4: Vertical overlap weld bead at initial temperature ( $T_{init}$ ) at 200°C . . . . .	178
A.4.4 Thermal simulation result of Exp.4: Vertical overlap weld bead at initial temperature ( $T_{init}$ ) at 300°C . . . . .	179
B.1.1 Design of experiment of single weld bead on cylinder substrate . . .	197
B.2.1 The result of Exp.3: single weld bead on cylinder substrate at $T_{init}=25^{\circ}\text{C}$ . . . . .	198
B.2.2 The result of Exp.3: single weld bead on cylinder substrate at $T_{init}=100^{\circ}\text{C}$ . . . . .	198
B.2.3 The result of Exp.3: single weld bead on cylinder substrate at $T_{init}=200^{\circ}\text{C}$ . . . . .	199
B.2.4 The result of Exp.3: single weld bead on cylinder substrate at $T_{init}=300^{\circ}\text{C}$ . . . . .	199
B.3.1 Design of experiment of lateral overlap weld bead . . . . .	200
B.4.1 Design of experiment of vertical overlap weld bead . . . . .	201
B.5.1 The result of Exp.4: Vertical overlap weld bead at $T_{init}= 100^{\circ}\text{C}$ . . .	202
B.5.2 The result of Exp.4: Vertical overlap weld bead at $T_{init}= 200^{\circ}\text{C}$ . . .	203
B.5.3 The result of Exp.4: Vertical overlap weld bead at $T_{init}= 300^{\circ}\text{C}$ . . .	203
C.1.1 Import library in Python . . . . .	205
C.1.2 Setting up the data for MLP Regressor in Python . . . . .	205
C.1.3 Using MLP Regressor and calculating the scores in Python . . . . .	207



# List of Tables

1.1	The mathematical function of weld bead cross-section profiles. . . . .	20
2.1	Nominal chemical composition (wt.%) of substrate and wire electrode material . . . . .	37
2.2	Process parameters for experiment . . . . .	38
2.3	Comparison of dimension between cylinders and thermal simulations	43
4.1	Weld beads measurements . . . . .	84
4.1	Weld beads measurements . . . . .	85
4.2	MLP regression model configuration for the training in Python . . . . .	94
4.3	Training performance of difference network architecture . . . . .	94
4.3	Training performance of difference network architecture . . . . .	95
4.3	Training performance of difference network architecture . . . . .	96
4.4	Case study of weld bead dimension prediction data (L1 to L8) . . . . .	99
A.1	Data surface deposition temperature ( $T_{dep}$ ) of Exp.1 . . . . .	129
A.1	Data surface deposition temperature ( $T_{dep}$ ) of Exp.1 . . . . .	130
A.1	Data surface deposition temperature ( $T_{dep}$ ) of Exp.1 . . . . .	131
A.1	Data surface deposition temperature ( $T_{dep}$ ) of Exp.1 . . . . .	132
A.1	Data surface deposition temperature ( $T_{dep}$ ) of Exp.1 . . . . .	133
A.2	Average surface temperature deposition ( $T_{dep}$ ) and standard deviation ( $\sigma$ ) of Exp.1: Single weld bead on flat substrate . . . . .	133
A.3	Data surface deposition temperature ( $T_{dep}$ ) of Exp.2 at initial temperature ( $T_{init}$ ) of 25°C . . . . .	137
A.3	Data surface deposition temperature ( $T_{dep}$ ) of Exp.2 at initial temperature ( $T_{init}$ ) of 25°C . . . . .	138
A.3	Data surface deposition temperature ( $T_{dep}$ ) of Exp.2 at initial temperature ( $T_{init}$ ) of 25°C . . . . .	139
A.3	Data surface deposition temperature ( $T_{dep}$ ) of Exp.2 at initial temperature ( $T_{init}$ ) of 25°C . . . . .	140



LIST OF TABLES

---

A.3	Data surface deposition temperature ( $T_{dep}$ ) of Exp.2 at initial temperature ( $T_{init}$ ) of 25°C . . . . .	141
A.3	Data surface deposition temperature ( $T_{dep}$ ) of Exp.2 at initial temperature ( $T_{init}$ ) of 25°C . . . . .	142
A.4	Data surface deposition temperature ( $T_{dep}$ ) of Exp.2 at initial temperature ( $T_{init}$ ) of 100°C . . . . .	142
A.4	Data surface deposition temperature ( $T_{dep}$ ) of Exp.2 at initial temperature ( $T_{init}$ ) of 100°C . . . . .	143
A.4	Data surface deposition temperature ( $T_{dep}$ ) of Exp.2 at initial temperature ( $T_{init}$ ) of 100°C . . . . .	144
A.4	Data surface deposition temperature ( $T_{dep}$ ) of Exp.2 at initial temperature ( $T_{init}$ ) of 100°C . . . . .	145
A.4	Data surface deposition temperature ( $T_{dep}$ ) of Exp.2 at initial temperature ( $T_{init}$ ) of 100°C . . . . .	146
A.5	Data surface deposition temperature ( $T_{dep}$ ) of Exp.2 at initial temperature ( $T_{init}$ ) of 200°C . . . . .	147
A.5	Data surface deposition temperature ( $T_{dep}$ ) of Exp.2 at initial temperature ( $T_{init}$ ) of 200°C . . . . .	148
A.5	Data surface deposition temperature ( $T_{dep}$ ) of Exp.2 at initial temperature ( $T_{init}$ ) of 200°C . . . . .	149
A.5	Data surface deposition temperature ( $T_{dep}$ ) of Exp.2 at initial temperature ( $T_{init}$ ) of 200°C . . . . .	150
A.5	Data surface deposition temperature ( $T_{dep}$ ) of Exp.2 at initial temperature ( $T_{init}$ ) of 200°C . . . . .	151
A.6	Data surface deposition temperature ( $T_{dep}$ ) of Exp.2 at initial temperature ( $T_{init}$ ) of 300°C . . . . .	151
A.6	Data surface deposition temperature ( $T_{dep}$ ) of Exp.2 at initial temperature ( $T_{init}$ ) of 300°C . . . . .	152
A.6	Data surface deposition temperature ( $T_{dep}$ ) of Exp.2 at initial temperature ( $T_{init}$ ) of 300°C . . . . .	153
A.6	Data surface deposition temperature ( $T_{dep}$ ) of Exp.2 at initial temperature ( $T_{init}$ ) of 300°C . . . . .	154
A.6	Data surface deposition temperature ( $T_{dep}$ ) of Exp.2 at initial temperature ( $T_{init}$ ) of 300°C . . . . .	155
A.6	Data surface deposition temperature ( $T_{dep}$ ) of Exp.2 at initial temperature ( $T_{init}$ ) of 300°C . . . . .	156

---

A.7	Data surface deposition temperature ( $T_{dep}$ ) of Exp.2 at initial temperature ( $T_{init}$ ) of 400°C . . . . .	156
A.7	Data surface deposition temperature ( $T_{dep}$ ) of Exp.2 at initial temperature ( $T_{init}$ ) of 400°C . . . . .	157
A.7	Data surface deposition temperature ( $T_{dep}$ ) of Exp.2 at initial temperature ( $T_{init}$ ) of 400°C . . . . .	158
A.7	Data surface deposition temperature ( $T_{dep}$ ) of Exp.2 at initial temperature ( $T_{init}$ ) of 400°C . . . . .	159
A.7	Data surface deposition temperature ( $T_{dep}$ ) of Exp.2 at initial temperature ( $T_{init}$ ) of 400°C . . . . .	160
A.8	Average surface temperature deposition ( $T_{dep}$ ) and standard deviation ( $\sigma$ ) of Exp.2: Single weld bead on cylinder substrate . . . . .	161
A.9	Data surface deposition temperature ( $T_{dep}$ ) of Exp.3 at initial temperature ( $T_{init}$ ) = 200°C . . . . .	163
A.9	Data surface deposition temperature ( $T_{dep}$ ) of Exp.3 at initial temperature ( $T_{init}$ ) = 200°C . . . . .	164
A.9	Data surface deposition temperature ( $T_{dep}$ ) of Exp.3 at initial temperature ( $T_{init}$ ) = 200°C . . . . .	165
A.9	Data surface deposition temperature ( $T_{dep}$ ) of Exp.3 at initial temperature ( $T_{init}$ ) = 200°C . . . . .	166
A.9	Data surface deposition temperature ( $T_{dep}$ ) of Exp.3 at initial temperature ( $T_{init}$ ) = 200°C . . . . .	167
A.10	Data surface deposition temperature ( $T_{dep}$ ) of Exp.3 at initial temperature ( $T_{init}$ ) = 300°C . . . . .	167
A.10	Data surface deposition temperature ( $T_{dep}$ ) of Exp.3 at initial temperature ( $T_{init}$ ) = 300°C . . . . .	168
A.10	Data surface deposition temperature ( $T_{dep}$ ) of Exp.3 at initial temperature ( $T_{init}$ ) = 300°C . . . . .	169
A.10	Data surface deposition temperature ( $T_{dep}$ ) of Exp.3 at initial temperature ( $T_{init}$ ) = 300°C . . . . .	170
A.10	Data surface deposition temperature ( $T_{dep}$ ) of Exp.3 at initial temperature ( $T_{init}$ ) = 300°C . . . . .	171
A.11	Data surface deposition temperature ( $T_{dep}$ ) of Exp.3 at initial temperature ( $T_{init}$ ) = 400°C . . . . .	172
A.11	Data surface deposition temperature ( $T_{dep}$ ) of Exp.3 at initial temperature ( $T_{init}$ ) = 400°C . . . . .	173

LIST OF TABLES

---

A.11	Data surface deposition temperature ( $T_{dep}$ ) of Exp.3 at initial temperature ( $T_{init}$ ) = 400°C . . . . .	174
A.11	Data surface deposition temperature ( $T_{dep}$ ) of Exp.3 at initial temperature ( $T_{init}$ ) = 400°C . . . . .	175
A.12	Average surface temperature deposition ( $T_{dep}$ ) and standard deviation ( $\sigma$ ) of Exp.3: Lateral overlap weld bead . . . . .	176
A.13	Data surface deposition temperature ( $T_{dep}$ ) of Exp.4 at initial temperature ( $T_{init}$ ) = 100°C . . . . .	179
A.13	Data surface deposition temperature ( $T_{dep}$ ) of Exp.4 at initial temperature ( $T_{init}$ ) = 100°C . . . . .	180
A.13	Data surface deposition temperature ( $T_{dep}$ ) of Exp.4 at initial temperature ( $T_{init}$ ) = 100°C . . . . .	181
A.13	Data surface deposition temperature ( $T_{dep}$ ) of Exp.4 at initial temperature ( $T_{init}$ ) = 100°C . . . . .	182
A.13	Data surface deposition temperature ( $T_{dep}$ ) of Exp.4 at initial temperature ( $T_{init}$ ) = 100°C . . . . .	183
A.14	Data surface deposition temperature ( $T_{dep}$ ) of Exp.4 at initial temperature ( $T_{init}$ ) = 200°C . . . . .	184
A.14	Data surface deposition temperature ( $T_{dep}$ ) of Exp.4 at initial temperature ( $T_{init}$ ) = 200°C . . . . .	185
A.14	Data surface deposition temperature ( $T_{dep}$ ) of Exp.4 at initial temperature ( $T_{init}$ ) = 200°C . . . . .	186
A.14	Data surface deposition temperature ( $T_{dep}$ ) of Exp.4 at initial temperature ( $T_{init}$ ) = 200°C . . . . .	187
A.15	Data surface deposition temperature ( $T_{dep}$ ) of Exp.4 at initial temperature ( $T_{init}$ ) = 300°C . . . . .	188
A.15	Data surface deposition temperature ( $T_{dep}$ ) of Exp.4 at initial temperature ( $T_{init}$ ) = 300°C . . . . .	189
A.15	Data surface deposition temperature ( $T_{dep}$ ) of Exp.4 at initial temperature ( $T_{init}$ ) = 300°C . . . . .	190
A.15	Data surface deposition temperature ( $T_{dep}$ ) of Exp.4 at initial temperature ( $T_{init}$ ) = 300°C . . . . .	191
A.16	Data surface deposition temperature ( $T_{dep}$ ) of Exp.4 at initial temperature ( $T_{init}$ ) = 400°C . . . . .	192
A.16	Data surface deposition temperature ( $T_{dep}$ ) of Exp.4 at initial temperature ( $T_{init}$ ) = 400°C . . . . .	193

A.16	Data surface deposition temperature ( $T_{dep}$ ) of Exp.4 at initial temperature ( $T_{init}$ ) = 400°C . . . . .	194
A.16	Data surface deposition temperature ( $T_{dep}$ ) of Exp.4 at initial temperature ( $T_{init}$ ) = 400°C . . . . .	195
A.17	Average surface temperature deposition ( $T_{dep}$ ) and standard deviation ( $\sigma$ ) of Exp.4: Vertical overlap weld bead . . . . .	196
C.1	Comparison of experiment and predicted results . . . . .	208
C.1	Comparison of experiment and predicted results . . . . .	209
C.2	Average surface temperature deposition ( $T_{dep}$ ) of validation part . . . . .	209
C.2	Average surface temperature deposition ( $T_{dep}$ ) of validation part . . . . .	210
C.2	Average surface temperature deposition ( $T_{dep}$ ) of validation part . . . . .	211
C.3	Cause study validation result . . . . .	211
C.3	Cause study validation result . . . . .	212
C.3	Cause study validation result . . . . .	213



# Introduction

## Context

### Additive Manufacturing (AM)

Over the past 30 years, Additive Manufacturing (AM) technologies have progressed steadily. The application of additive manufacturing has indeed increased in various industries such as biomedical, aerospace, automotive, etc [109]. This growth is expected to continue over the next few years [55]. AM technologies build physical objects created from a three dimensional (3D) model and are usually built layer by layer in contrast to subtractive manufacturing [13, 50]. In addition, different techniques of deposition can be identified for a variety of materials. It is known that the AM process is used for manufacturing parts based on layer by layer addition of materials with the assistance of 3D model made from Computer Aided Design (CAD) [6, 53]. As Figure 0.1.1 shows the diagram of the additive manufacturing process. Each layer is deposited on top of the other layers based on a given trajectory. The AM process starts with a Computer-Aided Design (CAD) file model. Which is sliced. From these slices, manufacturing trajectories are calculated. Finally, the part is manufactured layer by layer by melting and cooling a raw material, either plastic or metallic, powder or wire [63].

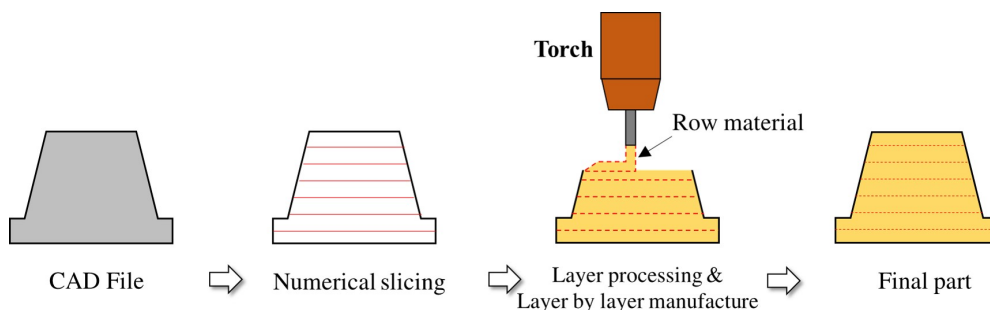


Figure 0.1.1 : Schematic diagram of Additive Manufacturing process

These technologies emerged from the industry of rapid prototyping (RP) [28] and rapid manufacturing (RM) [47]. Rapid prototyping is the creation of a fundamental concept that involves an idea *i.e.*, the process of creating prototypes to quickly evaluate an engineering product design visually and functionally. Rapid manufacturing is a technique that quickly directs fabrication. It is used for various applications and for manufacturing high-quality parts in relatively small lots [86]. That is why nowadays, the Additive Manufacturing (AM) technology has shifted to manufacture more complex metal parts without fixtures, tooling and mold [33, 135]. Within AM, most technologies can be classified into three main processes: liquid, powder, and solid processes [128, 32, 12] as shown in Figure 0.1.2. The directed energy deposition (DED) of the solid process is the environment of this research that will focus especially on WAAM process.

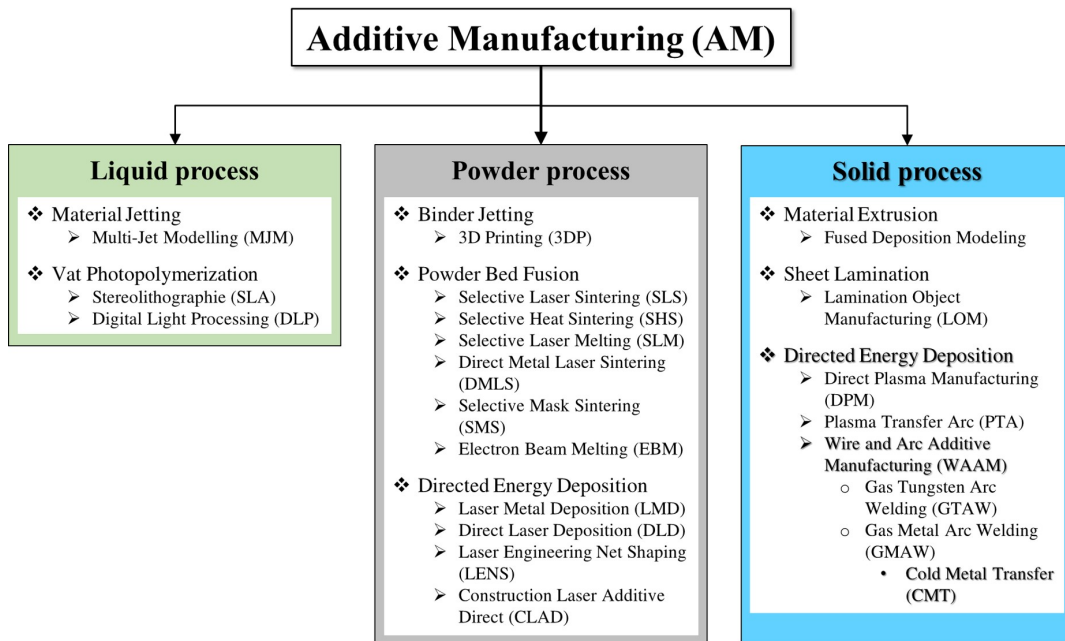


Figure 0.1.2 : Type of Additive Manufacturing process [86, 119]

## Directed Energy Deposition (DED)

Directed energy deposition (DED) [108] allows the fabrication of objects by melting a powdery or wiry metallic or plastic material (such as copper, aluminum, titanium, stainless steel) on a surface with a concentrated energy source such as a welding arc[110, 83]. DED technologies are ideally suited for repairing or adding material to existing components. The advantages of DED are high building rate, high-quality

parts and re-manufacturing [96]. Moreover, it can be used for multi-material range, large parts, easy material change and reduced material waste [27, 39]. As displayed in Figure 0.1.2 DED regroups a variety of technologies. In this research, the focus will be put on Wire and Arc Additive Manufacturing (WAAM). In WAAM, the heat source is an electric arc, and the feedstock material is a metallic wire [93].

## Wire and Arc Additive Manufacturing (WAAM)

WAAM uses either the Gas Tungsten Arc Welding process (GTAW) or the Gas Metal Arc Welding process (GMAW) [1, 34]. It has two main advantages: the deposition rate and consequently, the production efficiency [117, 82]. WAAM can be performed by a robotic system (Figure 0.1.3). A molten pool of liquid metal is formed when an electric arc occurs between a consumable wire electrode and substrate [61]. Under the protection of the shielding gas, the welding wire is fed into the molten pool [43]. Geometrical shapes are created layer by layer by controlling the trajectory of the robot at a defined speed [35].

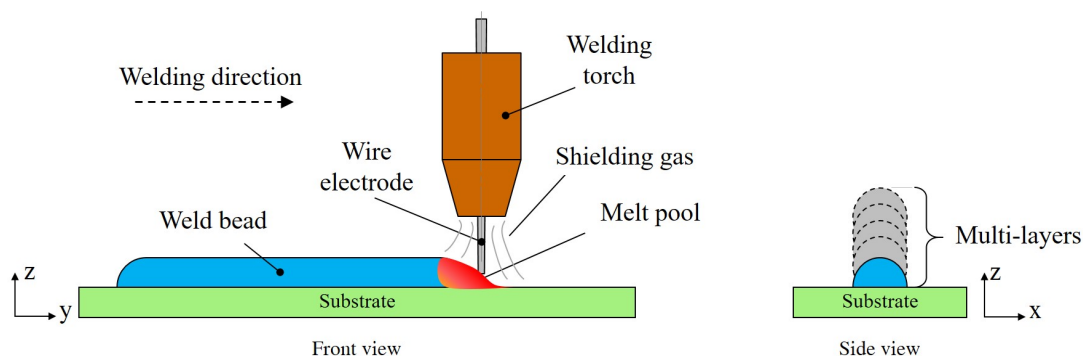


Figure 0.1.3 : Schematic representation of the Wire and Arc Additive Manufacturing (WAAM) process [35]

Ideally, the welding parameters must be controlled to be constant during the deposition process, to ensure the weld bead geometrical stability such as width ( $w$ ) and height ( $h$ ). To manage the WAAM process, there are at least three main parameters to take into consideration: wire feed speed ( $WFS$ ), travel speed ( $TS$ ), and energy modes.

However, it is known that thermal accumulation is an essential factor that significantly affects the geometrical stability and residual stresses [100, 84]. In order to deposit a weld bead, heat production or heat input must be managed, and sometimes reduced. One of the solutions to reduce it is by using a specific mode that



involve a lower amount of energy which is the cold metal transfer (CMT). CMT is a modified metal inert gas (MIG) welding process, which features low heat input [41]. It is based on a short-circuiting transfer process developed by Fronius of Austria [44]. CMT has been developed in various modes but this research focuses specifically on the management of the weld bead deposition process with cold metal transfer standard (CMT-STD) mode. The CMT-STD is ideal for welding aluminum alloy sheets and thin metal due to its low heat input and slight deformation [100]. The electrical welding cycle is divided into three phases: the peak current phase, the background current phase and the short-circuiting phase [44].

## **Cold Metal Transfer (CMT) technology**

Cold metal transfer (CMT) is an improved metal inert gas (MIG) welding process, mainly operating in short-circuiting transfer process [88]. CMT allows lower energy input [11]. The idea also comes from the consumer side that needs an optimal welding solution with just a few drops of molten metal on a very thin plate [57]. For this reason, intensive development work for the most suitable solutions for industrial applications has begun since then. The main difference between CMT and conventional gas metal arc welding (GMAW) [80], is that CMT allows full digital control of the welding process. The micro-controller controls the wire feeding for the CMT process through the feed motor. A high pulse current is initiated, producing an arc between the forward electrode and the electrode tip melting surface [100]. As soon as a short circuit is identified, the voltage drops. The current is further reduced to a low background value, and the wire then retracts [105]. This leads to the release of the molten droplet. Hence, the CMT process is characterized by an innovative solution for weld drop detachment. Unlike in a conventional pulsed arc, the droplet is not notched by a current impulse, instead it is a defined retraction motion of the wire which brings controlled droplet detachment. Figure 0.1.4 describes the principal phases of the CMT process [44].

The length of this cycle is not predetermined. Instead, it is optimized according to predefined arc characteristics. Thus, the movement of the wire controls what happens in the weld pool and vice versa [107].

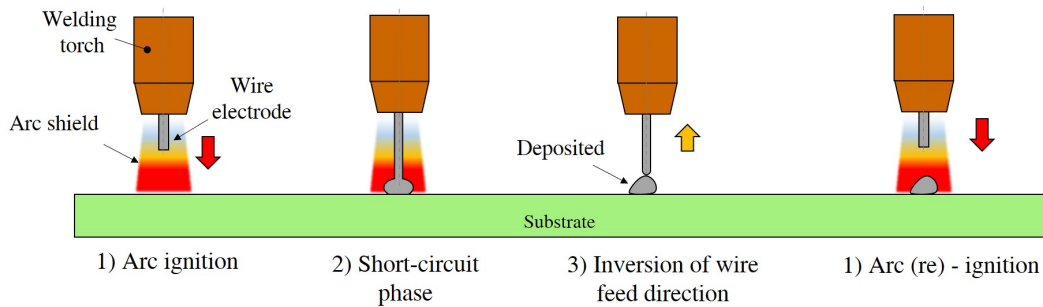


Figure 0.1.4 : The principal phases in the CMT process: 1) Arc (re)-ignition 2) Short circuit phase 3) Inversion of wire feed direction [44]

The characteristic curves for the CMT-process are shown in Figure 0.1.5. The upper curve shows the wire feed rate curve. The back and forth motion can be seen from the curve during the short circuit phase. The following curves indicate multiple variables that can be adjusted to optimize the welding process, such as power. The length of each cycle phases can also be adjusted. The CMT process is an integrated welding method that can be used for different types of applications, including low heat input [44, 107].

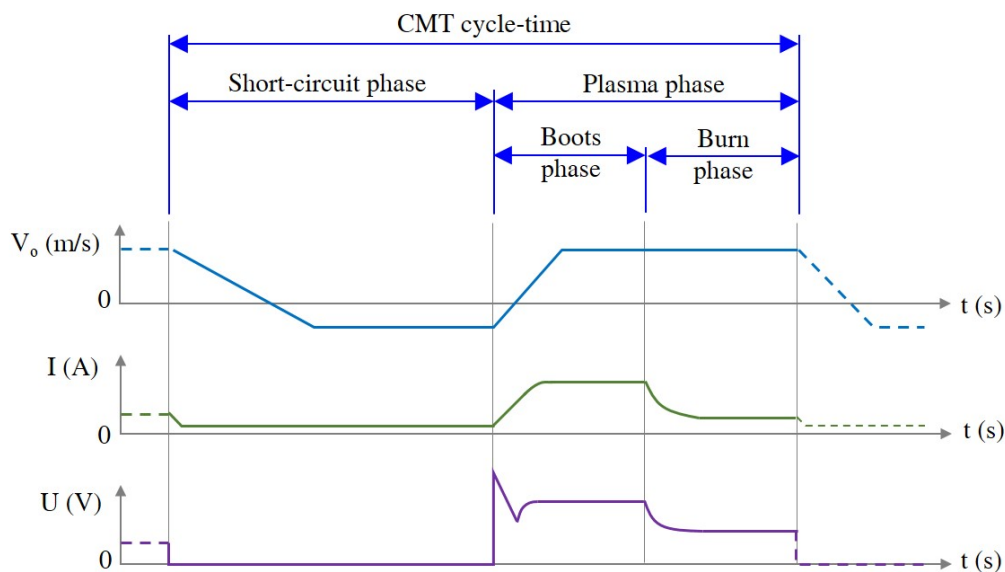


Figure 0.1.5 : Overview of the CMT characteristic parameters, Wire feed rate (m/s), current ( $I$ ) and voltage ( $V$ ) curve during a CMT cycle-time [44]

## Problematic

This research focuses on the management of weld bead quality deposited using CMT of WAAM. In terms of quality, this process still encounters many problems. Figure 0.2.1 displays the typology of defects that can be encountered on WAAM manufactured parts. These defect can be divided into two main types: geometric defects and materials defects. Geometric defects regroup dimensional, undulatory and distortion defects. Material defects refer to residual stress, cracking and porosity formation defects. All defects are primarily caused by thermal effects due to heigh heat input induced by the WAAM process.

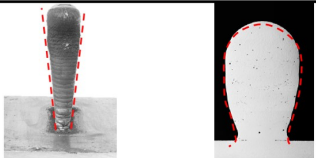
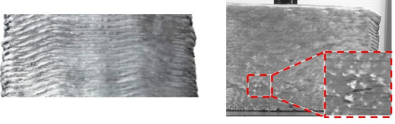


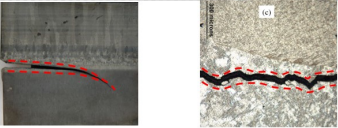
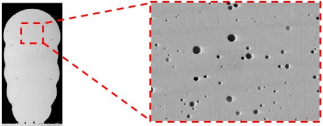
Types	Defects	Pictures
Geometric	(a) Dimensional	
	(b) Undulatory	
	(c) Distortion	
Materials	(d) Residual stress	
	(e) Cracking	
	(f) Porosity formation	

Figure 0.2.1 : Typology of defects in WAAM process: (a) dimensional defect [19], (b) Undulatory defect [48], (c)&(d) distortion and residual stress defects Wu et al. [120], Rodrigues et al. [93], Jafari et al. [59], (e) cracking defect [134, 133, 29] and (f) Porosity formation defect [29]

## **Geometric and Materials integrity defects**

### **(a) Dimensional**

In the WAAM process, the dimensional defects are physical, and it is impossible to avoid their generation altogether. The dimensional defect can lead to distortion of the geometry part and loss of geometric accuracy. [118] studied the effects of heat accumulation on arc characteristics and metal transfer behavior in WAAM of Ti6Al4V. They suggested to use the specific heat equation to quantify thermal accumulation for each layer of a thin-wall component. They explained that the geometry of the layers varies along deposition direction due to the changing heat dissipation conditions and increasing interpass temperature, namely, the temperature of the last deposited layer at the start of the subsequent layer deposition. Indeed, this interpass temperature significantly influences the geometry of the manufactured parts. [19] proposes to manufacture a thin-wall part with WAAM. The experiment was composed of sixty layers of 100 mm length. The deposition strategy was based on zigzag deposition path. In fact, during the deposition of thin-walled structures, the heat is mainly conducted from the molten pool to the substrate plate through conduction. Therefore, the heat dissipation is slower with increasing deposition. As a result, the molten pool increases, and its solidification is slowed down. This heat accumulation phenomenon can also be observed by its significant consequence: the increase of the part temperature during the production time [24]. [25] presented the effect of two thermal management approaches on geometry of thin-walled produced by WAAM. They compare two techniques of active cooling. First, near-immersion active cooling (NIAC) under a fixed set of deposition parameters. Then, secondly, the same experiment was performed with natural cooling (NC) in the air. To characterize the thermal management approaches, the interpass temperature was monitored by a trailing/leading infrared pyrometer during the deposition time. Finally, thin walls with a fixed-length were deposited using the NC, and NIAC reaches with equal interpass temperatures. The findings revealed that the NIAC approach effectively reduced heat buildup in aluminum WAAM and produced parts with a better quality. With the water cooling, there was no noticeable increase in porosity.

### **(b) Undulatory**

The undulation defects are mainly influenced by wire feed speed ( $WFS$ ), travel speed ( $TS$ ) and arc current ( $V$ ) [129]. [127] studies the effects of the main WAAM process parameters on the wall quality. They observed that, with other parameters being constant, the reduction of the layer temperature is related to the increased surface quality of thin-walled parts. They showed that wire feed speed ( $WFS$ ) is the critical influencing factor for the fabricated appearance of thin-walled parts. Moreover, by keeping the ratio of wire feed speed to travel speed ( $TS$ ) constant, the surface roughness increases with the increasing wire feed speed. [124] studied forming characteristics of multi-layer single-pass. The main objective is to show how the issue factors, such as the arc current, travel speed, and heat input, affect the undulatory appearance. The results show that arc current is the main factor affecting defects.

### **(c) Distortion & (d) Residual stress**

Distortion and residual stresses are present in the WAAM process, and their generation cannot be completely avoided. The process of reducing distortion starts with choosing the suitable parameters (heat input and dwell times), planning the path, and adding extra steps like heat treatment and high-impact rolling [66]. Residual stress is stress within a material that persists after stress removal. If this stress is greater than the local yield stress of the material, warping or distortion may happen [99]. Residual stress can lead to part distortion, loss of geometry tolerance, delamination of the layer during deposition, and the deterioration of the fatigue performance and fracture resistance of additive manufactured components [120].

### **(e) Cracking**

Cracking is typical in additively manufactured parts, including those manufactured by WAAM. These defects are caused by the material properties deposited and the temperature of the process [19]. The fabrication of defects is highly conditional on process temperature. Microstructure cracking occurs between subsequent heating and solidification, including porosity. Cracking can be classified into two types: solidification cracking and boundary cracking. Mainly, cracking is sometimes used to explain macroscopic cracks in the material [99].

### (f) Porosity formation

Porosity is another material defect problem that strongly affects the mechanical properties of WAAM produced parts. When processing most aluminum alloys, porosity is a general defect and should be avoided or kept as low as possible to alter the mechanical properties as little as possible [54]. [29] explained that the higher interpass temperature exposed 10.41% less porosity than the experiment prepared with the lower interpass temperature. [8] experiment showed the selection of the shielding gas, gas flow and deposition path affect the reduction of porosity defect lower than 0.035%.

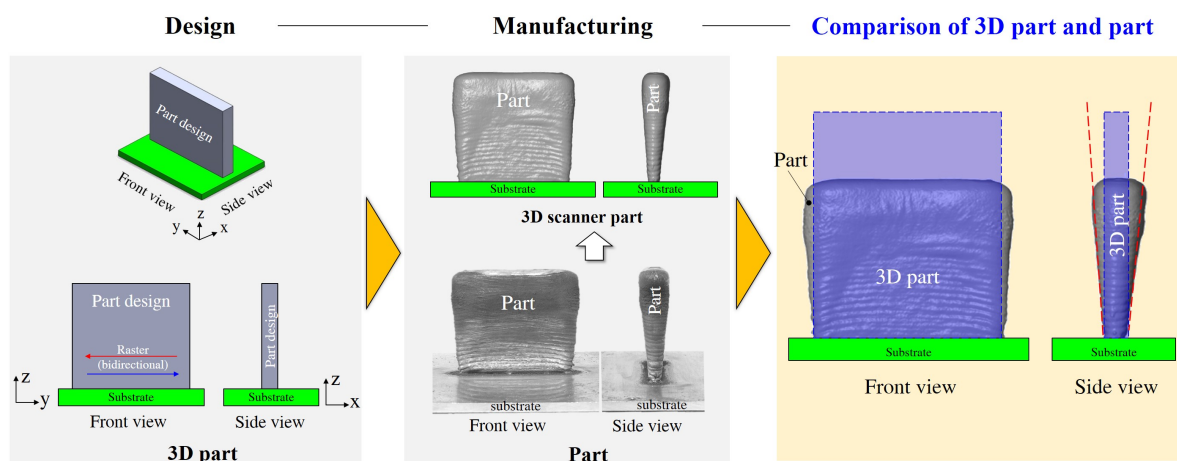


Figure 0.2.2 : Wall weld bead problem [19]

From the aforementioned typology of defects in WAAM process, the dimensional defect, *i.e.* the part shape, is a major problem. To better understand this issue, a solution is to compare the physical part with a three-dimensional (3D) model. The outcome of this comparison leads to the identification of shape deformation. In other words, the part is not produced correctly according to the 3D model. The results of the analysis reveal that heat accumulation [118, 19, 25] is the leading cause of the dimensional defect. Figure 0.2.2 shows a comparison between the 3D design and the part, noting that thin walls have different thicknesses and heights than the 3D design. The cause of the problem was analyzed in terms of the dimensional defect. For this reason, it can be explained that **heat accumulation affects the geometry of the weld bead.**

Now, the main issue is to understand this phenomenon, which is presented in the following research question section.

## **Scientific and technical issue**

As aforementioned, Heat accumulation is an issue that affects the weld bead shape and there are many reasons for this problem. This is why managing heat accumulation will lead to better precision of the weld bead dimensions. This leads to the main issue of the present scientific work:

**“How to manage weld bead shape with regard to process parameters and heat accumulation around the deposition point?”**

Hence, we proposed to answer this question in two steps:

- Study the effect of heat accumulation and process parameters on the weld bead shape,
- Create an interpolation model of weld bead shape depending on process parameters and thermal conditions.

In the next chapter, we will study the literature review and will propose an approach for this research.

# Chapter 1

## Literature review

The objectives of this chapter are to study how the influence of the WAAM process parameters on the shape of the product has been investigated in the literature. By the term “process parameters” we refer to the global parameters of the WAAM process grouped into two different categories: **the welding parameters and the deposition trajectory**. Welding parameters refer to the parameters of the welding process that can influence the shape of the weld bead. Also, the shape of the product is strongly linked to the superposition and juxtaposition of the weld beads via the deposition trajectory.

The section 1.1 of this chapter presents the influence of welding parameters and deposition trajectory on the weld bead shape. The section 1.2 presents various weld bead models including a variety of mathematical modeling functions for measuring the weld bead shape, as well as the arguments for choosing one of the models. These investigations allow us to retain the model that will be used for our experiments. The section 1.3 describes the tool involved in thermal simulation by finite element method (FEM). FEM tool helps to simulate various phenomena of weld bead deposition, such as the distortion, residual stress, strength, heat dissipation or temperature occurring during deposition. One of the presented tools will be used to predict temperature of the deposition surface in our experiments.



## 1.1 Influence of process parameters on the weld bead shape

### 1.1.1 Welding parameters

Welding parameters refers on the parameters of the welding process schematized in Figure 1.1.1 (a). Wire feed speed (*WFS*) is the wire feeding speed of materials during the welding deposition. Travel speed (*TS*) is the welding torch speed during the deposition process. Arc voltage (*V*) is the amount of voltage consumed during welding deposition. Arc current (*I*) is the amount of current consumed during welding deposition. Torch distance is the distance between the welding torch and the substrate. Gas flow is the flow rate of gas during the welding deposition.

Cold metal transfer (CMT) process is an arc welding process based on the modified MIG welding process. It is characterized by low heat input, no-spatter and high deposition rate [44, 11]. Recently CMT has been developed into different welding modes which are conventional CMT, CMT pulse (CMT-P), CMT advanced (CMT-ADV) and CMT pulse advanced (CMT-PADV). Each of them can be described as follows:

- In conventional CMT mode, like in a conventional welding pulsed arc, the droplet is notched by a current impulse. However, it is a defined rearward motion of the welding wire that leads to controlled droplet detachment [44, 105].
- CMT pulse mode (CMT-P) is a combination of conventional CMT mode with one droplet per pulse and a short circuit transfer mode during the cold metal transfer period [44, 132].
- In CMT advanced mode (CMT-ADV) positive and negative CMT cycles are combined using an alternate current (AC). This results in a procedure that is even cooler than standard CMT. The welding current reverses polarity in the short-circuit phase, resulting in decreased heat input, higher gap bridge ability, and faster deposition rates [44, 107, 92].
- CMT pulse advanced (CMT-PADV) is a combination of negatively poled CMT cycles and positively poled pulsing cycles. First comes the CMT negative phase where the wire moves towards the workpiece. It is followed by the initialization phase where the wire is retracted and the cycle is positive poled, which is followed by positive pole pulsed-arc cycles [44, 107].

## 1.1 Influence of process parameters on the weld bead shape

The welds bead shape can be defined by the weld bead width ( $w$ ), height ( $h$ ) and/or area ( $A$ ) as shown in [89, 138, 137] as shown in Figure 1.1.1 (b)

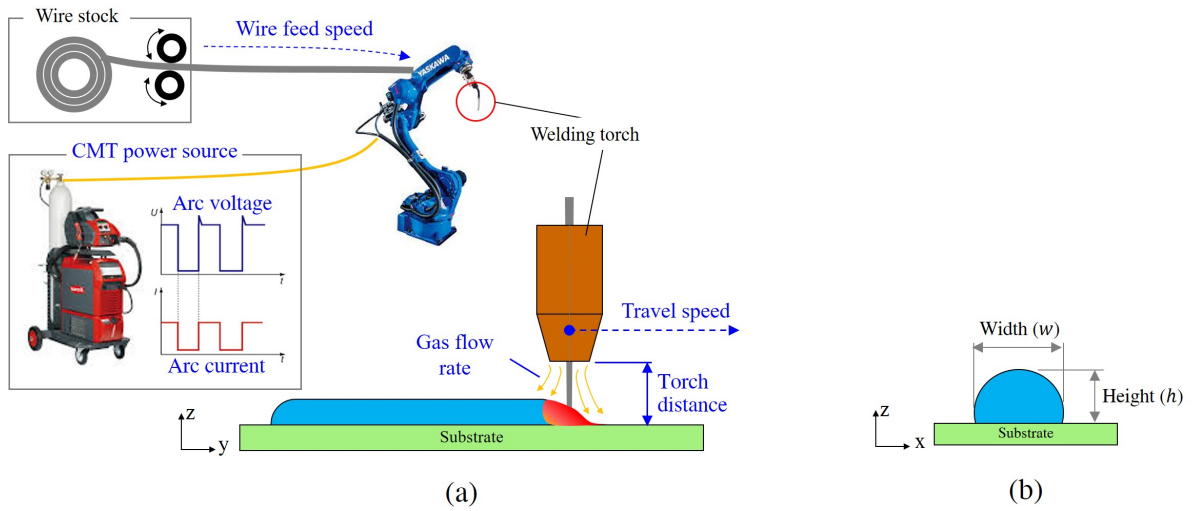


Figure 1.1.1 : (a) Definition of welding parameters [121], (b) weld bead structure [89, 138, 137]

[32] focus on the influence of  $TS$  on the weld bead geometry: height, width and area. The wire material used for the experiment is copper-clad steel with a diameter of 1.2 mm. The authors try experiment for a combination of one  $WFS$  and height different  $TS$ . Different models of the weld bead are proposed (CMT modes) and the ratio  $\lambda = WFS/TS$  is introduced indicating that all of the proposed models can accurately predict the weld bead geometry according to variation of  $TS$ , for ratio ranges for 9.1 to 25.

[104] have identified two welding parameters ( $WFS$ ,  $TS$ ) as primary process parameters and point out the influence of these primary processes on the weld beads geometry. The wire used for the experiment is a copper-coated mild steel (ER70S6) wire with a diameter of 0.8 mm. This is validated through a series of single-bead experiments comparing the predicted and measured geometries of the beads for various values of wire and torch speeds. These are the same two parameters ( $WFS$ ,  $TS$ ) that were retained by [122] in their study on weld bead section profile. [106] describe the irregularity of the weld bead, namely the abnormal area. The abnormal area is the unstable area of the weld and is divided into three areas: the beginning area, middle area, and end area of the weld bead. However, the low precision of WAAM limits the geometry control, especially in the arc striking (AS) at the beginning area and arc extinguishing (AE) at the end area of the weld bead. The chosen

welding parameters (travel speed ( $TS$ ), arc current ( $I$ )) have significant effects on the weld bead shape. As a result, the response surface method (RSM) approach is used to establish mathematical models for the bead width and height in the AS and AE areas. The results showed that the relationship models at both ends were applicable and preferable for the optimization of the weld beads.

In the study of [130], we still find the influence of  $WFS$  and  $TS$ , which are considered the most influential welding parameters on the weld bead geometry. The material substrate used for the experiment is steel (S355), and the wire material is a low-alloy high-strength steel (ER 120S-G) with a diameter of 1.2 mm. Compared to the papers above cited, we find in [130] the additional notion of heat input. Heat input helps to measure of how much energy has been supplied to per unit length of weld. In WAAM, every layer is deposited with an additional amount of heat, causing heat accumulation. This heat accumulation influences process stability, geometrical accuracy, and material properties [130].  $WFS$  and  $TS$  are the major process parameters controlling the heat input for the WAAM process. The ratio ( $\lambda$ ) also correlates almost perfectly linear with the heat input and can be a major parameter to control the heat input (and therefore the weld bead geometry), even if other welding parameters can also have an influence on the heat input, such as arc voltage [71, 94], arc current and process efficiency [82] and CMT modes [79, 9, 87, 88, 17]. As for, the influence of arc voltage, [7] show how arc voltage changes the effect onto the weld bead width. Generally, the weld bead width increases and the weld bead height decreases with the increase of the arc voltage, whatever travel speeds value. The highest decrease of the weld bead height with the increase in the welding voltage occurs at the highest welding traverse speed (540 mm/min). In contrast, the highest values of the weld bead height are measured at the slowest deposition. The results of this study are consistent with this literature [52, 2]. Also, the influence of arc voltage arc current and process efficiency are presented by [82]. In this study, the authors have introduced a method for optimizing the process parameters based on the heat source power modification and the selection of unique parameters for each deposition layer. One of the key points of this paper is that they highlight the fact that achieving an uninterrupted deposition process entails a modification of the heat input for each layer.

In addition to the above-mentioned welding parameters, a welding parameter that influences the weld bead shape is the mode of CMT. [79] propose CMT pulse (CMT-P) and CMT pulse advanced (CMT-PADV) for the deposition of the single weld bead and multi-bead thick walls using AA4043 and AA2319 materials, respectively.

### 1.1 Influence of process parameters on the weld bead shape

---

For both options, CMT-P and CMT-PADV are tested. The integrity of the parts defects level and deposition shape accuracy are accessed. As a results, the effective wall width (EWW) is in the order of 4 mm while utilizing CMT-PADV, and only switching to CMT-P could achieve an EWW of 6 mm. Surface tension is more significant in CMT-PADV than in the other processes because of its narrow form and high bead height. Surface tension has a significant impact on the connection between two weld beads. In the literature [9], similar results were observed. Because CMT-P has a higher heat input, the wetting between the weld beads is smoother, resulting in an effective wall width that is comparable to single-bead values. In hotter processes, the narrowing due to surface tension is less significant, and is consistent with the literature [87, 88]. [103] have studied the cross-section weld bead geometry when comparing metal inert gas (MIG) and CMT. The determination of welding parameters reveals relations between wire feed speed ( $WFS$ ) and travel speed ( $TS$ ). The results show that for CMT process, the weld bead width and penetration depth have lower errors of 3.8% and 15.3%, respectively when compared to MIG with errors of 21.6%. [23] describe four different CMT processes with the variation of heat input employed in the welding of Al-Cu alloy with ER2319 wire. Their influences on the weld bead shape and porosity were investigated and the mechanism of porosity generation was also discussed. It is observed that, for the conventional CMT, CMT-P, and CMT-ADV processes, width ( $w$ ) and height ( $h$ ) of weld bead are reduced with the increase of travel speed ( $TS$ ), corresponding to the decrease of heat input ( $HI$ ). Height is stabilized with higher heat input ( $HI$ ), which denotes that height is about 2.2, 2.1, and 1.5 mm, respectively. Compared to the CMT-P process, a narrow molten pool is developed using the conventional CMT process, which means that with a similar width ( $w$ ) the height ( $h$ ) is higher than that of the CMT-P process and the melting area of the weld bead is lower than that of the CMT-P process. Unlike the above three processes, a spherical-shaped weld bead is achieved with very low dilution using the CMT-PADV process. Height ( $h$ ) is only about 0.4 mm with a different travel speed ( $TS$ ) of 0.5~0.4 m/min. As a result, it can be concluded that the various CMT modes and their influence on the heat input has significant effects on the weld bead shape in CMT process. [40] investigated the influence of arc modes on microstructure parameters and mechanical qualities while depositing 5183 aluminum alloy using CMT, CMT-P, and CMT-ADV arc modes. The results obtained are the influence of the heat input during high deposition. Furthermore, the interlayer fine-grain area and layer column grain size are included in CMT and CMT-A, but the CMT-P process, which has the highest heat input, contributes

to the generation of column grains. As a consequence, CMT-ADV has the most excellent mechanical qualities than 290 MPa, whereas CMT had lower values (280 MPa) and CMT-P had the lowest with 270 MPa.

This bibliographic study shows us that among the many welding parameters, three main ones influence the shape of the weld bead: *WFS*, *TS*, CMT modes. These parameters are influential because they are directly related to the heat input induced by the process, in addition to being linked to the amount of deposited material. As already mentioned, this heat input influences process stability, geometrical accuracy, and material properties of the weld beads. It is therefore a key point to master the final geometry of the part in WAAM. However, heat accumulation is not constant during the deposition process. Thus, determining the right welding parameters before manufacturing and keeping them constant during the deposition process will not make it possible to control neither the weld beads geometry nor the part. It is essential then to master the heat input, a parameter which cannot be imposed, that is induced by other welding parameters.

Since the part is created by deposition of several weld beads, the following section focuses on the influence of the deposition trajectory on the obtained shape.

### 1.1.2 Deposition trajectory

Ordinarily, a part fabricated by WAAM consists of several layers with constant or different thicknesses overlapping each other according to a predefined overlapping strategy [136, 70]. [116] said the path planning was one of the most important interfaces between the CAD model and the solid workpiece in WAAM. This is because the weld bead geometry of the forming path significantly influences the workpiece surface roughness.

A variety of strategies for trajectory planning dedicated for WAAM are given as examples by [116, 42] as shown in Figure 1.1.2.

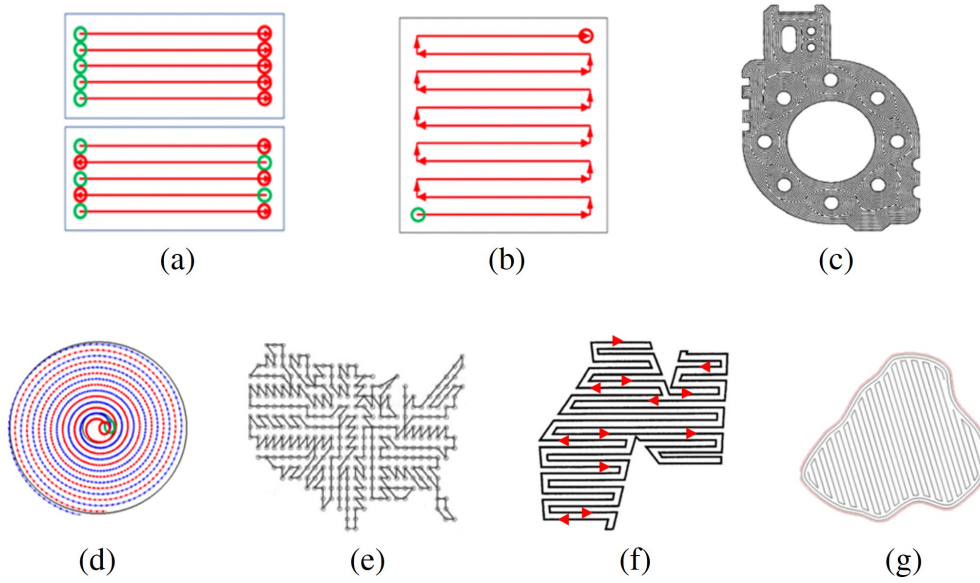


Figure 1.1.2 : Examples of strategies for trajectory planning in WAAM: (a) Raster, (b) Zig-Zag, (c) Contour, (d) Spiral, (e) Fractal space curves, (f) Continuous, and (g) Hybrid [116, 42]

In these examples Figure 1.1.2 (a) shows the two classical pattern strategies for trajectory planning developed for AM, namely raster unidirectional or raster bidirectional. The raster strategy is probably the most basic one, which is the deposition of weld beads in a similar direction. Once the raster strategy is used, appropriate parametrization is applied to the various starts and stops, resulting in a flexible strategy. For example, setting dwell times between stops and starts may help to prevent material and heat accumulation [31, 30, 116]. Figure 1.1.2 (b) shows the Zig-Zag strategy as one of the most common approaches utilized in commercial AM systems derived from the raster strategy. While the raster technique fills geometries line by line in one direction, the zigzag approach merges the different parallel lines into one continuous pass, reducing the number of tool-path passes [90, 62]. Figure 1.1.2 (c) shows contour strategy, the contour follows the subsequently inscribed edges of an external geometry through parallel displacements (pre-established offsets) relative to the geometry edges [42]. Figure 1.1.2 (d) shows spiral strategy generated by numerically controlled (NC) machining. The spiral strategy has been extensively used, particularly for 2D pocket milling and uniform pocket cutting. This approach may be used to solve zigzag tool path issues in the AM process. However, it is only appropriate for particular geometrical models [115, 91, 65]. Figure 1.1.2 (e) shows fractal space-filling curves strategy. In the fused deposition modeling process, this

strategy is especially effective for decreasing shrinkage during AM fabrication. However, this strategy produces a high number of path direction turning movements that are unsuitable for WAAM [31]. Figure 1.1.2 (f) shows a continuous strategy adaptation of the Zig-Zag strategy. This strategy consists of Zig-Zag trajectories planned to leave staggering gaps between the paths. The gaps are sequentially closed by another Zig-Zag trajectory in the inversed direction. The continuous strategy of the hybrid type is adapted to other strategies, for example the spiral strategy [37]. In Figure 1.1.2 (g) shows continuous hybrid path planning strategy is developed for AM. In this method, the 2D geometry is initially broken down into a collection of monotone polygons. A closed zigzag curve is then produced for each monotone polygon. Finally, a series of closed zigzag curves are connected to form a continuous torch path. As a result, the number of welding passes is greatly reduced when using a continuous path planning strategy [37].

In all of previously mentioned strategies, there is an uncertainty about heat accumulation. For raster strategy mentioned, [113] investigate the issue of trajectory deposition which needs to be optimized to minimize various mechanical properties and weld bead shape defects. The authors focus on the trajectory deposition (raster bi-directional strategy) for the WAAM process applied to the manufacture of T-crossing features. In the experiment, the choice of a path must be carried out as a compromise between productivity, energy input and material usage efficiency. Indeed, high productivity is synonymous with reduced idle times, which has an influence on heat input and therefore on bead geometries and mechanical properties of the manufactured parts. The geometry of the previously deposited layers has also to be taken into account for insuring a constant height for each layer. In the experiment, a pause of seventy seconds is introduced every two layers, to enable the cooling of the part and the height measuring of the deposited material. [45] investigated the influence of the multi-layers between layers and deposition strategies on the Ti-6Al-4V sample. In this experiment, four different tool paths were considered. They are all connected by zigzag tool paths. The difference between them is in the way layers and layers are lined up. The first and third tool-path methods are identical; the distinction is that one is primarily for side wire feeding, while the other is for front and back wire feeding to assess the impact of wire-feeding directions. The second tool path is interlaced with the previous layer, and the fourth tool path is moved 3 mm outward in the horizontal direction. The multi-layers between layers and layers in the deposition strategies has been discovered to affect the shaping quality and, in particular, the mechanical characteristics of the manufactured samples. As a result,

surface quality (smooth or undulating) and defects within or on the surface of the components vary across samples.

As mentioned, the heat accumulation affects weld bead shape. The raster strategies (unidirectional and bidirectional) have advantages: as starts and stops are imposed, dwell time can be used to manage heat accumulation, which can be found in the literature. In our research we decide to use raster strategies in order to benefit from the advantages of starts and stops to manage heat accumulation. But this management will not be based solely on the dwell time. Temperature modeling will be use as a tool to control initial temperature and has to be studied (see section 1.3 of this chapter).

The following section shows the weld modeling related to trajectory deposition: the deposition process can occur in several directions, vertical and horizontal and choosing a good deposition strategy must also be appropriate for the deposition direction. The weld bead shape can be represented by various models as it is presented in the next section.

## **1.2 Weld beads modeling**

The AM method entails slicing a 3D CAD model into 2.5D layer contours with a fixed or adaptive thickness and depositing material. These contours are filled to produce components layer by layer from the bottom to the top (superposition of weld beads) [32]. In WAAM, this building strategy incorporates the deposition of many single weld beads side by side (juxtaposition of weld beads). Therefore, accurate models for single bead geometry and multi-bead overlapping play a critical role in determining fabricated surface quality and dimensional accuracy [17, 32, 34]. The weld bead deposition process consists of the continuous overlapping weld bead and weld bead models overlap in two directions as follows:



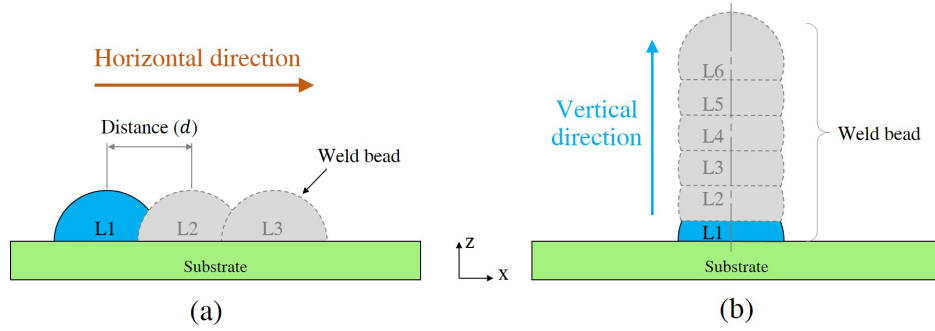


Figure 1.2.1 : Overlapping weld bead models (a) Horizontal overlapping [104, 17, 123], (b) Vertical overlapping [75]

Figure 1.2.1 (a) shows horizontal direction overlapping for the multi-weld bead deposition. The distance of adjacent weld beads is referred as a step over increment ( $d$ ) of the center [104, 17, 123, 69]. In the studies, the shape-forming process of multi-layer weld beads is influenced by interactions between adjacent weld beads in the layers. Table 1.1 presents the mathematical function for dealing with overlapping beads, where  $a$ ,  $b$  and  $c$  are curvilinear coefficients to be estimated for the model.

Table 1.1 : The mathematical function of weld bead cross-section profiles.

Models	Model function	References
Circular arc	$y = \sqrt{a^2 - x^2} + b$	[4, 104, 122, 32]
Parabola	$y = ax^2 + c$	[17, 122, 32]
Gaussian	$y = ae^{-(x-b)^2/c^2}$	[17]
Logistic	$\ln y = a + bx^2 + c^{-x}$	[17]
Sine	$y = a \sin(2\pi x/c + b)$	[17]
Cosine	$y = a \cos(bx)$	[122, 32]

All these studies present the mathematical model function for curve fitting weld beads and develop the overlapping model of adjacent weld beads. Adjacent determination is significant as it directly affects the surface quality and weld bead shape. [17] propose the mathematical model of the single weld bead in horizontal overlapping direction. A mathematical model of the weld bead section is developed to analyze the weld bead geometry, based on the "surfacing of equivalent area" method. The overlapping coefficient and optimum-overlapping coefficient concepts

are introduced, and the developed overlapping model is examined. Under experimental circumstances, the ideal overlapping coefficient is calculated to be 63.66%. According to the findings, the edge detection of the weld bead section with the Canny operator [16] is continuous and distinct. The sine function has a greater accuracy to suit the measured data than the Gaussian, logistic, and parabola functions. The "surfacing of equivalent area" method is shown to be reasonable and achievable by the experiments. [104] propose single weld beads and overlapping multiple weld beads models. In contrast, the individual weld bead geometry is influenced by the welding parameters (wire feed speed, travel speed). Therefore, this research assumes a parabola cross-sectional profile of the weld bead, and step-over increment ( $d$ ) uses 66.66% of weld bead width. [32] study curve fitting models with three mathematical models for single weld beads and propose a new multi-weld bead overlapping model for the concept of center distance of the weld bead. The welding parameters use a wire feed speed set at 5 m/min and the travel speed varies from 200 to 550 mm/min. The step over increment ( $d$ ) is significantly set at 73.8% of weld bead width [32, 70].

[122] highlight an experimental study carried out to determine the optimal model of the weld bead cross-section profile fit with mathematical model function by comparing the actual area of the weld bead section with the predicted areas of the three models. In addition, an important condition for the overlapping of adjacent weld beads is proposed. The result showed that the circular arc function is more accurate than the other two functions, with a ratio greater than 12.5 between wire feed speed and travel speed.

[4] present the ratio of distance ( $d$ ) because it plays an important role in the quality of parts. The ratio ( $\lambda$ ) of width ( $w$ ) to height ( $h$ ) is  $\lambda = w/h$ . In their analysis, they assume the beads as overlapping circular arcs. This research applies circular function to measure the weld bead cross-section, but they have not taken into account the overlapping zone.

The vertical direction overlapping (Figure 1.2.1 (b)) is the weld bead deposition on the previous layer. [75] describe the effect of process parameters on the vertical overlapping (wall weld bead) and develop two concepts of weld bead cross-section predicting models. The first concept is to predict the weld bead shape using static fluid capillary-gravity analysis. The second concept is that the thermal analysis calculates the amount of molten pool as a function of the WAAM parameters. [60] mention heat input effects on the weld bead of the wall. All these have not been mentioned as the mathematical function for measuring the weld bead cross-section. Using PAW-based WAAM, [10] create a 3D numerical model to study metal pool

flow and heat transmission characteristics during the multilayer depositing process (wall weld bead). They discover that the number of deposit layers increases, and the metal pool shape changes, with the width, increasing and the height decreasing.

[112] presents built using a strategy that include the deposition of a pair of layers in sequential order. Both thick and thin walls weld beads can be used. For the building of these walls, two alternative methodologies are adopted. The deposition of three overlapping weld beads per layer is one technique. The deposition is done in this order: the weld bead in the middle, then the beads on the sides, with the torch inclined 20 degrees from vertical. The amount of overlapping employed was 50 percent of the width of the weld beads. The deposition of a single weld bead per layer is the other approach used for the thin walls. The dwell period between successive layer depositions is 3 minutes in both instances. In order to limit the buildup of material at the arc ignition and extinction zones, *i.e.*, the start and end zones of the weld bead, the direction of deposition of the weld beads in each layer and between superposed layers is alternated (raster bi-directional strategy). As a result, each layer grew evenly and in a regulated manner, which is critical in the WAAM process.

The main focus of all the literature reviews is to develop a weld bead model to verify single and multi-layer weld beads. The researchers present a mathematical model involved in developing weld cross-sections, such as the circular arc function, parabola function, Gaussian function, logistic function, sine function, and cosine function, to calculate the step-over distance between welds of the horizontal overlapping. Some studies use the ratio of width to height to determine step over distance. The papers found in the literature which use the circular model do not specify however on which zone of the weld bead it applies. This is an important element to take into account because, due to heat accumulation, the weld bead is not regular over its entire length: the start and the stop of the bead differ from the center which is in a zone of stabilized temperature.

In this research work, the weld bead model will be used in a thermally stable zone of the weld beads. Next section presents thermal simulations research for the analysis and prediction of heat accumulation during the welding process. It helps us to decide which model that would best fit to the profiles to be considered in our experimentation's.

## 1.3 Thermal simulation

WAAM process is a layered filling technology which is prone to geometric and material defects that affect the weld bead shape quality. The cause of this phenomenon is uneven temperature and heat accumulation during the deposition process [119]. Process simulation is a powerful tool for solving such problems. This makes it possible to test the effects of different deposition patterns. It can also simulate working in a variety of environments [67]. From a simulation perspective, the WAAM process is similar to the multi-pass welding process. The transfer of heat and mass between the arc and the workpiece is controlled by the molten pool, which is characterized by a complex physical phenomenon. Although some works focus on molten pool and arc dynamic simulation [56], it is impossible to implement such complex techniques at the component scale, due to acceptable calculation time requirements. Therefore, this process is often simulated by coupled thermo-mechanical Finite-Element (FE) analyses [76]. In general, the heat transfer from the arc to the melt pool is simulated using a heat source model, which determines the heat generation per unit volume in the molten pool area. The material deposition is taken into account by means of enabling specific algorithms [73].

The heat source model proposed by [49] is frequently used. In this model the heat input is a double-ellipsoidal, defined in a moving frame of reference as shown in Figure 1.3.1 (a) where x axis is oriented in the deposition direction. On Figure 1.3.1 (b) the model is defined by two Gaussian distributed power densities allowing to better take into account the asymmetries of heat distribution in the molten pool [49, 19].

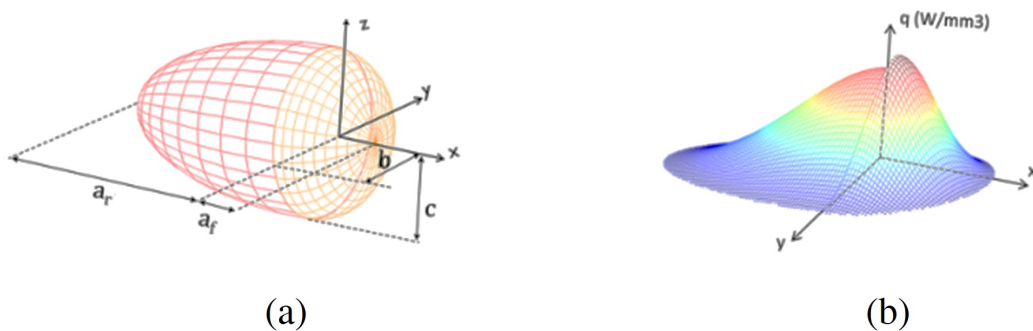


Figure 1.3.1 : Goldak double ellipsoidal heat source model [49]

The power density distribution for this model. Hence, expressed in a moving Cartesian coordinate system (x, y, and z). The source is expressed by the following Equations 1.3.1 and 1.3.2

Distribution inside the front quadrant:

$$q_f(x, y, z, t) = \frac{6\sqrt{3}f_f Q}{abc_f \pi \sqrt{\pi}} \exp \left\{ -3 \left( \frac{x^2}{a_f^2} + \frac{y^2}{b^2} + \frac{(z + vt)^2}{c^2} \right) \right\} \quad (1.3.1)$$

Similarly, for the rear quadrant:

$$q_r(x, y, z, t) = \frac{6\sqrt{3}f_r Q}{abc_r \pi \sqrt{\pi}} \exp \left\{ -3 \left( \frac{x^2}{a_r^2} + \frac{y^2}{b^2} + \frac{(z + vt)^2}{c^2} \right) \right\} \quad (1.3.2)$$

Where  $q_f$  and  $q_r$  are the power density distributions in front and rear quadrants.  $x$ ,  $y$ , and  $z$  are the position coordinates.  $f_f$  and  $f_r$  are the heat distribution parameters in the front and rear quadrants.  $a_f$  and  $a_r$  are the lengths of the front and rear quadrants.  $b$  and  $c$  are the half-width ( $y$  semi-axis) and the depth ( $z$  semi-axis) of the source.  $Q = \eta VI$  is the total input power heat source,  $\eta$  is the heat distribution factors of the front and rear quadrants.  $V$  is welding arc voltage and welding arc current ( $I$ ).

It is not easy to determine of the length (semi-axes) of the heat source and experimental comparisons must be made by measuring the temperature or observing the area of the molten pool. In the absence of such information, [49] recommend using the length of  $a_f$  equal to half the depth  $c$ .  $a_r$  length equal to the penetration depth of the source.

Many researchers mention improving the thermal simulation of WAAM as follows; [76] present a more realistic heat flow distribution in the filler material. The WAAM process is simulated using a unique definition of the heat source based on a modified Goldak model. The Goldak model is addressed in the paper, focusing on its limitations. The simulation method and heat source model that have been proposed are then presented. Finally, the observed distortion of a WAAM-manufactured test case component is compared to FE findings produced with the suggested tool for thermal simulation and Goldak heat source models. [20] FE model is proposed in order to model metal deposition in the WAAM process. This technique allows a gradually construction of the mesh representing the deposited regions along the deposition path. The heat source model proposed by Goldak is adapted and combined with the proposed metal deposition technique taking into account the energy dis-

tribution between the filler material and the molten pool. The effectiveness of the proposed method is validated by a series of experiments. In this technique, each deposited droplet is modeled by a set of elements, representing together a numerical droplet. Every numerical droplet is created at its corresponding time-step in the deposition phase simulation. The newly created elements are then added to the elements already created in the previous time steps. Thus, the mesh representing the deposited regions is constructed gradually along the deposition path. The results show that the temperature curves generated by the FE model match fairly well those recorded in the experiment rather well. The average difference between simulated and experimental results is about 5%. The margin is higher in the first peaks and the thermal inertia of the thermocouples used in the experiments could be a cause of such an error.

[36] describe the thermo-mechanical behavior of the multi-layer wall structure made by the WAAM process. This research uses a 3D thermo-elastic-plastic transient model as well as a model based on an enhanced steady-state thermal analysis. This modeling approach shows a significant advantage concerning computational time. The temperature simulations and distortion predictions are compared with the experimental results from thermo-couples and laser scanners. At the same time, the residual stresses are verified with the neutron diffraction strain scanner ENGIN-X. The stress throughout the deposited wall is found uniform with very little influence of the preceding layers on the following layers. Due to the bending distortion of the sample, the stress is redistributed after unclamping, with a substantially lower value at the top of the wall than at the interface. And [131] use FE to predict material behavior under consideration of the microstructure and thermal stresses during the deposition process [22, 51]. [102]) propose to use FE analysis to predict thermal and mechanical conditions throughout manufacture, as well as distortions, strength, and residual stresses at the end of the process. These findings show the importance of constraint and thermal history in shaping evolving local property distributions in finished parts. They propose a modeling framework for predicting relevant engineering characteristics like strength and residual stress distributions in additively manufactured parts. [126] develops FE model to calculate the heat transfer of circular thin-wall part. Temperature simulations at certain sites correlate with thermocouple measurements in some cases. The high-temperature areas of the substrate and molten pool expand as the deposition process progresses. While increasing deposition height, the temperature gradient in the molten pool reduces. The heat dissipation situation in the molten pool of the current layer strongly de-

depends on the deposition direction of the previous layer. Heat conduction in the axial direction is the primary heat dissipation orientation at the time of deposit finishing, while the circumferential orientation becomes the main direction of heat dissipation in the top layers. [125] has developed a circular thin-wall part to investigate the thermal behavior in gas metal arc welding (GMAW) additive manufacturing. The main issues of reducing thermal stress is preventing cracking of the manufactured parts. Meanwhile, using thermal cycle tests, the validation experiment is carried out to assess the efficiency of the finite element model. The calculated thermal cycle curves closely match the experimental findings. In addition, the validated model investigated the influence of substrate preheating on thermal behavior. Modeling results demonstrate that preheating the substrate can smooth thermal cycles and reduce the rate of melt pool cooling. [26] propose a comprehensive FE model using a five-step strategy, which is then used to acquire temperature history at the positions of thermocouples. Those values are heat source parameters, welding efficiency, dwell-time, arc extinguishing mode, and heat transfer coefficient. A bead-on-plate welding thermal model has been developed using the presented techniques, which are based on a systematic approach and realistic circumstances and can reliably forecast the transient thermal history of the weld.

The literature reviews on thermal simulation, the finite elements method (FEM) can assist in analyzing the causes of heat accumulation on weld beads shape. Therefore, thermal simulations will be used to predict the heat accumulation during deposition of the weld bead and to correlate the results to the actual weld bead shape see in Chapter 2.

From the literature review of the above three sections, it can be summarized as follows:

- *Influence of process parameters on the weld bead shape*

Welding parameters and deposition trajectory influence weld bead shape. Note that these variables are controlled during the deposition process. In addition, it has been seen that heat accumulation has a great influence on the weld bead shape. Heat accumulation is directly linked to the initial temperature before the deposition process, the surface deposition temperature during the manufacturing process and the actual surface geometry. These variables occur during the deposition process and cannot be directly controlled, contrary to the welding parameters and deposition trajectory. In other words, controlled and uncontrolled parameters must be mastered in order to avoid heat accumulation during the manufacturing process. Therefore,

a method for managing the deposition process should be developed. It is presented in the next chapter.

- *Weld bead modeling*

The development of weld bead modeling is essential for weld bead shape, a mathematical model being applied to weld bead shape for multi-layer deposition. To determine the distance between two weld beads, it is crucial to choose the optimal model the use of an inappropriate model which can lead to a wrong measurement of the weld distance.

- *Thermal simulation*

Thermal simulation by finite element method (FEM) simulates the temperature during the deposition process, and the resulting temperature can be predicted. The data help improving the management of heat accumulation and can also be developed for measuring the weld bead shape.



All literature review can describe the causes of heat accumulation into two main groups of parameters, controlled and uncontrolled, both having an effect onto the shape of the weld beads. Some of the variables that are currently not taken into account in the literature review are the initial temperature ( $T_{init}$ ), the actual surface geometry and the surface deposition temperature ( $T_{dep}$ ) as shown in Figure 1.3.2.

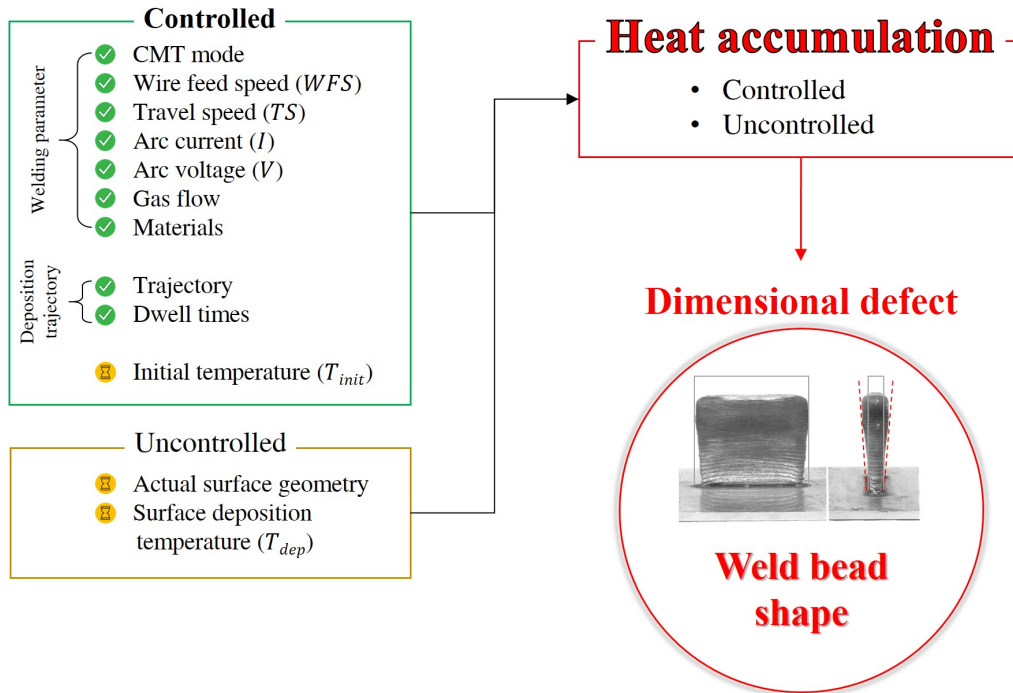


Figure 1.3.2 : Heat accumulation of weld bead shape

## Research question and approach

As shown in Scientific and technical issue section, the main purpose is to manage weld bead shape with regard to heat accumulation around the deposition point and process parameters.

The literature review points out that heat is an important issue that have not been addressed yet.

Thus, this PhD work proposes to address the following research question:

***How to predict the weld bead shape related to heat accumulation?***

In the literature review and our previous research, we identified three scientific obstacles to overcome in order to answer this question:

- Create and control stable thermal conditions during the deposition process,
- Propose a geometric model of the weld bead and identify its parameters from deposited weld bead,
- Propose an interpolation solution to predict the weld bead shape parameters as a function of heat accumulation,

The main steps proposed to answer this question and address these obstacles are (as shown in figure 1.4.1):

- Problem identification: Identifying problems related to the thermal effect on the weld bead shape.
- Design of experiment: Design several experiments to cover the thermal effect that can occur on the WAAM process. Then, thermal simulation monitored the temperature occurring during the weld bead deposition.
- Geometrical identification: The weld bead measurement uses a curve fitting model to verification of the weld bead shape.
- Interpolation and validation: The outputs of the neural network optimal prediction are analyzed and discussed.
- Conclusions and perspectives

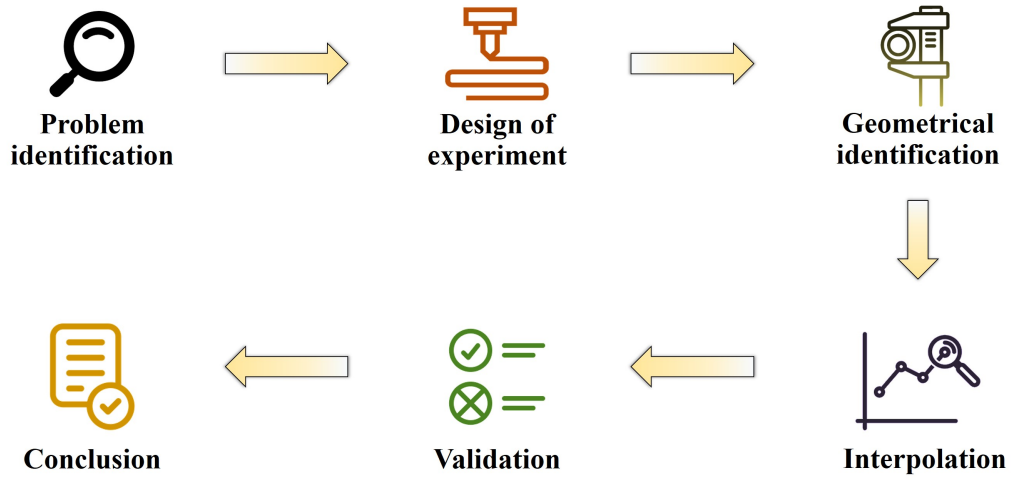


Figure 1.4.1 : Thesis approach

The following section presents the whole structure of this thesis manuscript.

## Thesis outline

The chapter of this research will be organized as follow:

**Chapter 1** Literature review about Wire and Arc Additive Manufacturing (WAAM): presents the state of the art for this research, thesis approach, and research outline.

**Chapter 2** Design of experiment: This chapter focuses on studying the experimental design of the division task into two main parts: The first part, the design is based on the weld deposition basis. The main focus is the direction of weld bead deposition as vertically, horizontally, and the weld bead deposition of the curved substrate. All of these are characteristics of the design. In the second part, the thermal simulation is examined and the thermal phenomena during deposition are examined and identified to determine the thermal history of their occurrence.

**Chapter 3** Geometrical identification: proposes the experimental measurement procedure by explaining the reasons for measuring welds. The principle of determining the measurement position is derived from temperature simulations for consideration.

**Chapter 4** Interpolation & validation: This chapter proposes developing a Multi-Layers Perceptron (MLP) regression model for interpolating experimental weld bead shape. The main objective is to interpolate the weld bead shape as surface deposition temperature changes during deposition. Moreover, create the most efficient Multi-Layers Perceptron (MLP) regression model. MLP regression model is used to interpolate the shape of the weld bead and compare it to the results of other experiments to make sure the results were correct.

**Chapter 5** Conclusion: presents the conclusions and perspectives of the thesis.



## Chapter 2

# Design of Experiment and procedure

It is necessary to find a way to effectively manage the weld bead shape, as shown in Figure 2.0.1. To reach this aim a phenomenological approach based on series of experiment is presented. This chapter propose the design of the experimental procedure to study the influence of the temperature on the weld bead shape. First, the essential characteristics of WAAM are listed such as material, welding parameters, temperature or deposition surface geometry. The goal is to confirm that temperature is a key parameter that influence the weld bead shape, as stated in Chapter 1, and to scope its importance as well as for other factors. The issue is that temperature is not a parameter that can be directly controlled. A possibility is to drive it through the initial temperature of the substrate. The verification of this statement is done through finite element simulations. The objective of these simulations is to verify that deposition temperature varies with the initial temperature and to determine the relationship between these two. At this point, parameters are identified and steps of experiment can be defined. Finally, the last section resumes the experimental procedure and the main results.

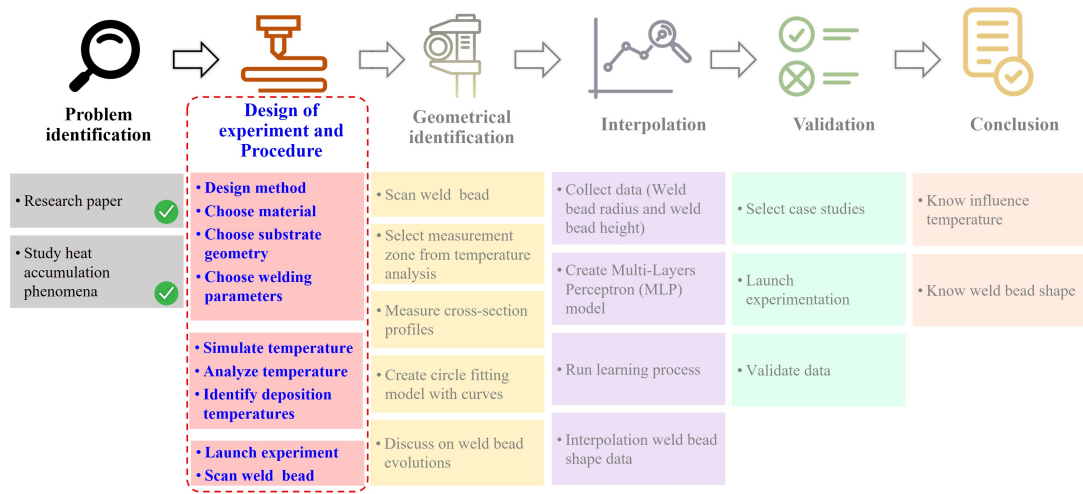


Figure 2.0.1 : Research approach of design of experiment and procedure

## 2.1 Geometry of deposition surface

To realize parts in WAAM, the process starts from a 3D model of the part. From this 3D model, the appropriate trajectory has to be determined. The deposition trajectory has vertical and horizontal directions displacements and run until the final part is built, as shown in the Figure 2.1.1. Elementary situations have to be identified from usual trajectories to define the different deposition surface geometry that could be encountered.

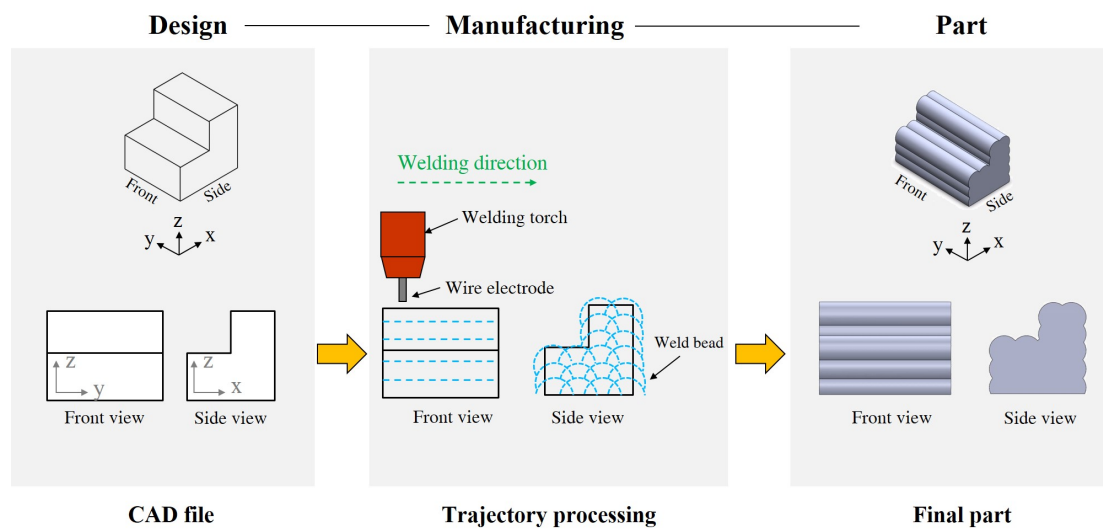


Figure 2.1.1 : The conceptual design of WAAM process

Figure 2.1.2 (a) shows the different surface geometry that has been identified on usual deposition process. The first layer (case a) is usually deposited onto a flat surface. It is characteristic of usual substrate geometry (flat surface). Then, the WAAM process consists in depositing material layer by layer usually in the vertical direction. In the case of thin walls (case d), the deposition surface is then close to a portion of cylinder. To investigate this case, the weld bead (b) is deposited on a cylindrical substrate of various diameter as shown Figure 2.1.2 (b). In case of horizontal deposition (coating, massive parts, the first bead is deposited on a flat surface (c\_L1) and the next bead are deposited partly on a flat surface and partly on a portion of cylinder (c\_L2) as shown in Figure 2.1.2 (c). The last experiment is made for verification purpose as it has various substrate characteristics along the deposition. The first layer is deposited on a flat surface (d\_L1) and the second layer (d\_L2) being deposited on (d\_L1) is set down on a portion of cylinder. In fact, every other following layers are deposited on cylindrical substrate, its radius varying for each successive layer.

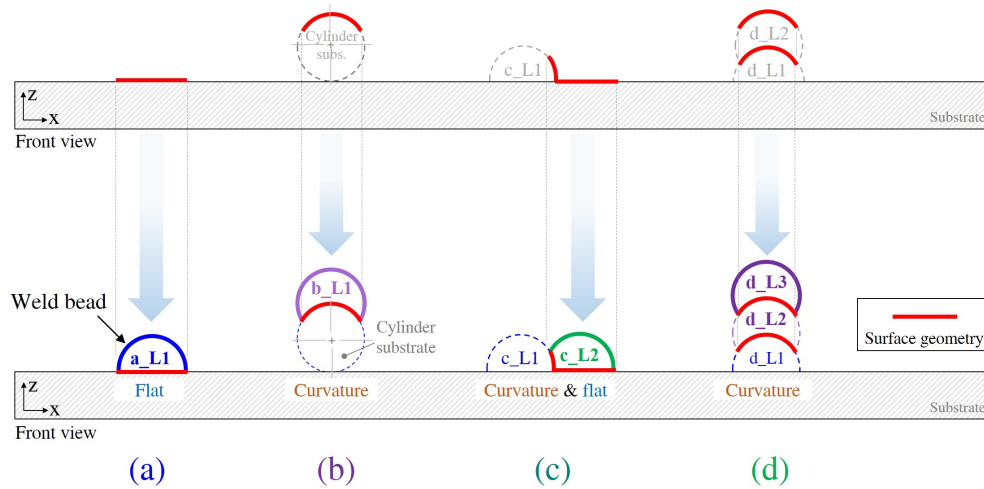


Figure 2.1.2 : Configuration of the weld bead deposition for design of experiment; a) Exp.1: Single weld bead on flat substrate, (b) Exp.2: Single weld bead on the cylinder substrate, (c) Exp.3: Lateral overlap weld bead and (d) Exp.4: Vertical overlap weld bead.



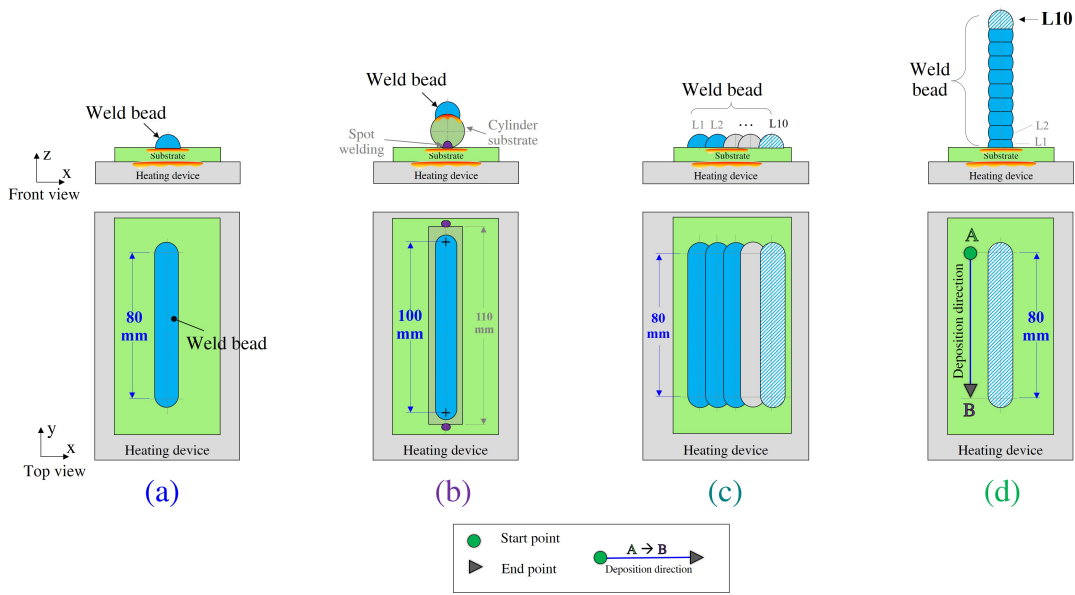


Figure 2.1.3 : Design of experiment: (a) Single weld bead on flat substrate, (b) Single weld bead on cylinder substrate (c) Lateral overlap weld bead and (d) Vertical overlap weld bead

All the experiment designed for this research are aiming to cover the WAAM deposition situations identified in Figure 2.1.3. (a) Exp.1: Single weld bead on flat substrate, (b) Exp.2: Single weld bead on the cylinder substrate, (c) Exp.3: Lateral overlap weld bead and (d) Exp.4: Vertical overlap weld bead.

### 2.1.1 Equipment

The equipment used is a welding robot equipped with a wire and arc additive production system. It is composed by of a YASKAWA MA1440 six-axis robot, a welding torch and a Fronius TPS CMT 4000 Advanced welding station (Fronius, Pettenach, Austria). In addition, a heating device has been designed. It consists of three heating resistances (6 kW) and a temperature closed loop control system allowing a preheating up to 500 °C. This heating device has been built for this research. It increases the initial temperature of the substrate and weld bead. It is used in these experiments to create different initial temperatures as it has been identified as a very important parameter in order to determine weld bead shape. Illustrations in Figure 2.1.4 show (a) the welding robot and the wire arc additive system and (b) the heating device.

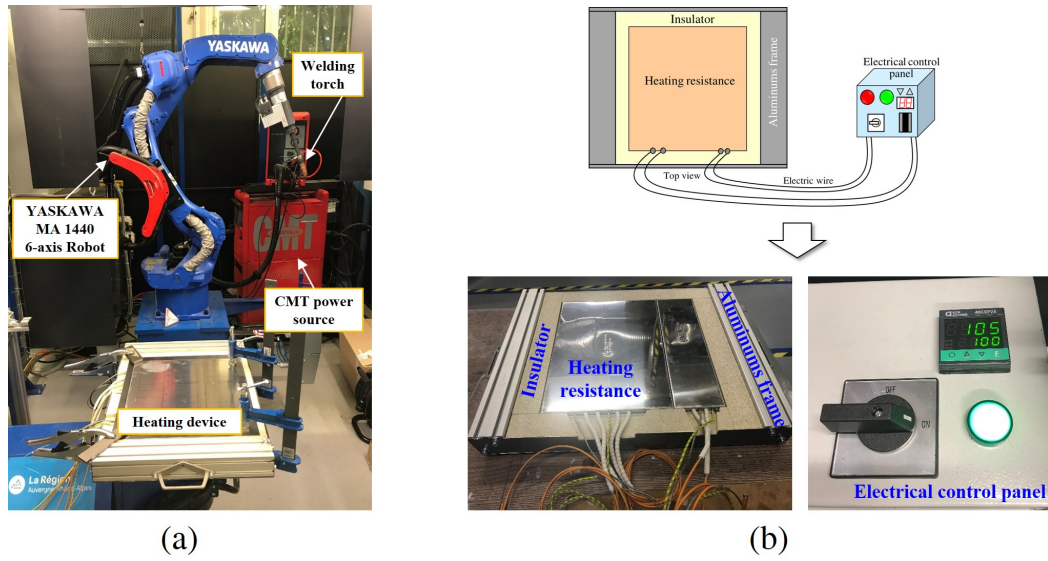


Figure 2.1.4 : Equipment set up: (a) robot wire and arc additive systems and (b) the heating device

### 2.1.2 Material properties

For this research two types of substrate have been used: plate (250 x 250 x 5 mm) and cylinder diameter 7 to 35 mm. The chosen grade is a AA5083 (AlMg4.5Mn0.7) aluminum alloy. In addition, the wire electrode is made of AA5356 (AlMg5Cr) alloy and its diameter is 1.20 mm. Table 2.1 shows the chemical composition of these two materials.

Table 2.1 : Nominal chemical composition (wt.%) of substrate and wire electrode material

Materials	Cu	Cr	Fr	Mg	Mn	Si	Ti	Zn	Other	Al
AA5083 (Substrate)	0.1	0.05 - 0.25	0.4	4.0 - 4.9	0.4 - 1.0	0.4	0.15	0.25	0.15	Bal.
AA5356 (Wire electrode)	0.1	0.05 - 0.20	0.4	4.0 - 5.5	0.05 - 0.2	0.25	0.06 - 0.2	0.01	0.15	Bal.

### 2.1.3 Process parameters

The process parameters used in the experiment are listed Table 2.2. They are divided in three categories:

- The material category including wire electrode and substrate material
- The dimension category, including the wire electrode diameter and substrates dimensions,
- The welding parameters category, defining the welding setup parameters.

All the experiment are done with these parameters. For each situation, different initial temperatures ( $T_{init}$ ) are tested as listed in Table 2.2

Table 2.2 : Process parameters for experiment

Process Parameters	Details	Unit	Types of Experiment			
			Exp.1	Exp.2	Exp.3	Exp.4
<b>Materials:</b>						
Wire electrode	Al 5356		O	O	O	O
Substrate flat & Cylinder substrate	Al 5083		O	O	O	O
<b>Dimension :</b>						
Wire electrode diameter	Ø1.20	mm	O	O	O	O
Substrate flat	250 x 250 x 5	mm <sup>3</sup>	O	X	O	O
Cylinder Substrate diameter(Length = 110 mm)	Ø7, Ø8, Ø9, Ø10, Ø12, Ø16, Ø20, Ø25, Ø30, Ø35	mm	X	O	X	X
Weld bead length	80	mm	O	X	O	O
	100	mm	-	O	X	X
<b>Welding Parameters :</b>						
Technology mode	CMT		O	O	O	O
Wire Feed Speed ( $WFS$ )	5	m/min	O	O	O	O
Travel Speed ( $TS$ )	0.60	m/min	O	O	O	O
Argon Gas Flow Rate	13	L/min	O	O	O	O
Working distance	15	mm	O	O	O	O
Torch orientation	Normal to the substrate surface		O	O	O	O
Initial temperatures ( $T_{init}$ )	25	°C	O	O	X	X
	100	°C	O	O	X	O
	200	°C	O	O	O	O
	300	°C	O	O	O	O
	400	°C	O	O	O	O

O = Selected, X = Not select

## 2.2 Thermal simulation

Heat accumulation is strongly influencing the weld bead shape. Indeed, the heat generated during deposition processes modifies the temperature and the weld bead shape. Measuring this heat accumulation or the temperature variation during WAAM deposition is very difficult considering the equipment available in the field of temperature measurement. On the other hand, the heat accumulation and its effect on the temperature can be predicted in various ways and with various degrees of accuracy. Thermal simulation using finite element models is a precise method to predict the heat generated during deposition and its effect on the temperature.

The surface deposition temperature ( $T_{dep}$ ) criterion [19] has been chosen to monitor the temperature at which a droplet is locally deposited. The fusion interface between the droplet mesh and the substrate mesh is used to calculate this criterion based on several control nodes on the top surface of the mesh, indicating the substrate section on which the next droplet will be deposited as shown Figure 2.2.1. As a result, the value of this criterion will be the surface temperature of the control nodes precisely before the droplet is deposited, as given in the equation 2.2.1. Furthermore, these control nodes positions change consistently throughout the deposit path, and are automatically different based on where the next droplet will be put. We suppose that this temperature is the correct criterion to link the thermal environment of the deposited drop and the weld bead shape. The question is then: Can we have a stable and controlled deposition temperature at least in a zone of the deposited weld bead?. The second question is then: Can we control the temperature deposition through the control of the initial temperature?.

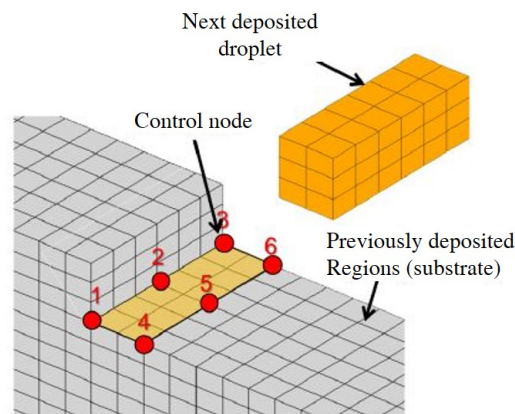


Figure 2.2.1 : Surface deposition temperature ( $T_{dep}$ ) criterion [19]

$$T_{dep} = \frac{1}{n} \sum_{i=1}^n T_i \quad (2.2.1)$$

These verifications will be done using finite element simulations. All the experiment planned will be simulated to monitor the surface deposition temperature ( $T_{dep}$ ) behaviors during the weld deposition process. It is presented as follows:

### 2.2.1 Thermal simulation of single weld bead deposited on flat substrates

Welding parameters were: a weld bead deposition length of 80 mm, wire feed speed ( $WFS$ ) of 5 m/min, travel speed ( $TS$ ) of 0.6 m/min and initial temperature ( $T_{init}$ ) of 25°C, 100°C, 200°C, 300°C and 400°C. An example of the thermal simulation results is given in Figure 2.2.2, detailing the building process of deposition temperature graphics. The first pictures (a) presents the deposition temperature at the starting position equivalent here to the initial temperature of 100°C. Figure 2.2.2 (b) illustrates the  $T_{dep}$  criterion at a distance of 40 mm from the starting point, here with  $T_{dep} = 541.96^\circ\text{C}$ . Finally, Figure 2.2.2 (c) shows the value of  $T_{dep}$  at the bead end, at 80 mm from the starting point. There, the surface deposition temperature ( $T_{dep}$ ) is  $543.81^\circ\text{C}$ . Thus, the thermal simulation gives access to the deposition temperature history of weld beads. All the results for the different initial temperatures ( $T_{init}$ ) of Exp.1 are shown in Figure 2.2.3. It appears that, after a quick rise,  $T_{dep}$  tends to stabilize at a relative constant temperature until the end of weld beads.

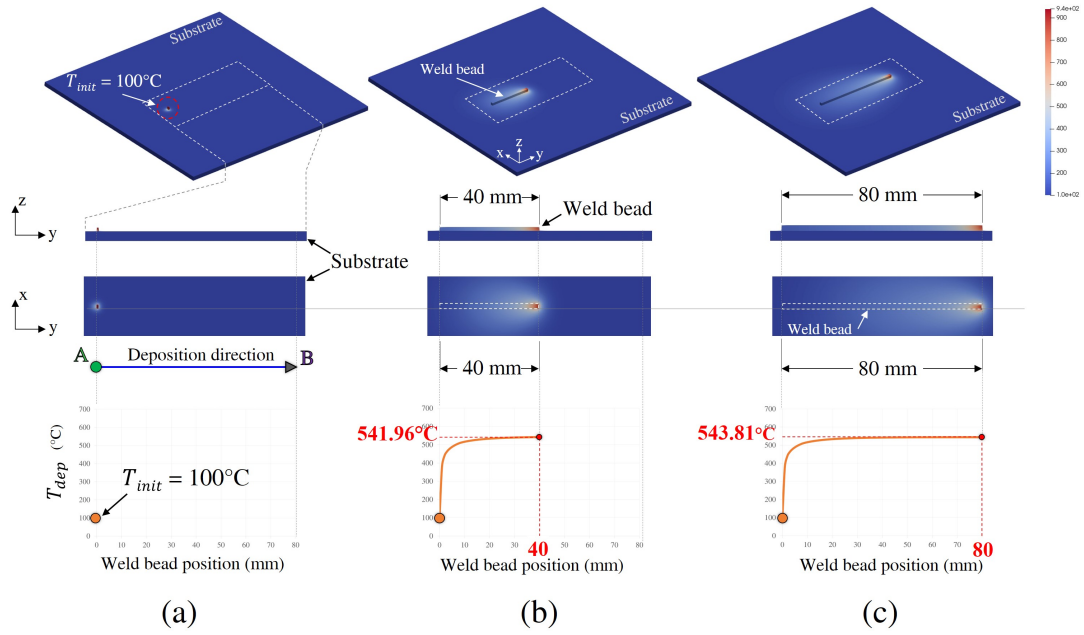


Figure 2.2.2 : Illustration of the building process of the deposition temperature criteria graphics for Exp.1 at the initial temperature ( $T_{init}$ ) of 100°C, (a)  $T_{dep}$  at start point, (b)  $T_{dep}$  at 40 mm, (c)  $T_{dep}$  at end point (endpoint)

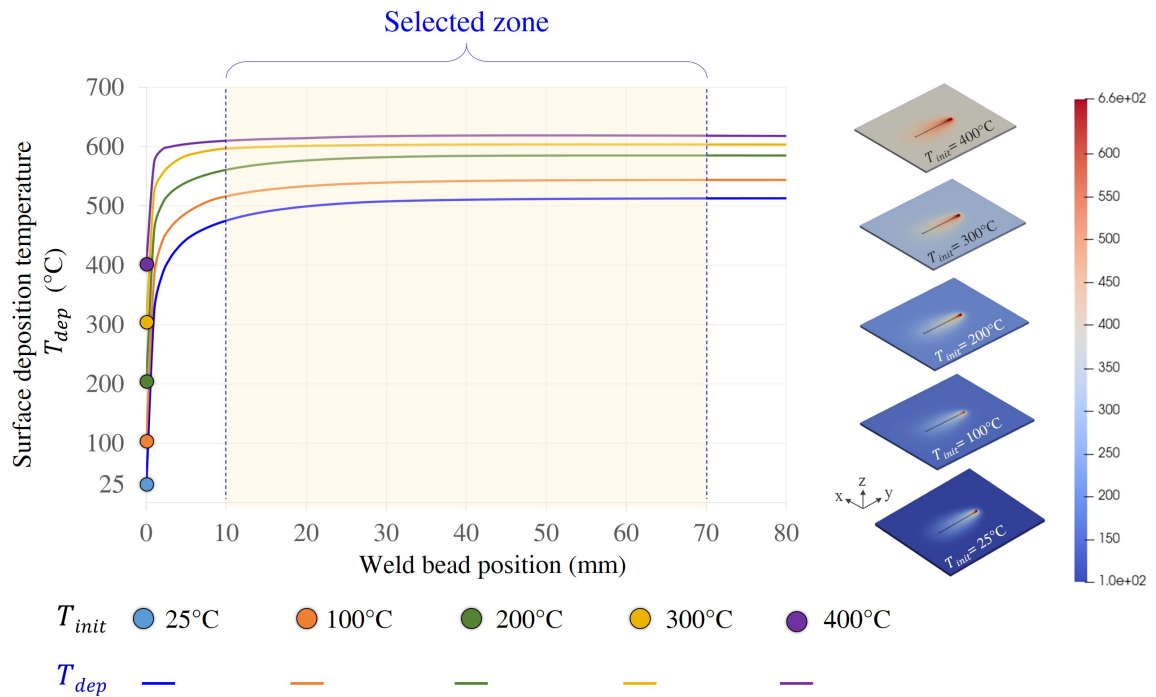


Figure 2.2.3 : Thermal simulation results of Exp.1 at different initial temperatures ( $T_{init}$ ) of 25°C, 100°C, 200°C, 300°C and 400°C

For each initial temperature ( $T_{init}$ ), this stable zone is found in the range of 10 to 70 mm. Detailed data of the surface deposition temperature ( $T_{dep}$ ) is available in Appendix A: Table A.1 and A.2. The average value of  $T_{dep}$  in these regions are gathered in Figure 2.2.4. It can be seen that this stable temperature can be directly related to the initial temperature and with a gap of about 200 to 400°C from  $T_{init}$ . It confirms the strong interest of a thermal simulation to help to analyze the thermal history occurring during the deposition process.

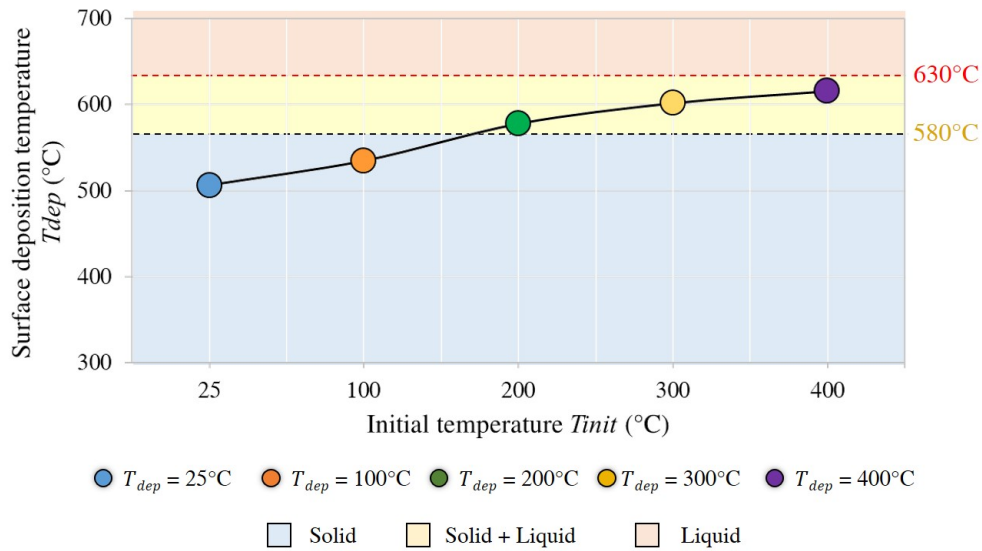


Figure 2.2.4 : Evolution of  $T_{dep}$  according to  $T_{init}$  for the deposition of single weld beads on flat substrates.

## 2.2.2 Thermal simulation of single weld beads deposited on cylinder substrates

For this experiment, meshing is the key element in obtaining accurate results from finite element analysis (FEA) models. It has been chosen to create a rectangular mesh instead of a cylinder as illustrated at Figure 2.2.5. It changes the cross-section from a circle profile to a rectangular one.  $D$  being the diameter of the cylinder and  $A_c$  its cross-section area, these primary parameters evolve for the rectangular substrate used in the simulation to:  $a$  the width,  $b$  the height and  $A_s$  the simulated area of the rectangular cross-section. Table 2.3 shows how this transition is pursued across those parameters.

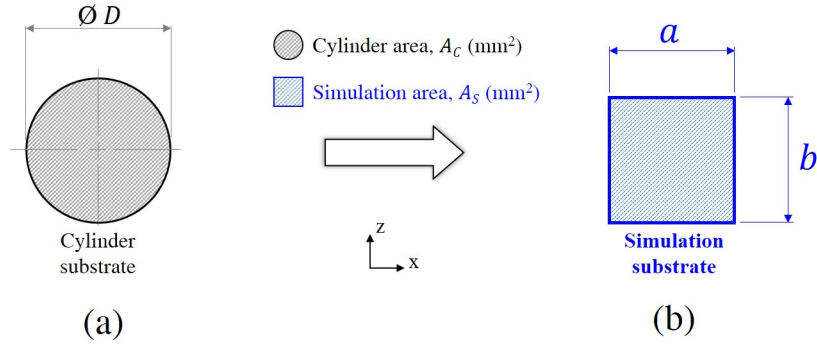


Figure 2.2.5 : Substrate area of temperature analysis: (a) cylinder area, (b) simulation area (rectangular)

Table 2.3 : Comparison of dimension between cylinders and thermal simulations

Cylinder substrate diameter	Cylinder substrate area	Simulation substrate area (rectangular)			Error
$\varnothing D$ (mm)	$A_c$ (mm <sup>2</sup> )	$a$ (mm)	$b$ (mm)	$A_s$ (mm <sup>2</sup> )	$[(A_s - A_c)/A_c]$
$\varnothing 7$	38.48	5	7	35	-0.09
$\varnothing 8$	50.27	7	7	49	-0.03
$\varnothing 9$	63.62	7	9	63	-0.01
$\varnothing 10$	78.54	9	9	81	0.03
$\varnothing 12$	113.10	9	13	117	0.03
$\varnothing 16$	201.06	13	15	195	-0.03
$\varnothing 20$	314.16	17	18	306	-0.03
$\varnothing 25$	490.87	21	23	483	-0.02
$\varnothing 30$	706.86	27	26	702	-0.01
$\varnothing 35$	962.11	31	31	961	0.00

The counterpart of Figure 2.2.2 for this experiment is available in Appendix A: Figure A.2.1. Figure 2.2.6 shows an example at  $T_{init} = 400^\circ\text{C}$  of the behavior of  $T_{dep}$  according to  $T_{init}$  considering the different cylinder diameters ( $\varnothing 7$ ,  $\varnothing 8$ ,  $\varnothing 9$ ,  $\varnothing 10$ ,  $\varnothing 12$ ,  $\varnothing 16$ ,  $\varnothing 20$ ,  $\varnothing 25$ ,  $\varnothing 30$  and  $\varnothing 35$  mm). Similar to the first experiment, it has



still to be noted that  $T_{dep}$ , being relatively constant between 20 mm and 80 mm, increases slightly at the end of the weld bead. This phenomenon is linked to the fact that heat is harder to evacuate here as there is a discontinuity in the matter and that calories are more easily conducted inside the metal rather than through the atmosphere. All experiments are show in Appendix A: 2.2.6 to 2.2.6.

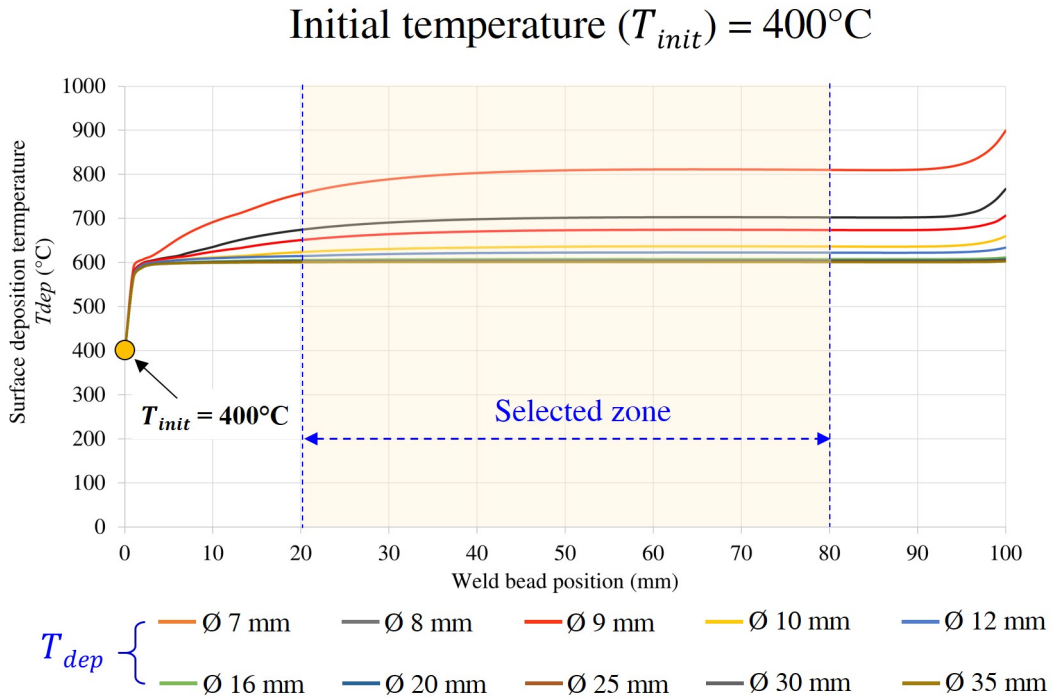


Figure 2.2.6 : Thermal simulation result of Exp.2: Single weld bead on cylinder substrate at initial temperature ( $T_{init}$ ) at 400°C

Figure 2.2.7 show the average value of  $T_{dep}$  in that range of 20-80 mm relatively to the cylinder substrate diameter. It was found that when the diameter of the cylinder is small, the surface temperature deposition ( $T_{dep}$ ) is at its maximum value. This heat spike could potentially be a problem, as it will be seen later, as its value surpasses the liquidus. Larger cylindrical substrate tend to lower  $T_{dep}$  to a certain limit close to the values found for the first experiment. All data surface temperature deposition ( $T_{dep}$ ) of this experiment are show in Appendix A: Table A.3 to A.7.

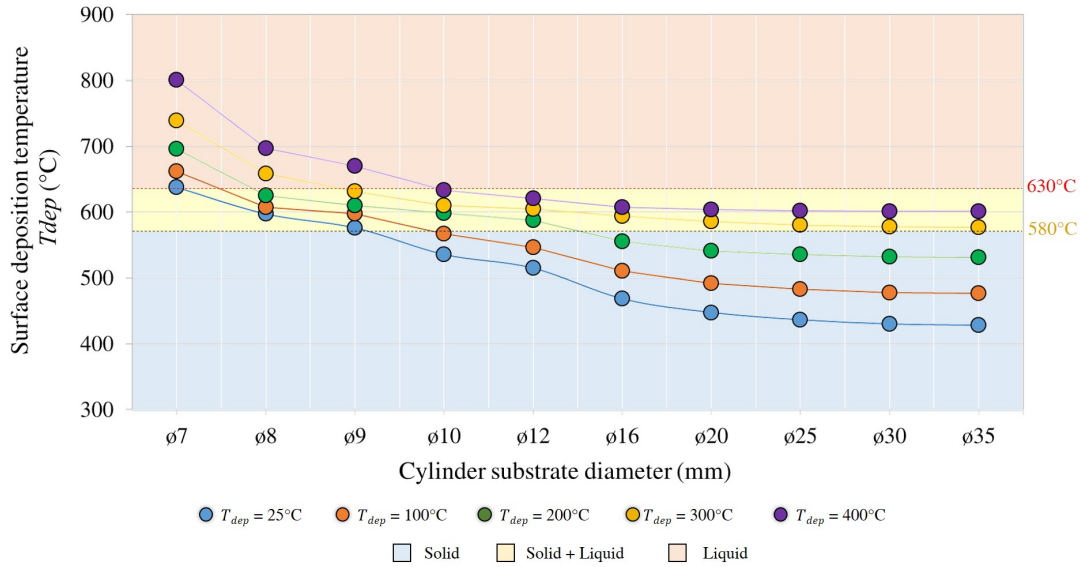


Figure 2.2.7 : Evolution of  $T_{dep}$  according to  $T_{init}$  for the deposition of single weld bead on cylinder substrate.

### 2.2.3 Thermal simulation of lateral overlap weld bead

The thermal simulation of this experiment is shown in Appendix A: Figure A.3.1. A lateral overlap weld bead is a weld bead that is deposited on the side of the previous weld. The distance between two consecutive weld beads is fixed at  $d = 0.738w$  according to [32]. Based on the same principle as the previous experiment, secondary layers present a lower temperature of deposition than the first one because of the heat dissipation area increases as the deposition process occurs. The measurement area of this experiment, as shown in Figure 2.2.8, can be determined from the surface temperature history during the weld bead deposition. The temperature is here again relatively stable in the middle zone, from 10 mm to 70 mm. All experiments are show in Appendix A: A.3.2 to A.3.3.

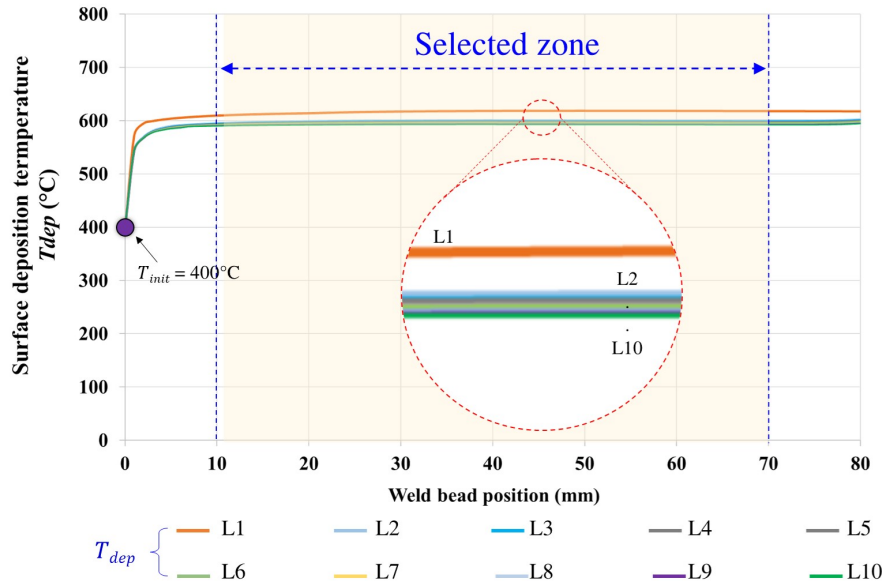


Figure 2.2.8 : Thermal simulation result of Exp.3: Lateral overlap weld bead at initial temperature ( $T_{init}$ ) at 400°C

Figure 2.2.9 shows the result of surface temperature deposition ( $T_{dep}$ ) in that range (10-70 mm) compared to the number of weld beads. All data surface temperature deposition ( $T_{dep}$ ) of this experiment are shown in Appendix A: Table A.9 to A.11 and Table A.12.

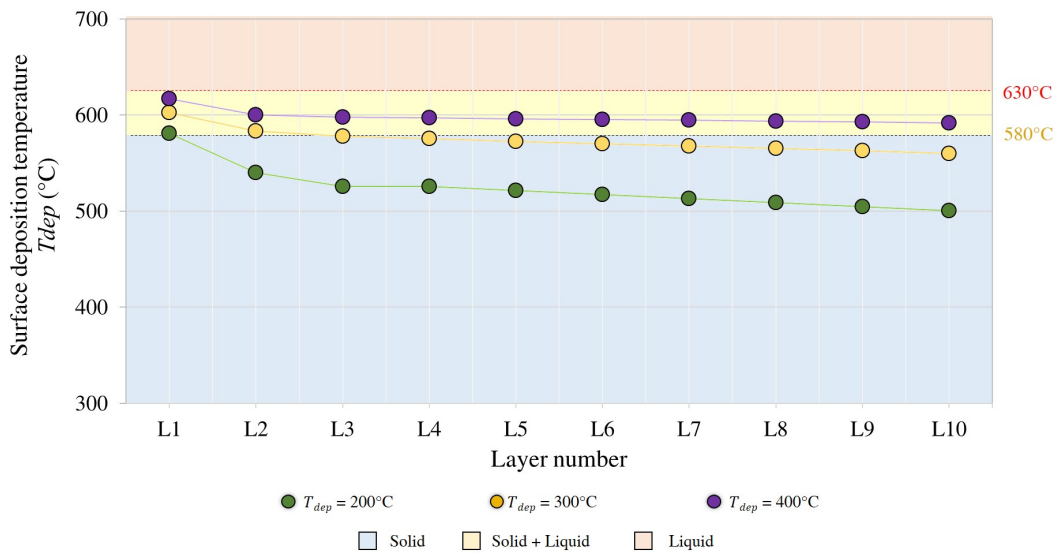


Figure 2.2.9 : Evolution of  $T_{dep}$  according to  $T_{init}$  for the deposition of lateral overlap weld bead.

### 2.2.4 Thermal simulation of vertical overlap weld bead

In this experiment, several layers have been stack up (from 2 to 10 layers) to produce walls. Here, four initial temperatures have been tested (100°C, 200°C, 300°C, and 400°C). Figure 2.2.10 at  $T_{init}$  400°C, the curves shape of  $T_{dep}$  values is comparable of behaviors highlighted in the second experiment: a quick rise in temperature is followed by a stable plateau and finished by a last and short increase of  $T_{dep}$ . All experiments are show in Appendix A: A.4.2 to A.4.4. The value of this plateau, always placed from 10 to 70 mm from the starting point, is not constant over the layers as show in Figure 2.2.11. It tends to rise with the number of layers but with a smaller increase for each step. Here too, this heat accumulation might be explain by the reduced amount of matter being able to transfer and stock this thermal energy. All data of the surface temperature deposition ( $T_{dep}$ ) of this experiment are gathered in Appendix A: Table A.13 to A.16 and Table A.17.

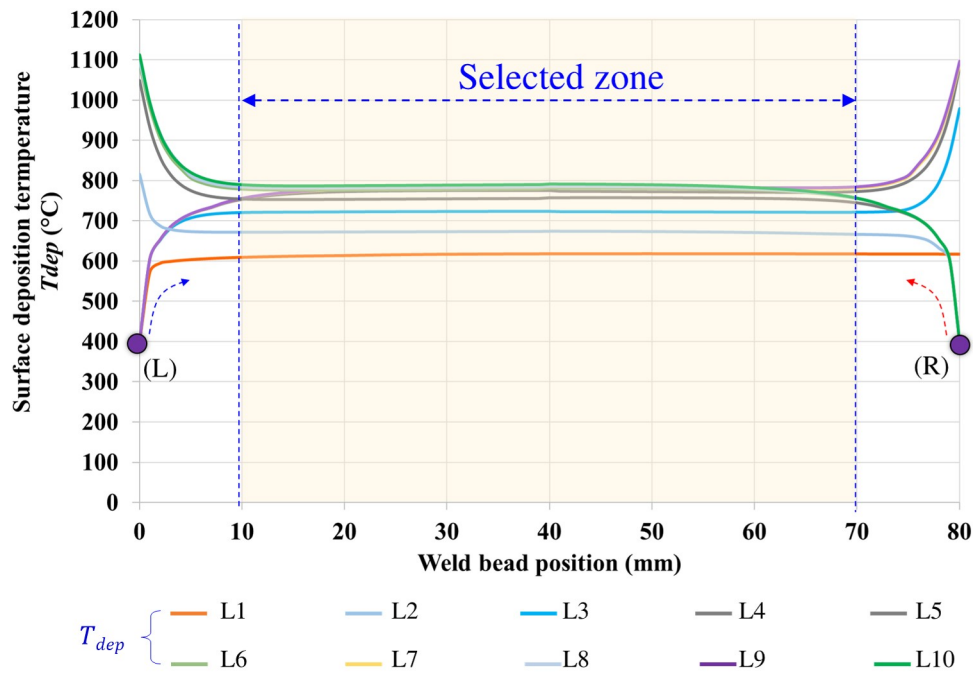


Figure 2.2.10 : Thermal simulation result of Exp.4: Vertical overlap weld bead at initial temperature ( $T_{init}$ ) at 400°C

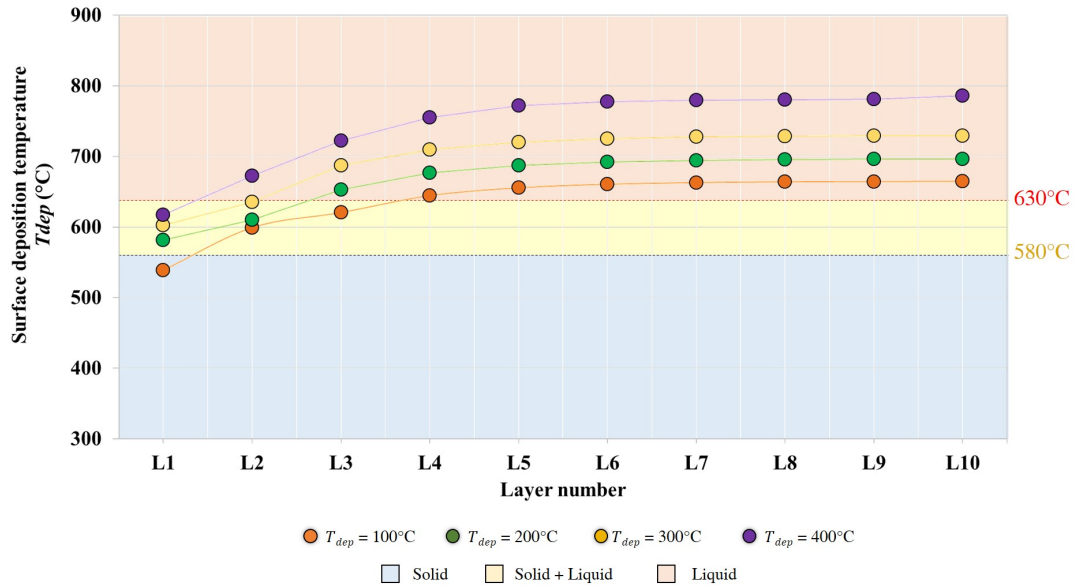


Figure 2.2.11 : Evolution of  $T_{dep}$  according to  $T_{init}$  for the deposition of vertical overlap weld bead.

The evolution of this deposition temperature give a lot of valuable information. Even if welding conditions are constant, the geometrical environment play a key role in the thermal cycle of a bead. Whether considering the initial temperature, the shape of the substrate, the presence of consecutive beads or the number of layers, many different factors influence the deposition conditions, without taking into account welding parameters. This short study clearly highlights the need to understand the melt pool environment and specifically the role played by the temperature which can have different sources.

In the next and last section of this chapter, the realization of weld beads is presented.

## 2.3 Experimental procedure

The above information describes the experiment and its implementation using equipment of the WAAM cell presented earlier in this chapter. This section presents the design implementation and the result of the experiments, which are detailed as follows:

### 2.3.1 Experimental procedure of single weld bead on flat substrate

A single weld bead deposited on a flat substrate is the basis of WAAM. For the needs of this experiment, the heating device is placed on the table of the WAAM robot. It will provide the thermal energy to reach the different initial temperatures. The substrate is then put on the heating device and clamped. After that, the working distance, the gap between the welding torch and the substrate, is fixed at 15 mm. The next step is very important. It is the validation of the surface temperature before the deposition by using a thermometer (FLUKE-50S). Once the correct temperature is insured (25°C, 100°C, 200°C, 300°C or 400°C), the deposition step in itself take place with a wire feed speed ( $WFS$ ) of 5 m/min, travel speed ( $TS$ ) of 0.60 m/min, while using the CMT-STD law n°875. Naturally, the process mentioned above is implemented for each initial temperature as shown in Figure 2.3.1.

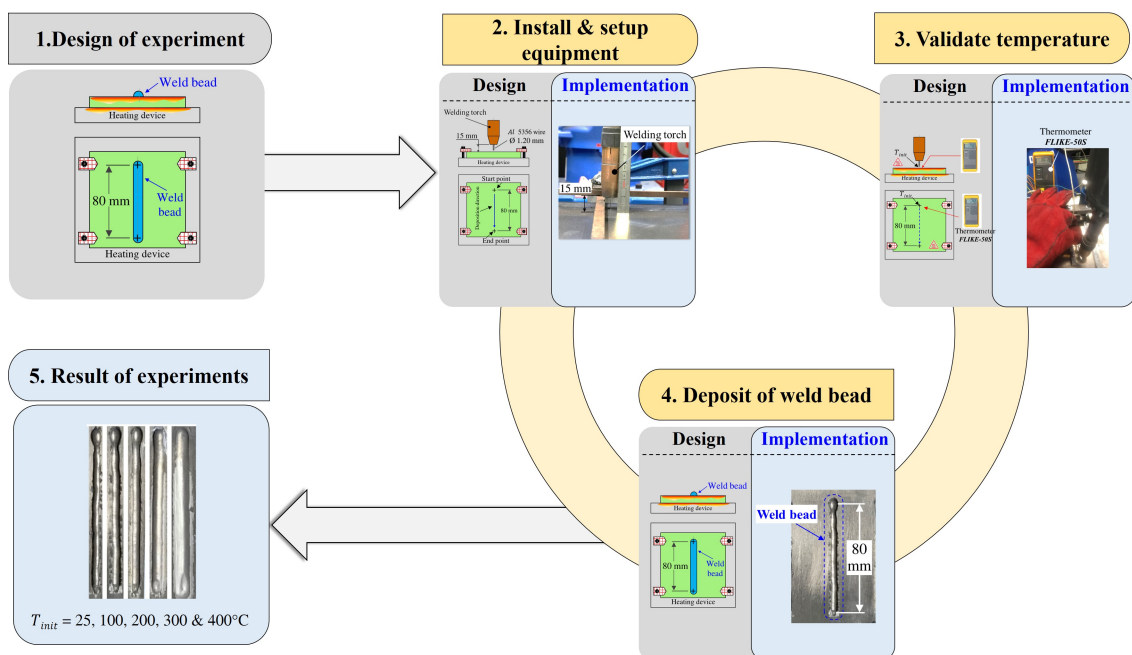


Figure 2.3.1 : Design of experiment of single weld bead on a flat substrate

All process parameters are controlled except the deposition temperature which is only estimated thanks to the thermal simulation presented in the previous section. The final picture of the four deposited weld beads is available in Figure 2.3.2. First observations with the naked eye already show that the weld bead shape changes as the initial temperature is modified. The higher it goes and the flatter the weld bead

is with an improvement of its regularity. Further analysis are proposed in the next chapter.

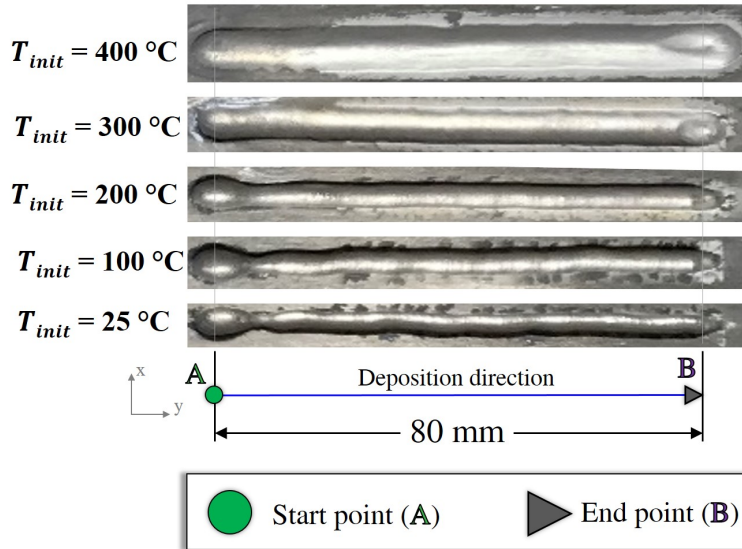


Figure 2.3.2 : The result of Exp.1: Single weld bead on flat substrate

### 2.3.2 Experimental procedure of single weld bead on cylinder substrate

This experiment is characterized by the use of non-flat substrate geometry. Indeed, cylindrical substrates have been set up to increase the diversity of conditions affecting the weld bead shape and to get closer to reality. Diameters of cylinders are listed as follow:  $\varnothing 7$ ,  $\varnothing 8$ ,  $\varnothing 9$ ,  $\varnothing 10$ ,  $\varnothing 12$ ,  $\varnothing 16$ ,  $\varnothing 20$ ,  $\varnothing 25$ ,  $\varnothing 30$  and  $\varnothing 35$  mm. The weld bead is deposited on the very top of cylinders. The weld bead deposition length is 100 mm. The welding parameters are: Wire Feed Speed ( $WFS$ ) = 5 m/min, Travel Speed ( $TS$ ) = 0.60 m/min and Argon gas flow rate = 13 L/min. This experiment contains the following initial temperatures ( $T_{init}$ ): 25°C, 100°C, 200°C, 300°C and 400°C, once more using the heating device, as shown in Appendix B: Figure B.1.1.

Figure 2.3.3 shows the produced weld beads for this experiment. The temperature here seems to affect in the same way the bead shape as in the previous experiment. To be noted, as expected from the thermal simulation, the smallest cylinders have been partially melt during the process. Especially for high  $T_{init}$ , this partial fusion of the substrates could cause difficulties to distinguish the weld bead from the cylinder. Being problematic for the next step of this research work, some conditions have not

been kept for the geometrical analysis: at  $T_{init} = 300^{\circ}\text{C}$  of  $\varnothing 7$ ,  $\varnothing 8$  mm and  $T_{init} = 400^{\circ}\text{C}$  of  $\varnothing 7$ ,  $\varnothing 8$ ,  $\varnothing 9$ ,  $\varnothing 10$  mm have been remove due to the defromation of cylinder substrates. All experiments result are show in Appendix B: B.2.1 to B.2.4.

**Initial temperature ( $T_{init}$ ) =  $400^{\circ}\text{C}$**

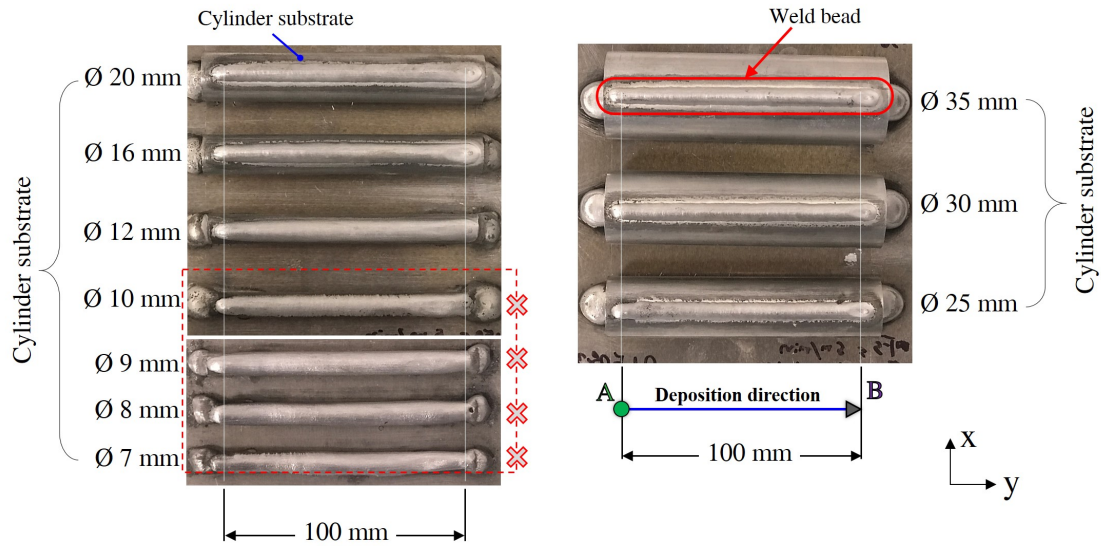


Figure 2.3.3 : The result of Exp.4 at  $T_{init}= 400^{\circ}\text{C}$

**2.3.3 Experimental procedure of lateral overlap weld beads**

The lateral overlap weld beads, this design of experiment is characteristic of substrate geometry (Non-flat and flat surface). The weld bead deposition length is 80 mm. The welding parameters are fixed at Wire Feed Speed ( $WFS$ ) = 5 m/min, Travel Speed ( $TS$ ) = 0.60 m/min and Argon gas flow rate = 13 L/min. This experiment is implemented with the following initial temperatures ( $T_{init}$ ):  $200^{\circ}\text{C}$ ,  $300^{\circ}\text{C}$  and  $400^{\circ}\text{C}$ , using heating device. The Figure 2.3.4 shows the trajectory design for the lateral direction overlap weld beads. This path is referenced as the unidirectional raster trajectory. The offset distance ( $D$ ) is fixed at  $0.738w$  according to [32]



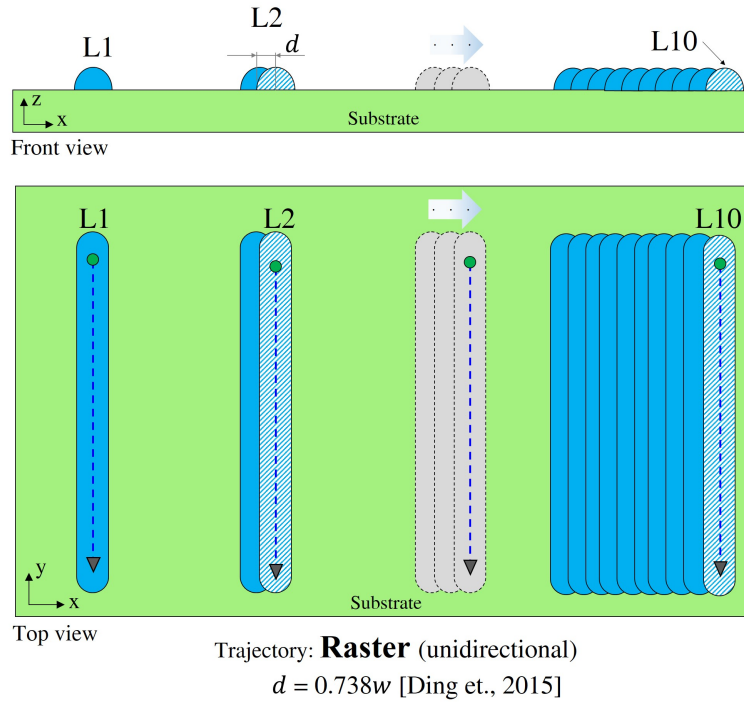


Figure 2.3.4 : Trajectory of lateral overlap weld bead deposition

The deposition process of this experiment is identical to the previous ones. Before starting the bead weld, the temperature on the surface beside of the previous layer is checked with a thermometer (FLUKE-50S). When the temperature reaches and stabilizes at the correct value, three points controlled to insure this state, then the next bead is deposited to form a new “layer”. All experiments had the same weld bead deposition process, changing only the initial temperature. This experiment contains built structure with a number of layers of one to ten for each value of  $T_{init}$  as shown in Appendix B: B.3.1. The results show that the initial temperature had a significant effect on the weld bead deposition, even of greater importance than for the other experiment. For the initial temperature ( $T_{init}$ ) of 200°C, when the second layer is deposited, the bead is deposited, not on the flat surface as expected, but on the near upper surface of the previous weld bead, at a closer distance than the one planned. Then, when the next layer is welded, it is deposited without continuity with the previous beads, like if it was a single deposition of Exp.1. This succession of recovery and gap is pursued as weld beads are deposited as visible in Figure 2.3.5. This behavior completely disappears for higher initial temperature (experiments where  $T_{init}$  is set up at 300°C and 400°C), and the deposition process results in a regular surface as shown in Figure 2.3.5. This phenomena could be

explain by the fact that, at low temperatures, the wetting angle being degraded, it results in a change of the shortest distance between the torch and the near matter. The electrical arc is thus ignited on the upper surface of the previous bead and, the molten droplets following the arc, changes drastically the deposited geometry. As the temperature increases, the wetting angle becomes more favorable and the deposition process is pursued correctly. In this context, the experiment at 200°C has been removed and further work will be done only considering value of  $T_{init}$  of 300 and 400°C for Exp.3.

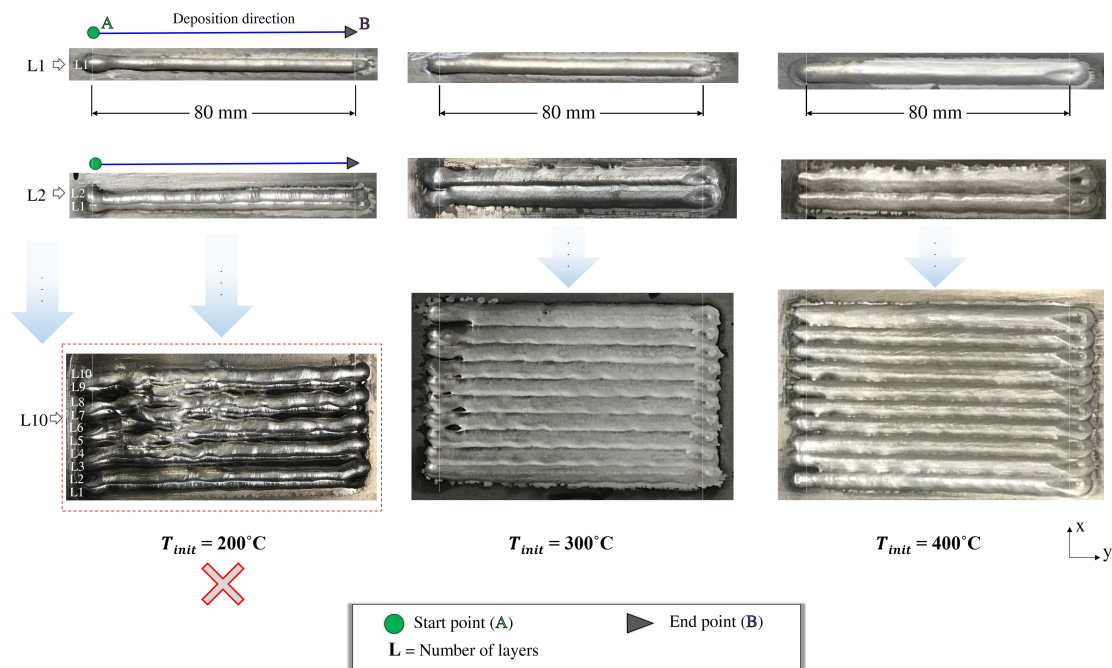


Figure 2.3.5 : The result of Exp.3: Lateral overlap weld beads at  $T_{init} = 200^\circ\text{C}$ ,  $300^\circ\text{C}$  and  $400^\circ\text{C}$

### 2.3.4 Experimental procedure of vertical overlap weld beads

For this last experiment, walls of 80 mm long, have been produced with the following welding parameters: Wire Feed Speed ( $WFS$ ) = 5 m/min, Travel Speed ( $TS$ ) = 0.60 m/min and Argon gas flow rate = 13 L/min. This experiment is built on the following initial temperatures ( $T_{init}$ ):  $100^\circ\text{C}$ ,  $200^\circ\text{C}$ ,  $300^\circ\text{C}$  and  $400^\circ\text{C}$  by using the heating device. The value of  $T_{init}$  at  $25^\circ\text{C}$  is specifically avoided as it induces conditions in terms of manufacturing time and temperatures that are too far from a real part production. For each condition, 9 walls have been generated from 2 to 10 layers. Figure 2.3.6 shows the trajectory design of the vertical overlap weld bead.

The welding trajectory is the bidirectional raster trajectory. Between each layer, an increment of the Z axis ( $\Delta H$ ) have been done of 2.4 mm.

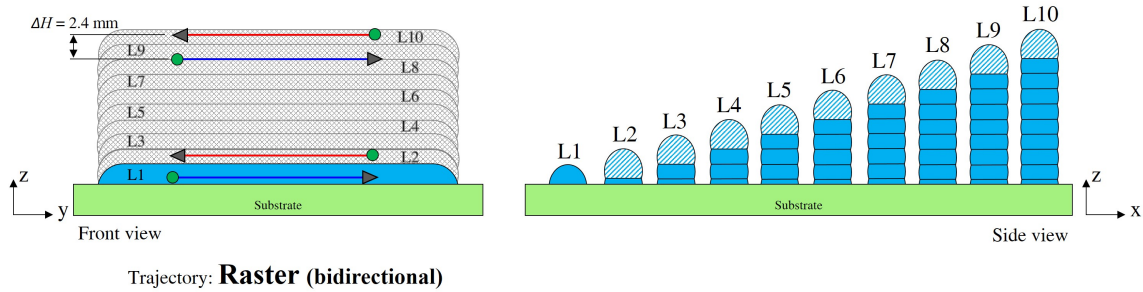


Figure 2.3.6 : Trajectory of vertical overlap weld bead

As the rest of experiment, a specific attention is given to the conditions in which weld bead are deposited. Before starting a weld, the temperature on the surface of the previous layer is controlled with a thermometer (FLUKE-50S) and the process starts only when this measure reaches and stabilizes at  $T_{init}$ . Photography of every walls thus produced are available in Appendix B: B.4.1. First observations show that every conditions have been processed until the end and that an increased initial temperature tends to generate smaller and thicker walls (illustration given Figure 2.3.7). All experiment results are show in Appendix B: B.5.1 to B.5.3

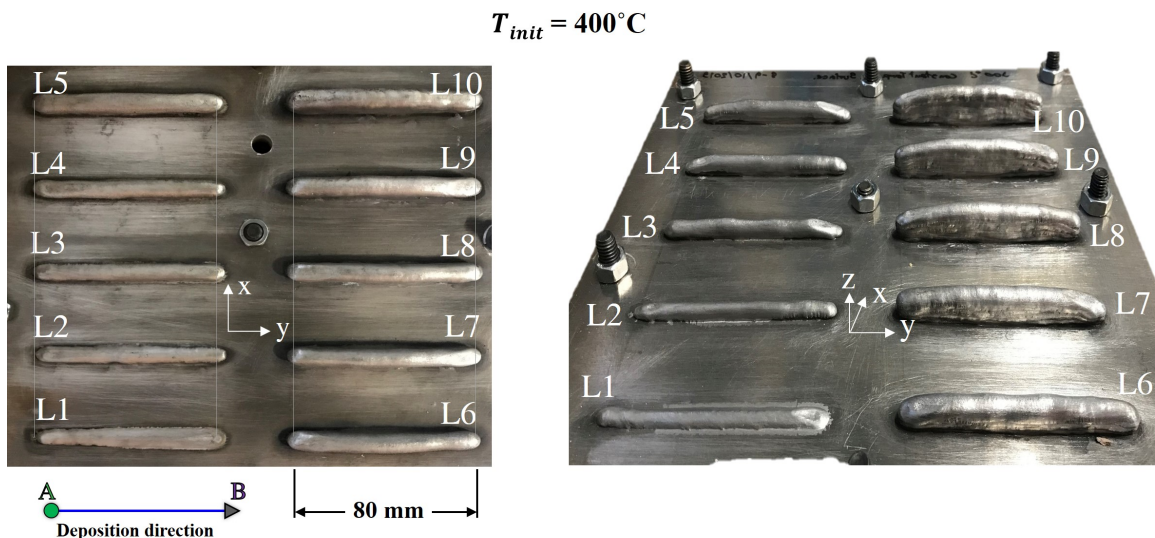


Figure 2.3.7 : The result of Exp.4: Vertical overlap weld bead at  $T_{init} = 400^{\circ}\text{C}$

## Conclusion

The work presented in this chapter has the ambition to design an experiment allowing to answer the problematic exposed in the first chapter of this manuscript. To achieve this goal, the WAAM process is decomposed to identify elementary configurations. These steps are implemented in four different experiment. They allow to isolate influencing parameters and make them controllable. They are identified as follow:

- Exp.1: Single weld bead on flat substrate.
- Exp.2: Single weld bead on the cylinder substrate.
- Exp.3: Lateral overlap weld bead.
- Exp.4: Vertical overlap weld bead.

However, the thermal problematic remains complex. While the use of a heating device allowed to control its order of magnitude, the temperature is still inaccessible due to its too many influencing factors. To overcome this problem, thermal simulations have been implemented. They investigate the deposition temperature behavior during the deposition process. First, the importance of the initial temperature ( $T_{init}$ ) concerning the surface deposition temperature ( $T_{dep}$ ) was thus determined. Then, the different experiments have each of them allowed to introduce geometrical components to the study. Thus, we have seen that the decrease of the substrate size tends to increase the deposition temperature, that in lateral overlap, secondary beads benefit of a lower value of this temperature and that, in the opposite, stacking layer in the vertical direction tends to rise the heat accumulated at the substrate surface. Most important, they identified the position of a portion of weld beads where process conditions, welding parameters and temperatures, are stable, which will be the basis of the next chapter.

Finally, the realization of these experiments is detailed, emphasizing the step of the initial temperature control to insure constant starting conditions. The quality of these experiments composed a good starting point for the next chapter which will be dedicating to connect the process parameters to the observe variations of weld beads dimensions.



# Chapter 3

## Geometrical identification

The main objective of this chapter is transiting from physical weld beads, whose production is described in the previous chapter, to a geometrical model with quantified dimensions. Evolutions of these data can be then tracked or even predicted with phenomenological or numerical models. This chapter deals with the different steps of this transition process, while the prediction step will be further discussed in the next and last chapter. At first, physical weld beads are scanned to obtain a numerical model of their shapes. After that, a zone of interest for each experimental condition is defined to retain only the portion with constant processing conditions. Especially, the start and end of weld beads will be excluded as different transiting phenomena occur, such as process parameters fluctuations or temperature behavior. This selection is based on the thermal simulation presented in the previous chapter. Then, a circular model, which have been presented in chapter 1, is used to represent weld cross-sections. Thanks to its simple and instant application, information on width and height are extracted for each conditions. Finally, their evolutions are finally discussed in the last section. Thus, this chapter focuses on the steps mentioned above which are illustrated in Figure 3.0.1

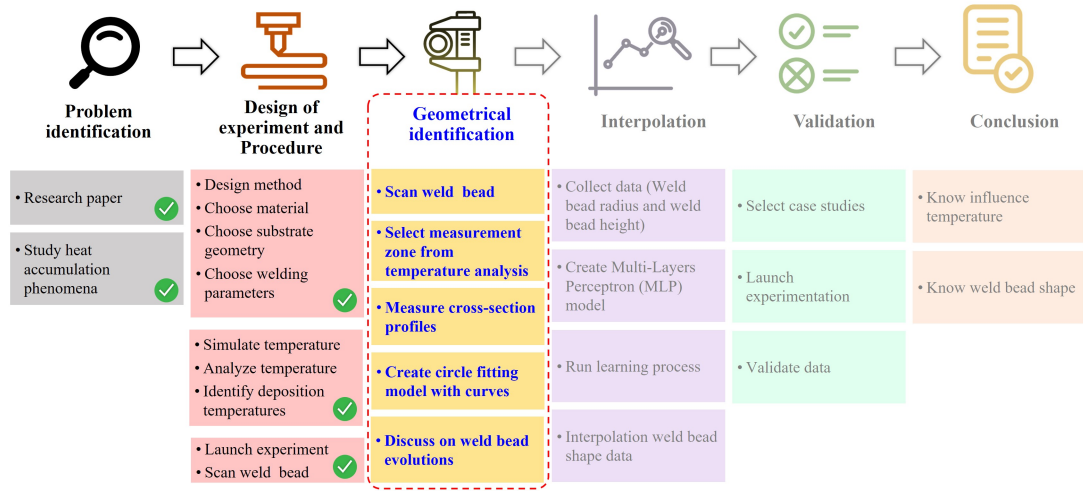


Figure 3.0.1 : Geometrical identification approach

### 3.1 Acquisition of numerical models of weld beads through 3D-scan correct

As previously described, a theoretical model of weld bead cross-section is required to obtain quantified dimensions. Their evolutions have to be representative of weld bead shapes evolutions along with variations of process conditions. In order to do that, a digitalization step of weld beads shapes is required in order to obtain a numerical object. It will easily allow the extraction of several information at any point on bead shapes. The 3D scanner HandySCAN 700 is used with a resolution of 0.05 mm. Technical specifications are shown in table 3.1. The associated software VXelements is used to export the numerical model in a STL file format. This file is then opened with GOM inspect software in order to measure cross-sections of the weld bead, as shown in 3.1.1.

3.1 Acquisition of numerical models of weld beads through 3D-scan correct

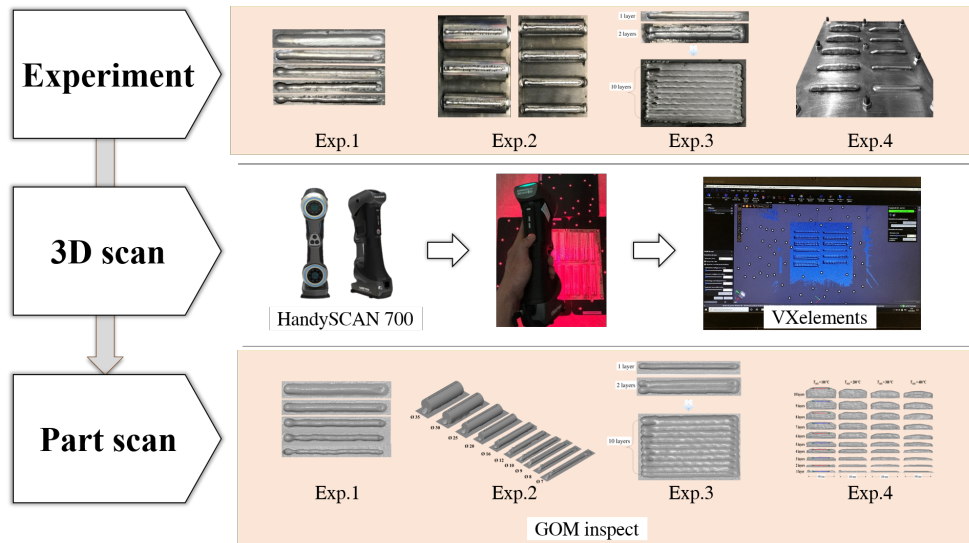


Figure 3.1.1 : The experiment 3D scan process

The scanning process is presented for each experiment in the next sections in order to show the shape of the different weld beads (single weld bead on flat substrate, single weld bead on the cylinder substrate, lateral overlap weld bead, and wall). A primary example is given Figure 3.1.2.



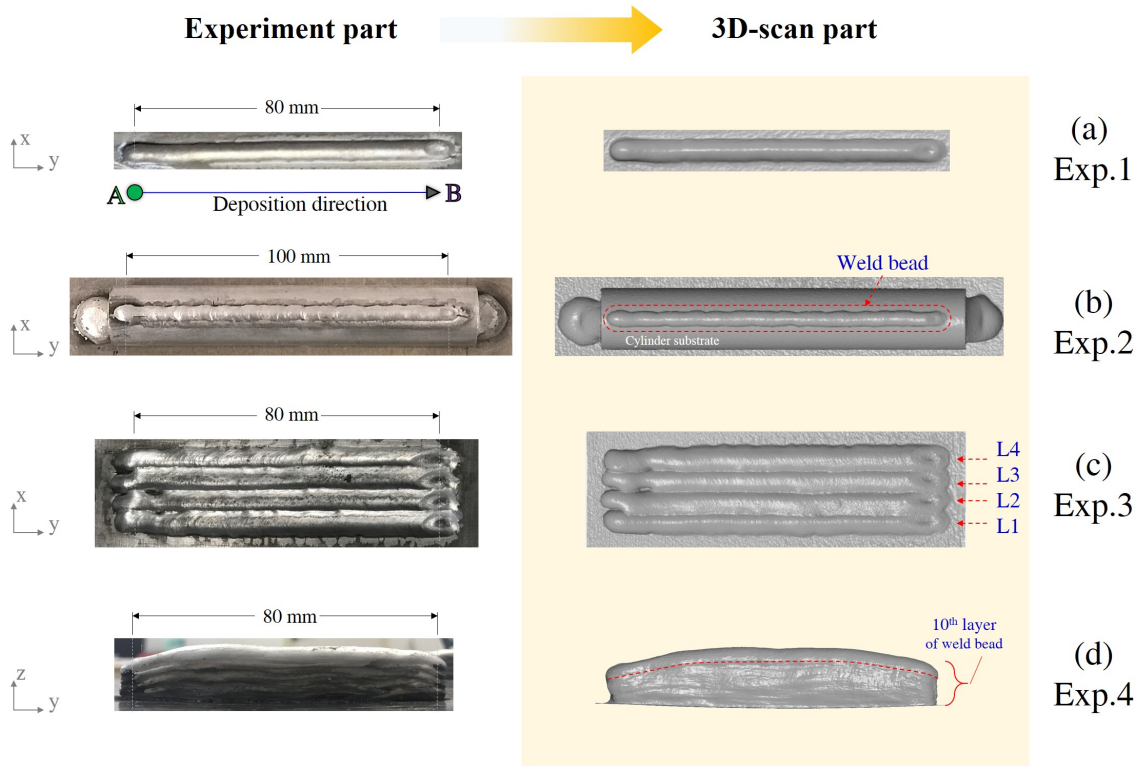


Figure 3.1.2 : Examples of experiments and scanner results (processed at  $WFS = 5\text{m/min}$ ,  $TS = 0.6\text{ m/min}$  and  $T_{init} = 300^\circ\text{C}$ ).

## 3.2 Cross-section profile measurement

Numerical models from the 3D-scanning process give information at any place on weld beads. However, it includes transiting zones where process conditions are not stables. These instabilities came from both welding parameters, where weld bead ignition and extinguish have punctual and specific conditions, and from thermal environment with can be specific either on a geometrical or temporal point of view. In this way, and thanks to thermal simulations presented in the previous chapter, it is possible to define a stable zone along the weld bead where constant conditions are found. These ranges are recalled here for every experiments : Exp. 1 : from 10 to 70 mm, Exp. 2 : from 20 to 80 mm, Exp. 3 : from 10 to 70 mm, Exp. 4 : from 10 to 70 mm, A series of cross-section profiles are extracted from those areas. As shown in Figure 3.2.1, a profile is read out every 1 mm all along the selected zone and recorded as a cloud of points.

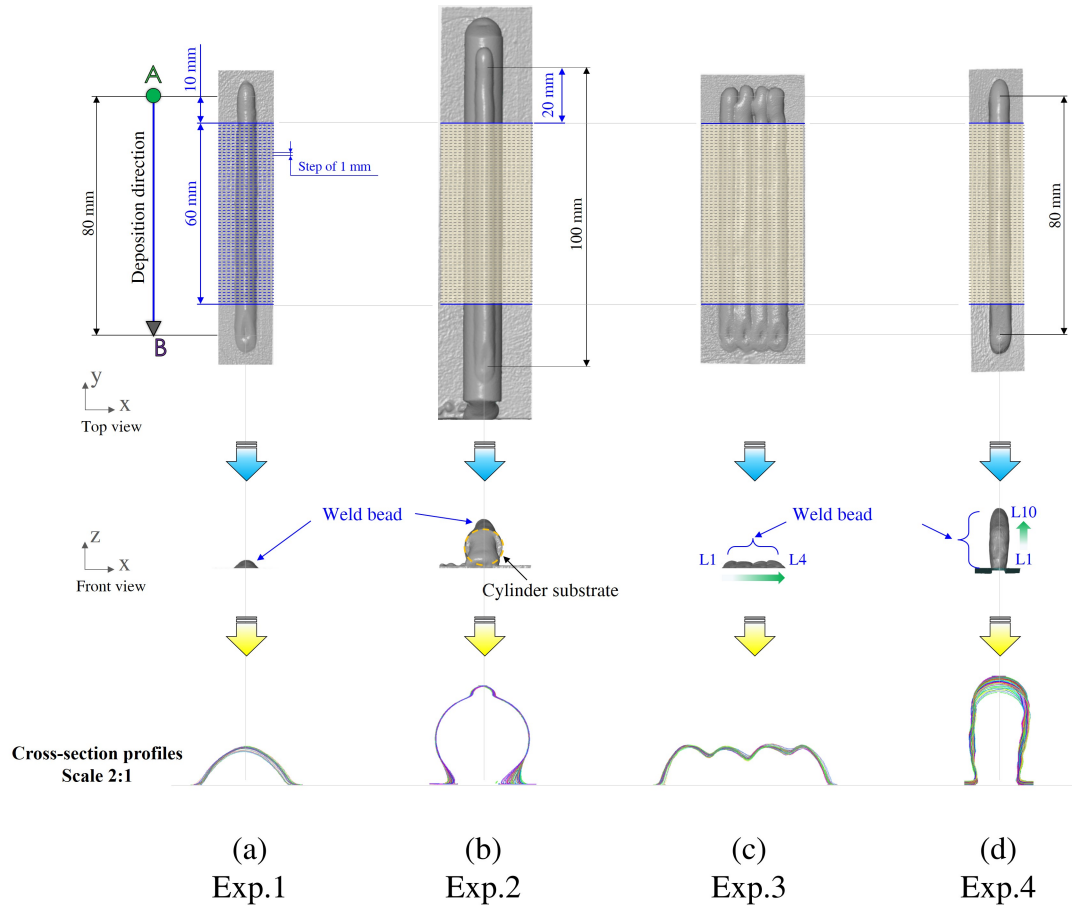


Figure 3.2.1 : Cross-sections extraction of experiment.

After profiles extraction, a circular model is implemented for geometrical representation of cross-sections. This modeling is fulfilled through an algorithm presented in the next section.

### 3.3 Weld bead cross-section modeling

Scanning and computational process results are composed of 60 clouds of points for each conditions. The use of a circular model allows obtaining quantifiable dimensions that can be tracked in order to start to understand influences from process parameters such as welding conditions and temperature. For instance, we have chosen to use one of the simplest models to represent a cross-section with a portion of a circle. The modeling is implemented for every condition profile through an algorithm detailed in the next section. Data are then presented and analyzed in the last section.

Using a simple model for the representation of weld bead cross-section offers the advantage to be easily implemented. As detailed in Figure 3.3.1, profiles are first straightened to ensure that the highest point is correctly identified. Then, it simplifies the selection of points from the upper surface (included in a distance  $d$  from the highest one) that will be taken into account for the circular model fitting. Only those points are used to fit the model as this selection does not induce any results deviation. In effect, they are less subject to errors during the scanning process, they are more likely to become the substrate of the next deposition, and including points from the whole bead section or not result in a deviation of a few hundredths for regular weld beads. The linear regression is then implemented through the least square method [5]. Therefore, the center and the radius of the fitted circle compose the raw results of this representation by a circular model. These data are then to be refined. An illustration of this process and its results can be found in Figure 3.3.2.

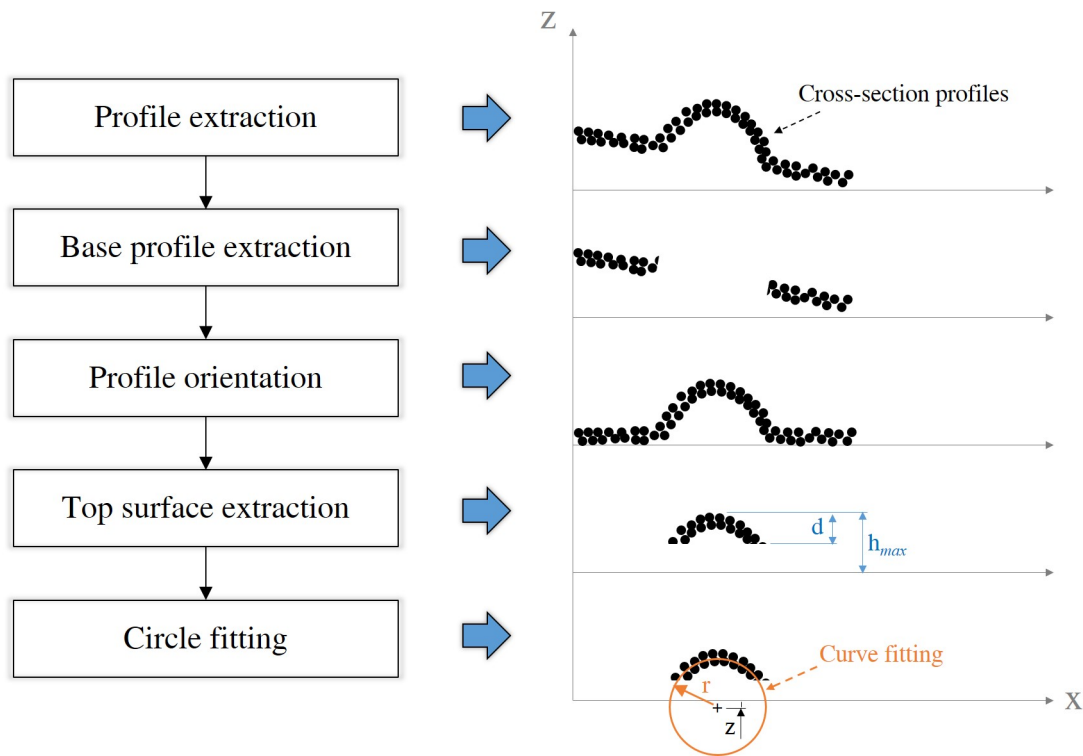


Figure 3.3.1 : Algorithm of circle fitting model.

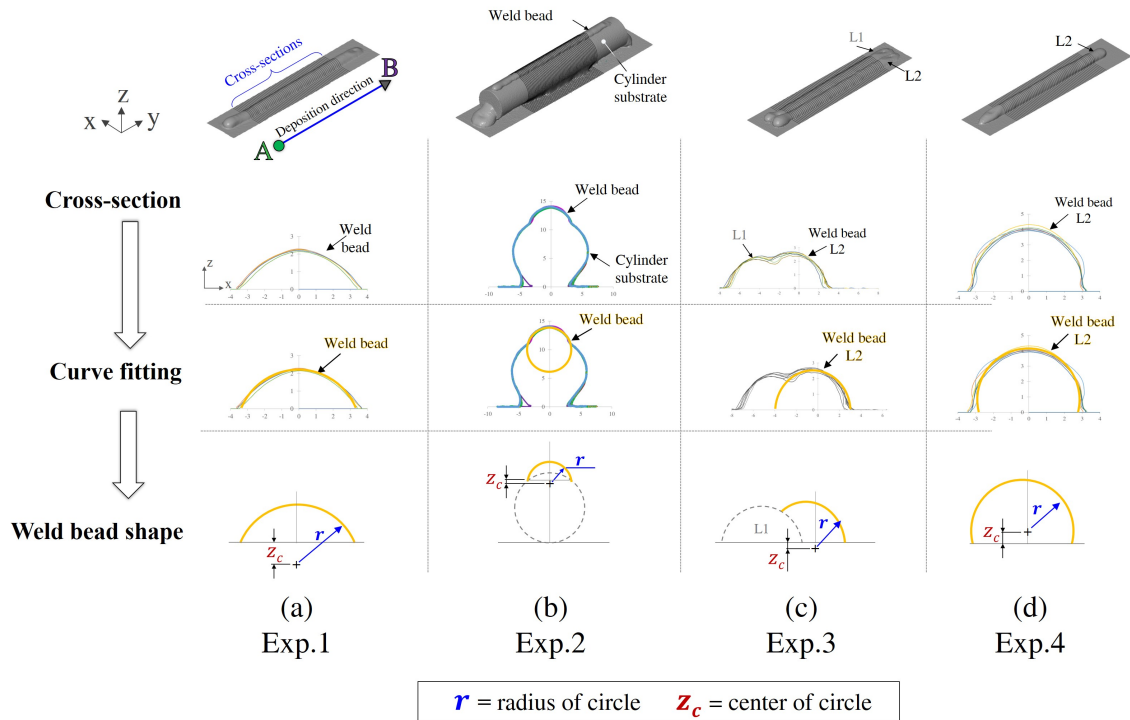


Figure 3.3.2 : Illustration of the process of bead cross-section modelling

### 3.3.1 Obtaining the representative dimensions of weld bead cross-sections

As a geometrical model now represents beads cross-sections, dimensions have to be extracted from this circular fitting and must transpose the different evolution of beads shape. Four factors have thus been chosen for this purpose :

$h$  (mm) : Weld bead height.

$w$  (mm) : Maximum width of weld bead.

$A$  (mm<sup>2</sup>) : Cross-section area of weld bead.

$\theta$  (°) : Wetting angle (only calculated for the first 3 experiments)

They are obtained according to the radius and the coordinates of the fitted circle. An illustration of their definition is given in Figure 3.3.3.

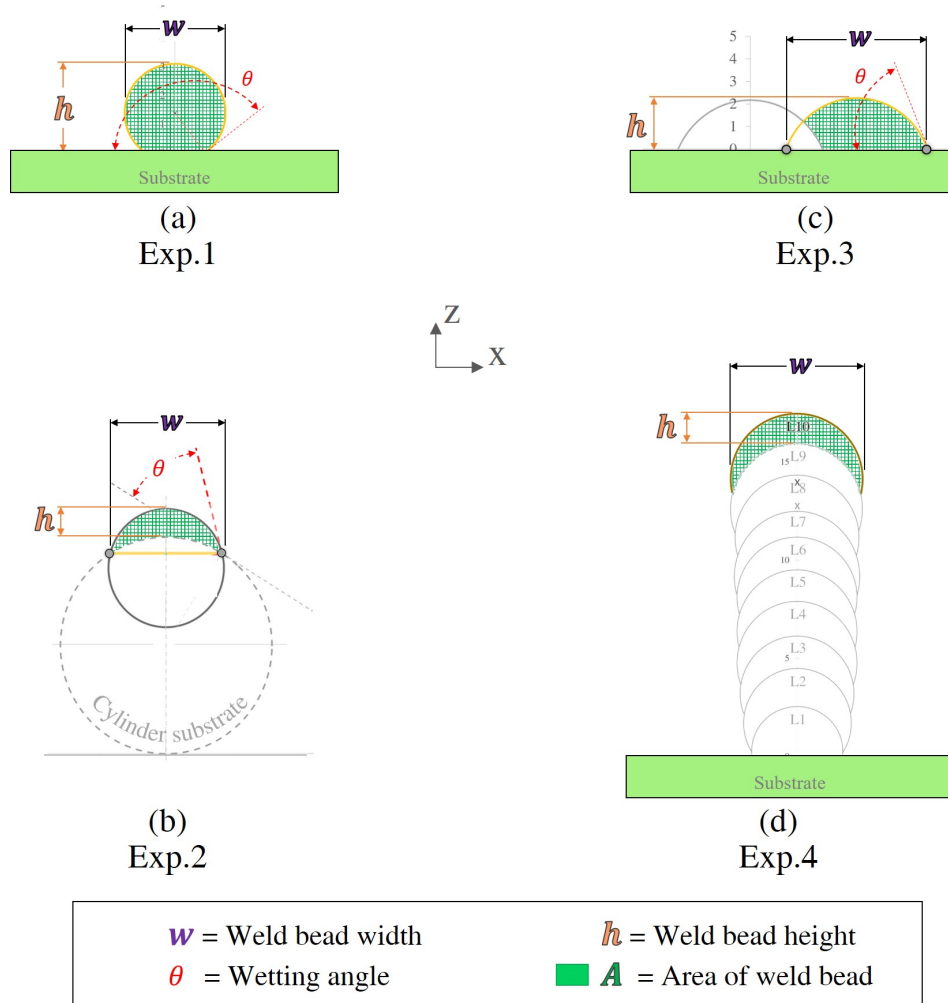


Figure 3.3.3 : Definition of weld bead dimensions

Before any discussion, the relevance of the circular model has been investigated. Using 3 parameters: highness, width at mid-height and cross-section area, the precision of this geometrical representation has been characterized through a comparison. This control has only been performed on the first experiment (single weld bead). The Figures 3.3.4 illustrate the results of this study. Thus, the difference between the maximum height of points profiles obtained through the scanning process and the one calculated from the circles parameter is very satisfying. The measured deviation does not exceed  $\pm 0.05$  mm, of a similar order of magnitude as the scanner precision. With a slightly larger difference, the width deviation measured at mid-height remains under 0.2 mm of difference. This disparity of precision between the height and width can be explain by the fact that the circular model is fitted using points belonging to the upper part of the weld bead and, by doing so, defining this

region with a higher accuracy. Another explanation is that the circular model being the simplest, it is not able to represent exactly the cross-section profile. The weld bead being probably slightly elliptical, it might explain why the circular model tend to lightly underestimate the height and, on the contrary, overestimate the width of weld beads. All in all, the cross-section surfaces are rather accurate with a gap smaller than  $\pm 5 \text{ mm}^2$  between scanned profiles and circular model calculations. This parameter transposing the real amount of matter deposited during the weld bead, it is all the more important to be representative.

In this way, those data and the previous comparisons are satisfying and allow to validate the accuracy of the circular model and its implementation.

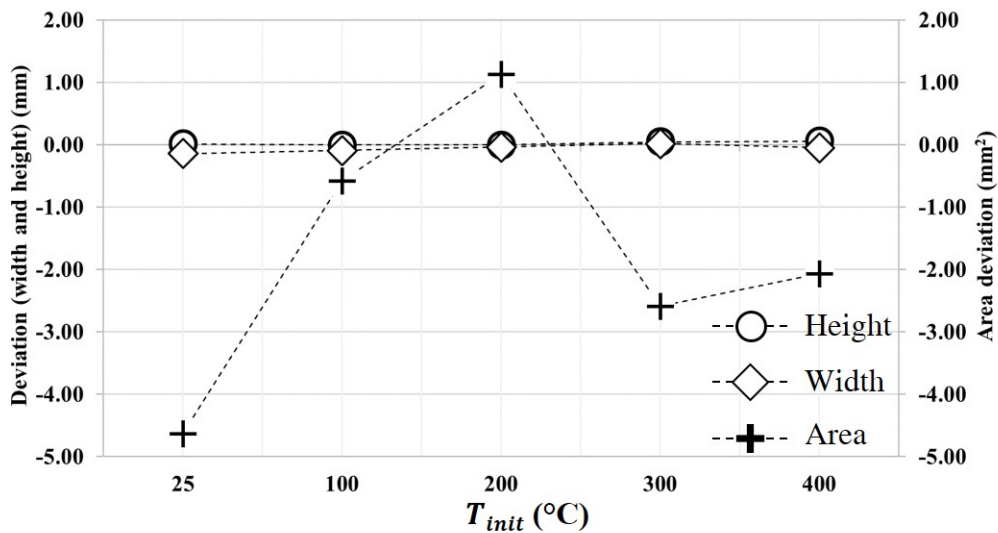


Figure 3.3.4 : Deviations of weld bead cross-section

## 3.4 First discussions on weld bead shape evolutions

### 3.4.1 Contribution of Exp.1

The first experiments have been set up in order to investigate the influence of the substrate temperature on the shape of single beads. From a physical point of view, we know that metals see their viscosity decreased with the temperature [81, 46]. In this way, the rise of the initial temperature, and so the rise of the deposition temperature, induces obviously a higher temperature during the weld bead. One can concludes on the decrease of the viscosity of the liquid metal that have also implications on weld bead shape and dimensions. In effect, as shown in Figure

3.4.1, this viscosity diminution with the temperature rise is directly visible with the decrease of the wetting angle ( $\theta$ ). This physical change affects all the weld bead dimensions: radius, highness and width as shown Figure 3.4.2. The molten pool being at a higher temperature, it is more fluid and requires longer time to cool down, inducing that the weld bead spreads. It can be seen as the width increase while the highness is lowered. These evolutions offset each other as the cross-section area remains rather constant across the different initial temperatures, as visible in Figure 3.4.3. Close to the theoretical value, which is supposed to be independent from the initial temperature and calculated according to the Equation 3.4.1, it seems that a small trend can be observed as the area appears to slightly increase with the temperature. Since it is not supposed to behave this way, it is assumed that the welding station is influenced by the temperature and its effects through its control loop, inducing a larger amount of deposited matter.

$$A_{th} = \frac{\pi \cdot r_{wire}^2 \cdot WFS}{TS} \quad (3.4.1)$$

Where  $A_{th}$  is cross-sectional of calculation ( $mm^2$ ).  $r_{wire}$  is radius of wire diameter (mm).  $WFS$  and  $TS$  are wire feed speed and travel speed, respectively, and their unit is meter per minute (m/min).

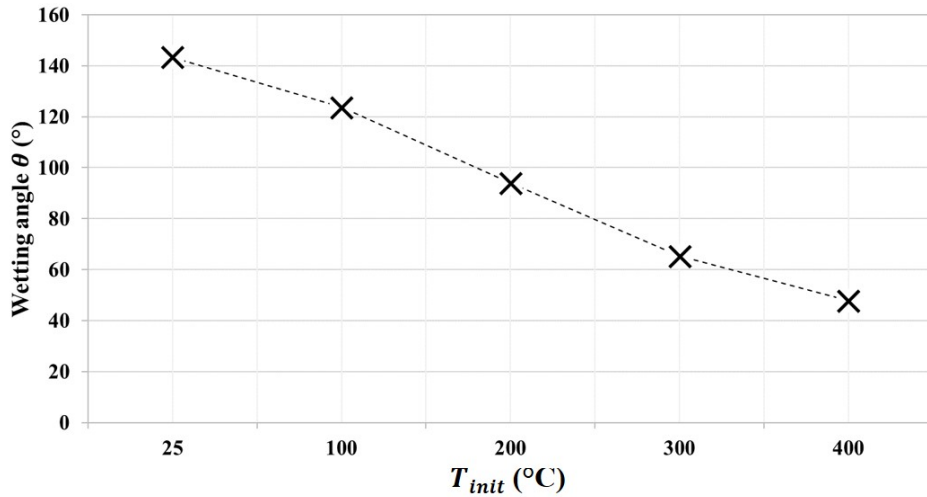


Figure 3.4.1 : Wetting angles for each initial temperature ( $T_{init}$ )

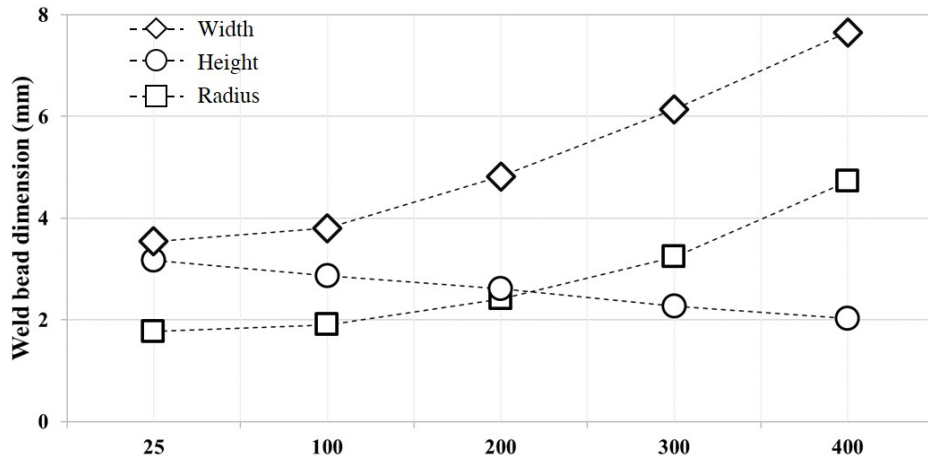


Figure 3.4.2 : Weld bead dimensions of each initial temperature ( $T_{init}$ )

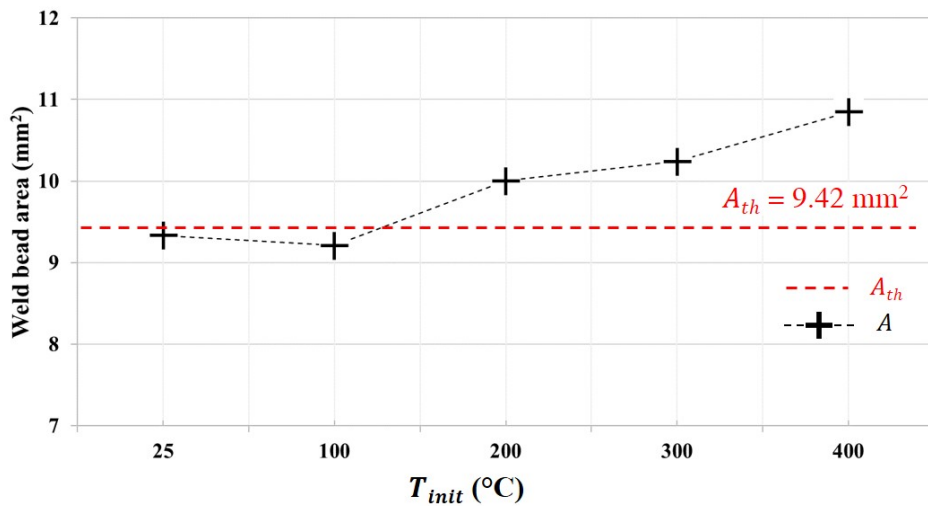


Figure 3.4.3 : Comparison cross-sectional of calculation ( $A_{th}$ ) and curve fitting area

### 3.4.2 Contribution of Exp.2

In this experiment, the radius of curvature of the substrate have been instigated in addition to the initial temperature variation. The goal is to highlight the relation of these factors on the weld bead shape. As the welding parameters  $WFS$  and  $TS$  are identical to the first experiment, changes are likely to come from the fact that matter and energy are deposited on a cylinder substrate. Compared to a flat substrate, it is a smaller environment and therefore it will be less efficient to evacuate the thermal energy. Thus, this alteration is firstly shown on the deposition temperature as



seen in the previous chapter.  $T_{dep}$  reaches different values depending on the formal radius of the cylinder. If bead dimensions are then plot according to  $T_{dep}$ , interesting information are exposed. For example, as visible on figures 3.4.4 and 3.4.5, the radius and width do not undergo any other influence from the cylinder radius other than its consequence on the deposition temperature. These dimensions present a similar behavior to single weld beads deposited on flat substrate: they increase with the temperature, independently of the substrate curvature. To be noted that the choice here to represent these data according to  $T_{dep}$  highlights that there is an inflection point around the value of the liquidus where radius and width increase suddenly. We assumed that, in these conditions the bead is collapsed.

Conclusions are more challenging to draw on the smallest cylinder as  $T_{dep}$  reaches quickly this melting temperature. The substrate losing its integrity, it is more difficult to build an argument on the evolution of weld bead shape.

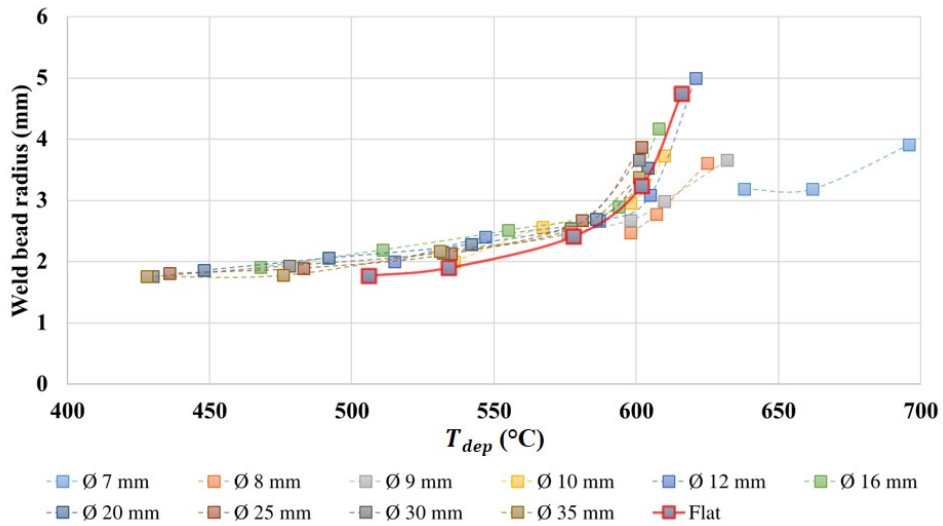


Figure 3.4.4 : Radius of weld bead deposited on cylinder substrates.

### 3.4 First discussions on weld bead shape evolutions

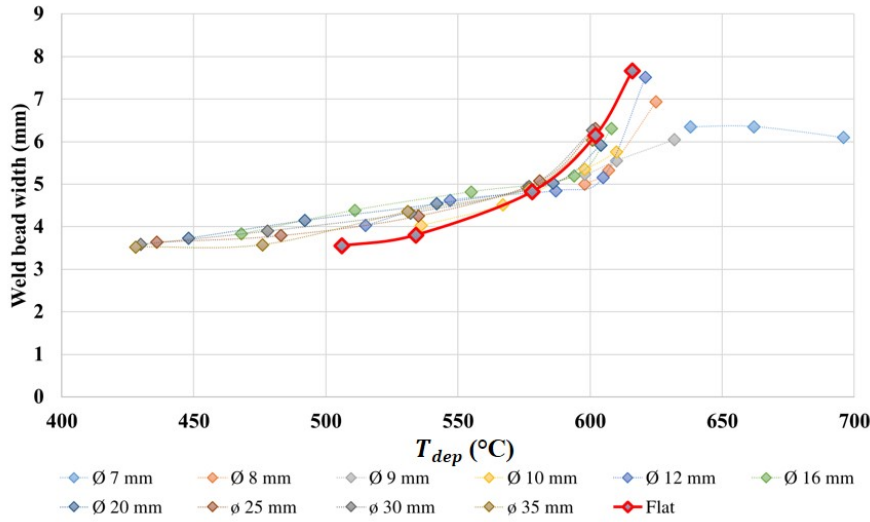


Figure 3.4.5 : Width of weld bead deposited on cylinder substrates.

Concerning wetting angles, with the way they are calculated, they seem to have a direct linear relationship with the initial temperature, as illustrated in Figure 3.4.6. In the same way as a weld bead deposited on substrate, the metal tends to spread more easily with the rise of temperature and thus produce weld beads with lower wetting angles. However, on the opposite of the two previous data, these angles depend also on the size of cylinders, independently of the influence of the latter on  $T_{dep}$ . As visible in Figure 3.4.7, wetting angles seem to be linearly related to the cylinder radius inverse ( $1/r_{cylinder}$ ). To explain this relation, we propose to approach it from the surface tension point of view. Surface tension is the force that tends to minimize the surface between two fluids (here, the liquid metal and the protective gas). This tension being less important with the rise of temperature, it allows the metal to flow and spread, inducing lower wetting angles on plates. Another way of saying it is that the surface tension will directly define the radius of weld beads. Thus, the radius depends on surface tension which depends on temperature and therefore, the weld bead radius depends only on the temperature  $T_{dep}$  as illustrated at Figure 3.4.4.

In the case of the cylinders experiment, a relatively constant amount of matter is deposited and therefore forming a weld bead with a relatively constant area of its cross-section. The radius and this area being quite fixed, the weld bead will then more or less envelops the cylinder. The matter will be more or less spread around the substrate surface, depending of the radius of this latter. In this experiment, wetting angles being defined from the normal of the cylinder at the frontier cylinder

/ weld bead / atmosphere, it is thus logical to find a linear relation between  $\theta$  and  $1/r_{cylinder}$ .

Evolutions of the highness of beads deposited on cylinder are identical to those of the wetting angle. As visible on Figures 3.4.8 to 3.4.9, height evolves linearly with the initial temperature and also presents a linear relation with the cylinder radius inverse. There too, the proposed is similar. In fact, the height as it is defined for this experiment, translates directly how much the deposited matter spread around the cylinder (keeping the same weld bead radius) a.k.a. until which point the weld bead embed around the cylinder. It is then possible to show a direct linear relationship between the weld bead height and its wetting angle, independently of its process conditions as visible Figure 3.4.10.

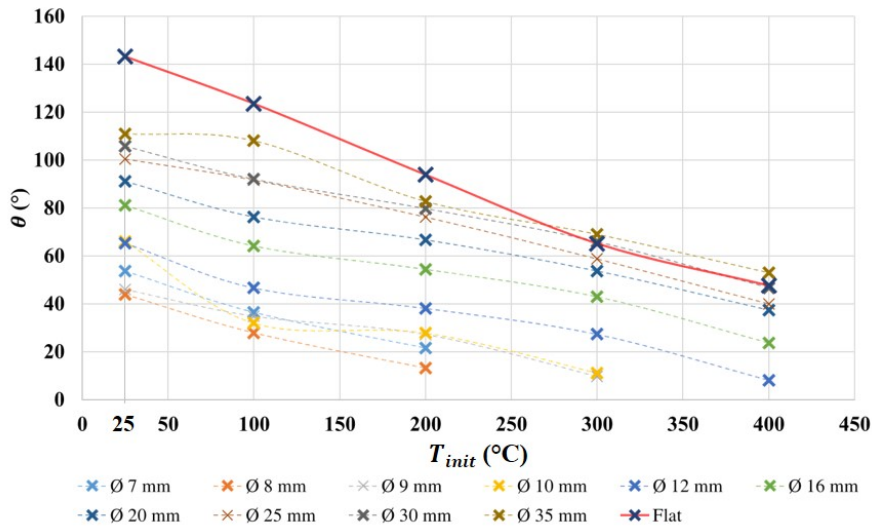


Figure 3.4.6 : Wetting angle of weld beads deposited on cylinder substrates

### 3.4 First discussions on weld bead shape evolutions

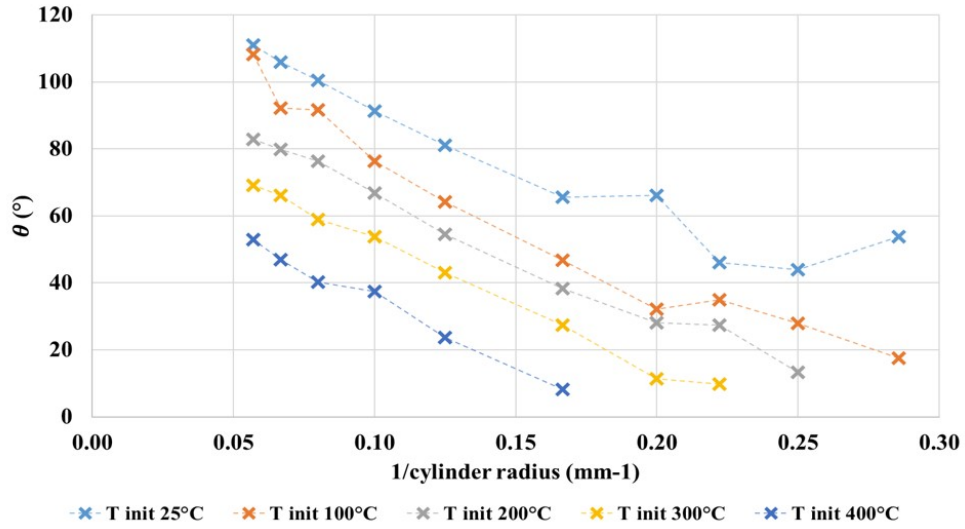


Figure 3.4.7 : Wetting angle of weld beads related to substrate curvatures

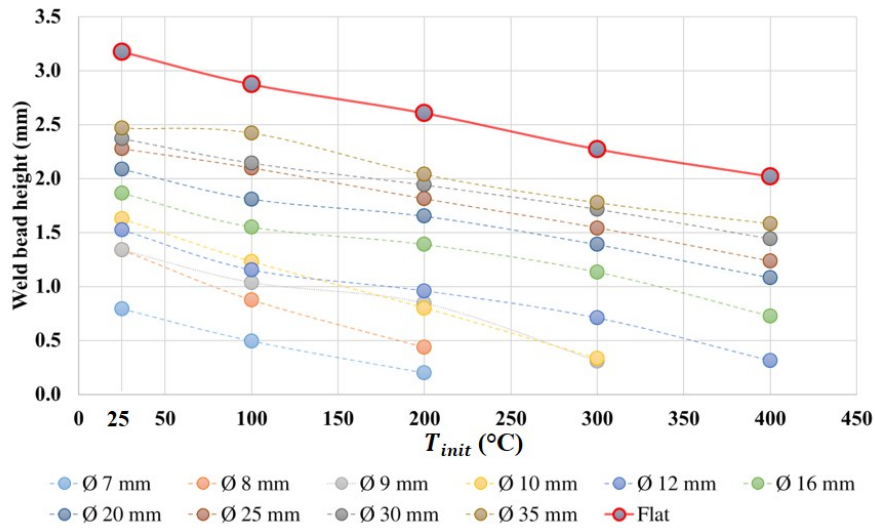


Figure 3.4.8 : Heights of weld beads deposited on cylinder substrates

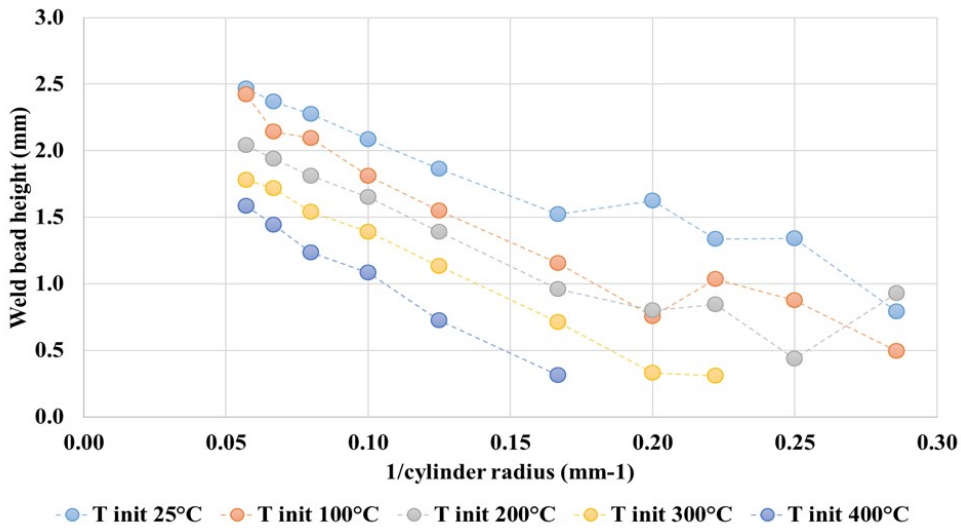


Figure 3.4.9 : Height of weld beads related to substrate curvatures

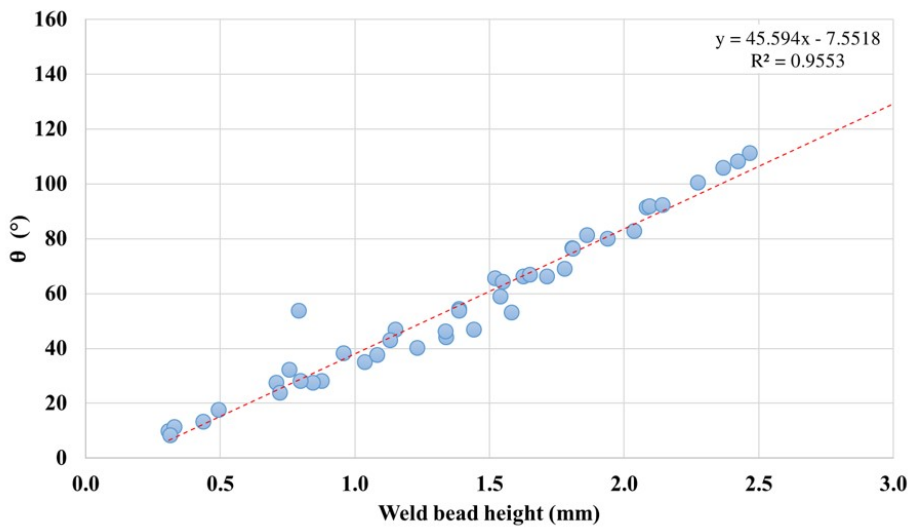


Figure 3.4.10 : Relation between wetting angles and heights of weld beads deposited on cylinder substrates (every conditions are shown)

Finally, concerning the area of cross-sections, this data tends to stay almost constant until an inflection temperature of deposition is reached near the liquidus as shown Figure 3.4.11. Before this point, it seems that a lower amount of matter is deposited considering the theoretical value driven by the selected welding conditions. On the opposite after the inflection point, the process tends to deposit a larger amount of matter. We link these deviations from the set point to the control loop of the welding station of which we are unaware.

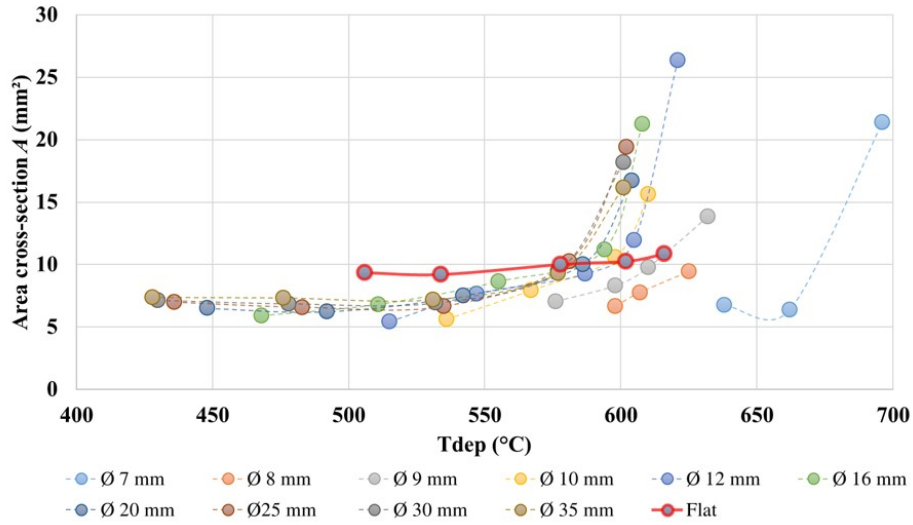


Figure 3.4.11 : Cross section area of weld beads deposited on cylinder substrates

### 3.4.3 Contribution of Exp.3

This experiment has consisted in depositing successive beads on a plate while staying in the same plan in order to understand the geometrical evolutions of the secondary weld beads. As previously explained, only two initial temperatures have been setup. It appears that our results tend to confirm the model of [32]. In principle, almost nothing change except that the matter, which should has occupied the space of the previous bead is reported higher on the z axis. As confirmed by our data available on Figures 3.4.12 and 3.4.13, heights and cross-section areas do not vary and are equal to those of single weld beads.

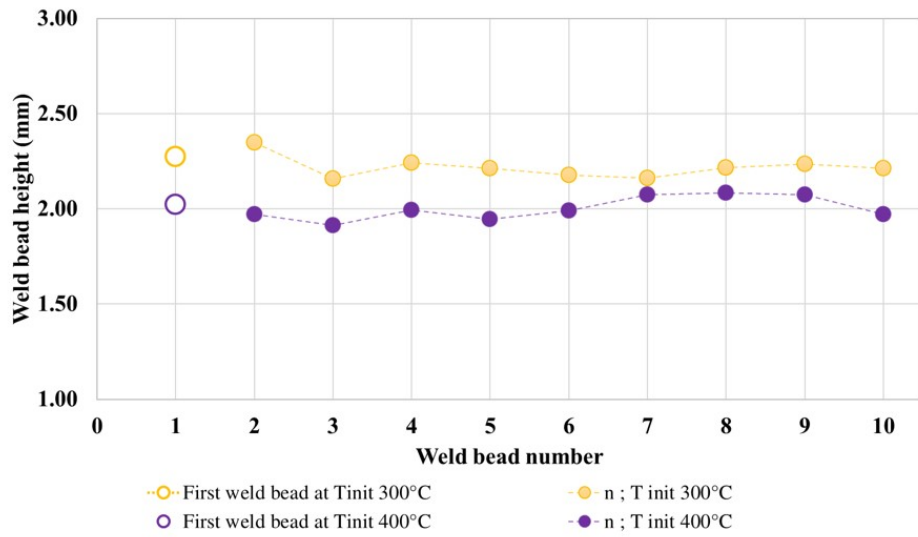


Figure 3.4.12 : Heights of weld beads deposited in the lateral direction

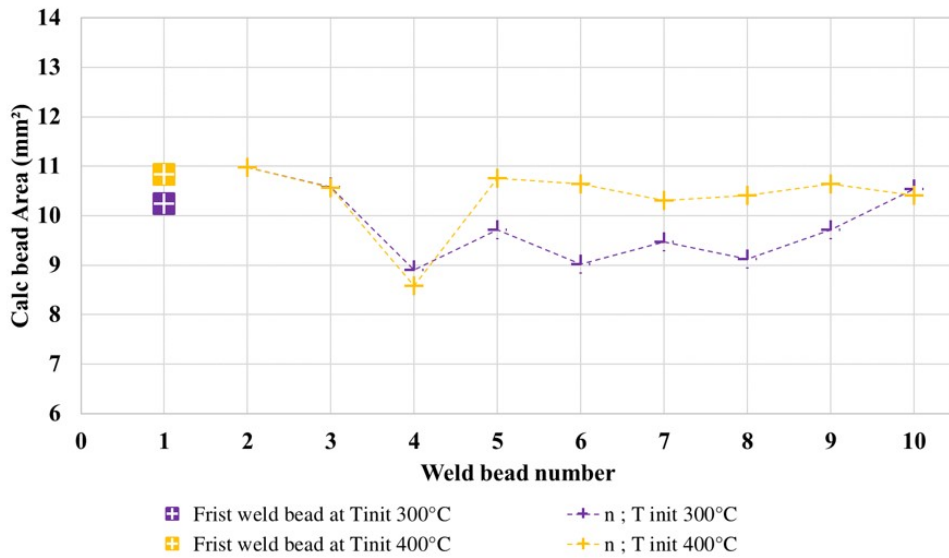


Figure 3.4.13 : Cross-section area of weld beads deposited in the lateral direction

On the other hand, this upward shift of matter induces greater radius for our circular model, which, combined with a constant height, tends to also increased the width and decrease the wetting angle compared to single weld beads set of data. However, the number of weld bead deposited in the lateral direction does not affect these parameters nor any other of them as shown from figure 3.4.14 to 3.4.16. These constancies imply that, except for the very first bead, every secondary deposition will be pursue in the exact same conditions as expected from the simulation of  $T_{dep}$

### 3.4 First discussions on weld bead shape evolutions

exposed in the previous chapter. Thus, it does not induce any evolutions of bead geometry, except those related to dispersion.

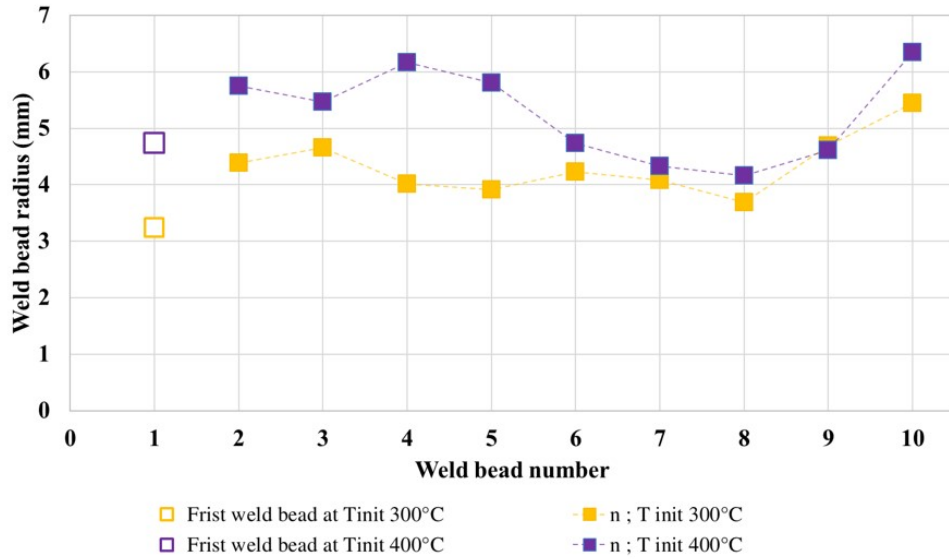


Figure 3.4.14 : Radius of weld beads deposited in the lateral direction

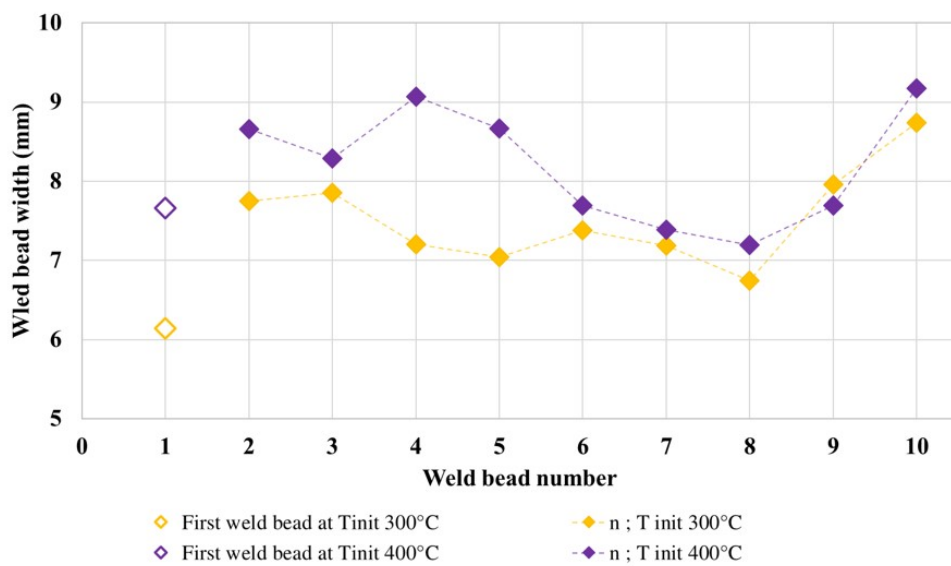


Figure 3.4.15 : Widths of weld beads deposited in the lateral direction



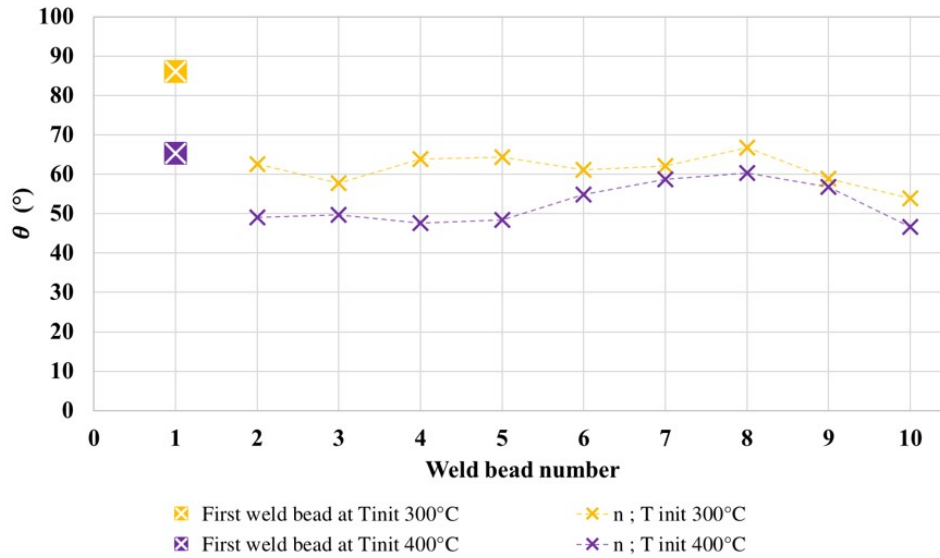


Figure 3.4.16 : Wetting angle of weld beads deposited in the lateral direction

### 3.4.4 Contribution of Exp.4

For this last experiment, walls were built at different heights, from 2 to 10 layers. As scans were performed once the production is over, there is no information available on previous layers. Therefore, only the ultimate layer has been accessible for analysis. This restriction implies that only weld bead radius and wall heights are directly accessible. For the others, dimensions assumptions have to be made when possible but some data are still out of reach. For example, the lack of information on the previous layer denies the evaluation of wetting angles and cross-section surfaces. Thus, layers height is assumed to be equal to the highness of the considered wall minus the highness of the wall with a lower number of layer by one. The width will be discussed in the following paragraphs.

Concerning the weld bead radius of the ultimate layers, it appears here that the temperature influences its value in the same way as in the previous experiments. However, it seems to be rather unchanged with the underneath number of layer as illustrated Figure 3.4.17.

### 3.4 First discussions on weld bead shape evolutions

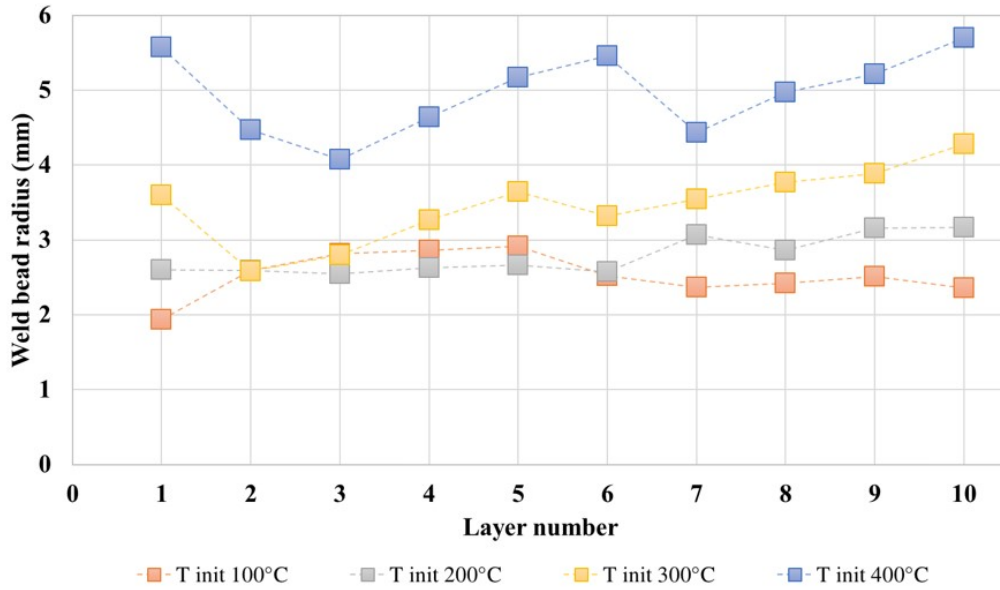


Figure 3.4.17 : Radius of the last layers of walls

Despite the fact that we do not have access to the previous layers for each wall, analysis on the total highness bring interesting information. As visible in Figure 3.4.18, walls height seems to follow a linear law according to the number of layers. Therefore, estimating the final highness of a wall can be easily done, on the number of layers and the initial temperature, as the linear coefficient seems driven by this parameter. As expected, the rise of the temperature induces a loss in the total height. The fact that it follows a linear law means that, except for the first layer, where the geometrical environment is different, every successive layer should present the same height, equivalent to the linear coefficient. This relation between the amount of layer and the total highness induces that the first weld bead presents a greater height compared to successive beads. Values extracted from these equations are very close to the ones determined in the first experiment.

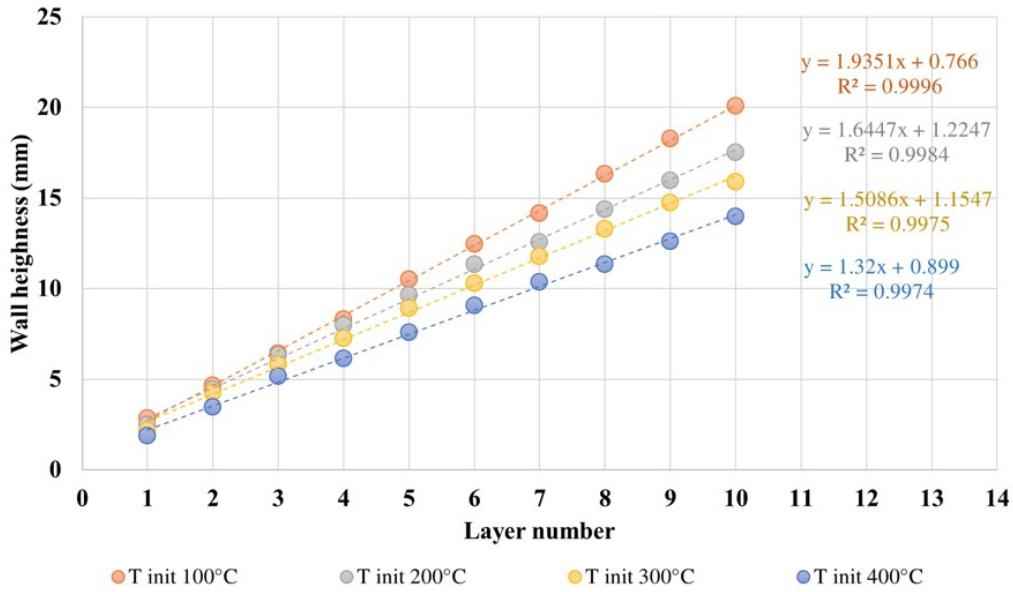


Figure 3.4.18 : Walls heights

Finally, since it is not possible to have access directly to the width and the wetting from the circular model, hypotheses are made. Considering that radius and layer height are relatively constant inside a wall and that this height value is smaller than the radius, it is assumed that the wetting angle is lower than  $90^\circ$ . Moreover, the width should be constant and it is proposed to estimate its value equal at two times the radius, at least when the bead is not collapsed. In order to verify this last assumption, the average width of walls has been extracted from scans and compared to the radius obtained through our fitting process. As shown in Figure 3.4.19, these data seem to confirm our hypothesis, especially for initial temperatures ( $T_{init}$ ) up to  $300^\circ\text{C}$ . Unfortunately, it appears to introduce a deviation about 2 mm for the highest initial temperature ( $T_{init}$ ). It might be caused by different factors, either that the temperature reaches a too high value and the weld bead collapsed or the circular model is not relevant anymore or also that specific phenomena are missed.

3.4 First discussions on weld bead shape evolutions

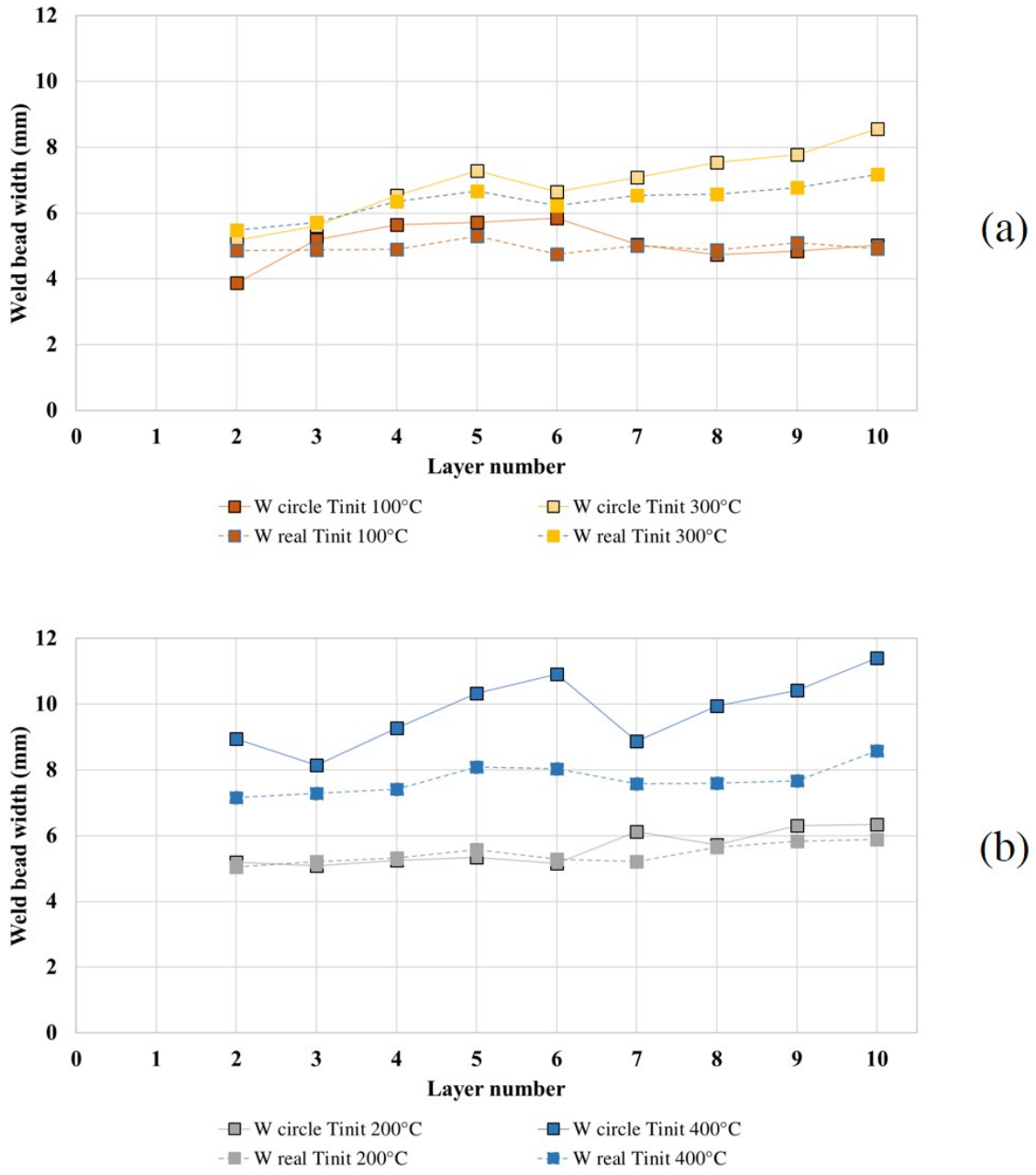


Figure 3.4.19 : Comparison of widths between data extracted from scans and circle models.

## Conclusion

In this chapter, the process of transforming a physical weld bead in a geometrical model with quantified data has been described. These data have then been studied in regards with experimental parameters such as initial temperature ( $T_{init}$ ), surface deposition temperature ( $T_{dep}$ ), or substrate radius.

Starting from the experimental scanning technique, specific weld bead portions have been selected applying temperature simulation techniques to assist in the identification of a stable the zone. It was found that the middle of the weld was an essential zone due to relatively stable conditions. There, cross-section profiles have been extracted every 1 mm. For all profiles, an algorithm allowed to fit a circle model giving access to representative weld bead data such as radius ( $r$ ), height ( $h$ ), width ( $w$ ), wetting angle ( $\theta$ ) and cross-section area ( $A$ ). As these information are gathered from a theoretical representation, a short verification have been set up in order to verify their accuracy. Precisions have been found around  $\pm 0.05$  mm and 0.2 mm, respectively, for the representation of height and width, confirming the validity of the circular model and its implementation. Results of experiment are remembered in the next paragraphs.

Single weld bead on flat substrate were deposited with fixed welding parameters,  $WFS = 5$  m/min and  $TS = 60$  cm/min and different initial temperatures ( $T_{init} = 25^\circ\text{C}$ ,  $100^\circ\text{C}$ ,  $200^\circ\text{C}$ ,  $300^\circ\text{C}$ , and  $400^\circ\text{C}$ ). As one can expect, the rise of the initial temperature, and thus of  $T_{dep}$ , induces a decrease in the viscosity of the liquid metal. This effect results in higher values of the radius ( $r$ ) and width ( $w$ ) of weld bead along with smaller heights. In short, a hotter metal will spread, forming a flatter bead. It seems that the temperature may also influence the quantity of deposited matter. It has been suggested that it might be related to the inner control of the welding station and should be further studied.

The introduction of different substrate geometry for the 2<sup>nd</sup> experiment, in terms of curvature ( $\emptyset 7$ ,  $\emptyset 8$ ,  $\emptyset 9$ ,  $\emptyset 10$ ,  $\emptyset 12$ ,  $\emptyset 16$ ,  $\emptyset 20$ ,  $\emptyset 25$ ,  $\emptyset 30$  and  $\emptyset 35$  mm), confirms this tendency and reveal a special influence of the substrate radius. In this way, it is recalled here that this radius have a direct influence on  $T_{dep}$ , additionally on  $T_{init}$ . Thus, weld bead radius ( $r$ ) and width ( $w$ ) seem to be only correlated to the temperature of deposition. However, it appears that the substrate curvature influences the wetting angle ( $\theta$ ) and the height ( $h$ ), not only through its implications on the temperature but also through a specific role. We suggest that the temperature fixes the surface tension, and thus the radius ( $r$ ), and that the matter, being rather

constant in quantity, only spreads more or less around the cylinder, depending on its temperature and its radius ( $r$ ). These intricate interactions highlight the importance for a weld bead deposition model through machine learning for weld predicting. In the next chapter, Chapter 4, such a model will be presented and tested.

Next experiment have consisted in a deposition of several weld beads. First, lateral deposition have been tested on a flat surface with the same welding parameters. However, only two values for the initial temperature ( $T_{init}$ ) have been implemented, at 300°C and 400°C. The first result of this experiment is that, as each weld bead is deposited at the exact same  $T_{init}$ , there is no difference in geometry between secondary weld beads. Being the second one or the 10<sup>th</sup>, each weld bead will present the same shape and dimensions. Radius ( $r$ ), height ( $h$ ) and width ( $w$ ) are not affected by the weld bead numerical position. Differences are found though between the very first weld bead and its following. Radius ( $r$ ) and width ( $w$ ) are found with higher values, while the wetting angle tends to be lowered. However, heights and amounts of deposited matter seem to be constant even over first and secondary weld beads.

Finally, weld beads have been stacking up to 10 layers in the vertical direction. Here, wall have been produced keeping identical welding parameters and four different initial temperature (100°C, 200°C, 300°C, and 400°C). Walls have been produced for each number of layers (4 different  $T_{init}$  and 10 layers giving thus 36 walls). Every weld bead has been deposited at the exact temperature corresponding to its definition. As scans have been performed at the end of production, extracted information are only available for the last layer. It appears that weld beads radius ( $r$ ), width ( $w$ ) and height ( $h$ ) do not depend on the layer number (except for the very first one like for the previous experiment) but rather rely on the initial temperature ( $T_{init}$ ).

All those experiments confirm that the temperature is a key parameter to understand and predict the geometry, and later properties, of parts manufactured by WAAM. The next chapter presents the interpolation of weld bead shape by using Multi-layers perceptron (MLP) techniques. The built model helps to interpolate the shape of the weld bead and predict parts shapes.



# Chapter 4

## Interpolation & Validation

Predicting weld bead shape (width and height) is essential for toolpath determination. From the information concerning the weld bead shape measured from the experiments described in Chapter 3, this chapter describes an artificial neural network model for interpolating the weld bead shape relative to the controllable process parameters (wire feed speed, travel speed) and non-controllable one (surface deposition temperature and substrate radius). Multi-layer perceptrons (MLPs) tools predicted the weld bead shape of experiment 2: a single weld bead on a cylinder substrate. As material deposit on a cylindrical curved surface (symmetrical). The focus is on predicting the weld bead shape deposited on a cylindrical surface. This explains the weld bead shape prediction as see in Figure 4.0.1. It is presented in the next section.

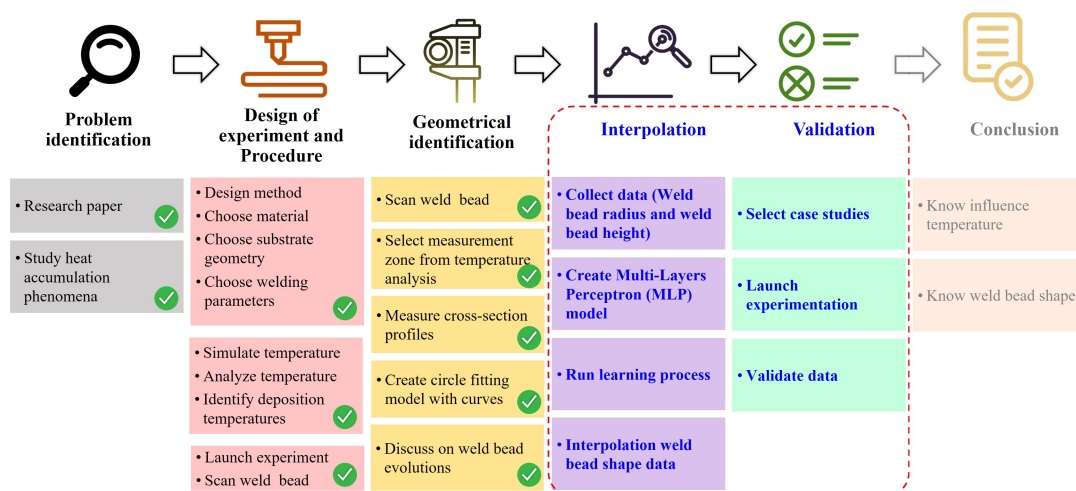


Figure 4.0.1 : Interpolation & validation approach



## 4.1 Data collection

The data collected are coming from the Exp.2 result. This experiment performs deposition on a cylinder of various diameter ranging from 3.5 to 17.5 mm. It has been done with various initial temperatures ( $T_{init}$ ) are 25°C, 100°C, 200°C, 300°C, and 400°C. The surface deposition temperatures ( $T_{dep}$ ) are obtained by thermal simulation (Chapter 2). The controllable process parameters are chosen as follows: a 5 m/min wire feed speed ( $WFS$ ) and a travel speed ( $TS$ ) of 0.60 m/min. The substrate radius is the radius of the cylinder substrate. The output parameters identified on the weld bead are its radius and height as presented in Chapter 3. All the input and output parameters are summarized in Table 4.1 All these data are gathered to create a model for predicting the weld bead shape.

Table 4.1 : Weld beads measurements

No.	$T_{init}$ (C°)	Input					Output	
		$T_{dep}$ (C°)	$WFS$ (m/min)	$TS$ (m/min)	$D$ (mm)	$R_{sub}$ (mm)	$r$ (mm)	$h$ (mm)
1	25	638.29	5	0.60	Ø7	3.50	3.33	0.79
2	25	597.66	5	0.60	Ø8	4.00	2.52	1.34
3	25	576.45	5	0.60	Ø9	4.50	2.49	1.34
4	25	535.98	5	0.60	Ø10	5.00	2.02	1.63
5	25	515.07	5	0.60	Ø12	6.00	2.02	1.52
6	25	468.43	5	0.60	Ø16	8.00	1.92	1.86
7	25	447.50	5	0.60	Ø20	10.00	1.87	2.09
8	25	436.21	5	0.60	Ø25	12.50	1.82	2.27
9	25	429.88	5	0.60	Ø30	15.00	1.79	2.37
10	25	427.98	5	0.60	Ø35	17.50	1.76	2.47
11	100	662.23	5	0.60	Ø7	3.50	3.25	0.50
12	100	607.03	5	0.60	Ø8	4.00	2.77	0.88
13	100	597.54	5	0.60	Ø9	4.50	2.73	1.04
14	100	566.81	5	0.60	Ø10	5.00	2.56	0.76
15	100	546.61	5	0.60	Ø12	6.00	2.44	1.15
16	100	510.72	5	0.60	Ø16	8.00	2.22	1.55
17	100	491.51	5	0.60	Ø20	10.00	2.08	1.81
18	100	482.68	5	0.60	Ø25	12.50	1.90	2.10

Table 4.1 : Weld beads measurements

No.	$T_{init}$ (C°)	Input					Output	
		$T_{dep}$ (C°)	$WFS$ (m/min)	$TS$ (m/min)	$D$ (mm)	$R_{sub}$ (mm)	$r$ (mm)	$h$ (mm)
19	100	477.75	5	0.60	Ø30	15.00	1.95	2.14
20	100	427.98	5	0.60	Ø35	17.50	1.79	2.42
21	200	696.28	5	0.60	Ø7	3.50	3.99	0.93
22	200	625.18	5	0.60	Ø8	4.00	3.62	0.44
23	200	609.75	5	0.60	Ø9	4.50	2.99	0.85
24	200	598.04	5	0.60	Ø10	5.00	3.02	0.80
25	200	587.48	5	0.60	Ø12	6.00	2.70	0.96
26	200	555.40	5	0.60	Ø16	8.00	2.52	1.39
27	200	541.59	5	0.60	Ø20	10.00	2.31	1.65
28	200	535.38	5	0.60	Ø25	12.50	2.13	1.81
29	200	531.90	5	0.60	Ø30	15.00	2.16	1.94
30	200	530.89	5	0.60	Ø35	17.50	2.18	2.04
31	300	631.75	5	0.60	Ø9	4.50	3.66	0.31
32	300	610.49	5	0.60	Ø10	5.00	3.80	0.33
33	300	604.71	5	0.60	Ø12	6.00	3.15	0.71
34	300	594.04	5	0.60	Ø16	8.00	2.92	1.13
35	300	585.51	5	0.60	Ø20	10.00	2.69	1.39
36	300	580.64	5	0.60	Ø25	12.50	2.69	1.54
37	300	577.44	5	0.60	Ø30	15.00	2.56	1.72
38	300	576.54	5	0.60	Ø35	17.50	2.51	1.78
39	400	620.89	5	0.60	Ø12	6.00	4.99	0.31
40	400	607.83	5	0.60	Ø16	8.00	4.25	0.72
41	400	603.98	5	0.60	Ø20	10.00	3.60	1.08
42	400	602.30	5	0.60	Ø25	12.50	3.85	1.23
43	400	601.38	5	0.60	Ø30	15.00	3.65	1.44
44	400	601.14	5	0.60	Ø35	17.50	3.38	1.58

This experiment has produced enough samples to launch a prediction model. The next section gives an overview of Artificial Neural Network (ANN) and the reason why the MLP regression model is chosen for this research.

## 4.2 Artificial Neural Network (ANN) and Multi-Layers Perceptron (MLP) model creation

### State of the art

Artificial neural networks (ANN) have been suggested in the field of additive manufacturing to optimize process parameters in order to obtain a good part quality. The weld bead shape is an important parameter to predict and manage. It is hard to develop an appropriate mathematical model for predicting the shape of a weld bead in a constantly changing welding process. There are many factors that affect the weld bead. [58] describes the neural network model as a viable method for predicting weld bead geometry. The neural network model was trained using back-propagation and the Levenberg-Marquardt training method. The results were built using the neural network and a mathematical model. The designed neural network is markedly more accurate than the regression equations [111]. [68] proposed an artificial neural network (ANN) model for predicting the weld bead geometry with a changing travel speed ( $TS$ ). [85] studied the three outputs of the weld beads *i.e.* the depth of penetration ( $DOP$ ), weld pool width ( $WW$ ), and reinforcement height ( $RH$ ). Four input parameters are welding voltage ( $WV$ ), welding current ( $WC$ ), welding speed ( $WS$ ), and flow rate ( $FR$ ). A back-propagation neural network (BPN) is used for the prediction of the weld bead geometry. The BPN model correctly predicts the shape of the weld bead with a high level of accuracy. [18] used the BPN model to predict weld bead geometry as well. The input parameters are welding current, welding speed, torch work angle, and molten pool width. Then, the results showed that this model could be used to predict the penetration of asymmetrical fillet welds. This is practical and reasonable for weld bead geometry.

[74] presented a prediction model to predict the weld bead geometry. There are three input parameters: plate thickness ( $t$ ), travel speed ( $TS$ ), and wire feed speed ( $WFS$ ). When one of them changes, the interpolation approach is used to create a new weld profile. If these parameters are not found in the database, the program uses the interpolation approach to get the maximum (P2) and lowest (P1) values

for each parameter.

The literature review on Artificial Neural Networks (ANNs) shows the prediction of weld bead shape relative to several inputs welding parameters (controlled) such as wire feed speed, travel speed, arc current, and flow rate. However, these variables are not covered with enough characteristics to predict the weld bead shape. Some of the variables that occur during the deposition process are surface temperature deposition ( $T_{dep}$ ) and actual surface geometry that we can consider as non-directly controlled parameters. These added variables play an essential role in predicting the weld bead shape and are the novelty of this research.

Artificial Neural Networks (ANNs) is largely established in Artificial Intelligence (AI) [58]. An Artificial Neural Networks (ANNs) usually involves a large number of processors running in parallel and arranged into levels as shown in Figure 4.2.1. The initial layer will receive raw input data, which is similar to the function of the brain and neural biological cell processing [111]. The neural structure is able to perform tasks: for example, classification, prediction, decision-making, visualization and others. Each successive level receives an output from the previous level and the last level generates the system output. This means that they will adapt as they learn from the initial training and subsequent runs [64]. The most basic learning model focuses on weighting the input stream. This is how each node weighs the importance of input from previous generations. The inputs leading to the correct answer have a higher weight. ANNs are usually trained from a lot of initial data. The training of the ANNs is accomplished through a learning process. During the training process, weights are modified to minimize output error. Sample data are processed by the network during the training process, and the weights are modified to better approximate the desired output [98].

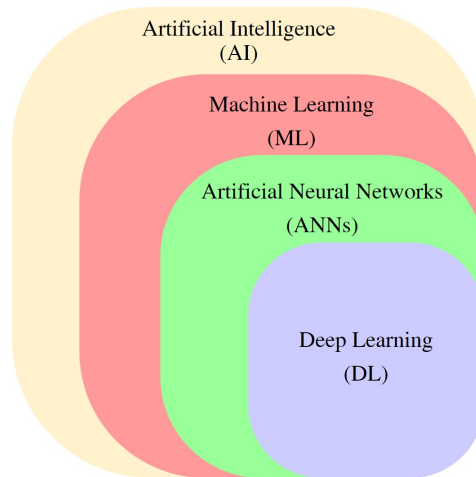


Figure 4.2.1 : Overview of Artificial Intelligence (AI) [64]

The types of neural networks are presented below. [14]

- Recurrent Neural Networks (RNNs)
- Convolutional Neural Networks (CNNs)
- Multi-layer Perceptrons (MLPs)

A multi-layer perceptrons (MLPs) or multi-layer neural network is a feed-forward artificial neural network (ANN) that maps the input data set to the appropriate output set. Also known as ANN feed-forward, a fully connected MLP consists of multiple layers of nodes in a directed graph. Each layer is completely connected to the next node except the input node. Each node is a neuron. MLP uses a supervised learning technique. The back-propagation network training, the MLP is an adaptation of the standard linear perception [78, 72]. MLP networks are an adaptation of one or more nonlinear hidden layers and a linear output layer. Each layer may contain one or more nonlinear processing units called neurons or nodes [38].

Among the several types of ANN, Multi-Layers Perceptrons (MLPs) have the objective to solve the following: Classification: A prediction model involves predicting a class label or class label probability for a determined input. Regression: Regression is a kind of predictive modeling that involves predicting a numeric result from a set of inputs. Therefore, regression solves the problem of a quantity predicting multiple input variables [98, 77]. For this research, Multi-Layers Perceptron (MLPs) regression was chosen to predict weld bead shape.

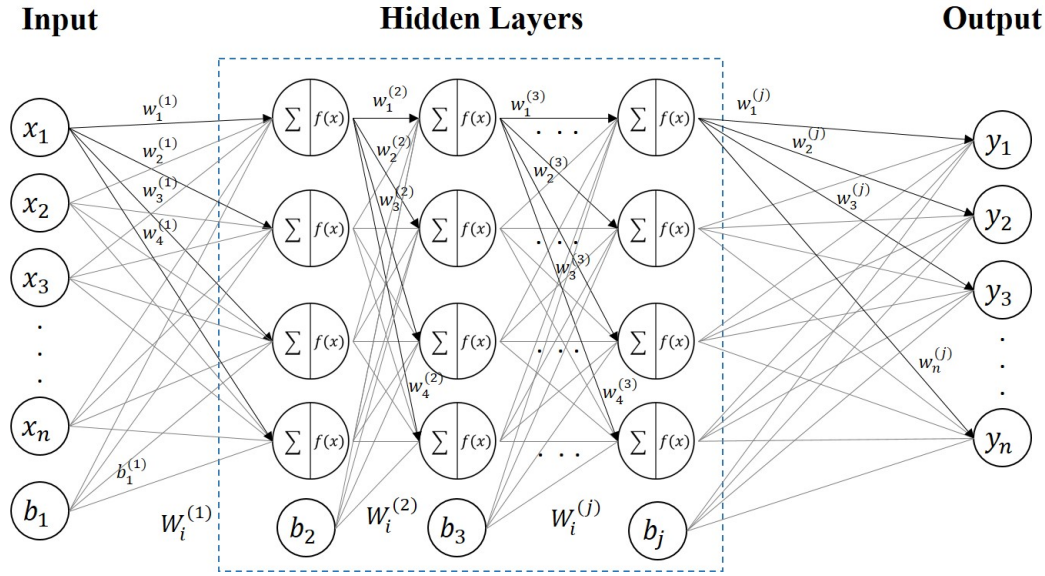


Figure 4.2.2 : Architecture of Multi-layers perceptron (MLPs) neural network [114]

The general architecture of MLP is presented in Figure 4.2.2 a neural network made of interconnected neurons. The network architecture can be divided into three main layers:

- Input layer : This is the first layer of the network, which accepts input and converts it into an output.
- Hidden layer : At least one hidden layer is required in the network. The hidden layers conduct calculations and operations on the incoming data to generate anything meaningful.
- Output layer : This layer is made up of neurons that produce the output variables.

Each neuron is characterized by its bias, its weight and its activation function. The input is feed to the input layer. The neurons perform linear conversion on this input using weights and bias. For instance, the equation 4.2.1

$$y_n = f \left[ \sum_j^n ((w_j^{(j)} * x_n) + b_j) \right] \left[ \sum_{i=1}^n ((w_n^{(1)} * x_n) + b_1) \right] \quad (4.2.1)$$

where  $y_n$  is the output of the neuron,  $f$  is the non-linear activation function,  $w$  is the random weight,  $w$  is the number of neurons in the previous layer,  $x_n$  is the input value,  $b$  is a bias. In neural networks, activation functions are conducted to transform

the weighted sum of input and biases to output. The use of activation functions assists the learning of high order polynomials beyond a single degree for deep neural network training by transforming linear input signals and modeling them as non-linear output signals. A particular property of the non-linear activation functions is that it is differentiable, which is very important. This allows them to function while being trained using the backpropagation technique. A neural network with numerous hidden layers and an output layer is known as a deep neural network [97].

Activation functions are an essential part of the neural network. The kind of neural network design determines which activation function is applied in hidden layers. This research chosen Multi-Layers Perceptron (MLPs) regression. Therefore, The ReLU activation function will be used in modern neural network models with common topologies, such as MLP and CNN [15] as show in Figure 4.2.3.

Rectified Linear Units (ReLU) is an activation function with strong biological and mathematical foundations. It was shown to enhance deep neural network training in the future [3]. It works by thresholding values at 0, i.e.  $f(x) = \max(0, x)$ . Simply put, it outputs 0 when  $x < 0$ , and conversely, it outputs a linear function when  $x \geq 0$  as shown in Figure 4.2.4 and equation 4.2.2.

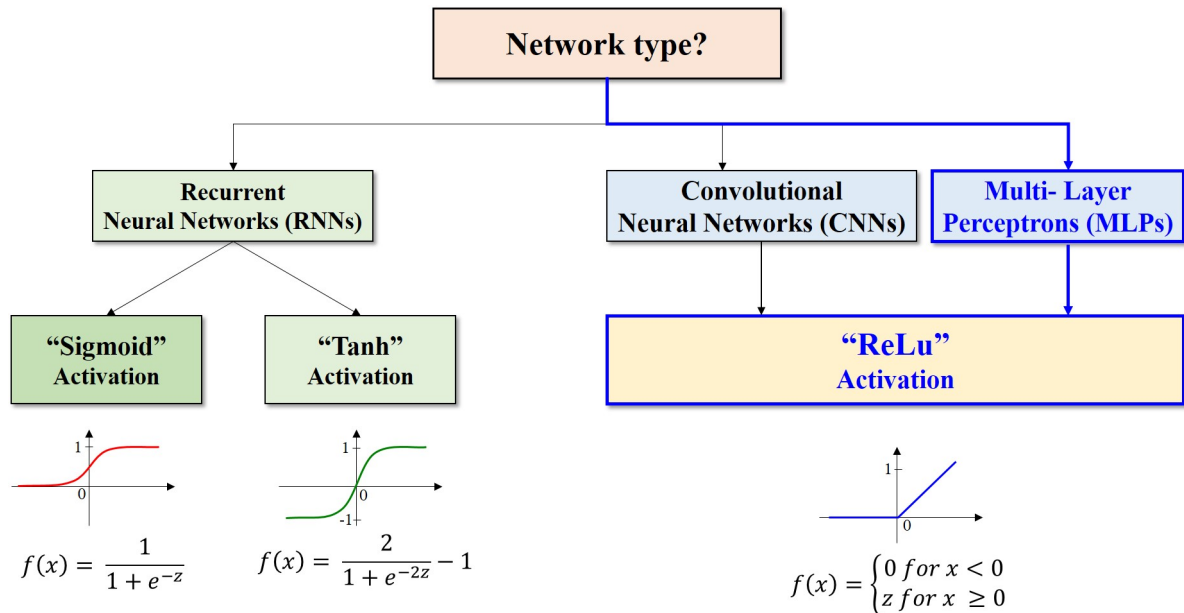


Figure 4.2.3 : How to choose an hidden layer activation function [14]

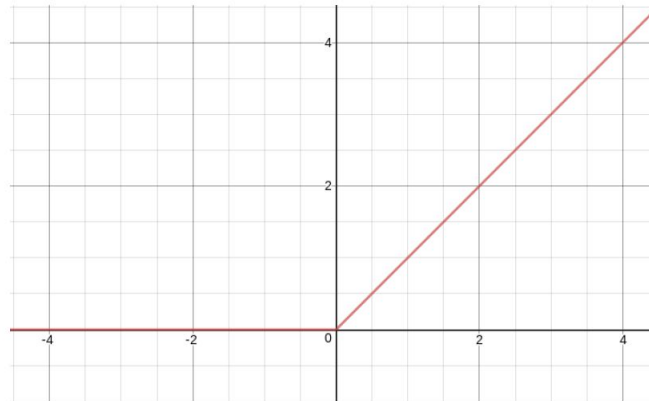


Figure 4.2.4 : The Rectified Linear Activation (ReLU) function [3]

$$f(x) = \begin{cases} 0 & \text{for } x < 0 \\ x & \text{for } x \geq 0 \end{cases} \quad (4.2.2)$$

To conclusions, this section presented the structure of the MLP regression model, which is essential in this research. The following section presents the application of the model to this research. First, a MLP regression model is used to predict the shape of the weld bead. Then, the MLP regression model is trained based on the experiments results. The MLP regression model will begin to predict the weld bead shape of experiment 4: a single weld bead on a cylinder substrate. It is an experiment on a cylindrical curved surface (symmetrical), that makes the initial modeling possible. Therefore, the model focuses mainly on predicting the shape of the weld bead deposited on a cylindrical surface and this is presented in the next section.

### 4.3 Training & Learning process

In this research, an attempt is made to construct a single multi-output MLP model to interpolate the weld bead shapes with one network, as welding parameters and weld bead shapes are interrelated in such a way that the solution should always be considered as a set. Henceforward, solving all with one network is a more logical approach in this case [85]. The neural network models and training are written in Python using the scikit-learn neural network (MLP Regressor) learning library. MLP model has three type of layers: input layer, hidden layer and output layer as shown in Figure 4.3.1.



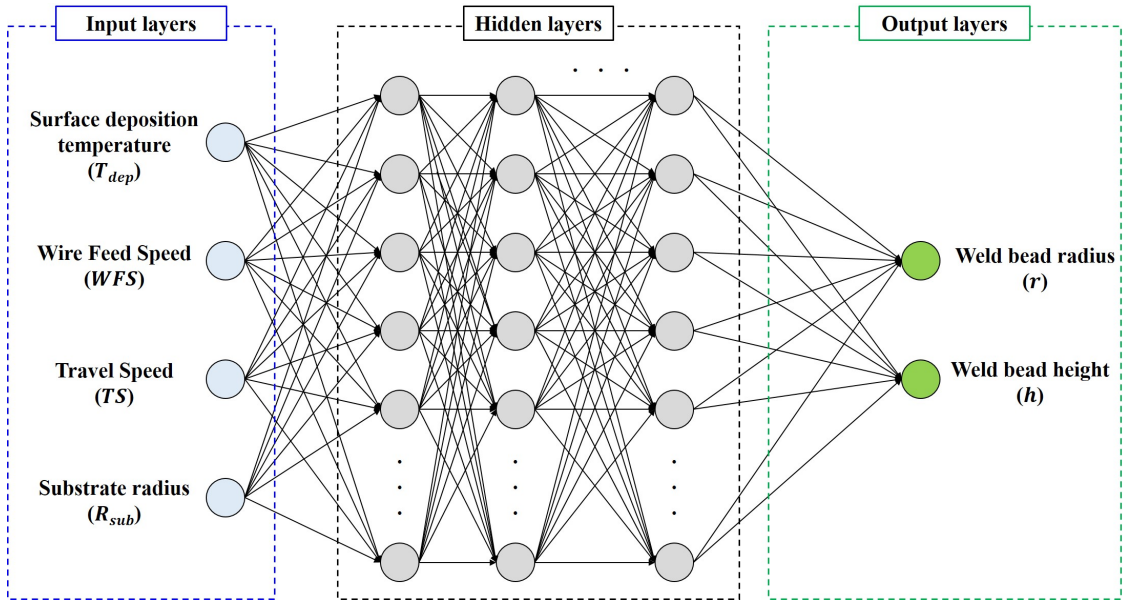


Figure 4.3.1 : Multi-Layer Perceptron (MLP) architecture for interpolating weld bead shape

Several welding parameters influence the weld bead shape. Typically, It has been observed that welding parameters or process temperature often cause heat accumulation that affects weld bead shape. Therefore, to predict the optimum weld bead shape, this model uses experimental data. The input parameters considered are the surface deposition temperature ( $T_{dep}$ ), the wire feed speed ( $WFS$ ), the travel speed ( $TS$ ), and the substrate radius ( $R_{sub}$ ). The output layer has two neurons, which gives the weld bead radius ( $r$ ) and height ( $h$ ). The weld bead shape is taken as the output parameter to design the framework of the model. The data set is divided into two parts; the training (80%) and testing (20%) data sets [101]. As shown in Table 4.1, this experimental data set contains a total of 44 samples. Therefore, the randomization is 35 training data sets, while the testing set will be selected from 9 samples. A coefficient of multiple determination calculates the accuracy of the network ( $R^2$ ). These networks have achieved good agreement with the training data and have yielded satisfactory modules. Neural network may effectively be implemented for estimating the weld bead shape. The results from the experiments indicate a relative error (%) between the predicted and experimental values as shown in Figure 4.3.2.

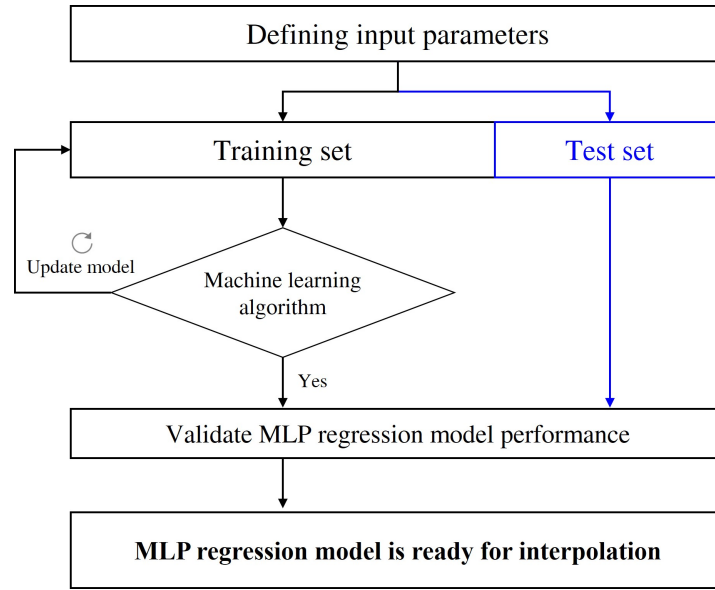


Figure 4.3.2 : Flowchart of the Machine Learning process [21]

The objective is to determine the best performance of the model based on the experiment and which can be used to predict the weld bead shape.

## 4.4 Interpolation analysis

### 4.4.1 Training procedure

The neural network configuration for the training set is created and formulated in Python with the specification given in Table 4.2. The training input is 4 neurons, the number of hidden layer is 1-5 layers, the number of neurons in hidden layers is 1-100 neurons, the output layer has 2 neurons, the activation function is ReLu, the maximum number of epoch is set 100 (with a step of 10), the training function is MLP Regression and the performance function is R-square ( $R^2$ ). Different number of hidden layers and number of neurons for each hidden layer has been tested as shown Table 4.3. in order to identify the optimum network structure. Finally the best setting in term of  $R^2$  has been chosen *i.e.* 3 hidden layer composed of 47 neuron each.

Table 4.2 : MLP regression model configuration for the training in Python

Parameter	Specification	Unit
Input	4	neuron
No. of hidden layer	1-5	layers
No. of neurons in hidden layer	1-100	neuron
Output	2	neuron
Activation function	ReLu	
Maximum epochs	100 (in steps of 10)	time
Training function	MLP Regression	
Performance function	R-squared ( $R^2$ )	

Table 4.3 : Training performance of difference network architecture

No.	Input	No. of hidden layer	No. of neurons in hidden layer	Output	Activation function	Maximum epochs	R-squared ( $R^2$ )
1	4	1	66	2	ReLu	10	0.8536
2	4	2	23-23	2	ReLu	10	0.7991
3	4	3	13-13-13	2	ReLu	10	0.8743
4	4	4	6-6-6-6	2	ReLu	10	0.8542
5	4	5	28-28-28-28-28	2	ReLu	10	0.8398
6	4	1	75	2	ReLu	20	0.8560
7	4	2	25-25	2	ReLu	20	0.8656
8	4	3	13-13-13	2	ReLu	20	0.8648
9	4	4	34-34-34-34	2	ReLu	20	0.8562
10	4	5	27-27-27-27-27	2	ReLu	20	0.8489
11	4	1	90	2	ReLu	30	0.8801
12	4	2	82-82	2	ReLu	30	0.8660
13	4	3	52-52-52	2	ReLu	30	0.8758
14	4	4	52-52-52-52	2	ReLu	30	0.8668
15	4	5	43-43-43-43-43	2	ReLu	30	0.8580

Table 4.3 : Training performance of difference network architecture

No.	Input	No. of hidden layer	No. of neurons in hidden layer	Output	Activation function	Maximum epochs	R-squared ( $R^2$ )
16	4	1	90	2	ReLu	40	0.8794
17	4	2	25-25	2	ReLu	40	0.8651
18	4	3	47-47-47	2	ReLu	40	0.8769
19	4	4	34-34-34-34	2	ReLu	40	0.8816
20	4	5	43-43-43-43-43	2	ReLu	40	0.8822
21	4	1	79	2	ReLu	50	0.8728
22	4	2	88-88	2	ReLu	50	0.0560
23	4	3	14-14-14	2	ReLu	50	0.8907
24	4	4	52-52-52-52	2	ReLu	50	0.8995
25	4	5	39-39-39-39-39	2	ReLu	50	0.8639
26	4	1	90	2	ReLu	60	0.8782
27	4	2	66-66	2	ReLu	60	0.8878
28	4	3	27-27-27	2	ReLu	60	0.8949
29	4	4	74-74-74-74	2	ReLu	60	0.8938
30	4	5	39-39-39-39-39	2	ReLu	60	0.8903
31	4	1	79	2	ReLu	70	0.8721
32	4	2	88-88	2	ReLu	70	0.8711
33	4	3	14-14-14	2	ReLu	70	0.8894
34	4	4	52-52-52-52	2	ReLu	70	0.9206
35	4	5	34-34-34-34-34	2	ReLu	70	0.8779
36	4	1	90	2	ReLu	80	0.8835
37	4	2	88-88	2	ReLu	80	0.8862
38	4	3	27-27-27	2	ReLu	80	0.8862
39	4	4	74-74-74-74	2	ReLu	80	0.9053
40	4	5	34-34-34-34-34	2	ReLu	80	0.8781
41	4	1	90	2	ReLu	90	0.9124
42	4	2	66-66	2	ReLu	90	0.8678
43	4	3	47-47-47	2	ReLu	90	0.9002
44	4	4	34-34-34-34	2	ReLu	90	0.9007
45	4	5	39-39-39-39-39	2	ReLu	90	0.8874

Table 4.3 : Training performance of difference network architecture

No.	Input	No. of hidden layer	No. of neurons in hidden layer	Output	Activation function	Maximum epochs	R-squared ( $R^2$ )
46	4	1	83	2	ReLu	100	0.8696
47	4	2	82-82	2	ReLu	100	0.8659
<b>48</b>	<b>4</b>	<b>3</b>	<b>47-47-47</b>	<b>2</b>	<b>ReLu</b>	<b>100</b>	<b>0.9223</b>
49	4	4	74-74-74-74	2	ReLu	100	0.8904
50	4	5	56-56-56-56-56	2	ReLu	100	0.8865

This neural network has then be used and the predicted radius ( $r$ ) and height ( $h$ ) for the 44 samples has been compared to the experimental results as shown Figure 4.4.1. In this figure the results are sorted by increasing value of the radius. The radius average relative error (%) between the experimental and the predicted radius is 6.38%. The height average relative error (%) between the experimental and the predicted height is 17.55%. Therefore, this prediction model is tested with on a case study to validate its ability to predict the built geometry. This is the object of the next section.

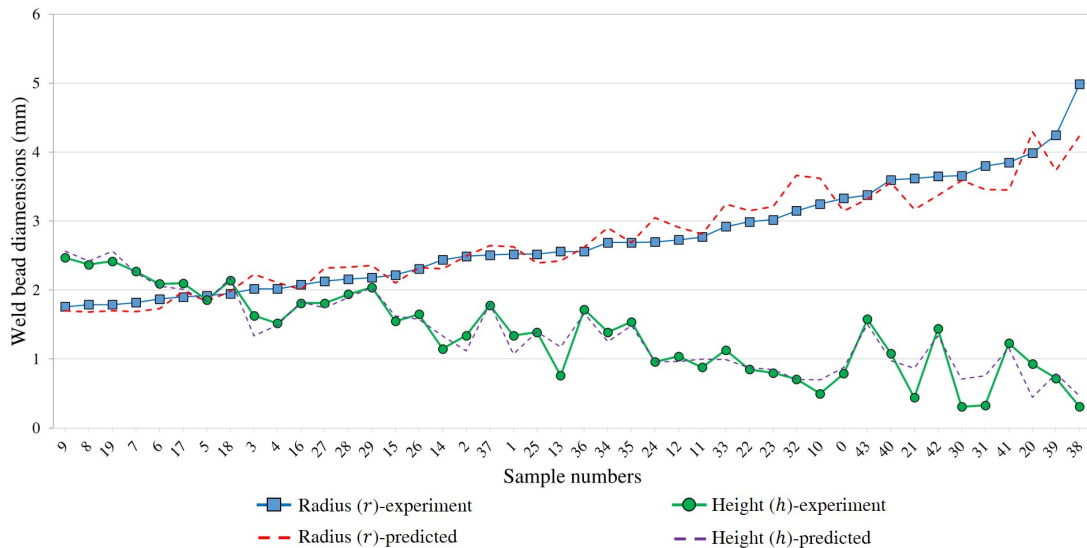


Figure 4.4.1 : Comparison of radius experiment and predicted values in data set

## 4.5 Validation

Figure 4.5.1 shows a case study proposed to validate the ability of the interpolation model to predict the built geometry. It consist in the built of a wall of 60 layers long of 60 mm. The welding parameters are wire feed speed ( $WFS$ ) = 5 m/min and travel speed ( $TS$ ) is 0.60 m/min. The welding trajectory is raster (bidirectional). The Dwell time is 2 sec per layer. The layer thickness (Z-axis direction) is 2.4 mm. First deposition temperature has been calculated as shown Figure 4.5.2. It was found that temperature increase drastically along the built due to short dwell time. The surface deposition temperature rises sharply from the fourth layer onwards, but there is a noticeable temperature difference between the deposition directions left-to-right ((L)→(R)) and right-to-left ((R)→(L)). The surface deposition temperatures are very different when considering the middle zone between the tenth to fifty millimeters of the weld bead. All thermal simulation result data are show in Appendix C: C.2.

Trajectory deposition: **Raster (bidirectional)**

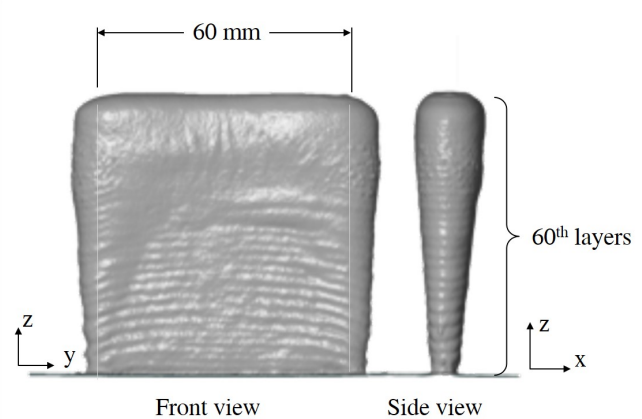
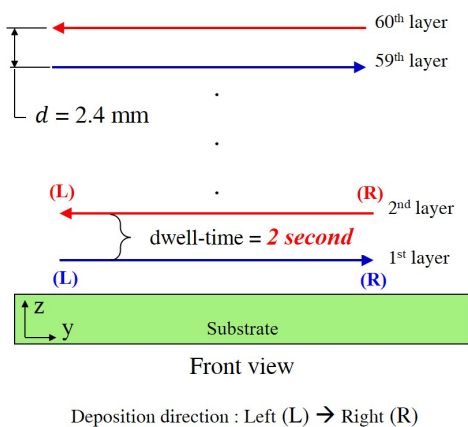


Figure 4.5.1 : Trajectory deposition and case study part

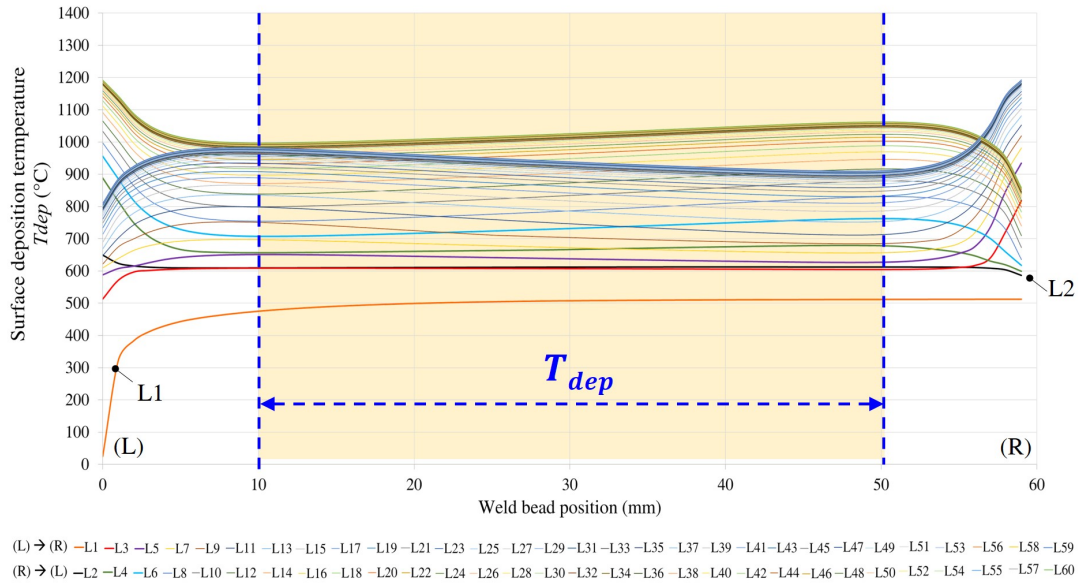


Figure 4.5.2 : Thermal simulation of case study

From these temperatures and the substrate surface geometry the weld bead geometry is predicted using the interpolation model (*i.e.* the neural network). The substrate geometry is flat for the first layer and cylindrical with the previous layer predicted radius for the next ones. Table 4.4 shows the prediction results for layer 1 to 8 and layer 60 and Figure 4.5.3 (a) shows the cross-section profile (A-A section) extracted from the built wall scan. Figure 4.5.3 (b) shows the weld bead shape prediction superposed with the cross-section of built wall. It is found that for the weld beads from layer 1 (L1) to layer 5 (L5), the prediction results are close to the cross-section of the built wall. In layer 6 (L6), the prediction results start to slip away from the experimental ones. The radius is 4.69 mm and the height 0.30 mm. For this layer  $T_{dep} = 638.88^{\circ}\text{C}$  which is over the maximum learning  $T_{dep}$ . The results continue to move away and for layer 8 (L8) of the predicted radius is 6.72 mm and the predicted height -0.47 mm. For this layer  $T_{dep} = 673.81^{\circ}\text{C}$ . The presented data shows that the weld bead prediction is different from the layer (L6) onwards. All weld bead dimension prediction data are shown in Appendix C: C.3.

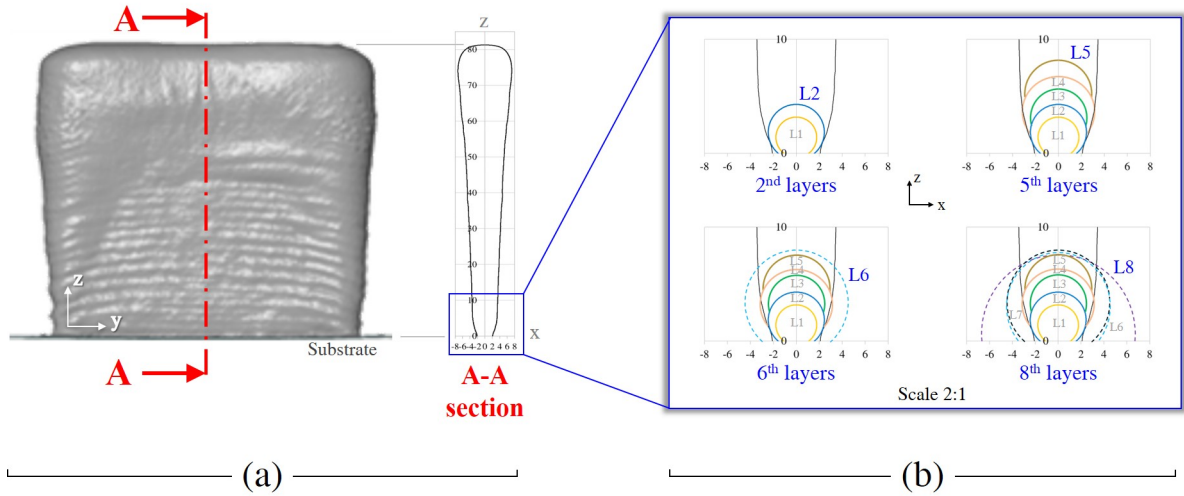


Figure 4.5.3 : Case study of weld bead cross-sections

Table 4.4 : Case study of weld bead dimension prediction data (L1 to L8)

No.	Input				Prediction output	
	$T_{dep}$ (°C)	$WFS$ (m/min)	$TS$ (m/min)	$R_{sub}$ (mm)	$r$ (mm)	$h$ (mm)
L1	503.19	5	0.60	Flat	1.77	3.17
L2	503.19	5	0.60	1.77	2.44	1.12
L3	611.29	5	0.60	2.44	2.44	1.14
L4	607.32	5	0.60	2.44	3.12	0.89
L5	667.70	5	0.60	3.12	2.92	0.96
L6	638.08	5	0.60	2.92	4.69	0.30
L7	733.34	5	0.60	4.69	4.53	0.36
L8	673.81	5	0.60	4.53	6.72	-0.47
.	.	.	.	.	.	.
.	.	.	.	.	.	.
.	.	.	.	.	.	.
L60	1,027.77	5	0.60	.	17.71	-4.60

It seems that prediction for  $T_{dep}$  over the maximum learning  $T_{dep}$  are not correct. To verify this point radius ( $r$ ) and height ( $h$ ) has been predicted for constant substrate radius,  $WFS$ ,  $TS$  and variable  $T_{dep}$  from 400°C to 1,000°C with an increment of 50°C. It is observed that for surface deposition temperature ( $T_{dep}$ ) over 650°C the



prediction starts to diverge. Weld bead height ( $h$ ) becomes lower and reach negative values indicating that the model fails to predict for surface deposition temperature ( $T_{dep}$ ) out of the training range. Figure 4.5.4 shows that for surface deposition temperature ( $T_{dep}$ ) over  $700^{\circ}\text{C}$  the weld bead height ( $h$ ) decreases to a negative value while the radius ( $r$ ) exceeds 4.5 mm. As a result, the accuracy of the weld bead prediction model is not suitable. Compared with the prediction data of the case study, L5 found that the radius ( $r$ ) and height ( $h$ ) is in the training data range (green region). On the other hand, the L6 radius is more significant than 4.5 mm outside the efficiency area, although the height is in the training data range (green region). Furthermore, L7 and L8 have the radius and height outside the training area of this model, resulting in imprecision on the weld bead dimensions prediction as well. Although, this prediction model has an initial performance accuracy of 92%. At the same time, case studies with different conditions and limitations validate the model effectiveness. It can be concluded that the surface deposition temperature ( $T_{dep}$ ) prediction does not exceed  $700^{\circ}\text{C}$  because the initial surface temperature model training is at a maximum of  $T_{dep} = 696.28^{\circ}\text{C}$ , which is results in a less effective of weld bead dimension prediction.

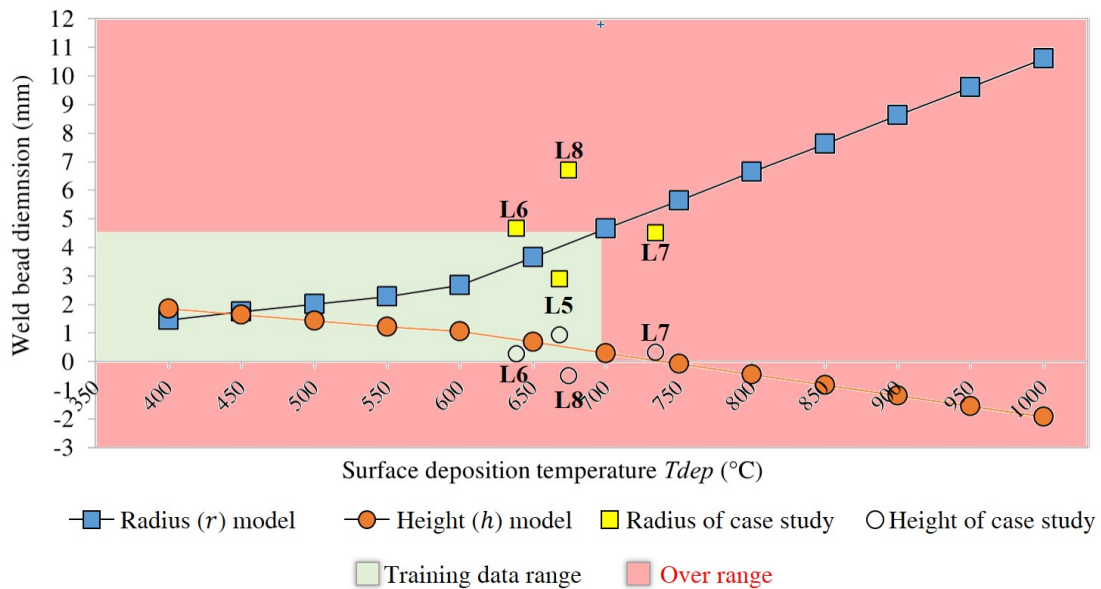


Figure 4.5.4 : Comparison between  $T_{dep}$  prediction and case study dimension

## Conclusion

The geometry of the weld bead (width and height) is critical for the deposition trajectory determination. However, determining the form of the weld bead from a physical model is difficult. Interpolating the geometric parameters from experimental results is an option. This chapter proposes to use an artificial neural network model to interpolate weld bead shape relative to controlled process parameter (wire feed speed ( $WFS$ ), travel speed ( $TS$ ), and uncontrolled factors (surface deposition temperature ( $T_{dep}$ ) and actual substrate radius ( $R_{sub}$ )). This neural network will then allow to predict the geometry of the weld bead depending on the process parameters and the uncontrolled factors. The prediction of the weld bead form when deposited on the substrate radius is accurate when we stay in the training range. However high level of errors appears when outside of this range and high level. We can then conclude that the interpolation model is not suitable for use outside of the training range.

The contributions of this chapter can be resumed as follows:

- *Data collection:* Data collection are from Exp.2 result. Thermal simulation allow to calculate the surface deposition temperature ( $T_{dep}$ ) as shown in Chapter 2. The welding parameters are constant with a 5 m/min wire feed speed ( $WFS$ ) and a travel speed ( $TS$ ) of 0.60 m/min. The substrate radius is variable. The circle fitting allows to calculate the radius and height of the weld bead in each sample (Chapter 3). Therefore, all these data are used to teach a model for interpolating the weld bead shape.
- *Multi-Layers Perceptron (MLP) model:* Multi-layers perception (MLP) regression can be used to interpolate many types of experimental results. For this research, Multi-Layers MLP regression is chosen to predict weld bead shape.
- *Training & learning process:* The model is based on experimental data for this investigation. The input parameters considered are surface deposition temperature ( $T_{dep}$ ), wire feed speed ( $WFS$ ), travel speed ( $TS$ ), and substrate radius ( $R_{sub}$ ). The output layer has two neurons, which gives the weld bead radius ( $r$ ) and height ( $h$ ). The data set is divided into two parts; the training(80%) and testing (20%) data sets.
- *Interpolation analysis:* The neural network configuration for the training set is created and formulated in Python with the specification. The input layer has 4 neurons, the number of hidden layers is 3 layers, the number of neurons

in hidden layers is 47 neurons, the output layer has 2 neurons, the activation function is ReLu, and the epochs are maximum 100 (with a step of 10) , the training function is MLP Regression. The R-square ( $R^2$ ) score determines the performance criteria.

- *Validation:* To verify the ability of the interpolation model to predict the built geometry, a case study has been proposed. Experimental and predicted results are compared. It shows that predictions are accurate when values stay in the learning range. However, the model is not suitable for use outside of the training range.

# Conclusion & Perspectives

## Conclusion

This research focuses on investigating the role of process parameters (direct and indirect) on weld beads shape deposited by Wire and Arc Additive Manufacturing (WAAM). WAAM process consist in melting a metallic wire and depositing it according to a defined trajectory. This technology generates heat during the fusion of the raw material. The difficulty of control we have on this thermal effect leads to various defects such as geometric deviation or poor mechanical properties. This is the critical reason for gaining knowledge in this matter. Therefore, as the first concern of this study relies on geometrical aspects, the objective is set as follow:

**“How to manage weld bead shape with regard to process parameters and heat accumulation around the deposition point?”**

The literature reveals the influence of WAAM process parameters on the shape of built parts. The term "process parameters" refers to the global WAAM process parameters split into welding parameters and deposition trajectories. In the literature, the direct influences of welding parameters are widely investigated and concern tension, intensity, travel speed and energy modulation. However, even if trajectory strategies are tackled, it is still rather badly known how the geometrical environment, such as substrate shape or trajectory, influences the weld bead dimensions. Especially, their crossed influences with the welding parameters on temperature are not enough considered yet. For this purpose, we managed to launch depositions at a fixed thermal state measured by the deposition temperature ( $T_{dep}$ ). In addition, we have proposed to control  $T_{dep}$ , which is the result of the cross influences of almost every other process parameters, through the experiment initial temperature ( $T_{init}$ ). The determination of  $T_{dep}$  relatively to  $T_{init}$ , and process parameters has been done thanks to a finite element simulation.

The goal of these simulations is to confirm that deposition temperature is stable and changes with regard to the initial temperature ( $T_{init}$ ), the welding parameters and the geometrical environment. Thus, four experiments are implemented in or-

der to cover as much configuration as possible. One set of welding parameters has been applied with five different initial temperatures, from room temperature up to 400°C, on four different geometrical configurations: single beads on flat surfaces and on cylinders with various diameters, lateral deposition on a flat surface, and finally walls of 10 layers. For every deposited weld bead, a specific attention is given to the initial temperature in order to insure its value at the start of every weld bead. The geometrical identification aims to associate simple geometrical models to the real shape. These simple models can be described with a limited number of parameters (here 2). With phenomenological or numerical models, the evolution of these parameters may be traced and even predicted. To this aim, physical weld beads are first scanned to create a numerical representation of their forms. Then, a zone of interest is determined to keep just the portions with constant processing circumstances (*i.e.*,  $T_{dep}$ ) for each experimental condition. As various transitory phenomena occur, such as process parameter variations or temperature behavior, the start and end of weld beads have been eliminated. This decision is based on the thermal simulation results. This showed that the middle zone of the weld bead was deposited at a relatively constant temperature. Hence, it is a suitable zone for the geometric identification. For this identification, first cross sections are extracted. Then, as far as a cylindrical model of the weld bead has been chosen, a circle is associated to each cross section using a mean square best fit. Information on width and height are then retrieved on each circle. Moreover, predicting the geometry of the weld bead (width and height) is critical to determine the correct deposition trajectory. Based on the data measured on the representative experiments, a neural network has been proposed and tested to interpolate weld bead radius and height over the controllable (wire feed speed, travel speed, and initial temperature ( $T_{init}$ )) and uncontrollable factors (surface deposition temperature ( $T_{dep}$ ) and actual substrate radius). We have fixed the objective to be able to predict the production of the wall composed by single weld bead. In order to build this model, data from Exp.2 have been used to train the ANN. This set of data is the most suited to reach this goal as this experiment has been designed on purpose to represent the stack of weld beads one on each other.

## Perspectives

The work presented in this manuscript could be deepened in the following areas:

### **Extension of the presented work to a wider range of welding conditions and materials**

The model proposes to characterize weld bead shape only in limited conditions and materials. It would be interesting, while time consuming, to extend the present work to variable  $WFS$ ,  $TS$ , substrate shape and materials. Such a work would require in the present condition at least 1 to 2h per weld bead. This work could be speeded up through online scanning, offline temperature conditioning and automation of the geometrical identification.

### **Determination of the optimal toolpath using knowledge**

The knowledge gained from this research concerns heat accumulation effects on the weld bead shape depending on CMT welding parameters (controlled and uncontrolled). Although it allows to predict the built shape, there is still some remaining work to use this knowledge to calculate the optimal toolpath and welding parameter values. This is part of the objectives of a French ANR project starting in G-SCOP laboratory.

### **Physical modeling of weld bead shape**

Generalizing the prediction of the weld bead geometry depending on controlled and uncontrolled process parameters is of key importance. This is not an easy task using a phenomenological model and a physical one would help. [75] presents the relationships between WAAM parameters and the deposited weld bead section based on a physical model. It's taking into account surface tension and hydrostatic pressure to calculate the contour of the section. Applying this model would help to generalize the present work. However, its analytical solving is only possible in specific cases described in [95] and a numerical solving would be a technical obstacle to overcome. In case such a solution would be achieved, the identification of physical parameters would also be a challenge.

## **Deposition shape control with a closed loop**

As energy input affects the temperature and consequently the weld bead shape and material properties, an incorrect thermal management can lead to geometrical defects and poor material health. To control in real time the deposition process is a key issue to manage the quality of the deposition. For example, using thermal imaging for no-contact thermal monitoring could be used to track heat accumulation before, during and after deposition in order to ensure appropriate thermal management and consequently, the geometric shape control. Indeed, a recent French ANR project has been launched in G-SCOP laboratory regarding this topic.

## **My personal perspective: development of additive manufacturing in Thailand**

This thesis can be applied to the author's future project in two ways as shown in Figure 5.0.1. One is an academic project, and another is an industrial project. First, my profession is lecturer in the department of Tools and Die engineering, one of the departments in faculty of engineering at Rajamangala University of Technology Lanna (RMUTL), Chiang Mai, Thailand. My responsibility is teaching and supervising students about plastic mould design, my major subject. This AM knowledge that I have reached in this thesis will be transferred to students as a new technology for making moulds. Today, the subtractive process is used as a mould-making process in Thailand. However, the problem of this subtractive process, in other words, its weak points, is the high cost of investment and significantly cutting tool. Moreover, it is a long process that always wastes our time. While the subtractive process is not the best choice nowadays, the new technology, AM, is a new way to solve these problems. In other words, AM is not only more friendly for our cost of mould making, but also it is time-saving. Therefore, we can predict that this AM technology will be a new trend in the future, especially in the industrial sectors of Thailand. That is why this thesis will be used as a knowledge base for building up students and help them prepare for their future careers.

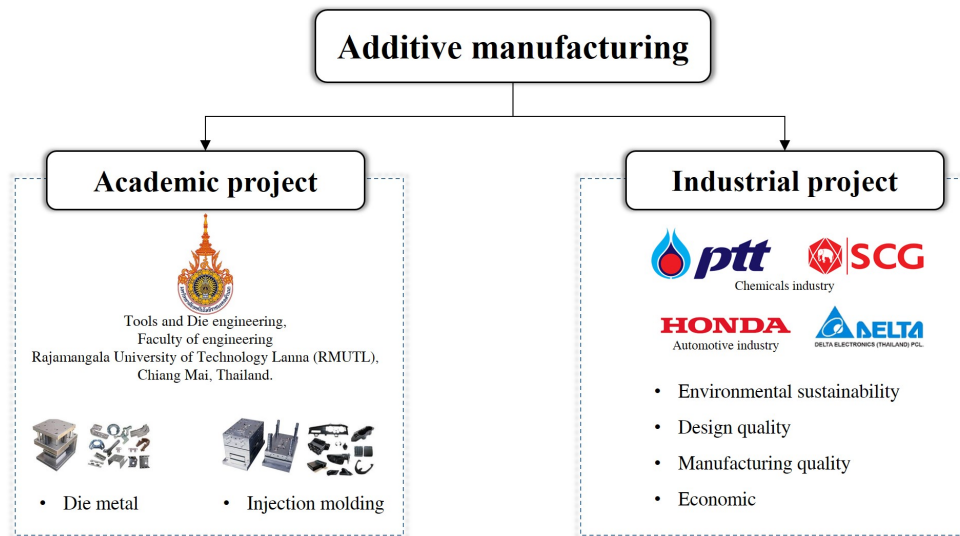


Figure 5.0.1 : The future projects in my career path

Furthermore, this AM research in this thesis will also be used in the industrial sector as Thailand is an industrial country. There are many industries, such as chemicals, electronics, automotive, and so on. Mould making is evidently a part of their manufacturing process. Although everything seems to run smoothly right now, if we look closely at it, these industries still use old technology, like the subtractive process. That's why the AM, the new technology, will help these industries in their mould-making process line. The benefices can be explained in 4 aspects. Environmental sustainability is the first aspect because, as we mentioned, the subtractive is the process of building the hold form of mould and then taking one part out to get the shape we want. While AM, we can build the whole mould without wasting the raw materials by making only the mould base. In other words, there is no exceeding part that we do not use. The second aspect is design quality. AM technology allows us to design many more shapes as we want with fewer limits than the old technology one. Moreover, the manufacturing quality is the third aspect of its advantage. The last one is the result of all three mentioned aspects. Finally, it is about an economic aspect. Using this AM technology, the industries will reduce their cost of raw materials and all of their capital (time, money, manpower) to make better-quality products to serve customers. Therefore, this thesis will transfer AM know-how to Thailand industries to help them develop their manufacturing processes, precisely, the mould-making process, re-manufacturing and repair. In addition, I desired to transfer the knowledge and know-how I have learned during my research to students and the industries in Thailand.



## List of published articles

### International conference

1. Supasit M., Frederic V., Matthieu M., and Maxime L. Process Parameters Effect on Weld Beads Geometry Deposited by Wire and Arc Additive Manufacturing (WAAM). *International Joint Conference on Mechanics, Design Engineering & Advanced Manufacturing, JCM 2020: Advances on Mechanics, Design Engineering and Manufacturing III*. pp.9-14. doi : 10.1007/978-3-030-70566-4\_3.
2. Supasit M., Frederic V., Matthieu M., and Maxime L. Model of weld beads geometry produced on surface temperatures by Wire and Arc Additive Manufacturing (WAAM). *11th International Conference on Manufacturing Science and Technology (ICMST 2020)*. IOP Conference Series: Materials Science and Engineering. 1063. September 2020. doi:10.1088/1757-899X/1063/1/012008.

# Bibliography

- [1] Adeyinka Adebayo. *Charecterisation of Intergrated WAAM and Machining Process*. PhD thesis, Cranfiled university, England, December 2013.
- [2] Mohamed Aesh. Optimization of Weld Bead Dimensions in GTAW of Aluminum-Magnesium Alloy. *Materials and Manufacturing Processes*, 16(5): 725–736, 2001. doi: 10.1081/AMP-100108632.
- [3] Abien Fred M Agarap. Deep Learning using Rectified Linear Units (ReLU). page 8, 2018.
- [4] Wurikaixi Aiyiti, Wanhua Zhao, Bingheng Lu, and Yiping Tang. Investigation of the overlapping parameters of MPAW-based rapid prototyping. *Rapid Prototyping Journal*, 12(3):165–172, May 2006. ISSN 1355-2546. doi: 10.1108/13552540610670744.
- [5] Z. Al-Nabulsi, J.T. Mottram, M. Gillie, N. Kourra, and M.A. Williams. Mechanical and X ray computed tomography characterisation of a WAAM 3D printed steel plate for structural engineering applications. *Construction and Building Materials*, 274:121700, March 2021. ISSN 09500618. doi: 10.1016/j.conbuildmat.2020.121700.
- [6] Pedro Almeida. *Process Control and Development in Wire and Arc Additive Manufacturing*. PhD thesis, Cranfield University, England, April 2012.
- [7] A. Aloraier, A. Almazrouee, T. Shehata, and John W. H. Price. Role of Welding Parameters Using the Flux Cored Arc Welding Process of Low Alloy Steels on Bead Geometry and Mechanical Properties. *Journal of Materials Engineering and Performance*, 21(4):540–547, April 2012. ISSN 1059-9495, 1544-1024. doi: 10.1007/s11665-011-9948-6.
- [8] Maider Arana, Eneko Ukar, Iker Rodriguez, Amaia Iturrioz, and Pedro Alvarez. Strategies to Reduce Porosity in Al-Mg WAAM Parts and Their Impact

- on Mechanical Properties. *Metals*, 11(3):524, March 2021. ISSN 2075-4701. doi: 10.3390/met11030524.
- [9] K F Ayarkwa, S Williams, and J Ding. Investigation of pulse advance cold metal transfer on aluminium wire arc additive manufacturing. *Int. J. Rapid Manufacturing*, 5(1):44–57, 2015. doi: 10.1504/IJRAPIDM.2015.073547.
- [10] Xingwang Bai, Paul Colegrove, Jialuo Ding, Xiangman Zhou, Chenglei Diao, Philippe Bridgeman, Jan Honnige, Haiou Zhang, and Stewart Williams. Numerical analysis of heat transfer and fluid flow in multilayer deposition of PAW-based wire and arc additive manufacturing. *International Journal of Heat and Mass Transfer*, page 13, 2018.
- [11] S Balamurugan and R Ranjith. Cold metal transfer (CMT) technology - A review. *International Journal of Pure and Applied Mathematics*, 119(12):12, 2018. ISSN 1314-3395 (on-line version).
- [12] Jørgen Blindheim, Øystein Grong, Ulf Roar Aakenes, Torgeir Welo, and Martin Steinert. Hybrid Metal Extrusion & Bonding (HYB) - a new technology for solid-state additive manufacturing of aluminium components. *Procedia Manufacturing*, 26:782–789, 2018. ISSN 23519789. doi: 10.1016/j.promfg.2018.07.092.
- [13] David Bourell, Jean Pierre Kruth, Ming Leu, Gideon Levy, David Rosen, Allison M. Beese, and Adam Clare. Materials for additive manufacturing. *CIRP Annals*, 66(2):659–681, 2017. ISSN 00078506. doi: 10.1016/j.cirp.2017.05.009.
- [14] Jason Brownlee. *Deep Learning With Python*. 2016.
- [15] Jason Brownlee. How to Choose an Activation Function for Deep Learning. <https://machinelearningmastery.com/choose-an-activation-function-for-deep-learning/>, January 2021.
- [16] John Canny. A Computational Approach to Edge Detection. page 20.
- [17] Yong Cao, Sheng Zhu, Xiubing Liang, and Wanglong Wang. Overlapping model of beads and curve fitting of bead section for rapid manufacturing by robotic MAG welding process. *Robotics and Computer-Integrated Manufacturing*, 27(3):641–645, June 2011. ISSN 07365845. doi: 10.1016/j.rcim.2010.11.002.

- 
- [18] Yushuo Chang, Jianfeng Yue, Rui Guo, Wenji Liu, and Liangyu Li. Penetration quality prediction of asymmetrical fillet root welding based on optimized BP neural network. *Journal of Manufacturing Processes*, 50:247–254, February 2020. ISSN 15266125. doi: 10.1016/j.jmapro.2019.12.022.
- [19] Mohammed Akram Chergui. *Simulation Based Deposition Strategies Evaluation and Optimization in Wire Arc Additive Manufacturing*. PhD thesis, Université Grenoble Alpes, France, March 2021.
- [20] Mohammed Akram Chergui, Nicolas Beraud, Frederic Vignat, and Francois Villeneuve. Finite Element Modeling and Validation of Metal Deposition in Wire Arc Additive Manufacturing. In *JCM 2020: Advances on Mechanics, Design Engineering and Manufacturing III*, Lecture Notes in Mechanical Engineering, pages 61–66, Aix-en Provence, France, 2020. Springer International Publishing. doi: 10.1007/978-3-030-70566-4\_11.
- [21] Mattia Chiesa, Giada Maioli, Gualtiero I. Colombo, and Luca Piacentini. GARS: Genetic Algorithm for the identification of a Robust Subset of features in high-dimensional datasets. *BMC Bioinformatics*, 21(1):54, December 2020. ISSN 1471-2105. doi: 10.1186/s12859-020-3400-6.
- [22] Michele Chiumenti, Miguel Cervera, Alessandro Salmi, Carlos Agelet de Saracibar, Narges Dialami, and Kazumi Matsui. Finite element modeling of multi-pass welding and shaped metal deposition processes. *Computer Methods in Applied Mechanics and Engineering*, 199(37-40):2343–2359, August 2010. ISSN 00457825. doi: 10.1016/j.cma.2010.02.018.
- [23] Baoqiang Cong, Ruijie Ouyang, Bojin Qi, and Jialuo Ding. Influence of Cold Metal Transfer Process and Its Heat Input on Weld Bead Geometry and Porosity of Aluminum-Copper Alloy Welds. *Rare Metal Materials and Engineering*, 45(3):606–611, March 2016. ISSN 18755372. doi: 10.1016/S1875-5372(16)30080-7.
- [24] Leandro João da Silva, Danielle Monteiro Souza, Douglas Bezerra de Araújo, Ruham Pablo Reis, and Américo Scotti. Concept and validation of an active cooling technique to mitigate heat accumulation in WAAM. *The International Journal of Advanced Manufacturing Technology*, 107(5-6):2513–2523, March 2020. ISSN 0268-3768, 1433-3015. doi: 10.1007/s00170-020-05201-4.

- [25] Leandro João da Silva, Henrique Nardon Ferraresi, Douglas Bezerra Araújo, Ruham Pablo Reis, and Américo Scotti. Effect of Thermal Management Approaches on Geometry and Productivity of Thin-Walled Structures of ER 5356 Built by Wire + Arc Additive Manufacturing. *Coatings*, 11(9):1141, September 2021. ISSN 2079-6412. doi: 10.3390/coatings11091141.
- [26] Djarot B. Darmadi, Anh Kiet Tieu, and John Norrish. A validated thermal model of bead-on-plate welding. *Heat and Mass Transfer*, 48(7):1219–1230, July 2012. ISSN 0947-7411, 1432-1181. doi: 10.1007/s00231-012-0970-5.
- [27] José Luis Dávila, Paulo Inforçatti Neto, Pedro Yoshito Noritomi, Reginaldo Teixeira Coelho, and Jorge Vicente Lopes da Silva. Hybrid manufacturing: A review of the synergy between directed energy deposition and subtractive processes. *The International Journal of Advanced Manufacturing Technology*, 110(11-12):3377–3390, October 2020. ISSN 0268-3768, 1433-3015. doi: 10.1007/s00170-020-06062-7.
- [28] Robert James Demey. *Development of Processing Strategies for the Additive Layer Manufacture of Aerospace Components in Inconel 718*. PhD thesis, The University of Sheffield, England, January 2012.
- [29] Karan Derekar, Jonathan Lawrence, Geoff Melton, Adrian Addison, Xiang Zhang, and Lei Xu. Influence of Interpass Temperature on Wire Arc Additive Manufacturing (WAAM) of Aluminium Alloy Components. *MATEC Web of Conferences*, 269:05001, 2019. ISSN 2261-236X. doi: 10.1051/mateconf/201926905001.
- [30] Dong-Hong Ding, Zeng-Xi Pan, Cuiuri Dominic, and Hui-Jun Li. Process Planning Strategy for Wire and Arc Additive Manufacturing. In Tzyh-Jong Tarn, Shan-Ben Chen, and Xiao-Qi Chen, editors, *Robotic Welding, Intelligence and Automation*, volume 363, pages 437–450. Springer International Publishing, Cham, 2015. ISBN 978-3-319-18996-3 978-3-319-18997-0. doi: 10.1007/978-3-319-18997-0\_37.
- [31] Donghong Ding, Zengxi Pan, Dominic Cuiuri, and Huijun Li. A tool-path generation strategy for wire and arc additive manufacturing. *The International Journal of Advanced Manufacturing Technology*, 73(1-4):173–183, July 2014. ISSN 0268-3768, 1433-3015. doi: 10.1007/s00170-014-5808-5.

- 
- [32] Donghong Ding, Zengxi Pan, Dominic Cuiuri, and Huijun Li. A multi-bead overlapping model for robotic wire and arc additive manufacturing (WAAM). *Robotics and Computer-Integrated Manufacturing*, 31:101–110, February 2015. ISSN 07365845. doi: 10.1016/j.rcim.2014.08.008.
- [33] Donghong Ding, Zengxi Pan, Dominic Cuiuri, and Huijun Li. Wire-feed additive manufacturing of metal components: Technologies, developments and future interests. *The International Journal of Advanced Manufacturing Technology*, 81(1-4):465–481, October 2015. ISSN 0268-3768, 1433-3015. doi: 10.1007/s00170-015-7077-3.
- [34] Donghong Ding, Zengxi Pan, Dominic Cuiuri, Huijun Li, Stephen van Duin, and Nathan Larkin. Bead modelling and implementation of adaptive MAT path in wire and arc additive manufacturing. *Robotics and Computer-Integrated Manufacturing*, 39:32–42, June 2016. ISSN 07365845. doi: 10.1016/j.rcim.2015.12.004.
- [35] Donghong Ding, Zengxi Pan, Stephen van Duin, Huijun Li, and Chen Shen. Fabricating Superior NiAl Bronze Components through Wire Arc Additive Manufacturing. *Materials*, 9(8):652, August 2016. ISSN 1996-1944. doi: 10.3390/ma9080652.
- [36] J. Ding, P. Colegrove, J. Mehnen, S. Ganguly, P.M. Sequeira Almeida, F. Wang, and S. Williams. Thermo-mechanical analysis of Wire and Arc Additive Layer Manufacturing process on large multi-layer parts. *Computational Materials Science*, 50(12):3315–3322, December 2011. ISSN 09270256. doi: 10.1016/j.commatsci.2011.06.023.
- [37] Rajeev Dwivedi and Radovan Kovacevic. Automated Torch Path Planning Using Polygon Subdivision for Solid Freeform Fabrication Based on Welding. *Journal of Manufacturing Systems*, 23(4):15, 2004.
- [38] Virginia Chika Ebhota, Joseph Isabona, and Viranjay M. Srivastava. Environment-Adaptation Based Hybrid Neural Network Predictor for Signal Propagation Loss Prediction in Cluttered and Open Urban Microcells. *Wireless Personal Communications*, 104(3):935–948, February 2019. ISSN 0929-6212, 1572-834X. doi: 10.1007/s11277-018-6061-2.
- [39] Engineering product design. Direct Energy Deposition (DED).

<https://engineeringproductdesign.com/knowledge-base/direct-energy-deposition/>, 2021.

- [40] Xuewei Fang, Lijuan Zhang, Guopeng Chen, Xiaofeng Dang, Ke Huang, Lei Wang, and Bingheng Lu. Correlations between Microstructure Characteristics and Mechanical Properties in 5183 Aluminium Alloy Fabricated by Wire-Arc Additive Manufacturing with Different Arc Modes. *Materials*, 11(11):2075, October 2018. ISSN 1996-1944. doi: 10.3390/ma11112075.
- [41] Xuewei Fang, Lijuan Zhang, Hui Li, Chaolong Li, Ke Huang, and Bingheng Lu. Microstructure Evolution and Mechanical Behavior of 2219 Aluminum Alloys Additively Fabricated by the Cold Metal Transfer Process. *Materials*, 11(5):812, May 2018. ISSN 1996-1944. doi: 10.3390/ma11050812.
- [42] Rafael Pereira Ferreira and Américo Scotti. The Concept of a Novel Path Planning Strategy for Wire + Arc Additive Manufacturing of Bulky Parts: Pixel. *Metals*, 11(3):498, March 2021. ISSN 2075-4701. doi: 10.3390/met11030498.
- [43] William E. Frazier. Metal Additive Manufacturing: A Review. *Journal of Materials Engineering and Performance*, 23(6):1917–1928, June 2014. ISSN 1059-9495, 1544-1024. doi: 10.1007/s11665-014-0958-z.
- [44] Fronius. *Fronius RCU 5000 Operating Manual*. 2017.
- [45] Jie Fu, Kun Qiu, Lin Gong, Changmeng Liu, Qianru Wu, Jiping Lu, and Hongli Fan. Effect of Tool-Path on Morphology and Mechanical Properties of Ti-6Al-4V Fabricated by Wire and Arc Additive Manufacturing. *MATEC Web of Conferences*, 128:05009, 2017. ISSN 2261-236X. doi: 10.1051/mateconf/201712805009.
- [46] Rui Fu, Shuiyuan Tang, Jiping Lu, Yinan Cui, Zixiang Li, Haorui Zhang, Tianqiu Xu, Zhuo Chen, and Changmeng Liu. Hot-wire arc additive manufacturing of aluminum alloy with reduced porosity and high deposition rate. *Materials & Design*, 199:109370, February 2021. ISSN 02641275. doi: 10.1016/j.matdes.2020.109370.
- [47] Ian Gibson, David W. Rosen, and Brent Stucker. *Additive Manufacturing Technologies: 3D Printing, Rapid Prototyping and Direct Digital Manufacturing*. Springer, New York London, 2nd edition edition, 2015. ISBN 978-1-4939-2113-3.

- 
- [48] Maximilian Gierth, Philipp Henckell, Yarop Ali, Jonas Scholl, and Jean Pierre Bergmann. Wire Arc Additive Manufacturing (WAAM) of Aluminum Alloy AlMg5Mn with Energy-Reduced Gas Metal Arc Welding (GMAW). *Materials*, 13(12):2671, June 2020. ISSN 1996-1944. doi: 10.3390/ma13122671.
- [49] John Goldak, Aditya Chakravarti, and Malcolm Bibby. A new finite element model for welding heat sources. *Metallurgical Transactions B*, 15(2):299–305, June 1984. ISSN 0360-2141, 1543-1916. doi: 10.1007/BF02667333.
- [50] J. González, I. Rodríguez, J-L. Prado-Cerqueira, J.L. Diéguez, and A. Pereira. Additive manufacturing with GMAW welding and CMT technology. *Procedia Manufacturing*, 13:840–847, 2017. ISSN 23519789. doi: 10.1016/j.promfg.2017.09.189.
- [51] M. Graf, K. P. Pradjadhiana, A. Hälsig, Y. H. P. Manurung, and B. Awiszus. Numerical simulation of metallic wire arc additive manufacturing (WAAM). In *PROCEEDINGS OF THE 21ST INTERNATIONAL ESAFORM CONFERENCE ON MATERIAL FORMING: ESAFORM 2018*, page 140010, Palermo, Italy, 2018. doi: 10.1063/1.5035002.
- [52] V. Gunaraj and N. Murugan. Prediction and Comparison of the Area of the Heat-Affected Zone for the Bead-on-Plate and Bead-on-Joint in Submerged Arc Welding of Pipes. *Journal of Materials Processing Technology*, 95(1-3): 246–261, 1999. doi: 10.1016/S0924-0136(99)00296-4.
- [53] Nannan Guo and Ming C. Leu. Additive manufacturing: Technology, applications and research needs. *Frontiers of Mechanical Engineering*, 8(3):215–243, September 2013. ISSN 2095-0233, 2095-0241. doi: 10.1007/s11465-013-0248-8.
- [54] Tobias Hauser, Raven T. Reisch, Philipp P. Breese, Benjamin S. Lutz, Matteo Pantano, Yogesh Nalam, Katharina Bela, Tobias Kamps, Joerg Volpp, and Alexander F.H. Kaplan. Porosity in wire arc additive manufacturing of aluminium alloys. *Additive Manufacturing*, 41:101993, May 2021. ISSN 22148604. doi: 10.1016/j.addma.2021.101993.
- [55] Diogo Horst, Charles Duvoisin, and Rogerio Vieira. Additive Manufacturing at Industry 4.0: A Review. *International Journal of Engineering and Technical Research (IJETR)*, 8(8), August 2018. ISSN 2321-0869.



- [56] J. Hu and H.L. Tsai. Heat and mass transfer in gas metal arc welding. Part I: The arc. *International Journal of Heat and Mass Transfer*, 50(5-6):833–846, March 2007. ISSN 00179310. doi: 10.1016/j.ijheatmasstransfer.2006.08.025.
- [57] N. E. Imoudu, Y. Z. Ayele, and A. Barabadi. *The Characteristic of Cold Metal Transfer (CMT) and Its Application for Cladding*. PhD thesis, The arctic university of norway, Norway, December 2017.
- [58] Mohd Idris Shah Ismail, Yasuhiro Okamoto, and Akira Okada. Neural Network Modeling for Prediction of Weld Bead Geometry in Laser Microwelding. *Advances in Optical Technologies*, 2013:1–7, December 2013. ISSN 1687-6393, 1687-6407. doi: 10.1155/2013/415837.
- [59] Davoud Jafari, Tom H.J. Vaneker, and Ian Gibson. Wire and arc additive manufacturing: Opportunities and challenges to control the quality and accuracy of manufactured parts. *Materials & Design*, 202:109471, April 2021. ISSN 02641275. doi: 10.1016/j.matdes.2021.109471.
- [60] Fengchun Jiang, Laibo Sun, Ruisheng Huang, Hui Jiang, Guangyong Bai, Xiaopeng Qi, Chuanming Liu, Yan Su, Chunhuan Guo, and Jiandong Wang. Effects of Heat Input on Morphology of Thin-Wall Components Fabricated by Wire and Arc Additive Manufacturing. *Advanced Engineering Materials*, 23(4):2001443, April 2021. ISSN 1438-1656, 1527-2648. doi: 10.1002/adem.202001443.
- [61] Wanwan Jin, Chaoqun Zhang, Shuoya Jin, Yingtao Tian, Daniel Wellmann, and Wen Liu. Wire Arc Additive Manufacturing of Stainless Steels: A Review. *Applied Sciences*, 10(5):1563, February 2020. ISSN 2076-3417. doi: 10.3390/app10051563.
- [62] Hyun-Chul Kim and Min-Yang Yang. Incomplete mesh-based tool path generation for optimum zigzag milling. *The International Journal of Advanced Manufacturing Technology*, 35(7-8):803–813, January 2008. ISSN 0268-3768, 1433-3015. doi: 10.1007/s00170-006-0757-2.
- [63] A. Sandeep Kranthi Kiran, Jagadeesh Babu Veluru, Sireesha Merum, A. V. Radhamani, Mukesh Doble, T. S. Sampath Kumar, and Seeram Ramakrishna. Additive manufacturing technologies: An overview of challenges and perspective of using electrospraying. *Nanocomposites*, 4(4):190–214, October 2018. ISSN 2055-0324, 2055-0332. doi: 10.1080/20550324.2018.1558499.

- 
- [64] Vijay Kotu and Bala Deshpande. Introduction. In *Data Science*, pages 1–18. Elsevier, 2019. ISBN 978-0-12-814761-0. doi: 10.1016/B978-0-12-814761-0.00001-0.
- [65] Prashant Kulkarni, Anne Marsan, and Debasish Dutta. A review of process planning techniques in layered manufacturing. *Rapid Prototyping Journal*, 6(1):18–35, March 2000. ISSN 1355-2546. doi: 10.1108/13552540010309859.
- [66] Geir Langelandsvik, Odd M. Akselsen, Trond Furu, and Hans J. Roven. Review of Aluminum Alloy Development for Wire Arc Additive Manufacturing. *Materials*, 14(18):5370, September 2021. ISSN 1996-1944. doi: 10.3390/ma14185370.
- [67] Seung Hwan Lee. CMT-Based Wire Arc Additive Manufacturing Using 316L Stainless Steel: Effect of Heat Accumulation on the Multi-Layer Deposits. *Metals*, 10(2):278, February 2020. ISSN 2075-4701. doi: 10.3390/met10020278.
- [68] Ran Li, Manshu Dong, and Hongming Gao. Prediction of Bead Geometry with Changing Welding Speed Using Artificial Neural Network. *Materials*, 14(6):1494, March 2021. ISSN 1996-1944. doi: 10.3390/ma14061494.
- [69] Yongzhe Li, Qinglin Han, Guangjun Zhang, and Imre Horváth. A layers-overlapping strategy for robotic wire and arc additive manufacturing of multi-layer multi-bead components with homogeneous layers. *The International Journal of Advanced Manufacturing Technology*, 96(9-12):3331–3344, June 2018. ISSN 0268-3768, 1433-3015. doi: 10.1007/s00170-018-1786-3.
- [70] Yongzhe Li, Yunfei Sun, Qinglin Han, Guangjun Zhang, and Imre Horváth. Enhanced beads overlapping model for wire and arc additive manufacturing of multi-layer multi-bead metallic parts. *Journal of Materials Processing Technology*, 252:838–848, February 2018. ISSN 09240136. doi: 10.1016/j.jmatprotec.2017.10.017.
- [71] Mariacira Liberini, Antonello Astarita, Gianni Campatelli, Antonio Scippa, Filippo Montevicchi, Giuseppe Venturini, Massimo Durante, Luca Boccarusso, Fabrizio Memola Capece Minutolo, and A. Squillace. Selection of Optimal Process Parameters for Wire Arc Additive Manufacturing. *Procedia CIRP*, 62:470–474, 2017. ISSN 22128271. doi: 10.1016/j.procir.2016.06.124.

- [72] Der-Chang Lo, Chih-Chiang Wei, and En-Ping Tsai. Parameter Automatic Calibration Approach for Neural-Network-Based Cyclonic Precipitation Forecast Models. *Water*, 7(12):3963–3977, July 2015. ISSN 2073-4441. doi: 10.3390/w7073963.
- [73] Richard Martukanitz, Pan Michaleris, Todd Palmer, Tarasankar DebRoy, Zi-Kui Liu, Richard Otis, Tae Wook Heo, and Long-Qing Chen. Toward an integrated computational system for describing the additive manufacturing process for metallic materials. *Additive Manufacturing*, 1–4:52–63, October 2014. ISSN 22148604. doi: 10.1016/j.addma.2014.09.002.
- [74] Sónia Meco, Gonçalo Pardal, Alexander Eder, and L. Quintino. Software development for prediction of the weld bead in CMT and pulsed-MAG processes. *The International Journal of Advanced Manufacturing Technology*, 64(1-4):171–178, January 2013. ISSN 0268-3768, 1433-3015. doi: 10.1007/s00170-012-3990-x.
- [75] Mohammad Sadegh Mohebbi, Michael Kühn, and Vasily Ploshikhin. A thermo-capillary-gravity model for geometrical analysis of single-bead wire and arc additive manufacturing (WAAM). *The International Journal of Advanced Manufacturing Technology*, 109(3-4):877–891, July 2020. ISSN 0268-3768, 1433-3015. doi: 10.1007/s00170-020-05647-6.
- [76] Filippo Montevicchi, Giuseppe Venturini, Antonio Scippa, and Gianni Campatelli. Finite Element Modelling of Wire-arc-additive-manufacturing Process. *Procedia CIRP*, 55:109–114, 2016. ISSN 22128271. doi: 10.1016/j.procir.2016.08.024.
- [77] Fionn Murtagh. Multilayer perceptrons for classification and regression. *Neurocomputing*, 2(5-6):183–197, July 1991. ISSN 09252312. doi: 10.1016/0925-2312(91)90023-5.
- [78] Jamal M Nazzal, Ibrahim M El-Emary, and Salam A Najim. Multilayer Perceptron Neural Network (MLPs) For Analyzing the Properties of Jordan Oil Shale. page 8, 2008.
- [79] Leonor Neto. Studying the Application of Additive Manufacturing to Large Parts. *materials science*, 2017.

- [80] John Norrish. Gas metal arc welding. In *Advanced Welding Processes*, pages 100–135. Elsevier, 2006. ISBN 978-1-84569-130-1. doi: 10.1533/9781845691707.100.
- [81] Arturo Gomez Ortega, Luis Corona Galvan, Mehdi Salem, Kamel Moussaoui, Stephane Segonds, Sébastien Rouquette, and Frédéric Deschaux-Beaume. Characterisation of 4043 aluminium alloy deposits obtained by wire and arc additive manufacturing using a Cold Metal Transfer process. *Science and Technology of Welding and Joining*, 24(6):538–547, August 2019. ISSN 1362-1718, 1743-2936. doi: 10.1080/13621718.2018.1564986.
- [82] Kohei Oyama, Spyros Diplas, Mohammed M’hamdi, Anette E. Gunnæs, and Amin S. Azar. Heat source management in wire-arc additive manufacturing process for Al-Mg and Al-Si alloys. *Additive Manufacturing*, 26:180–192, March 2019. ISSN 22148604. doi: 10.1016/j.addma.2019.01.007.
- [83] Ester M. Palmero and Alberto Bollero. 3D and 4D Printing of Functional and Smart Composite Materials. In *Encyclopedia of Materials: Composites*, pages 402–419. Elsevier, 2021. ISBN 978-0-12-819731-8. doi: 10.1016/B978-0-12-819724-0.00008-2.
- [84] L.A. Parry, I.A. Ashcroft, and R.D. Wildman. Geometrical effects on residual stress in selective laser melting. *Additive Manufacturing*, 25:166–175, January 2019. ISSN 22148604. doi: 10.1016/j.addma.2018.09.026.
- [85] N Pavan Kumar, Praveen K Devarajan, S Arungalai Vendan, and N. Shanmugam. Prediction of bead geometry in cold metal transfer welding using back propagation neural network. *The International Journal of Advanced Manufacturing Technology*, 93(1-4):385–392, October 2017. ISSN 0268-3768, 1433-3015. doi: 10.1007/s00170-016-9562-8.
- [86] Ivan Peko, Nikola Gjeldum, and Bozenko Bilic. Application of AHP, Fuzzy AHP and PROMETHEE Method in Solving Additive Manufacturing Process Selection Problem. *Tehnicki vjesnik - Technical Gazette*, 25(2), April 2018. ISSN 13303651, 18486339. doi: 10.17559/TV-20170124092906.
- [87] C. G. Pickin and K. Young. Evaluation of cold metal transfer (CMT) process for welding aluminium alloy. *Science and Technology of Welding and Joining*, 11(5):583–585, September 2006. ISSN 1362-1718, 1743-2936. doi: 10.1179/174329306X120886.

- [88] C.G. Pickin, S.W. Williams, and M. Lunt. Characterisation of the cold metal transfer (CMT) process and its application for low dilution cladding. *Journal of Materials Processing Technology*, 211(3):496–502, March 2011. ISSN 09240136. doi: 10.1016/j.jmatprotec.2010.11.005.
- [89] Jesús Pinto-Lopera, José S. T. Motta, and Sadek Absi Alfaro. Real-Time Measurement of Width and Height of Weld Beads in GMAW Processes. *Sensors*, 16(9):1500, September 2016. ISSN 1424-8220. doi: 10.3390/s16091500.
- [90] V.T. Rajan, V. Srinivasan, and K. Tarabanis. The optimal zigzag direction for filling a two-dimensional region. *Rapid Prototyping Journal*, 7(5):231–241, 2001. ISSN 45112178. doi: 10.1108/13552540110410431.
- [91] Fei Ren, Yuwen Sun, and Dongming Guo. Combined reparameterization-based spiral toolpath generation for five-axis sculptured surface machining. *The International Journal of Advanced Manufacturing Technology*, 40(7-8):760–768, February 2009. ISSN 0268-3768, 1433-3015. doi: 10.1007/s00170-008-1385-9.
- [92] P. Robert, M. Museau, and H. Paris. Effect of Temperature on the Quality of Welding Beads Deposited with CMT Technology. In *2018 IEEE International Conference on Industrial Engineering and Engineering Management (IEEM)*, pages 680–684, Bangkok, December 2018. IEEE. ISBN 978-1-5386-6786-6. doi: 10.1109/IEEM.2018.8607636.
- [93] Tiago A. Rodrigues, V. Duarte, R.M. Miranda, Telmo G. Santos, and J.P. Oliveira. Current Status and Perspectives on Wire and Arc Additive Manufacturing (WAAM). *Materials*, 12(7):1121, April 2019. ISSN 1996-1944. doi: 10.3390/ma12071121.
- [94] Nor Ana Rosli, Mohd Rizal Alkahari, Faiz Redza Ramli, Shafizal Mat, and Ahmad Anas Yusof. Influence of process parameters on dimensional accuracy in GMAW based additive manufacturing. page 4, 2019.
- [95] François Rouchon. *Contributions to the Geometric Modeling of Material Deposition for the Development of a Digital Twin of the WAAM Process*. PhD thesis, June 2022.
- [96] Abdollah Saboori, Alberta Aversa, Giulio Marchese, Sara Biamino, Mariangela Lombardi, and Paolo Fino. Application of Directed Energy Deposition-Based

- Additive Manufacturing in Repair. *Applied Sciences*, 9(16):3316, August 2019. ISSN 2076-3417. doi: 10.3390/app9163316.
- [97] Abhinav Sagar. A New Activation Function for Training Deep Neural Networks to Avoid Local Minimum. page 11, June 2020.
- [98] Wesam Salah Alaloul and Abdul Hannan Qureshi. Data Processing Using Artificial Neural Networks. In Dinesh G. Harkut, editor, *Dynamic Data Assimilation - Beating the Uncertainties*. IntechOpen, October 2020. ISBN 978-1-83968-083-0 978-1-83968-084-7. doi: 10.5772/intechopen.91935.
- [99] W. J. Sames, F. A. List, S. Pannala, R. R. Dehoff, and S. S. Babu. The metallurgy and processing science of metal additive manufacturing. *International Materials Reviews*, 61(5):315–360, July 2016. ISSN 0950-6608, 1743-2804. doi: 10.1080/09506608.2015.1116649.
- [100] S. Selvi, A. Vishvaksenan, and E. Rajasekar. Cold metal transfer (CMT) technology - An overview. *Defence Technology*, 14(1):28–44, February 2018. ISSN 22149147. doi: 10.1016/j.dt.2017.08.002.
- [101] Vivek Singh, M. Chandrasekaran, S. Samanta, and M. Thirugnanasambandam. Artificial neural network modelling of weld bead characteristics during GMAW of nitrogen strengthened austenitic stainless steel. In *INTERNATIONAL CONFERENCE ON MATERIALS, MANUFACTURING AND MACHINING 2019*, page 020024, Tamilnadu, India, 2019. doi: 10.1063/1.5117936.
- [102] Michael E. Stender, Lauren L. Beghini, Joshua D. Sugar, Michael G. Veilleux, Samuel R. Subia, Thale R. Smith, Christopher W. San Marchi, Arthur A. Brown, and Daryl J. Dagle. A thermal-mechanical finite element workflow for directed energy deposition additive manufacturing process modeling. *Additive Manufacturing*, 21:556–566, May 2018. ISSN 22148604. doi: 10.1016/j.addma.2018.04.012.
- [103] Harley Stinson, Richard Ward, Justin Quinn, and Cormac McGarrigle. Comparison of Properties and Bead Geometry in MIG and CMT Single Layer Samples for WAAM Applications. *Metals*, 11(10):1530, September 2021. ISSN 2075-4701. doi: 10.3390/met11101530.

- [104] S. Suryakumar, K.P. Karunakaran, Alain Bernard, U. Chandrasekhar, N. Raghavender, and Deepak Sharma. Weld bead modeling and process optimization in Hybrid Layered Manufacturing. *Computer-Aided Design*, 43(4): 331–344, April 2011. ISSN 00104485. doi: 10.1016/j.cad.2011.01.006.
- [105] R Talalaev, R Veinthal, A Laansoo, and M Sarkans. Cold metal transfer (CMT) welding of thin sheet metal products. *Estonian Journal of Engineering*, 18(3):243, 2012. ISSN 1736-6038. doi: 10.3176/eng.2012.3.09.
- [106] Shangyong Tang, Guilan Wang, Cheng Huang, Runsheng Li, Siyu Zhou, and Haiou Zhang. Investigation, modeling and optimization of abnormal areas of weld beads in wire and arc additive manufacturing. *Rapid Prototyping Journal*, 26(7):1183–1195, June 2020. ISSN 1355-2546, 1355-2546. doi: 10.1108/RPJ-08-2019-0229.
- [107] Jaakko Tapiola. Cold Metal Transfer cladding of wear and corrosion resistant coatings in engine applications. 2017. doi: 10.13140/RG.2.2.15573.52963.
- [108] Shivraman Thapliyal. Challenges associated with the wire arc additive manufacturing (WAAM) of aluminum alloys. *Materials Research Express*, 6(11): 112006, October 2019. ISSN 2053-1591. doi: 10.1088/2053-1591/ab4dd4.
- [109] Mary Kathryn Thompson, Giovanni Moroni, Tom Vaneker, Georges Fadel, R. Ian Campbell, Ian Gibson, Alain Bernard, Joachim Schulz, Patricia Graf, Bhriagu Ahuja, and Filomeno Martina. Design for Additive Manufacturing: Trends, opportunities, considerations, and constraints. *CIRP Annals*, 65(2): 737–760, 2016. ISSN 00078506. doi: 10.1016/j.cirp.2016.05.004.
- [110] C. J. Todaro, M. A. Easton, D. Qiu, D. Zhang, M. J. Bermingham, E. W. Lui, M. Brandt, D. H. StJohn, and M. Qian. Grain structure control during metal 3D printing by high-intensity ultrasound. *Nature Communications*, 11(1):142, December 2020. ISSN 2041-1723. doi: 10.1038/s41467-019-13874-z.
- [111] Hossein Towsyfyhan, Gholamreza Davoudi, Bahram Heidarian Dehkordy, and Ahmad Kariminasab. Comparing the Regression Analysis and Artificial Neural Network in Modeling the Submerged Arc Welding (SAW) Process. *Research Journal of Applied Sciences, Engineering and Technology*, 5(9):2701–2706, March 2013. ISSN 20407459, 20407467. doi: 10.19026/rjaset.5.4794.

- [112] Lexuri Vazquez, Maria Nieves Rodriguez, Iker Rodriguez, and Pedro Alvarez. Influence of Post-Deposition Heat Treatments on the Microstructure and Tensile Properties of Ti-6Al-4V Parts Manufactured by CMT-WAAM. *Metals*, 11(8):1161, July 2021. ISSN 2075-4701. doi: 10.3390/met11081161.
- [113] Giuseppe Venturini, Filippo Montevercchi, Antonio Scippa, and Gianni Campatelli. Optimization of WAAM Deposition Patterns for T-crossing Features. *Procedia CIRP*, 55:95–100, 2016. ISSN 22128271. doi: 10.1016/j.procir.2016.08.043.
- [114] Haifeng Wang and Teng Wu. Knowledge-Enhanced Deep Learning for Wind-Induced Nonlinear Structural Dynamic Analysis. *Journal of Structural Engineering*, 146(11):04020235, November 2020. ISSN 0733-9445, 1943-541X. doi: 10.1061/(ASCE)ST.1943-541X.0002802.
- [115] Hongcheng Wang, Peter Jang, and James A. Stori. A Metric-Based Approach to Two-Dimensional (2D) Tool-Path Optimization for High-Speed Machining. *Journal of Manufacturing Science and Engineering*, 127(1):33–48, February 2005. ISSN 1087-1357, 1528-8935. doi: 10.1115/1.1830492.
- [116] Xiaolong Wang, Aimin Wang, and Yuebo Li. A sequential path-planning methodology for wire and arc additive manufacturing based on a water-pouring rule. *The International Journal of Advanced Manufacturing Technology*, 103(9-12):3813–3830, August 2019. ISSN 0268-3768, 1433-3015. doi: 10.1007/s00170-019-03706-1.
- [117] S. W. Williams, F. Martina, A. C. Addison, J. Ding, G. Pardal, and P. Colegrove. Wire + Arc Additive Manufacturing. *Materials Science and Technology*, 32(7):641–647, May 2016. ISSN 0267-0836, 1743-2847. doi: 10.1179/1743284715Y.0000000073.
- [118] Binta Wu, Donghong Ding, Zengxi Pan, Dominic Cuiuri, Huijun Li, Jian Han, and Zhenyu Fei. Effects of heat accumulation on the arc characteristics and metal transfer behavior in Wire Arc Additive Manufacturing of Ti6Al4V. *Journal of Materials Processing Technology*, 250:304–312, December 2017. ISSN 09240136. doi: 10.1016/j.jmatprotec.2017.07.037.
- [119] Binta Wu, Zengxi Pan, Donghong Ding, Dominic Cuiuri, and Huijun Li. Effects of heat accumulation on microstructure and mechanical properties of



- Ti6Al4V alloy deposited by wire arc additive manufacturing. *Additive Manufacturing*, 23:151–160, October 2018. ISSN 22148604. doi: 10.1016/j.addma.2018.08.004.
- [120] Binta Wu, Zengxi Pan, Donghong Ding, Dominic Cuiuri, Huijun Li, Jing Xu, and John Norrish. A review of the wire arc additive manufacturing of metals: Properties, defects and quality improvement. *Journal of Manufacturing Processes*, 35:127–139, October 2018. ISSN 15266125. doi: 10.1016/j.jmapro.2018.08.001.
- [121] Wei Wu, Jiayang Xue, Wei Xu, Hongyan Lin, Heqing Tang, and Ping Yao. Parameters Optimization of Auxiliary Gas Process for Double-Wire SS316L Stainless Steel Arc Additive Manufacturing. *Metals*, 11(2):190, January 2021. ISSN 2075-4701. doi: 10.3390/met11020190.
- [122] Jun Xiong, Guangjun Zhang, Hongming Gao, and Lin Wu. Modeling of bead section profile and overlapping beads with experimental validation for robotic GMAW-based rapid manufacturing. *Robotics and Computer-Integrated Manufacturing*, 29(2):417–423, April 2013. ISSN 07365845. doi: 10.1016/j.rcim.2012.09.011.
- [123] Jun Xiong, Guangjun Zhang, Jianwen Hu, and Yongzhe Li. Forecasting process parameters for GMAW-based rapid manufacturing using closed-loop iteration based on neural network. *The International Journal of Advanced Manufacturing Technology*, 69(1-4):743–751, October 2013. ISSN 0268-3768, 1433-3015. doi: 10.1007/s00170-013-5038-2.
- [124] Jun Xiong, Guangjun Zhang, and Weihua Zhang. Forming appearance analysis in multi-layer single-pass GMAW-based additive manufacturing. *The International Journal of Advanced Manufacturing Technology*, 80(9-12):1767–1776, October 2015. ISSN 0268-3768, 1433-3015. doi: 10.1007/s00170-015-7112-4.
- [125] Jun Xiong, Yangyang Lei, and Rong Li. Finite element analysis and experimental validation of thermal behavior for thin-walled parts in GMAW-based additive manufacturing with various substrate preheating temperatures. *Applied Thermal Engineering*, 126:43–52, November 2017. ISSN 13594311. doi: 10.1016/j.applthermaleng.2017.07.168.
- [126] Jun Xiong, Rong Li, Yangyang Lei, and Hui Chen. Heat propagation of circular thin-walled parts fabricated in additive manufacturing using gas metal

- arc welding. *Journal of Materials Processing Technology*, 251:12–19, January 2018. ISSN 09240136. doi: 10.1016/j.jmatprotec.2017.08.007.
- [127] Jun Xiong, Yanjiang Li, Rong Li, and Ziqiu Yin. Influences of process parameters on surface roughness of multi-layer single-pass thin-walled parts in GMAW-based additive manufacturing. *Journal of Materials Processing Technology*, 252:128–136, February 2018. ISSN 09240136. doi: 10.1016/j.jmatprotec.2017.09.020.
- [128] Mostafa Yakout, M.A. Elbestawi, and Stephen C. Veldhuis. A Review of Metal Additive Manufacturing Technologies. *Solid State Phenomena*, 278:1–14, July 2018. ISSN 1662-9779. doi: 10.4028/www.scientific.net/SSP.278.1.
- [129] Yuri Yehorov, Leandro João da Silva, and Américo Scotti. Balancing WAAM Production Costs and Wall Surface Quality through Parameter Selection: A Case Study of an Al-Mg<sub>5</sub> Alloy Multilayer-Non-Oscillated Single Pass Wall. *Journal of Manufacturing and Materials Processing*, 3(2):32, April 2019. ISSN 2504-4494. doi: 10.3390/jmmp3020032.
- [130] Ahmet Suat Yildiz, Kemal Davut, Barış Koc, and Oguzhan Yilmaz. Wire arc additive manufacturing of high-strength low alloy steels: Study of process parameters and their influence on the bead geometry and mechanical characteristics. *The International Journal of Advanced Manufacturing Technology*, 108(11-12):3391–3404, June 2020. ISSN 0268-3768, 1433-3015. doi: 10.1007/s00170-020-05482-9.
- [131] Kai Zeng, Deepankar Pal, and Brent Stucker. A review of thermal analysis methods in Laser Sintering and Selective Laser Melting. In *2012 International Solid Freeform Fabrication Symposium*, page 19, 2012.
- [132] H.T. Zhang, J.C. Feng, P. He, B.B. Zhang, J.M. Chen, and L. Wang. The arc characteristics and metal transfer behaviour of cold metal transfer and its use in joining aluminium to zinc-coated steel. *Materials Science and Engineering: A*, 499(1-2):111–113, January 2009. ISSN 09215093. doi: 10.1016/j.msea.2007.11.124.
- [133] Jikui Zhang, Xueyuan Wang, Sanjooram Paddea, and Xiang Zhang. Fatigue crack propagation behaviour in wire+arc additive manufactured Ti-6Al-4V: Effects of microstructure and residual stress. *Materials & Design*, 90:551–561, January 2016. ISSN 02641275. doi: 10.1016/j.matdes.2015.10.141.

- [134] Jikui Zhang, Xiang Zhang, Xueyuan Wang, Jialuo Ding, Yéli Traoré, Sanjooram Paddea, and Stewart Williams. Crack path selection at the interface of wrought and wire+arc additive manufactured Ti-6Al-4V. *Materials & Design*, 104:365–375, August 2016. ISSN 02641275. doi: 10.1016/j.matdes.2016.05.027.
- [135] Yicha Zhang. Evaluating the Design for Additive Manufacturing: A Process Planning Perspective. *Procedia CIRP*, page 7, 2014. doi: 10.1016/j.procir.2014.03.179.
- [136] YuMing Zhang, Yiwei Chen, Pengjiu Li, and Alan T Male. Weld deposition-based rapid prototyping: A preliminary study. *Journal of Materials Processing Technology*, 135(2-3):347–357, April 2003. ISSN 09240136. doi: 10.1016/S0924-0136(02)00867-1.
- [137] Yun-tao Zhao, Wei-gang Li, and Ao Liu. Optimization of geometry quality model for wire and arc additive manufacture based on adaptive multi-objective grey wolf algorithm. *Soft Computing*, 24(22):17401–17416, November 2020. ISSN 1432-7643, 1433-7479. doi: 10.1007/s00500-020-05027-y.
- [138] Kai Zhou, Guoliang Ye, Xiangdong Gao, Kaihong Zhong, Jianwen Guo, and Bing Zhang. Weld Bead Width and Height Measurement Using RANSAC. In *2019 4th International Conference on Control and Robotics Engineering (ICCRE)*, pages 35–39, Nanjing, China, April 2019. IEEE. ISBN 978-1-72811-593-1. doi: 10.1109/ICCRE.2019.8724363.

# Appendix



# Appendix A

## The result of thermal simulation

### A.1 Exp.1: Single weld bead on substrate thermal simulation

#### A.1.1 Thermal simulation of single weld bead deposited on flat substrates data

Table A.1 : Data surface deposition temperature ( $T_{dep}$ ) of Exp.1

Weld bead position (mm)	$T_{init}$ (°C)					
	0	25	100	200	300	400
1		322.58	381.74	459.19	523.63	573.86
2		383.82	439.96	502.90	553.56	595.04
3		412.09	462.95	521.40	568.51	599.55
4		429.98	477.38	531.81	578.15	602.19
5		443.20	488.00	539.46	584.59	604.15
6		452.38	496.35	545.43	588.18	605.72
7		459.54	503.18	550.28	591.10	607.01
8		465.56	508.92	554.33	593.56	608.09
9		470.71	513.07	557.78	595.64	609.03
10		475.15	516.25	560.75	596.77	609.83

Appendix A The result of thermal simulation

Table A.1 : Data surface deposition temperature ( $T_{dep}$ ) of Exp.1

Weld bead position (mm)	$T_{init}$ (°C)				
	0	25	100	200	300
11	479.04	519.01	563.33	597.49	610.53
12	482.44	521.43	565.58	598.12	611.15
13	485.45	523.57	567.56	598.68	611.70
14	488.12	525.46	569.31	599.18	612.18
15	490.49	527.15	570.87	599.63	612.61
16	492.61	528.66	572.26	600.02	612.99
17	494.51	530.01	573.50	600.38	613.33
18	496.23	531.23	574.62	600.70	613.63
19	497.77	532.33	575.62	600.99	613.90
20	499.17	533.31	576.53	601.24	614.23
21	500.43	534.21	577.35	601.48	614.72
22	501.58	535.02	578.10	601.69	615.17
23	502.62	535.75	578.77	601.88	615.57
24	503.57	536.43	579.39	602.05	615.93
25	504.44	537.04	579.94	602.21	616.26
26	505.24	537.60	580.45	602.35	616.56
27	505.97	538.11	580.91	602.48	616.82
28	506.64	538.58	581.34	602.60	617.06
29	507.18	539.01	581.72	602.71	617.28
30	507.60	539.40	582.07	602.81	617.47
31	507.99	539.76	582.40	602.90	617.65
32	508.35	540.09	582.69	602.98	617.80
33	508.68	540.40	582.96	603.05	617.95

A.1 Exp.1: Single weld bead on substrate thermal simulation

Table A.1 : Data surface deposition temperature ( $T_{dep}$ ) of Exp.1

Weld bead position (mm)	$T_{init}$ (°C)				
	0	25	100	200	300
34	508.98	540.68	583.21	603.11	618.07
35	509.26	540.94	583.43	603.17	618.18
36	509.52	541.18	583.64	603.23	618.28
37	509.76	541.40	583.83	603.28	618.37
38	509.98	541.60	583.99	603.32	618.45
39	510.18	541.79	584.11	603.36	618.52
40	510.37	541.96	584.20	603.40	618.58
41	510.55	542.12	584.29	603.43	618.63
42	510.71	542.26	584.37	603.46	618.67
43	510.86	542.40	584.44	603.49	618.71
44	511.01	542.52	584.50	603.51	618.74
45	511.14	542.64	584.56	603.53	618.76
46	511.26	542.74	584.62	603.55	618.78
47	511.37	542.84	584.67	603.56	618.79
48	511.48	542.93	584.71	603.57	618.80
49	511.58	543.02	584.75	603.58	618.80
50	511.67	543.09	584.78	603.59	618.80
51	511.75	543.16	584.82	603.60	618.80
52	511.83	543.23	584.84	603.61	618.79
53	511.91	543.29	584.87	603.61	618.78
54	511.98	543.34	584.89	603.61	618.77
55	512.04	543.39	584.91	603.61	618.75
56	512.10	543.44	584.92	603.62	618.73



Appendix A The result of thermal simulation

Table A.1 : Data surface deposition temperature ( $T_{dep}$ ) of Exp.1

Weld bead position (mm)	$T_{init}$ (°C)				
	0	25	100	200	300
57	512.16	543.48	584.94	603.61	618.71
58	512.21	543.52	584.95	603.61	618.68
59	512.26	543.55	584.96	603.61	618.66
60	512.30	543.59	584.97	603.61	618.63
61	512.35	543.62	584.97	603.60	618.60
62	512.39	543.64	584.98	603.60	618.57
63	512.42	543.67	584.98	603.59	618.53
64	512.46	543.69	584.98	603.58	618.50
65	512.49	543.71	584.98	603.58	618.46
66	512.52	543.72	584.98	603.57	618.43
67	512.55	543.74	584.97	603.56	618.39
68	512.58	543.75	584.97	603.55	618.35
69	512.60	543.76	584.97	603.54	618.31
70	512.62	543.77	584.96	603.53	618.26
71	512.65	543.78	584.95	603.52	618.22
72	512.67	543.79	584.94	603.51	618.18
73	512.68	543.80	584.94	603.50	618.13
74	512.70	543.80	584.93	603.49	618.09
75	512.72	543.81	584.92	603.48	618.04
76	512.73	543.81	584.90	603.46	617.99
77	512.75	543.81	584.89	603.45	617.95
78	512.76	543.81	584.88	603.44	617.90
79	512.78	543.81	584.87	603.43	617.85

## A.2 Exp.2: Single weld bead on cylinder substrate thermal simulation

Table A.1 : Data surface deposition temperature ( $T_{dep}$ ) of Exp.1

Weld bead position (mm)	$T_{init}$ (°C)				
0	25	100	200	300	400
80	512.79	543.81	584.85	603.41	617.80

Table A.2 : Average surface temperature deposition ( $T_{dep}$ ) and standard deviation ( $\sigma$ ) of Exp.1: Single weld bead on flat substrate

$T_{init}$ °C	$T_{dep}$ (°C)	$\sigma$
25	506.17	10.55
100	534.49	5.34
200	577.56	2.89
300	601.52	2.01
400	615.51	1.54

## A.2 Exp.2: Single weld bead on cylinder substrate thermal simulation

### A.2.1 Thermal simulation process of Exp.2

Figure A.2.1 (a) shows an example of initial temperature ( $T_{init}$ ) at 200°C and a cylinder diameter of Ø20 mm or  $a = 17$  mm x  $b = 18$  mm. The cylinder substrate is 110 mm. The results show a history of surface deposition temperatures ( $T_{dep}$ ) occurring during deposition. Figure A.2.1 (b) shows the initial temperature at start point. Figure A.2.1 (c), the weld bead deposition is 50 mm and surface deposition temperatures ( $T_{dep}$ ) is 542.39°C. Figure A.2.1 (d) The weld bead deposition is 100 mm (endpoint). Therefore, it shows the weld deposition temperature. When the deposition begins, the temperature rises rapidly. Then the temperature is relatively stable until the end of the weld deposition.

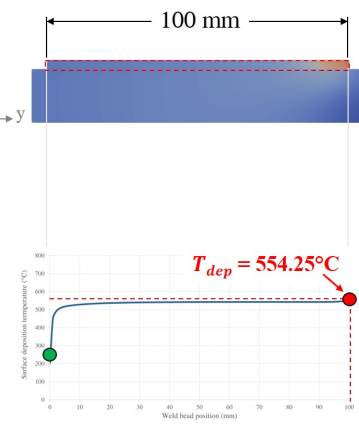
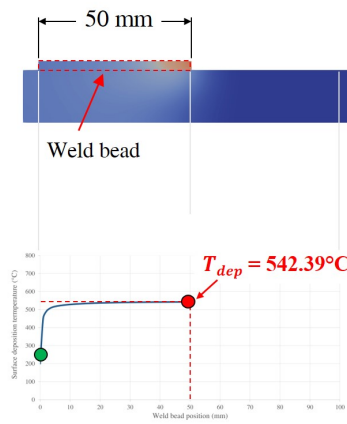
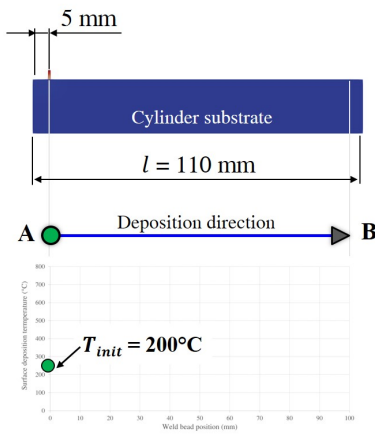
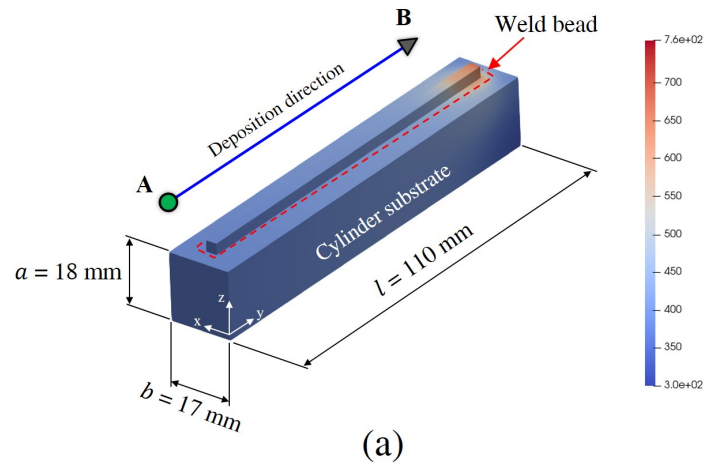


Figure A.2.1 : Exp.4 Single weld bead on cylinder substrate thermal simulation at initial temperature ( $T_{init}$ )= 200°C: (a) Cylinder substrate at  $\text{Ø}20$  mm or  $17 \times 18 \times 110$  mm ( $a \times b \times l$ ), (b) At start point, (c) Weld bead position is 50 mm, (d) Weld bead position is 100 mm

### A.2.2 Thermal simulation of single weld beads deposited on cylinder substrates at $T_{init} = 25^\circ\text{C}$ , $100^\circ\text{C}$ , $200^\circ\text{C}$ , $300^\circ\text{C}$

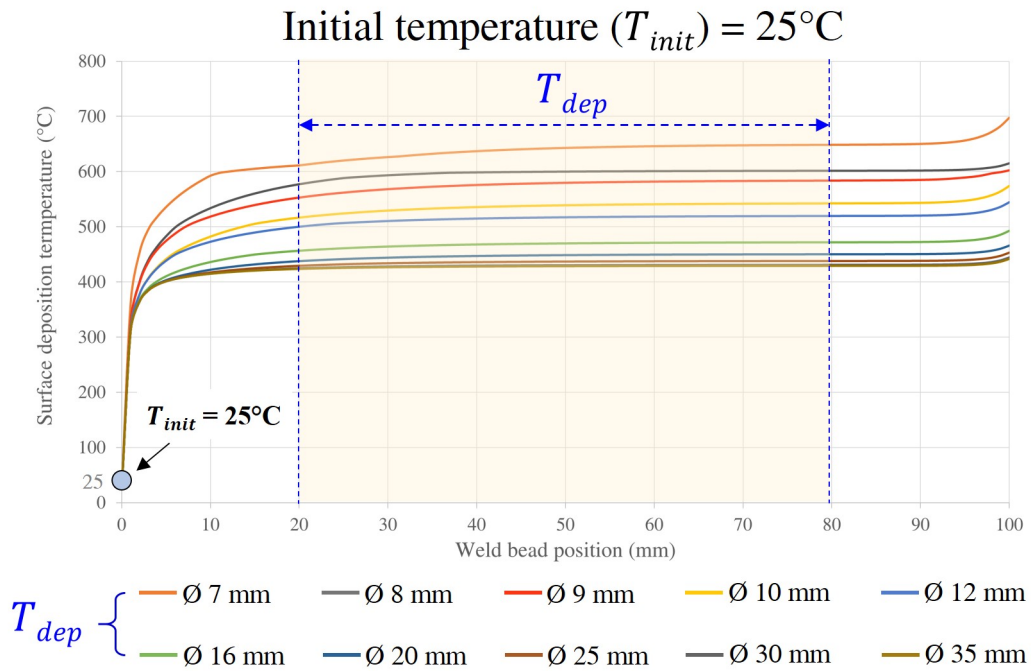


Figure A.2.2 : Thermal simulation result of Exp.2: Single weld bead on cylinder substrate at initial temperature ( $T_{init}$ ) of  $25^\circ\text{C}$

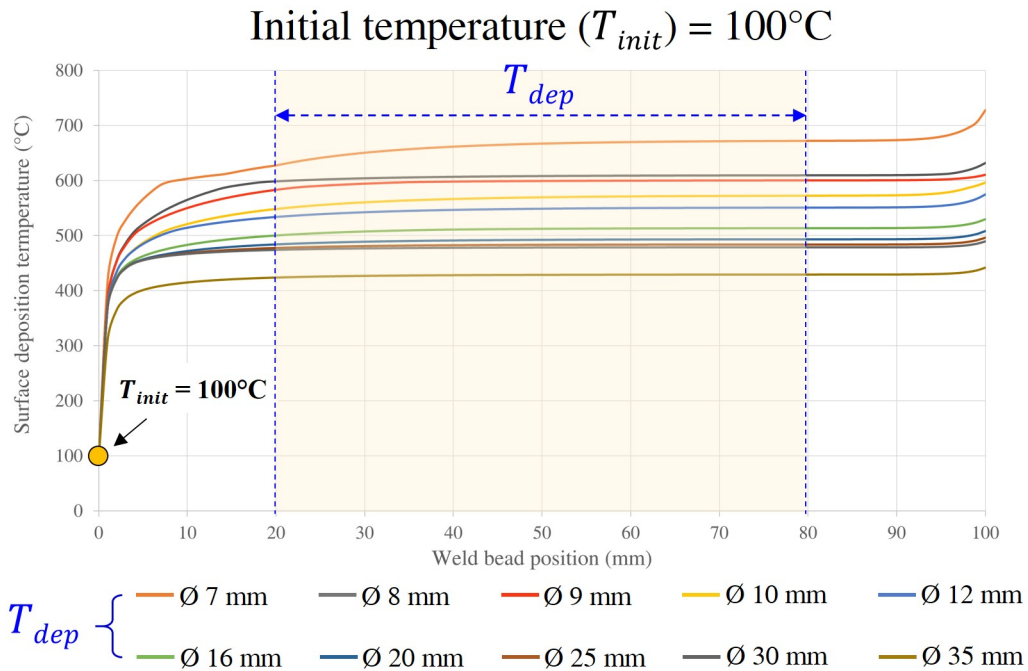


Figure A.2.3 : Thermal simulation result of Exp.2: Single weld bead on cylinder substrate at initial temperature ( $T_{init}$ ) of 100°C

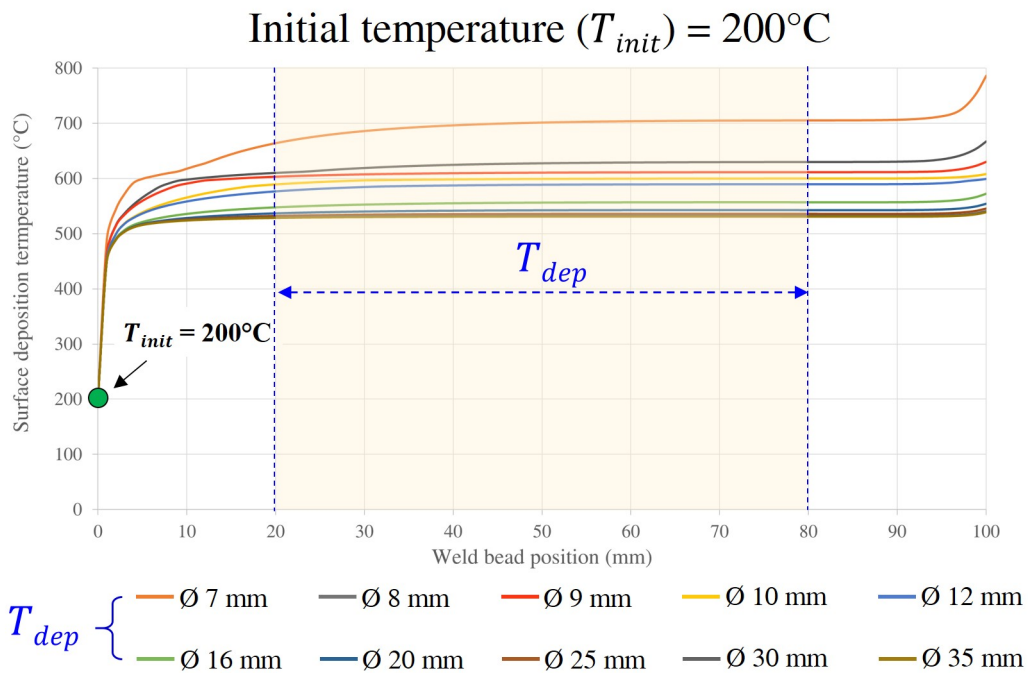


Figure A.2.4 : Thermal simulation result of Exp.2: Single weld bead on cylinder substrate at initial temperature ( $T_{init}$ ) of 200°C

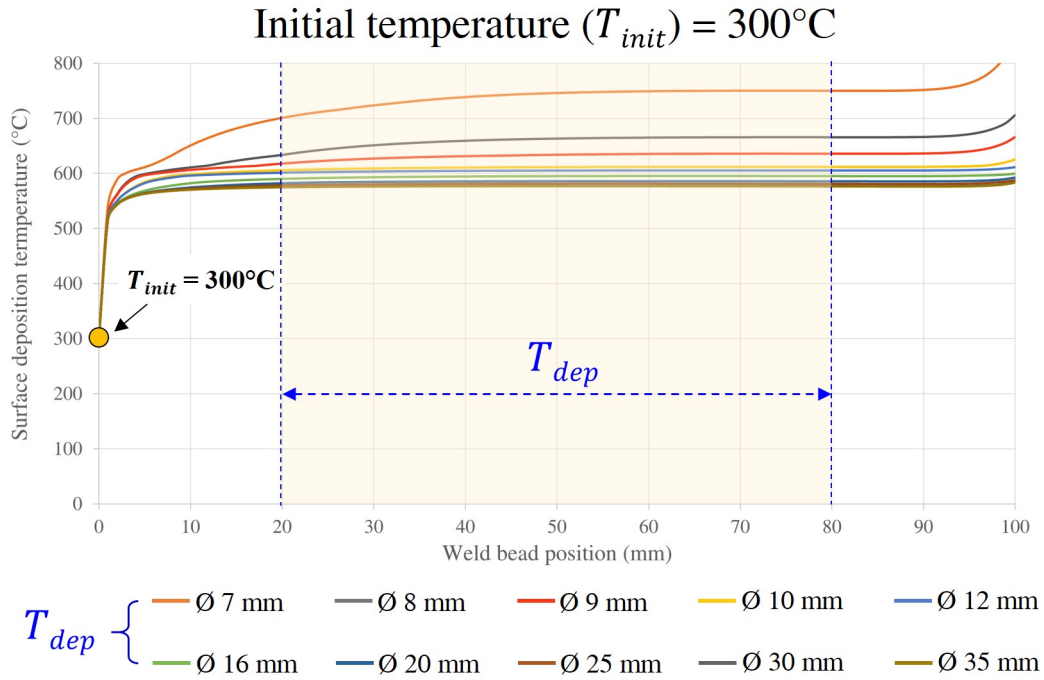


Figure A.2.5 : Thermal simulation result of Exp.2: Single weld bead on cylinder substrate at initial temperature ( $T_{init}$ ) of 300°C

### A.2.3 Thermal simulation of single weld beads deposited on cylinder substrate data

- Initial temperature ( $T_{init}$ ) of 25°C

Table A.3 : Data surface deposition temperature ( $T_{dep}$ ) of Exp.2 at initial temperature ( $T_{init}$ ) of 25°C

Weld bead position (mm)	Cylinder substrate diameter (mm)									
	Ø7	Ø8	Ø9	Ø10	Ø12	Ø16	Ø20	Ø25	Ø30	Ø35
0	25.00	25.00	25.00	25.00	25.00	25.00	25.00	25.00	25.00	25.00
1	361.16	327.53	327.08	316.63	316.58	312.32	311.83	311.76	311.76	311.76
2	452.95	400.39	398.61	377.58	377.28	366.49	364.84	364.57	364.52	364.53
3	495.24	440.09	436.07	407.04	406.21	388.80	385.49	384.85	384.71	384.70
4	517.92	464.45	458.76	426.47	424.76	401.62	396.43	395.25	394.96	394.94

Appendix A The result of thermal simulation

Table A.3 : Data surface deposition temperature ( $T_{dep}$ ) of Exp.2 at initial temperature ( $T_{init}$ ) of 25°C

Weld bead position (mm)	Cylinder substrate diameter (mm)									
	Ø7	Ø8	Ø9	Ø10	Ø12	Ø16	Ø20	Ø25	Ø30	Ø35
5	535.73	483.08	474.70	441.38	438.45	410.58	403.52	401.72	401.20	401.15
6	550.51	498.74	487.61	452.89	449.27	417.56	408.77	406.29	405.49	405.40
7	563.18	509.91	498.52	461.61	456.64	423.33	412.99	409.83	408.71	408.58
8	574.20	518.87	506.72	469.25	462.83	428.25	416.56	412.75	411.29	411.08
9	583.89	526.86	512.99	476.04	468.15	432.54	419.65	415.24	413.42	413.14
10	592.42	533.99	518.60	482.15	472.79	436.31	422.36	417.40	415.23	414.88
11	597.46	540.41	523.65	487.66	476.89	439.65	424.77	419.30	416.80	416.36
12	599.78	546.21	528.23	492.67	480.55	442.64	426.91	420.99	418.17	417.64
13	601.67	551.45	532.38	497.24	483.84	445.32	428.83	422.49	419.37	418.75
14	603.40	556.21	536.16	501.42	486.81	447.74	430.56	423.84	420.44	419.73
15	604.98	560.55	539.62	505.23	489.52	449.93	432.11	425.04	421.39	420.60
16	606.44	564.51	542.79	507.97	491.98	451.65	433.52	426.12	422.24	421.37
17	607.76	568.13	545.70	510.37	494.24	453.12	434.79	427.10	423.00	422.05
18	608.98	571.44	548.37	512.58	496.32	454.46	435.95	427.98	423.68	422.66
19	610.10	574.49	550.83	514.61	498.24	455.69	437.00	428.78	424.30	423.21
20	611.13	577.29	553.09	516.49	500.00	456.82	437.96	429.51	424.86	423.70
21	613.01	579.88	555.18	518.23	501.63	457.86	438.85	430.17	425.36	424.15
22	614.95	582.28	557.12	519.84	503.14	458.82	439.66	430.77	425.82	424.55
23	616.74	584.49	558.91	521.33	504.54	459.71	440.40	431.31	426.24	424.92
24	618.40	586.53	560.56	522.71	505.80	460.54	441.09	431.81	426.62	425.25
25	619.93	588.44	562.11	524.00	506.70	461.30	441.73	432.27	426.97	425.55
26	621.35	589.67	563.54	525.19	507.54	462.01	442.32	432.69	427.29	425.83
27	622.68	590.74	564.87	526.30	508.32	462.68	442.86	433.08	427.58	426.08

*A.2 Exp.2: Single weld bead on cylinder substrate thermal simulation*

Table A.3 : Data surface deposition temperature ( $T_{dep}$ ) of Exp.2 at initial temperature ( $T_{init}$ ) of 25°C

Weld bead position (mm)	Cylinder substrate diameter (mm)									
	Ø7	Ø8	Ø9	Ø10	Ø12	Ø16	Ø20	Ø25	Ø30	Ø35
28	623.91	591.73	566.11	527.34	509.05	463.29	443.37	433.44	427.85	426.31
29	625.05	592.66	567.26	528.30	509.72	463.87	443.84	433.77	428.10	426.52
30	626.12	593.52	568.34	529.20	510.36	464.40	444.27	434.07	428.33	426.72
31	627.10	594.32	569.34	530.04	510.95	464.90	444.68	434.35	428.54	426.89
32	628.38	595.07	570.27	530.82	511.49	465.37	445.06	434.61	428.73	427.06
33	629.71	595.77	571.14	531.55	512.01	465.80	445.41	434.85	428.91	427.21
34	630.96	596.42	571.96	532.23	512.49	466.21	445.74	435.08	429.08	427.35
35	632.12	597.03	572.72	532.87	512.94	466.59	446.05	435.29	429.23	427.48
36	633.20	597.60	573.44	533.47	513.36	466.95	446.34	435.48	429.38	427.60
37	634.21	598.09	574.11	534.03	513.75	467.28	446.61	435.66	429.51	427.71
38	635.16	598.32	574.73	534.55	514.12	467.59	446.86	435.83	429.63	427.81
39	636.04	598.53	575.32	535.05	514.47	467.89	447.10	435.99	429.75	427.91
40	636.87	598.73	575.87	535.51	514.79	468.16	447.32	436.13	429.85	428.00
41	637.64	598.92	576.39	535.94	515.10	468.42	447.52	436.27	429.95	428.08
42	638.36	599.10	576.87	536.34	515.38	468.66	447.72	436.40	430.04	428.15
43	639.04	599.27	577.33	536.72	515.65	468.89	447.90	436.52	430.13	428.22
44	639.67	599.42	577.76	537.08	515.91	469.10	448.07	436.63	430.21	428.29
45	640.27	599.57	578.16	537.42	516.14	469.30	448.23	436.73	430.29	428.35
46	640.82	599.71	578.54	537.73	516.36	469.49	448.38	436.83	430.36	428.41
47	641.35	599.84	578.90	538.03	516.57	469.66	448.52	436.92	430.42	428.46
48	641.84	599.96	579.23	538.31	516.77	469.83	448.66	437.01	430.48	428.51
49	642.30	600.08	579.55	538.57	516.95	469.98	448.78	437.09	430.54	428.56
50	642.73	600.18	579.84	538.82	517.13	470.13	448.90	437.17	430.60	428.60



Appendix A The result of thermal simulation

Table A.3 : Data surface deposition temperature ( $T_{dep}$ ) of Exp.2 at initial temperature ( $T_{init}$ ) of 25°C

Weld bead position (mm)	Cylinder substrate diameter (mm)									
	Ø7	Ø8	Ø9	Ø10	Ø12	Ø16	Ø20	Ø25	Ø30	Ø35
51	643.13	600.29	580.12	539.05	517.29	470.27	449.01	437.24	430.65	428.64
52	643.51	600.38	580.39	539.27	517.45	470.40	449.11	437.30	430.69	428.68
53	643.87	600.47	580.64	539.48	517.59	470.52	449.21	437.37	430.74	428.71
54	644.20	600.56	580.87	539.67	517.73	470.63	449.30	437.43	430.78	428.74
55	644.52	600.64	581.09	539.85	517.85	470.74	449.39	437.48	430.82	428.77
56	644.81	600.71	581.30	540.02	517.98	470.84	449.47	437.53	430.86	428.80
57	645.09	600.78	581.49	540.19	518.09	470.94	449.54	437.58	430.89	428.83
58	645.35	600.85	581.68	540.34	518.20	471.03	449.61	437.63	430.92	428.86
59	645.60	600.91	581.85	540.48	518.30	471.11	449.68	437.67	430.95	428.88
60	645.83	600.97	582.01	540.62	518.39	471.19	449.74	437.71	430.98	428.90
61	646.04	601.03	582.17	540.75	518.48	471.27	449.80	437.75	431.01	428.92
62	646.25	601.08	582.31	540.87	518.57	471.34	449.86	437.79	431.03	428.94
63	646.44	601.13	582.45	540.98	518.65	471.40	449.91	437.82	431.06	428.96
64	646.62	601.18	582.58	541.09	518.72	471.47	449.96	437.85	431.08	428.98
65	646.79	601.22	582.70	541.19	518.79	471.53	450.01	437.88	431.10	428.99
66	646.95	601.26	582.82	541.28	518.86	471.58	450.05	437.91	431.12	429.01
67	647.10	601.30	582.93	541.37	518.92	471.63	450.10	437.94	431.14	429.02
68	647.24	601.34	583.03	541.46	518.98	471.68	450.14	437.96	431.15	429.03
69	647.37	601.37	583.13	541.54	519.04	471.73	450.17	437.98	431.17	429.05
70	647.50	601.40	583.22	541.62	519.09	471.77	450.20	438.01	431.19	429.06
71	647.62	601.44	583.30	541.69	519.14	471.81	450.23	438.03	431.20	429.07
72	647.73	601.46	583.39	541.75	519.19	471.85	450.25	438.05	431.21	429.08
73	647.84	601.49	583.46	541.82	519.23	471.89	450.27	438.07	431.23	429.09

*A.2 Exp.2: Single weld bead on cylinder substrate thermal simulation*

---

Table A.3 : Data surface deposition temperature ( $T_{dep}$ ) of Exp.2 at initial temperature ( $T_{init}$ ) of 25°C

Weld bead position (mm)	Cylinder substrate diameter (mm)									
	Ø7	Ø8	Ø9	Ø10	Ø12	Ø16	Ø20	Ø25	Ø30	Ø35
74	647.93	601.52	583.54	541.88	519.27	471.93	450.30	438.08	431.24	429.10
75	648.03	601.54	583.61	541.94	519.31	471.96	450.32	438.10	431.25	429.11
76	648.12	601.57	583.67	541.99	519.35	471.99	450.34	438.11	431.26	429.11
77	648.20	601.59	583.73	542.04	519.38	472.02	450.36	438.13	431.27	429.12
78	648.28	601.61	583.79	542.09	519.42	472.05	450.37	438.14	431.28	429.13
79	648.36	601.63	583.85	542.14	519.45	472.07	450.39	438.16	431.29	429.14
80	648.44	601.65	583.91	542.19	519.49	472.10	450.41	438.17	431.30	429.14
81	648.51	601.67	583.97	542.23	519.52	472.13	450.43	438.18	431.31	429.15
82	648.59	601.69	584.02	542.28	519.55	472.15	450.44	438.20	431.32	429.16
83	648.67	601.71	584.08	542.33	519.59	472.18	450.46	438.21	431.33	429.16
84	648.75	601.74	584.15	542.39	519.62	472.21	450.48	438.23	431.34	429.17
85	648.85	601.76	584.23	542.45	519.67	472.25	450.50	438.24	431.35	429.18
86	648.97	601.79	584.32	542.52	519.72	472.29	450.53	438.27	431.37	429.19
87	649.12	601.83	584.44	542.62	519.79	472.35	450.57	438.29	431.39	429.21
88	649.32	601.89	584.59	542.75	519.88	472.42	450.61	438.33	431.41	429.23
89	649.58	601.95	584.79	542.92	520.00	472.51	450.68	438.38	431.45	429.27
90	649.95	602.05	585.08	543.15	520.16	472.64	450.77	438.46	431.51	429.31
91	650.47	602.19	585.48	543.49	520.40	472.83	450.89	438.57	431.59	429.39
92	651.22	602.38	586.06	543.96	520.74	473.10	451.08	438.73	431.71	429.49
93	652.30	602.66	586.89	544.65	521.24	473.50	451.36	438.96	431.90	429.66
94	653.88	603.07	588.11	545.65	521.96	474.08	451.76	439.32	432.19	429.92
95	656.18	603.66	589.35	547.11	523.02	474.94	452.37	439.87	432.63	430.32
96	659.54	604.53	591.00	549.25	524.61	476.23	453.30	440.71	433.32	430.96

Appendix A The result of thermal simulation

---

Table A.3 : Data surface deposition temperature ( $T_{dep}$ ) of Exp.2 at initial temperature ( $T_{init}$ ) of 25°C

Weld bead position (mm)	Cylinder substrate diameter (mm)									
	Ø7	Ø8	Ø9	Ø10	Ø12	Ø16	Ø20	Ø25	Ø30	Ø35
97	664.43	605.80	593.40	552.38	526.98	478.17	454.71	442.02	434.43	432.00
98	671.61	607.66	596.94	556.98	530.55	481.13	456.92	444.12	436.24	433.71
99	682.10	610.39	599.18	563.78	535.99	485.73	460.42	447.55	439.28	436.62
100	697.44	615.17	602.42	573.86	544.38	493.00	466.16	453.34	444.56	441.74

- Initial temperature ( $T_{init}$ ) of 100°C

Table A.4 : Data surface deposition temperature ( $T_{dep}$ ) of Exp.2 at initial temperature ( $T_{init}$ ) of 100°C

Weld bead position (mm)	Cylinder substrate diameter (mm)									
	Ø7	Ø8	Ø9	Ø10	Ø12	Ø16	Ø20	Ø25	Ø30	Ø35
0	100.00	100.00	100.00	100.00	100.00	100.00	100.00	100.00	100.00	100.00
1	419.10	386.70	386.24	376.00	375.94	371.69	371.20	371.14	371.13	371.14
2	497.15	454.13	452.67	434.00	433.70	423.15	421.51	421.25	421.20	421.21
3	527.99	485.73	482.45	459.48	458.80	444.46	441.21	440.57	440.44	440.44
4	549.75	507.54	502.59	475.17	473.77	455.42	451.24	450.28	450.04	450.03
5	566.82	521.05	514.85	487.14	484.75	462.77	457.14	455.68	455.26	455.23
6	580.95	532.41	524.20	496.93	493.34	468.44	461.45	459.46	458.82	458.76
7	592.56	542.23	532.10	505.30	500.36	473.06	464.87	462.35	461.46	461.35
8	598.27	550.85	538.95	511.76	506.27	476.96	467.72	464.70	463.53	463.37
9	601.06	558.49	545.00	516.66	510.82	480.32	470.17	466.67	465.22	465.01
10	603.59	565.32	550.38	521.05	514.15	483.26	472.30	468.37	466.65	466.37
11	605.88	571.45	555.22	525.02	517.08	485.86	474.18	469.85	467.87	467.52

*A.2 Exp.2: Single weld bead on cylinder substrate thermal simulation*

Table A.4 : Data surface deposition temperature ( $T_{dep}$ ) of Exp.2 at initial temperature ( $T_{init}$ ) of 100°C

Weld bead position (mm)	Cylinder substrate diameter (mm)									
	Ø7	Ø8	Ø9	Ø10	Ø12	Ø16	Ø20	Ø25	Ø30	Ø35
12	607.94	576.97	559.59	528.63	519.70	488.18	475.84	471.16	468.93	468.51
13	609.82	581.98	563.56	531.92	522.05	490.25	477.33	472.33	469.86	469.37
14	611.52	586.54	567.18	534.91	524.18	492.11	478.66	473.37	470.68	470.12
15	614.37	589.77	570.48	537.65	526.12	493.79	479.85	474.29	471.40	470.79
16	617.52	592.24	573.50	540.16	527.90	495.32	480.93	475.13	472.05	471.37
17	620.41	594.50	576.26	542.47	529.52	496.72	481.91	475.87	472.64	471.89
18	623.06	596.58	578.81	544.59	531.01	498.00	482.79	476.55	473.16	472.36
19	625.50	597.89	581.16	546.55	532.38	499.17	483.60	477.16	473.63	472.78
20	627.76	598.71	583.32	548.35	533.64	500.25	484.34	477.71	474.06	473.15
21	630.96	599.46	585.32	550.01	534.81	501.25	485.02	478.21	474.44	473.49
22	633.92	600.15	587.16	551.55	535.89	502.17	485.64	478.67	474.79	473.80
23	636.64	600.79	588.58	552.98	536.89	503.02	486.21	479.09	475.11	474.07
24	639.15	601.39	589.62	554.30	537.82	503.80	486.73	479.47	475.40	474.32
25	641.48	601.95	590.58	555.52	538.68	504.53	487.22	479.82	475.66	474.55
26	643.63	602.46	591.47	556.66	539.49	505.21	487.67	480.13	475.90	474.76
27	645.63	602.94	592.30	557.72	540.23	505.84	488.08	480.43	476.12	474.95
28	647.49	603.39	593.07	558.70	540.93	506.43	488.47	480.70	476.32	475.12
29	649.21	603.80	593.79	559.62	541.57	506.97	488.83	480.94	476.51	475.28
30	650.81	604.19	594.46	560.48	542.18	507.48	489.16	481.17	476.68	475.43
31	652.29	604.55	595.08	561.27	542.74	507.95	489.47	481.38	476.84	475.56
32	653.67	604.88	595.66	562.02	543.27	508.39	489.76	481.58	476.98	475.68
33	654.96	605.20	596.21	562.71	543.76	508.81	490.02	481.76	477.11	475.79
34	656.16	605.49	596.71	563.36	544.21	509.19	490.27	481.93	477.24	475.90

Appendix A The result of thermal simulation

Table A.4 : Data surface deposition temperature ( $T_{dep}$ ) of Exp.2 at initial temperature ( $T_{init}$ ) of 100°C

Weld bead position (mm)	Cylinder substrate diameter (mm)									
	Ø7	Ø8	Ø9	Ø10	Ø12	Ø16	Ø20	Ø25	Ø30	Ø35
35	657.28	605.76	597.19	563.97	544.64	509.55	490.50	482.08	477.35	475.99
36	658.32	606.02	597.50	564.53	545.04	509.89	490.72	482.23	477.45	476.08
37	659.29	606.25	597.70	565.07	545.41	510.20	490.92	482.36	477.55	476.16
38	660.19	606.48	597.88	565.56	545.76	510.49	491.11	482.48	477.64	476.23
39	661.04	606.69	598.04	566.03	546.09	510.77	491.29	482.60	477.72	476.30
40	661.83	606.88	598.20	566.46	546.39	510.96	491.45	482.71	477.80	476.36
41	662.57	607.07	598.35	566.87	546.68	511.14	491.60	482.81	477.87	476.42
42	663.25	607.24	598.49	567.25	546.95	511.31	491.75	482.90	477.94	476.47
43	663.90	607.40	598.62	567.61	547.20	511.46	491.88	482.98	478.00	476.52
44	664.50	607.55	598.74	567.94	547.44	511.61	492.01	483.06	478.05	476.57
45	665.06	607.69	598.86	568.26	547.65	511.75	492.12	483.14	478.11	476.61
46	665.58	607.82	598.96	568.55	547.86	511.87	492.23	483.21	478.15	476.65
47	666.08	607.94	599.06	568.83	548.05	511.99	492.33	483.27	478.20	476.69
48	666.53	608.06	599.16	569.09	548.23	512.11	492.43	483.33	478.24	476.72
49	666.96	608.17	599.25	569.33	548.40	512.21	492.52	483.39	478.28	476.75
50	667.36	608.27	599.33	569.56	548.56	512.31	492.60	483.44	478.31	476.78
51	667.74	608.37	599.41	569.77	548.71	512.40	492.68	483.49	478.35	476.80
52	668.09	608.46	599.48	569.97	548.85	512.49	492.75	483.53	478.38	476.83
53	668.42	608.54	599.55	570.16	548.98	512.57	492.82	483.57	478.41	476.85
54	668.73	608.62	599.62	570.33	549.10	512.64	492.88	483.61	478.43	476.87
55	669.02	608.69	599.68	570.50	549.22	512.71	492.94	483.65	478.45	476.89
56	669.29	608.76	599.73	570.65	549.32	512.78	492.99	483.68	478.48	476.90
57	669.54	608.83	599.79	570.80	549.42	512.84	493.04	483.71	478.50	476.92

*A.2 Exp.2: Single weld bead on cylinder substrate thermal simulation*

Table A.4 : Data surface deposition temperature ( $T_{dep}$ ) of Exp.2 at initial temperature ( $T_{init}$ ) of 100°C

Weld bead position (mm)	Cylinder substrate diameter (mm)									
	Ø7	Ø8	Ø9	Ø10	Ø12	Ø16	Ø20	Ø25	Ø30	Ø35
58	669.77	608.89	599.84	570.94	549.52	512.89	493.09	483.74	478.51	476.93
59	670.00	608.95	599.88	571.06	549.60	512.95	493.13	483.76	478.53	476.94
60	670.20	609.00	599.93	571.18	549.69	513.00	493.17	483.79	478.55	476.95
61	670.39	609.05	599.97	571.30	549.76	513.04	493.21	483.81	478.56	476.96
62	670.57	609.10	600.01	571.40	549.83	513.08	493.24	483.83	478.57	476.97
63	670.74	609.14	600.04	571.50	549.90	513.12	493.27	483.85	478.58	476.98
64	670.90	609.18	600.08	571.59	549.96	513.16	493.30	483.86	478.59	476.99
65	671.05	609.22	600.11	571.68	550.02	513.19	493.33	483.88	478.60	476.99
66	671.18	609.26	600.14	571.76	550.07	513.22	493.35	483.89	478.61	477.00
67	671.31	609.29	600.17	571.83	550.12	513.25	493.37	483.90	478.61	477.00
68	671.43	609.32	600.19	571.90	550.17	513.28	493.39	483.91	478.62	477.00
69	671.54	609.35	600.22	571.96	550.21	513.30	493.41	483.92	478.62	477.00
70	671.65	609.38	600.24	572.02	550.25	513.32	493.43	483.93	478.63	477.01
71	671.74	609.40	600.26	572.08	550.28	513.34	493.44	483.94	478.63	477.01
72	671.83	609.43	600.28	572.13	550.32	513.36	493.45	483.94	478.63	477.01
73	671.92	609.45	600.30	572.18	550.35	513.38	493.47	483.94	478.63	477.00
74	671.99	609.47	600.32	572.23	550.38	513.39	493.48	483.95	478.63	477.00
75	672.07	609.49	600.33	572.27	550.40	513.41	493.48	483.95	478.63	477.00
76	672.13	609.51	600.35	572.31	550.43	513.42	493.49	483.95	478.63	477.00
77	672.20	609.52	600.36	572.34	550.45	513.43	493.50	483.95	478.63	477.00
78	672.26	609.54	600.37	572.37	550.47	513.44	493.50	483.95	478.63	476.99
79	672.31	609.55	600.38	572.41	550.49	513.44	493.50	483.95	478.62	476.99
80	672.37	609.57	600.40	572.44	550.50	513.45	493.51	483.95	478.62	476.98

Appendix A The result of thermal simulation

Table A.4 : Data surface deposition temperature ( $T_{dep}$ ) of Exp.2 at initial temperature ( $T_{init}$ ) of 100°C

Weld bead position (mm)	Cylinder substrate diameter (mm)									
	Ø7	Ø8	Ø9	Ø10	Ø12	Ø16	Ø20	Ø25	Ø30	Ø35
81	672.42	609.58	600.41	572.47	550.52	513.46	493.51	483.95	478.62	476.98
82	672.48	609.60	600.42	572.50	550.54	513.47	493.51	483.95	478.61	476.97
83	672.54	609.61	600.43	572.53	550.56	513.48	493.52	483.94	478.61	476.97
84	672.61	609.63	600.45	572.57	550.58	513.49	493.52	483.94	478.60	476.97
85	672.69	609.65	600.46	572.62	550.61	513.50	493.53	483.95	478.60	476.96
86	672.79	609.68	600.48	572.68	550.65	513.52	493.54	483.95	478.60	476.96
87	672.92	609.71	600.51	572.75	550.70	513.55	493.56	483.96	478.61	476.96
88	673.10	609.76	600.55	572.86	550.77	513.59	493.59	483.98	478.62	476.97
89	673.35	609.83	600.60	573.02	550.88	513.65	493.63	484.01	478.64	476.99
90	673.71	609.92	600.67	573.23	551.03	513.74	493.71	484.05	478.67	477.01
91	674.23	610.06	600.78	573.55	551.25	513.88	493.82	484.13	478.73	477.06
92	674.99	610.25	600.93	574.01	551.57	514.08	493.98	484.25	478.82	477.14
93	676.08	610.54	601.15	574.68	552.05	514.38	494.24	484.43	478.96	477.26
94	677.68	610.95	601.47	575.66	552.76	514.84	494.62	484.72	479.18	477.46
95	680.02	611.56	601.94	577.10	553.81	515.51	495.21	485.16	479.54	477.79
96	683.41	612.68	602.63	579.20	555.37	516.53	496.10	485.86	480.11	478.31
97	688.37	615.20	603.64	582.27	557.69	518.08	497.48	486.95	481.03	479.17
98	695.58	618.87	605.12	586.49	561.18	520.43	499.64	488.71	482.54	480.60
99	706.08	624.22	607.30	590.68	566.47	524.07	503.06	491.58	485.09	483.04
100	728.31	632.05	610.56	596.33	574.55	529.83	508.65	496.42	489.51	487.32

- Initial temperature ( $T_{init}$ ) of 200°C

A.2 Exp.2: Single weld bead on cylinder substrate thermal simulation

Table A.5 : Data surface deposition temperature ( $T_{dep}$ ) of Exp.2 at initial temperature ( $T_{init}$ ) of 200°C

Weld bead position (mm)	Cylinder substrate diameter (mm)									
	Ø7	Ø8	Ø9	Ø10	Ø12	Ø16	Ø20	Ø25	Ø30	Ø35
0	200.00	200.00	200.00	200.00	200.00	200.00	200.00	200.00	200.00	200.00
1	489.06	463.55	463.17	454.99	454.94	451.50	451.09	451.03	451.02	451.03
2	543.19	514.55	513.45	498.67	498.42	489.98	488.65	488.43	488.39	488.39
3	571.96	536.86	534.42	518.67	518.15	506.86	504.24	503.72	503.61	503.61
4	591.85	552.88	548.73	529.93	528.88	516.07	512.75	511.81	511.57	511.56
5	599.18	565.60	559.57	538.53	536.74	521.42	517.42	516.36	516.06	516.03
6	603.20	576.28	568.36	545.54	542.88	525.53	520.58	519.15	518.68	518.63
7	606.71	585.49	575.76	551.50	547.86	528.86	523.07	521.26	520.61	520.53
8	609.81	591.38	582.19	556.70	552.04	531.65	525.12	522.96	522.11	522.00
9	612.57	596.07	587.63	561.31	555.61	534.04	526.86	524.37	523.32	523.17
10	617.61	598.23	590.92	565.44	558.72	536.12	528.38	525.58	524.33	524.13
11	622.56	599.99	593.89	569.17	561.47	537.95	529.70	526.62	525.19	524.94
12	627.04	601.59	596.51	572.55	563.92	539.57	530.87	527.55	525.94	525.64
13	632.77	603.04	597.64	575.62	566.13	541.02	531.91	528.36	526.59	526.24
14	638.51	604.37	598.67	578.42	568.12	542.33	532.85	529.09	527.16	526.76
15	643.74	605.59	599.62	580.98	569.93	543.51	533.68	529.73	527.67	527.22
16	648.50	606.70	600.49	583.33	571.59	544.58	534.44	530.31	528.12	527.63
17	652.85	607.72	601.29	585.49	573.10	545.55	535.12	530.83	528.52	527.99
18	656.83	608.65	602.03	586.90	574.49	546.45	535.74	531.30	528.88	528.31
19	660.48	609.51	602.71	588.10	575.77	547.26	536.30	531.73	529.21	528.60
20	663.83	610.31	603.34	589.20	576.95	548.02	536.81	532.11	529.50	528.86
21	666.91	611.04	603.93	590.22	578.04	548.71	537.28	532.45	529.77	529.09
22	669.75	611.72	604.47	591.16	579.04	549.35	537.71	532.77	530.01	529.30



Table A.5 : Data surface deposition temperature ( $T_{dep}$ ) of Exp.2 at initial temperature ( $T_{init}$ ) of 200°C

Weld bead position (mm)	Cylinder substrate diameter (mm)									
	Ø7	Ø8	Ø9	Ø10	Ø12	Ø16	Ø20	Ø25	Ø30	Ø35
23	672.36	612.35	604.97	592.03	579.98	549.94	538.11	533.06	530.22	529.49
24	674.77	613.26	605.43	592.84	580.84	550.49	538.47	533.32	530.42	529.66
25	677.00	614.45	605.86	593.59	581.64	550.99	538.80	533.56	530.60	529.82
26	679.06	615.56	606.26	594.29	582.39	551.46	539.11	533.78	530.76	529.96
27	680.97	616.58	606.63	594.94	583.08	551.90	539.40	533.98	530.91	530.09
28	682.73	617.53	606.98	595.54	583.72	552.30	539.66	534.16	531.05	530.20
29	684.36	618.42	607.30	596.10	584.32	552.68	539.91	534.33	531.17	530.31
30	685.88	619.24	607.60	596.62	584.88	553.03	540.13	534.48	531.29	530.41
31	687.29	620.01	607.88	596.84	585.39	553.35	540.34	534.62	531.39	530.49
32	688.59	620.72	608.14	597.05	585.86	553.66	540.54	534.76	531.49	530.57
33	689.81	621.38	608.38	597.25	586.16	553.94	540.72	534.88	531.58	530.65
34	690.93	622.00	608.61	597.43	586.43	554.20	540.89	534.99	531.66	530.72
35	691.98	622.58	608.82	597.60	586.69	554.44	541.04	535.09	531.73	530.78
36	692.96	623.12	609.01	597.76	586.93	554.67	541.19	535.18	531.80	530.83
37	693.86	623.62	609.20	597.91	587.15	554.88	541.32	535.27	531.86	530.88
38	694.70	624.08	609.37	598.05	587.36	555.08	541.45	535.35	531.92	530.93
39	695.49	624.52	609.53	598.18	587.55	555.26	541.56	535.43	531.97	530.97
40	696.22	624.93	609.68	598.31	587.73	555.43	541.67	535.49	532.02	531.01
41	696.90	625.31	609.82	598.42	587.90	555.59	541.77	535.56	532.06	531.05
42	697.53	625.66	609.95	598.53	588.06	555.74	541.86	535.61	532.10	531.08
43	698.12	626.00	610.08	598.63	588.20	555.87	541.95	535.67	532.14	531.11
44	698.67	626.31	610.19	598.72	588.34	556.00	542.03	535.72	532.17	531.13
45	699.18	626.60	610.30	598.81	588.47	556.12	542.10	535.76	532.20	531.16

A.2 Exp.2: Single weld bead on cylinder substrate thermal simulation

Table A.5 : Data surface deposition temperature ( $T_{dep}$ ) of Exp.2 at initial temperature ( $T_{init}$ ) of 200°C

Weld bead position (mm)	Cylinder substrate diameter (mm)									
	Ø7	Ø8	Ø9	Ø10	Ø12	Ø16	Ø20	Ø25	Ø30	Ø35
46	699.65	626.87	610.40	598.89	588.58	556.23	542.17	535.80	532.23	531.18
47	700.10	627.12	610.49	598.96	588.70	556.33	542.23	535.84	532.25	531.20
48	700.51	627.35	610.58	599.03	588.80	556.43	542.29	535.87	532.27	531.21
49	700.89	627.57	610.66	599.10	588.89	556.51	542.34	535.90	532.29	531.23
50	701.25	627.78	610.73	599.16	588.98	556.59	542.39	535.93	532.31	531.24
51	701.58	627.97	610.81	599.22	589.07	556.67	542.43	535.96	532.33	531.25
52	701.89	628.15	610.87	599.28	589.14	556.74	542.47	535.98	532.34	531.26
53	702.17	628.31	610.93	599.33	589.21	556.80	542.51	536.00	532.35	531.27
54	702.44	628.47	610.99	599.37	589.28	556.86	542.54	536.02	532.36	531.28
55	702.69	628.61	611.04	599.42	589.34	556.91	542.57	536.04	532.37	531.29
56	702.92	628.74	611.09	599.46	589.40	556.96	542.60	536.05	532.38	531.29
57	703.13	628.87	611.14	599.49	589.45	557.00	542.63	536.06	532.39	531.29
58	703.33	628.98	611.18	599.53	589.50	557.04	542.65	536.07	532.39	531.30
59	703.51	629.09	611.22	599.56	589.54	557.08	542.67	536.08	532.40	531.30
60	703.68	629.19	611.26	599.59	589.58	557.11	542.68	536.09	532.40	531.30
61	703.83	629.28	611.29	599.62	589.62	557.14	542.70	536.09	532.40	531.30
62	703.97	629.37	611.32	599.64	589.65	557.17	542.71	536.10	532.40	531.29
63	704.11	629.45	611.35	599.67	589.68	557.19	542.72	536.10	532.40	531.29
64	704.23	629.52	611.38	599.69	589.71	557.21	542.73	536.10	532.39	531.29
65	704.34	629.58	611.40	599.71	589.73	557.23	542.73	536.10	532.39	531.28
66	704.44	629.65	611.42	599.73	589.75	557.24	542.74	536.10	532.39	531.28
67	704.53	629.70	611.44	599.74	589.77	557.25	542.74	536.10	532.38	531.27
68	704.62	629.75	611.46	599.76	589.79	557.26	542.74	536.09	532.38	531.27

Table A.5 : Data surface deposition temperature ( $T_{dep}$ ) of Exp.2 at initial temperature ( $T_{init}$ ) of 200°C

Weld bead position (mm)	Cylinder substrate diameter (mm)									
	Ø7	Ø8	Ø9	Ø10	Ø12	Ø16	Ø20	Ø25	Ø30	Ø35
69	704.69	629.80	611.48	599.77	589.81	557.27	542.74	536.09	532.37	531.26
70	704.76	629.84	611.49	599.78	589.82	557.28	542.74	536.08	532.36	531.25
71	704.82	629.88	611.51	599.79	589.83	557.28	542.73	536.07	532.35	531.24
72	704.88	629.91	611.52	599.80	589.84	557.28	542.73	536.06	532.34	531.23
73	704.93	629.95	611.53	599.81	589.84	557.28	542.72	536.05	532.33	531.22
74	704.97	629.97	611.54	599.82	589.85	557.27	542.71	536.04	532.32	531.21
75	705.01	630.00	611.55	599.82	589.85	557.27	542.70	536.03	532.31	531.20
76	705.05	630.02	611.55	599.83	589.85	557.26	542.69	536.02	532.29	531.18
77	705.08	630.04	611.56	599.83	589.86	557.25	542.68	536.01	532.28	531.17
78	705.10	630.05	611.57	599.83	589.86	557.25	542.67	535.99	532.27	531.16
79	705.13	630.07	611.57	599.84	589.85	557.24	542.66	535.98	532.25	531.14
80	705.15	630.08	611.57	599.84	589.85	557.22	542.64	535.96	532.24	531.13
81	705.17	630.10	611.58	599.84	589.85	557.21	542.63	535.95	532.22	531.11
82	705.20	630.11	611.58	599.84	589.85	557.20	542.61	535.93	532.20	531.10
83	705.22	630.13	611.59	599.85	589.85	557.19	542.60	535.91	532.19	531.08
84	705.26	630.15	611.59	599.85	589.85	557.18	542.59	535.90	532.17	531.07
85	705.32	630.18	611.60	599.86	589.85	557.18	542.58	535.88	532.16	531.05
86	705.39	630.22	611.62	599.87	589.86	557.18	542.57	535.87	532.14	531.04
87	705.50	630.27	611.64	599.88	589.88	557.19	542.57	535.87	532.13	531.03
88	705.66	630.36	611.67	599.91	589.92	557.21	542.57	535.87	532.13	531.02
89	705.90	630.48	611.72	599.94	589.97	557.26	542.60	535.87	532.13	531.02
90	706.25	630.66	611.79	600.00	590.06	557.33	542.64	535.90	532.15	531.03
91	706.77	630.92	611.89	600.08	590.19	557.45	542.71	535.95	532.18	531.06

A.2 Exp.2: Single weld bead on cylinder substrate thermal simulation

Table A.5 : Data surface deposition temperature ( $T_{dep}$ ) of Exp.2 at initial temperature ( $T_{init}$ ) of 200°C

Weld bead position (mm)	Cylinder substrate diameter (mm)									
	Ø7	Ø8	Ø9	Ø10	Ø12	Ø16	Ø20	Ø25	Ø30	Ø35
92	707.53	631.31	612.05	600.20	590.38	557.64	542.83	536.03	532.24	531.11
93	708.63	631.88	612.27	600.37	590.67	557.93	543.02	536.16	532.34	531.20
94	710.25	633.04	612.60	600.63	591.11	558.36	543.32	536.38	532.51	531.35
95	712.61	634.88	613.30	601.01	591.76	559.02	543.78	536.73	532.78	531.59
96	716.05	637.57	614.67	601.57	592.72	560.01	544.48	537.27	533.23	532.00
97	722.93	641.47	616.68	602.38	594.15	561.50	545.56	538.13	533.95	532.68
98	736.25	647.13	619.61	603.56	596.17	563.77	547.24	539.50	535.14	533.80
99	756.68	655.37	623.90	605.30	597.51	567.26	549.91	541.74	537.13	535.71
100	785.84	667.30	630.25	607.89	599.55	572.72	554.25	545.52	540.59	539.07

- Initial temperature ( $T_{init}$ ) of 300°C

Table A.6 : Data surface deposition temperature ( $T_{dep}$ ) of Exp.2 at initial temperature ( $T_{init}$ ) of 300°C

Weld bead position (mm)	Cylinder substrate diameter (mm)									
	Ø7	Ø8	Ø9	Ø10	Ø12	Ø16	Ø20	Ø25	Ø30	Ø35
0	300.00	300.00	300.00	300.00	300.00	300.00	300.00	300.00	300.00	300.00
1	543.06	526.36	526.07	520.50	520.46	517.68	517.28	517.23	517.22	517.23
2	588.94	562.26	561.18	550.36	550.17	544.30	543.35	543.19	543.16	543.17
3	600.91	583.00	580.62	565.92	565.40	556.19	554.33	553.95	553.87	553.87
4	606.75	593.96	591.33	576.39	575.35	563.31	560.46	559.79	559.62	559.61
5	611.44	598.52	596.76	584.37	582.63	568.30	564.49	563.48	563.18	563.16
6	617.32	601.55	599.21	588.86	587.17	572.12	567.44	566.07	565.62	565.57

Appendix A The result of thermal simulation

Table A.6 : Data surface deposition temperature ( $T_{dep}$ ) of Exp.2 at initial temperature ( $T_{init}$ ) of 300°C

Weld bead position (mm)	Cylinder substrate diameter (mm)									
	Ø7	Ø8	Ø9	Ø10	Ø12	Ø16	Ø20	Ø25	Ø30	Ø35
7	624.90	604.21	601.31	592.50	590.19	575.19	569.75	568.03	567.40	567.33
8	633.27	606.57	603.15	595.68	592.72	577.76	571.65	569.59	568.78	568.68
9	642.57	608.70	604.79	596.98	594.89	579.96	573.25	570.90	569.90	569.75
10	650.90	610.61	606.27	598.15	596.18	581.88	574.64	572.00	570.82	570.63
11	658.39	612.34	607.61	599.21	596.95	583.56	575.85	572.96	571.61	571.38
12	665.14	614.16	608.83	600.18	597.64	584.72	576.92	573.80	572.29	572.01
13	671.25	617.32	609.94	601.07	598.27	585.59	577.87	574.55	572.88	572.55
14	676.79	620.19	610.96	601.88	598.83	586.37	578.72	575.20	573.39	573.02
15	681.82	622.81	611.89	602.63	599.35	587.08	579.48	575.79	573.85	573.44
16	686.40	625.21	612.75	603.32	599.83	587.73	580.17	576.32	574.26	573.81
17	690.57	627.40	613.53	603.95	600.26	588.31	580.79	576.79	574.62	574.13
18	694.38	629.41	614.96	604.53	600.66	588.85	581.35	577.21	574.95	574.42
19	697.87	631.26	616.43	605.07	601.03	589.34	581.86	577.59	575.24	574.68
20	701.07	633.28	617.80	605.56	601.37	589.80	582.32	577.94	575.50	574.91
21	704.01	635.71	619.06	606.02	601.68	590.21	582.75	578.25	575.74	575.12
22	706.70	637.96	620.22	606.45	601.97	590.60	583.14	578.53	575.95	575.30
23	709.18	640.03	621.30	606.84	602.24	590.95	583.49	578.79	576.15	575.47
24	711.47	641.95	622.29	607.20	602.49	591.28	583.82	579.02	576.32	575.62
25	713.57	643.72	623.21	607.54	602.72	591.58	584.04	579.23	576.48	575.76
26	715.51	645.36	624.07	607.86	602.94	591.86	584.22	579.42	576.62	575.88
27	717.62	646.87	624.86	608.15	603.14	592.12	584.38	579.60	576.75	575.99
28	719.84	648.28	625.59	608.42	603.32	592.36	584.54	579.76	576.87	576.09
29	721.89	649.58	626.28	608.67	603.49	592.58	584.68	579.91	576.98	576.19

*A.2 Exp.2: Single weld bead on cylinder substrate thermal simulation*

Table A.6 : Data surface deposition temperature ( $T_{dep}$ ) of Exp.2 at initial temperature ( $T_{init}$ ) of 300°C

Weld bead position (mm)	Cylinder substrate diameter (mm)									
	Ø7	Ø8	Ø9	Ø10	Ø12	Ø16	Ø20	Ø25	Ø30	Ø35
30	723.79	650.79	626.91	608.91	603.65	592.79	584.81	580.04	577.07	576.27
31	725.55	651.91	627.50	609.12	603.80	592.98	584.93	580.16	577.16	576.34
32	727.17	652.95	628.05	609.33	603.94	593.16	585.04	580.27	577.24	576.41
33	729.05	653.92	628.56	609.51	604.07	593.32	585.14	580.37	577.31	576.47
34	730.80	654.82	629.03	609.69	604.19	593.47	585.24	580.47	577.38	576.53
35	732.42	655.65	629.47	609.85	604.30	593.61	585.33	580.55	577.44	576.57
36	733.91	656.43	629.88	610.00	604.41	593.74	585.41	580.63	577.49	576.62
37	735.30	657.15	630.26	610.15	604.50	593.87	585.48	580.70	577.54	576.66
38	736.59	657.82	630.62	610.28	604.59	593.98	585.55	580.76	577.59	576.69
39	737.78	658.44	630.95	610.40	604.67	594.08	585.61	580.82	577.63	576.73
40	738.88	659.02	631.26	610.51	604.75	594.18	585.67	580.88	577.66	576.75
41	739.90	659.56	631.54	610.62	604.82	594.26	585.72	580.92	577.69	576.78
42	740.85	660.06	631.81	610.72	604.89	594.35	585.77	580.97	577.72	576.80
43	741.72	660.53	632.05	610.81	604.95	594.42	585.82	581.01	577.75	576.82
44	742.53	660.96	632.28	610.89	605.01	594.49	585.86	581.04	577.77	576.84
45	743.28	661.36	632.52	610.97	605.06	594.55	585.89	581.07	577.79	576.85
46	743.97	661.73	632.83	611.05	605.11	594.61	585.93	581.10	577.80	576.86
47	744.60	662.08	633.11	611.11	605.16	594.66	585.96	581.12	577.82	576.87
48	745.19	662.39	633.38	611.18	605.20	594.71	585.98	581.14	577.83	576.88
49	745.74	662.69	633.62	611.23	605.24	594.76	586.01	581.16	577.84	576.88
50	746.24	662.96	633.85	611.29	605.27	594.79	586.03	581.18	577.84	576.89
51	746.69	663.22	634.06	611.34	605.31	594.83	586.05	581.19	577.85	576.89
52	747.12	663.45	634.25	611.38	605.34	594.86	586.06	581.20	577.85	576.89

Appendix A The result of thermal simulation

Table A.6 : Data surface deposition temperature ( $T_{dep}$ ) of Exp.2 at initial temperature ( $T_{init}$ ) of 300°C

Weld bead position (mm)	Cylinder substrate diameter (mm)									
	Ø7	Ø8	Ø9	Ø10	Ø12	Ø16	Ø20	Ø25	Ø30	Ø35
53	747.50	663.66	634.43	611.42	605.36	594.89	586.07	581.21	577.85	576.89
54	747.86	663.86	634.59	611.46	605.39	594.92	586.09	581.21	577.85	576.89
55	748.18	664.04	634.74	611.50	605.41	594.94	586.10	581.21	577.85	576.89
56	748.47	664.21	634.88	611.53	605.43	594.96	586.10	581.21	577.85	576.88
57	748.74	664.36	635.01	611.56	605.45	594.97	586.11	581.21	577.84	576.87
58	748.98	664.50	635.12	611.58	605.47	594.99	586.11	581.21	577.84	576.87
59	749.20	664.63	635.23	611.61	605.48	595.00	586.12	581.21	577.83	576.86
60	749.40	664.74	635.32	611.63	605.49	595.01	586.12	581.20	577.82	576.85
61	749.57	664.85	635.40	611.65	605.50	595.01	586.11	581.19	577.81	576.84
62	749.73	664.94	635.48	611.67	605.51	595.02	586.11	581.18	577.80	576.83
63	749.87	665.02	635.55	611.68	605.52	595.02	586.11	581.17	577.79	576.81
64	749.99	665.10	635.61	611.69	605.53	595.02	586.10	581.16	577.77	576.80
65	750.09	665.16	635.66	611.70	605.53	595.02	586.10	581.14	577.76	576.79
66	750.18	665.22	635.70	611.71	605.54	595.01	586.09	581.13	577.74	576.77
67	750.25	665.27	635.74	611.72	605.54	595.01	586.08	581.11	577.72	576.75
68	750.31	665.31	635.77	611.73	605.54	595.00	586.07	581.09	577.70	576.74
69	750.36	665.34	635.80	611.73	605.54	594.99	586.06	581.07	577.68	576.72
70	750.39	665.37	635.82	611.73	605.54	594.98	586.04	581.05	577.66	576.70
71	750.42	665.39	635.83	611.74	605.54	594.97	586.03	581.03	577.64	576.68
72	750.43	665.41	635.84	611.74	605.54	594.96	586.02	581.01	577.62	576.66
73	750.44	665.42	635.85	611.73	605.53	594.94	586.00	580.98	577.59	576.63
74	750.43	665.42	635.85	611.73	605.53	594.93	585.98	580.96	577.57	576.61
75	750.42	665.42	635.84	611.73	605.52	594.91	585.96	580.93	577.54	576.58

*A.2 Exp.2: Single weld bead on cylinder substrate thermal simulation*

Table A.6 : Data surface deposition temperature ( $T_{dep}$ ) of Exp.2 at initial temperature ( $T_{init}$ ) of 300°C

Weld bead position (mm)	Cylinder substrate diameter (mm)									
	Ø7	Ø8	Ø9	Ø10	Ø12	Ø16	Ø20	Ø25	Ø30	Ø35
76	750.39	665.42	635.84	611.73	605.52	594.89	585.95	580.90	577.52	576.56
77	750.37	665.41	635.83	611.72	605.51	594.87	585.93	580.87	577.49	576.53
78	750.33	665.40	635.81	611.71	605.50	594.85	585.91	580.84	577.46	576.51
79	750.30	665.39	635.79	611.71	605.49	594.83	585.88	580.81	577.43	576.48
80	750.26	665.37	635.78	611.70	605.49	594.81	585.86	580.78	577.40	576.45
81	750.22	665.36	635.76	611.69	605.48	594.79	585.84	580.74	577.37	576.42
82	750.19	665.34	635.74	611.69	605.47	594.76	585.82	580.71	577.34	576.39
83	750.18	665.33	635.72	611.68	605.46	594.74	585.80	580.68	577.30	576.36
84	750.18	665.33	635.71	611.68	605.45	594.72	585.77	580.64	577.27	576.33
85	750.21	665.34	635.71	611.68	605.45	594.70	585.75	580.61	577.24	576.30
86	750.29	665.37	635.72	611.68	605.45	594.69	585.74	580.58	577.21	576.27
87	750.45	665.42	635.76	611.68	605.45	594.68	585.72	580.56	577.19	576.25
88	750.71	665.52	635.83	611.70	605.45	594.68	585.71	580.54	577.16	576.22
89	751.14	665.69	635.95	611.73	605.47	594.69	585.71	580.53	577.15	576.21
90	751.79	665.94	636.14	611.78	605.50	594.73	585.73	580.53	577.14	576.20
91	752.78	666.33	636.43	611.86	605.55	594.79	585.76	580.56	577.16	576.21
92	754.25	666.92	636.88	611.97	605.63	594.89	585.82	580.62	577.20	576.24
93	756.42	667.78	637.55	612.15	605.75	595.06	585.93	580.74	577.28	576.31
94	759.60	669.05	638.54	612.41	605.93	595.32	586.10	580.93	577.43	576.44
95	764.24	670.92	640.00	612.80	606.20	595.72	586.37	581.24	577.68	576.67
96	770.98	673.63	642.12	613.37	606.60	595.97	586.78	581.75	578.08	577.04
97	780.73	677.56	645.22	614.42	607.20	596.34	587.43	582.55	578.76	577.67
98	794.73	683.25	649.73	616.76	608.10	596.91	588.44	583.77	579.87	578.72



Appendix A The result of thermal simulation

---

Table A.6 : Data surface deposition temperature ( $T_{dep}$ ) of Exp.2 at initial temperature ( $T_{init}$ ) of 300°C

Weld bead position (mm)	Cylinder substrate diameter (mm)									
	Ø7	Ø8	Ø9	Ø10	Ø12	Ø16	Ø20	Ø25	Ø30	Ø35
99	814.66	691.45	656.34	620.19	609.45	597.79	590.03	585.09	581.73	580.50
100	842.93	705.67	665.99	625.25	611.51	599.15	592.61	587.32	584.35	583.49

- Initial temperature ( $T_{init}$ ) of 400°C

Table A.7 : Data surface deposition temperature ( $T_{dep}$ ) of Exp.2 at initial temperature ( $T_{init}$ ) of 400°C

Weld bead position (mm)	Cylinder substrate diameter (mm)									
	Ø7	Ø8	Ø9	Ø10	Ø12	Ø16	Ø20	Ø25	Ø30	Ø35
0	400.00	400.00	400.00	400.00	400.00	400.00	400.00	400.00	400.00	400.00
1	590.74	576.39	576.11	570.91	570.88	568.59	568.31	568.28	568.27	568.28
2	606.07	598.03	597.71	593.44	593.32	589.49	588.87	588.76	588.74	588.75
3	613.96	603.88	603.16	598.80	598.65	595.98	595.36	595.11	595.06	595.06
4	625.79	608.18	606.94	601.69	601.37	597.85	597.02	596.83	596.78	596.78
5	639.49	611.69	609.88	603.92	603.39	599.16	598.06	597.76	597.68	597.67
6	652.79	614.76	612.29	605.79	605.00	600.18	598.82	598.42	598.29	598.28
7	664.32	620.47	614.36	607.40	606.32	601.02	599.43	598.93	598.75	598.73
8	674.46	625.55	617.97	608.83	607.44	601.73	599.94	599.34	599.10	599.07
9	683.46	630.12	621.51	610.11	608.40	602.35	600.37	599.69	599.39	599.35
10	691.49	635.00	624.70	611.26	609.25	602.89	600.76	599.99	599.64	599.59
11	698.69	640.78	627.59	612.31	610.01	603.37	601.09	600.25	599.85	599.79
12	705.17	646.01	630.22	613.27	610.68	603.80	601.39	600.48	600.04	599.96
13	711.06	650.74	632.62	614.14	611.29	604.18	601.66	600.69	600.20	600.11

*A.2 Exp.2: Single weld bead on cylinder substrate thermal simulation*

Table A.7 : Data surface deposition temperature ( $T_{dep}$ ) of Exp.2 at initial temperature ( $T_{init}$ ) of 400°C

Weld bead position (mm)	Cylinder substrate diameter (mm)									
	Ø7	Ø8	Ø9	Ø10	Ø12	Ø16	Ø20	Ø25	Ø30	Ø35
14	718.14	655.04	635.88	615.32	611.85	604.53	601.90	600.87	600.34	600.24
15	725.33	658.96	638.99	616.94	612.35	604.85	602.12	601.04	600.47	600.35
16	732.65	662.53	641.84	618.43	612.82	605.13	602.31	601.18	600.58	600.45
17	739.31	665.80	644.45	619.79	613.24	605.39	602.49	601.31	600.68	600.54
18	745.38	668.78	646.85	621.05	613.63	605.63	602.65	601.43	600.77	600.62
19	750.92	671.52	649.05	622.20	613.99	605.85	602.79	601.54	600.85	600.69
20	755.98	674.03	651.07	623.27	614.32	606.05	602.92	601.63	600.93	600.76
21	760.62	676.34	652.94	624.25	614.66	606.24	603.04	601.72	600.99	600.81
22	764.87	678.46	654.66	625.15	615.29	606.41	603.15	601.80	601.05	600.86
23	768.77	680.41	656.25	625.99	615.87	606.56	603.25	601.87	601.10	600.91
24	772.34	682.21	657.71	626.76	616.40	606.71	603.35	601.93	601.15	600.95
25	775.63	683.87	659.06	627.47	616.90	606.84	603.43	601.99	601.19	600.99
26	778.66	685.40	660.31	628.13	617.36	606.97	603.51	602.04	601.23	601.02
27	781.44	686.81	661.47	628.75	617.78	607.08	603.58	602.09	601.26	601.05
28	784.00	688.12	662.54	629.31	618.18	607.18	603.64	602.13	601.30	601.08
29	786.36	689.32	663.52	629.84	618.54	607.28	603.70	602.17	601.32	601.10
30	788.53	690.44	664.44	630.32	618.88	607.37	603.76	602.21	601.35	601.12
31	790.53	691.47	665.29	630.77	619.20	607.45	603.81	602.24	601.37	601.14
32	792.37	692.43	666.07	631.19	619.49	607.53	603.85	602.27	601.39	601.16
33	794.07	693.31	666.80	631.58	619.76	607.60	603.90	602.30	601.41	601.17
34	795.63	694.12	667.47	631.93	620.00	607.66	603.93	602.32	601.42	601.19
35	797.07	694.88	668.09	632.26	620.24	607.72	603.97	602.34	601.44	601.20
36	798.40	695.58	668.67	632.57	620.45	607.78	604.00	602.36	601.45	601.21

Appendix A The result of thermal simulation

Table A.7 : Data surface deposition temperature ( $T_{dep}$ ) of Exp.2 at initial temperature ( $T_{init}$ ) of 400°C

Weld bead position (mm)	Cylinder substrate diameter (mm)									
	Ø7	Ø8	Ø9	Ø10	Ø12	Ø16	Ø20	Ø25	Ø30	Ø35
37	799.62	696.22	669.20	632.86	620.65	607.83	604.03	602.38	601.46	601.22
38	800.74	696.82	669.69	633.12	620.83	607.87	604.06	602.39	601.47	601.22
39	801.78	697.37	670.15	633.36	621.00	607.92	604.08	602.40	601.48	601.23
40	802.73	697.88	670.57	633.58	621.15	607.96	604.10	602.42	601.49	601.24
41	803.60	698.35	670.96	633.79	621.29	607.99	604.12	602.43	601.49	601.24
42	804.40	698.78	671.31	633.98	621.42	608.02	604.14	602.44	601.50	601.24
43	805.13	699.18	671.64	634.16	621.54	608.05	604.15	602.44	601.50	601.25
44	805.80	699.54	671.95	634.38	621.65	608.08	604.17	602.45	601.50	601.25
45	806.42	699.88	672.22	634.61	621.75	608.10	604.18	602.45	601.51	601.25
46	806.97	700.19	672.48	634.83	621.85	608.12	604.19	602.46	601.51	601.25
47	807.48	700.47	672.71	635.02	621.93	608.14	604.20	602.46	601.51	601.25
48	807.94	700.73	672.93	635.20	622.00	608.16	604.20	602.46	601.51	601.25
49	808.36	700.96	673.12	635.36	622.07	608.17	604.21	602.46	601.51	601.25
50	808.74	701.18	673.30	635.50	622.13	608.18	604.21	602.46	601.51	601.25
51	809.08	701.37	673.46	635.64	622.19	608.19	604.22	602.46	601.50	601.24
52	809.38	701.55	673.60	635.76	622.24	608.20	604.22	602.46	601.50	601.24
53	809.66	701.71	673.73	635.86	622.28	608.21	604.22	602.46	601.50	601.24
54	809.89	701.85	673.85	635.96	622.32	608.21	604.22	602.46	601.49	601.23
55	810.11	701.98	673.95	636.04	622.35	608.22	604.22	602.45	601.49	601.23
56	810.29	702.09	674.04	636.12	622.37	608.22	604.22	602.45	601.49	601.22
57	810.45	702.19	674.12	636.18	622.40	608.22	604.22	602.45	601.48	601.22
58	810.58	702.28	674.19	636.23	622.42	608.22	604.21	602.44	601.47	601.21
59	810.69	702.35	674.25	636.28	622.43	608.22	604.21	602.43	601.47	601.21

*A.2 Exp.2: Single weld bead on cylinder substrate thermal simulation*

---

Table A.7 : Data surface deposition temperature ( $T_{dep}$ ) of Exp.2 at initial temperature ( $T_{init}$ ) of 400°C

Weld bead position (mm)	Cylinder substrate diameter (mm)									
	Ø7	Ø8	Ø9	Ø10	Ø12	Ø16	Ø20	Ø25	Ø30	Ø35
60	810.78	702.41	674.29	636.32	622.44	608.22	604.20	602.43	601.46	601.20
61	810.85	702.46	674.33	636.35	622.44	608.21	604.20	602.42	601.46	601.20
62	810.91	702.51	674.36	636.37	622.45	608.21	604.19	602.41	601.45	601.19
63	810.94	702.54	674.38	636.38	622.45	608.20	604.18	602.41	601.44	601.18
64	810.96	702.56	674.40	636.39	622.44	608.20	604.17	602.40	601.43	601.17
65	810.96	702.58	674.41	636.39	622.43	608.19	604.16	602.39	601.42	601.17
66	810.95	702.58	674.41	636.39	622.42	608.18	604.15	602.38	601.41	601.16
67	810.92	702.58	674.40	636.38	622.41	608.17	604.14	602.37	601.40	601.15
68	810.89	702.58	674.39	636.36	622.40	608.16	604.13	602.36	601.39	601.14
69	810.83	702.56	674.37	636.34	622.38	608.15	604.12	602.35	601.38	601.13
70	810.77	702.54	674.34	636.32	622.36	608.14	604.11	602.34	601.37	601.12
71	810.70	702.51	674.31	636.29	622.33	608.12	604.10	602.32	601.36	601.11
72	810.62	702.48	674.28	636.25	622.31	608.11	604.08	602.31	601.35	601.10
73	810.52	702.44	674.24	636.21	622.28	608.10	604.07	602.30	601.34	601.09
74	810.42	702.40	674.19	636.17	622.25	608.08	604.05	602.28	601.33	601.08
75	810.31	702.35	674.14	636.12	622.22	608.06	604.04	602.27	601.31	601.06
76	810.19	702.30	674.09	636.07	622.18	608.05	604.02	602.26	601.30	601.05
77	810.07	702.24	674.03	636.02	622.15	608.03	604.01	602.24	601.29	601.04
78	809.95	702.18	673.98	635.96	622.11	608.01	603.99	602.23	601.27	601.03
79	809.82	702.12	673.91	635.90	622.07	607.99	603.97	602.21	601.26	601.01
80	809.69	702.06	673.85	635.84	622.03	607.98	603.96	602.20	601.24	601.00
81	809.56	701.99	673.79	635.78	621.99	607.96	603.94	602.18	601.23	600.99
82	809.44	701.93	673.73	635.72	621.95	607.94	603.92	602.16	601.21	600.97

Appendix A The result of thermal simulation

Table A.7 : Data surface deposition temperature ( $T_{dep}$ ) of Exp.2 at initial temperature ( $T_{init}$ ) of 400°C

Weld bead position (mm)	Cylinder substrate diameter (mm)									
	Ø7	Ø8	Ø9	Ø10	Ø12	Ø16	Ø20	Ø25	Ø30	Ø35
83	809.33	701.87	673.67	635.66	621.91	607.92	603.90	602.15	601.20	600.96
84	809.24	701.83	673.61	635.60	621.88	607.90	603.89	602.13	601.18	600.94
85	809.19	701.79	673.57	635.56	621.84	607.88	603.87	602.11	601.17	600.93
86	809.19	701.77	673.54	635.52	621.81	607.87	603.85	602.10	601.15	600.92
87	809.27	701.79	673.54	635.51	621.79	607.85	603.84	602.08	601.14	600.90
88	809.46	701.85	673.57	635.52	621.78	607.85	603.83	602.07	601.13	600.89
89	809.81	701.98	673.65	635.57	621.80	607.84	603.82	602.06	601.11	600.88
90	810.40	702.20	673.81	635.69	621.83	607.85	603.82	602.05	601.11	600.87
91	811.33	702.56	674.08	635.89	621.91	607.86	603.82	602.05	601.10	600.86
92	812.75	703.12	674.50	636.21	622.05	607.90	603.84	602.06	601.11	600.87
93	814.88	703.97	675.16	636.72	622.27	607.96	603.87	602.08	601.12	600.88
94	818.03	705.62	676.14	637.49	622.61	608.06	603.94	602.13	601.15	600.90
95	822.64	708.37	677.59	638.64	623.13	608.23	604.04	602.20	601.21	600.96
96	829.30	712.37	679.73	640.33	623.92	608.47	604.21	602.32	601.31	601.05
97	838.86	718.15	682.84	642.81	625.09	608.85	604.47	602.53	601.47	601.20
98	852.45	729.07	687.36	646.43	626.85	609.43	604.88	602.85	601.75	601.46
99	871.70	744.64	693.89	651.69	629.49	610.31	605.53	603.38	602.21	601.90
100	898.95	766.74	706.63	659.33	633.47	611.69	606.58	604.28	603.01	602.67

### A.3 Exp.3: Lateral overlap weld bead thermal simulation

Table A.8 : Average surface temperature deposition ( $T_{dep}$ ) and standard deviation ( $\sigma$ ) of Exp.2: Single weld bead on cylinder substrate

$T_{init}$	25°C		100°C		200°C		300°C		400°C	
Diameters	$T_{dep}$	$\sigma$	$T_{dep}$	$\sigma$	$T_{dep}$	$\sigma$	$T_{dep}$	$\sigma$	$T_{dep}$	$\sigma$
Ø7	638.29	10.55	662.23	11.72	696.28	10.85	739.23	14.08	801.10	14.19
Ø8	597.66	5.69	607.03	2.87	625.18	5.72	658.89	8.50	697.26	7.46
Ø9	576.45	8.14	597.54	4.01	609.75	2.19	631.75	4.87	670.05	6.11
Ø10	535.98	6.80	566.81	6.38	598.04	2.54	610.49	1.64	633.68	3.49
Ø12	515.07	4.93	546.61	4.47	587.48	3.26	604.71	1.11	620.89	2.19
Ø16	468.43	4.04	510.72	3.44	555.40	2.46	594.04	1.36	607.83	0.55
Ø20	447.50	3.28	491.51	2.42	541.59	1.56	585.51	0.89	603.98	0.31
Ø25	436.21	2.24	482.68	1.62	535.38	1.02	580.64	0.80	602.30	0.19
Ø30	429.88	1.65	477.75	1.18	531.90	0.73	577.44	0.55	601.38	0.13
Ø35	427.98	1.39	476.29	0.98	530.89	0.60	576.54	0.46	601.14	0.11

## A.3 Exp.3: Lateral overlap weld bead thermal simulation

### A.3.1 Thermal simulation process of Exp.3

Figure A.3.1 (a) shows the initial temperature is 200°C at the starting position. Figure A.3.1 (b) In the temperature analysis, the weld bead deposition is 40 mm and surface deposition temperature ( $T_{dep}$ ) is 529.72°C. Figure A.3.1 (c) The weld bead deposition is 80 mm (endpoint). The surface deposition temperature ( $T_{dep}$ ) is 542.87°C. In this example, the first and fourth layers are compared.

### A.3.2 Thermal simulation of lateral overlap weld bead at $T_{init} = 200^\circ\text{C}$ and $300^\circ\text{C}$

### A.3.3 Thermal simulation of lateral overlap weld bead data

- Initial temperature ( $T_{init}$ ) of 200°C

Appendix A The result of thermal simulation

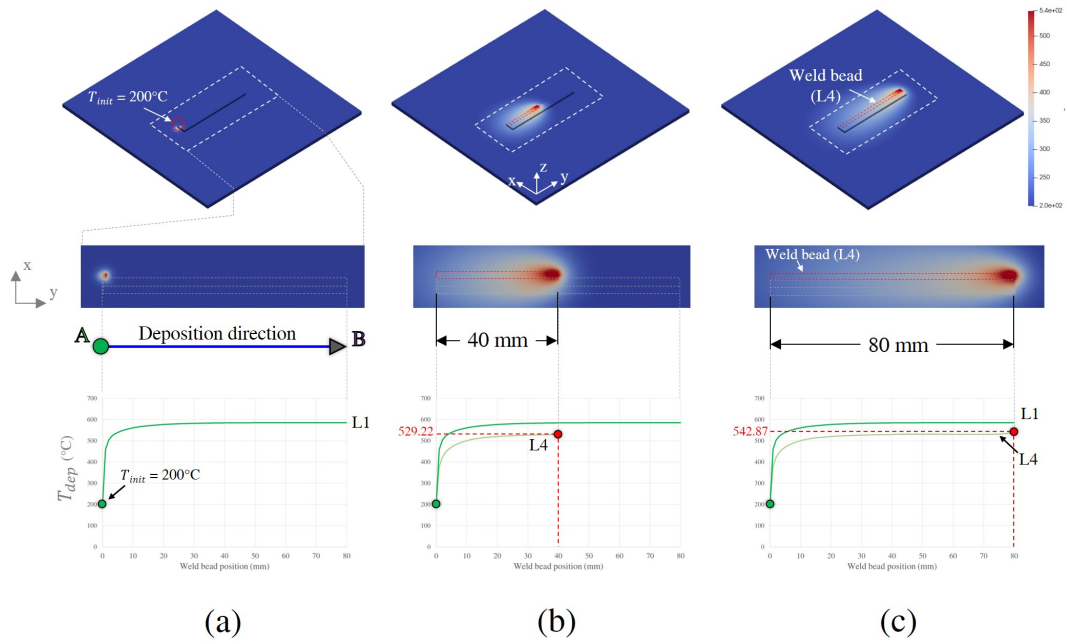


Figure A.3.1 : Thermal simulation of Exp.3 Lateral overlap weld bead (L4) at initial temperature ( $T_{init}$ ) =  $200^\circ\text{C}$ , (a) At start point, (b) Weld bead position is 40 mm and (c) Weld bead position is 80 mm (endpoint)

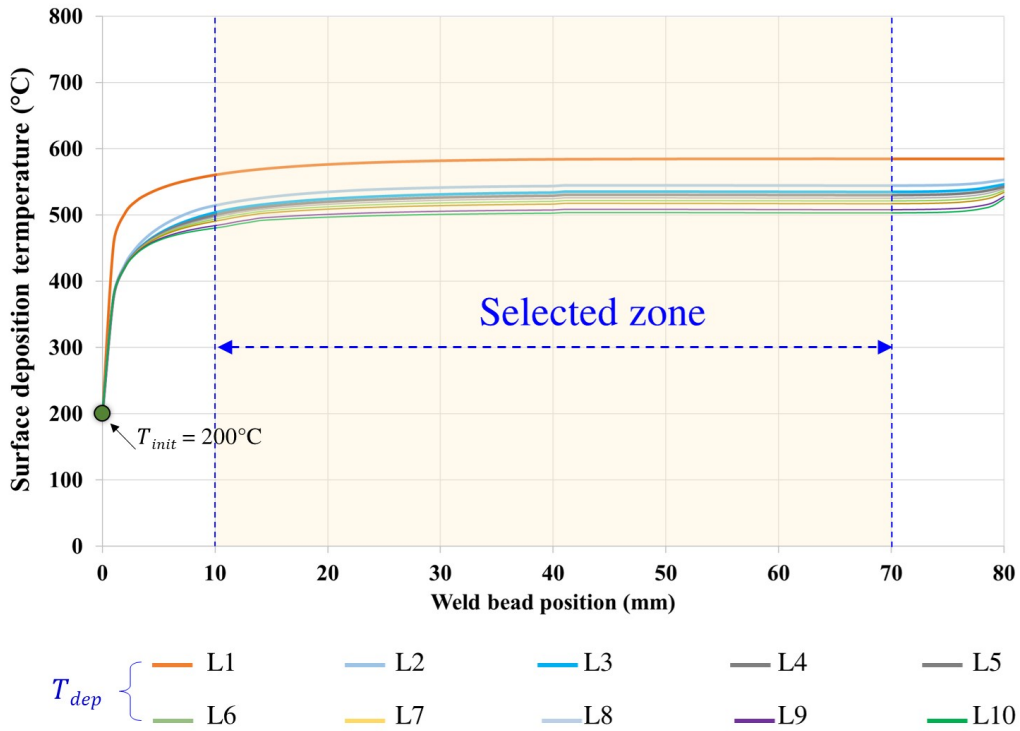


Figure A.3.2 : Thermal simulation result of Exp.3: Single weld bead on cylinder substrate at initial temperature ( $T_{init}$ ) of  $200^\circ\text{C}$

### A.3 Exp.3: Lateral overlap weld bead thermal simulation

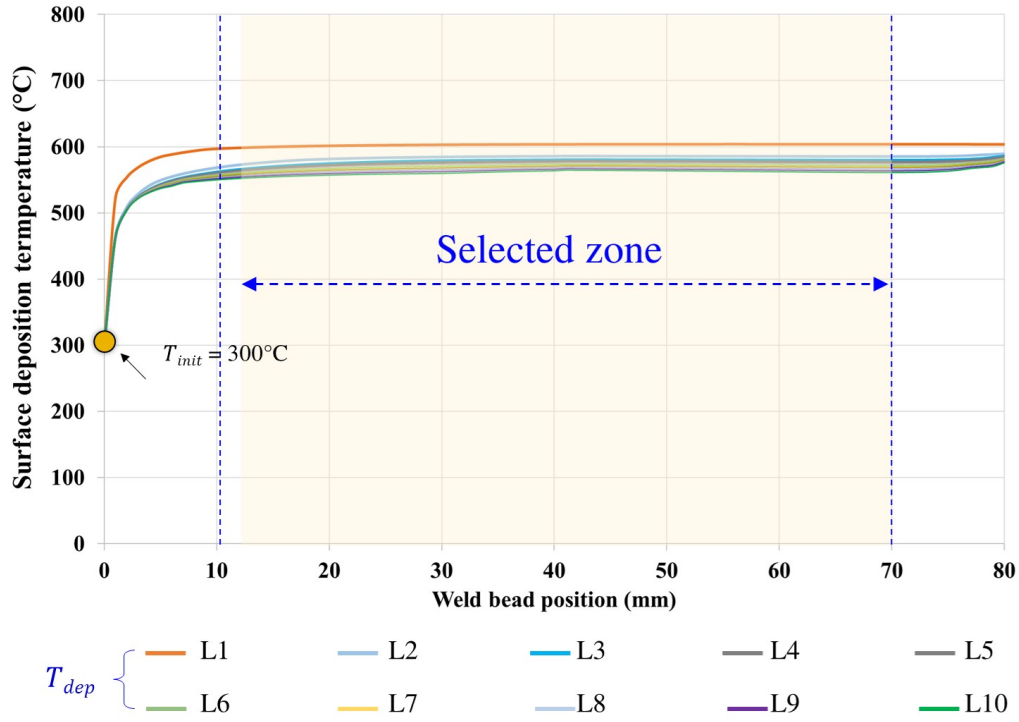


Figure A.3.3 : Thermal simulation result of Exp.3: Single weld bead on cylinder substrate at initial temperature ( $T_{init}$ ) of  $300^{\circ}\text{C}$

Table A.9 : Data surface deposition temperature ( $T_{dep}$ ) of Exp.3 at initial temperature ( $T_{init}$ ) =  $200^{\circ}\text{C}$

Weld bead position (mm)	Number of layers									
	L1	L2	L3	L4	L5	L6	L7	L8	L9	L10
0	200.00	200.00	200.00	200.00	200.00	200.00	200.00	200.00	200.00	200.00
1	459.19	379.23	377.88	377.82	377.76	377.70	377.65	377.59	377.53	377.47
2	502.90	425.67	422.08	421.84	421.60	421.36	421.13	420.89	420.65	420.41
3	521.40	450.73	444.89	444.33	443.78	443.22	442.67	442.11	441.55	441.00
4	531.81	467.87	460.18	459.21	458.24	457.27	456.30	455.34	454.37	453.40
5	539.46	480.67	471.57	470.15	468.73	467.31	465.88	464.46	463.04	461.61
6	545.43	490.67	480.54	478.66	476.78	474.90	473.03	471.15	469.27	467.40
7	550.28	498.74	487.85	485.55	483.24	480.94	478.64	476.33	474.03	471.73



Appendix A The result of thermal simulation

Table A.9 : Data surface deposition temperature ( $T_{dep}$ ) of Exp.3 at initial temperature ( $T_{init}$ ) = 200°C

Weld bead position (mm)	Number of layers									
	L1	L2	L3	L4	L5	L6	L7	L8	L9	L10
0	200.00	200.00	200.00	200.00	200.00	200.00	200.00	200.00	200.00	200.00
8	554.33	505.43	493.95	491.27	488.58	485.89	483.21	480.52	477.83	475.14
9	557.78	510.62	499.15	496.12	493.09	490.06	487.04	484.01	480.98	477.95
10	560.75	514.49	503.62	500.29	496.97	493.64	490.31	486.98	483.66	480.33
11	563.33	517.83	507.43	503.92	500.42	496.92	493.41	489.91	486.40	482.90
12	565.58	520.75	510.50	507.04	503.57	500.11	496.65	493.18	489.72	486.26
13	567.56	523.32	513.02	509.57	506.11	502.66	499.20	495.75	492.29	488.84
14	569.31	525.59	515.15	511.81	508.47	505.13	501.78	498.44	495.10	491.76
15	570.87	527.60	517.05	513.59	510.13	506.68	503.22	499.76	496.30	492.84
16	572.26	529.40	518.75	515.18	511.62	508.05	504.49	500.92	497.36	493.79
17	573.50	531.01	520.27	516.61	512.95	509.29	505.63	501.98	498.32	494.66
18	574.62	532.45	521.64	517.89	514.15	510.41	506.67	502.92	499.18	495.44
19	575.62	533.75	522.87	519.05	515.24	511.42	507.60	503.78	499.97	496.15
20	576.53	534.92	523.99	520.10	516.22	512.34	508.45	504.57	500.68	496.80
21	577.35	535.98	525.00	521.05	517.11	513.17	509.22	505.28	501.34	497.40
22	578.10	536.94	525.91	521.92	517.92	513.93	509.93	505.93	501.94	497.94
23	578.77	537.80	526.75	522.70	518.66	514.62	510.57	506.53	502.49	498.44
24	579.39	538.50	527.50	523.42	519.33	515.25	511.16	507.07	502.99	498.90
25	579.94	539.13	528.20	524.07	519.95	515.82	511.70	507.57	503.45	499.32
26	580.45	539.70	528.83	524.67	520.51	516.35	512.19	508.03	503.87	499.71
27	580.91	540.21	529.40	525.21	521.02	516.83	512.64	508.45	504.26	500.07
28	581.34	540.69	529.93	525.71	521.49	517.27	513.05	508.83	504.61	500.40

### A.3 Exp.3: Lateral overlap weld bead thermal simulation

Table A.9 : Data surface deposition temperature ( $T_{dep}$ ) of Exp.3 at initial temperature ( $T_{init}$ ) = 200°C

Weld bead position (mm)	Number of layers									
	L1	L2	L3	L4	L5	L6	L7	L8	L9	L10
0	200.00	200.00	200.00	200.00	200.00	200.00	200.00	200.00	200.00	200.00
29	581.72	541.12	530.41	526.16	521.92	517.68	513.43	509.19	504.95	500.70
30	582.07	541.52	530.84	526.58	522.31	518.05	513.78	509.52	505.25	500.99
31	582.40	541.88	531.25	526.96	522.67	518.39	514.10	509.82	505.53	501.25
32	582.69	542.21	531.61	527.31	523.01	518.70	514.40	510.10	505.79	501.49
33	582.96	542.51	531.95	527.63	523.31	518.99	514.67	510.35	506.03	501.71
34	583.21	542.77	532.25	527.92	523.59	519.25	514.92	510.58	506.25	501.92
35	583.43	542.98	532.54	528.19	523.84	519.49	515.15	510.80	506.45	502.11
36	583.64	543.17	532.79	528.43	524.07	519.72	515.36	511.00	506.64	502.28
37	583.83	543.35	533.03	528.66	524.29	519.92	515.55	511.18	506.81	502.44
38	583.99	543.51	533.24	528.86	524.48	520.10	515.72	511.35	506.97	502.59
39	584.11	543.66	533.44	529.05	524.66	520.27	515.89	511.50	507.11	502.72
40	584.20	543.80	533.62	529.22	524.83	520.43	516.03	511.64	507.24	502.85
41	584.29	544.84	535.02	530.56	526.10	521.64	517.18	512.72	508.26	503.80
42	584.37	544.85	535.03	530.57	526.10	521.64	517.18	512.72	508.26	503.80
43	584.44	544.85	535.03	530.57	526.11	521.64	517.18	512.72	508.26	503.79
44	584.50	544.85	535.03	530.57	526.10	521.64	517.18	512.71	508.25	503.79
45	584.56	544.84	535.03	530.56	526.10	521.64	517.17	512.71	508.24	503.78
46	584.62	544.84	535.02	530.56	526.09	521.63	517.16	512.70	508.23	503.77
47	584.67	544.83	535.01	530.55	526.08	521.62	517.15	512.69	508.22	503.76
48	584.71	544.82	535.00	530.54	526.07	521.60	517.14	512.67	508.21	503.74
49	584.75	544.81	534.99	530.52	526.06	521.59	517.12	512.66	508.19	503.72

Appendix A The result of thermal simulation

Table A.9 : Data surface deposition temperature ( $T_{dep}$ ) of Exp.3 at initial temperature ( $T_{init}$ ) = 200°C

Weld bead position (mm)	Number of layers									
	L1	L2	L3	L4	L5	L6	L7	L8	L9	L10
0	200.00	200.00	200.00	200.00	200.00	200.00	200.00	200.00	200.00	200.00
50	584.78	544.80	534.97	530.51	526.04	521.57	517.10	512.64	508.17	503.70
51	584.82	544.79	534.96	530.49	526.02	521.55	517.08	512.62	508.15	503.68
52	584.84	544.78	534.94	530.47	526.00	521.53	517.06	512.59	508.13	503.66
53	584.87	544.76	534.92	530.45	525.98	521.51	517.04	512.57	508.10	503.63
54	584.89	544.74	534.90	530.43	525.95	521.48	517.01	512.54	508.07	503.60
55	584.91	544.73	534.87	530.40	525.93	521.46	516.99	512.52	508.05	503.57
56	584.92	544.71	534.85	530.37	525.90	521.43	516.96	512.49	508.02	503.54
57	584.94	544.69	534.82	530.35	525.87	521.40	516.93	512.46	507.98	503.51
58	584.95	544.67	534.79	530.32	525.85	521.37	516.90	512.42	507.95	503.48
59	584.96	544.65	534.76	530.29	525.82	521.34	516.87	512.39	507.92	503.44
60	584.97	544.62	534.73	530.26	525.78	521.31	516.83	512.36	507.88	503.41
61	584.97	544.60	534.70	530.23	525.75	521.28	516.80	512.32	507.85	503.37
62	584.98	544.58	534.67	530.20	525.72	521.24	516.77	512.29	507.81	503.34
63	584.98	544.56	534.65	530.17	525.69	521.21	516.73	512.26	507.78	503.30
64	584.98	544.53	534.62	530.14	525.66	521.18	516.70	512.22	507.75	503.27
65	584.98	544.51	534.59	530.11	525.63	521.15	516.67	512.19	507.72	503.24
66	584.98	544.49	534.57	530.09	525.61	521.13	516.65	512.17	507.69	503.21
67	584.97	544.48	534.55	530.07	525.59	521.11	516.63	512.15	507.67	503.19
68	584.97	544.47	534.54	530.06	525.58	521.11	516.63	512.15	507.67	503.19
69	584.97	544.47	534.55	530.07	525.59	521.12	516.64	512.16	507.68	503.20
70	584.96	544.48	534.58	530.10	525.63	521.15	516.67	512.20	507.72	503.24

### A.3 Exp.3: Lateral overlap weld bead thermal simulation

Table A.9 : Data surface deposition temperature ( $T_{dep}$ ) of Exp.3 at initial temperature ( $T_{init}$ ) = 200°C

Weld bead position (mm)	Number of layers									
	L1	L2	L3	L4	L5	L6	L7	L8	L9	L10
0	200.00	200.00	200.00	200.00	200.00	200.00	200.00	200.00	200.00	200.00
71	584.95	544.52	534.65	530.17	525.69	521.22	516.74	512.27	507.79	503.32
72	584.94	544.60	534.77	530.29	525.82	521.34	516.87	512.39	507.92	503.44
73	584.94	544.73	534.97	530.50	526.02	521.54	517.07	512.59	508.11	503.64
74	584.93	544.97	535.31	530.83	526.35	521.87	517.38	512.90	508.42	503.94
75	584.92	545.36	535.85	531.36	526.86	522.37	517.88	513.38	508.89	504.40
76	584.90	546.01	536.68	532.19	527.70	523.20	518.71	514.22	509.73	505.24
77	584.89	547.03	537.92	533.48	529.04	524.61	520.17	515.73	511.29	506.85
78	584.88	548.60	539.85	535.51	531.17	526.83	522.49	518.15	513.81	509.47
79	584.87	550.86	542.85	538.72	534.58	530.44	526.30	522.16	518.02	513.88
80	584.85	553.16	545.93	542.87	539.82	536.76	533.71	530.65	527.60	524.54

- Initial temperature ( $T_{init}$ ) of 300°C

Table A.10 : Data surface deposition temperature ( $T_{dep}$ ) of Exp.3 at initial temperature ( $T_{init}$ ) = 300°C

Weld bead position (mm)	Number of layers									
	L1	L2	L3	L4	L5	L6	L7	L8	L9	L10
0	300.00	300.00	300.00	300.00	300.00	300.00	300.00	300.00	300.00	300.00
1	523.63	465.51	464.21	464.16	464.10	464.04	463.99	463.93	463.87	463.82
2	553.56	508.53	505.16	504.93	504.70	504.47	504.24	504.01	503.78	503.55

Appendix A The result of thermal simulation

Table A.10 : Data surface deposition temperature ( $T_{dep}$ ) of Exp.3 at initial temperature ( $T_{init}$ ) = 300°C

Weld bead position (mm)	Number of layers									
	L1	L2	L3	L4	L5	L6	L7	L8	L9	L10
0	300.00	300.00	300.00	300.00	300.00	300.00	300.00	300.00	300.00	300.00
3	568.51	528.38	524.06	523.63	523.20	522.76	522.33	521.90	521.47	521.04
4	578.15	541.07	535.46	534.72	533.98	533.24	532.51	531.77	531.03	530.29
5	584.59	549.21	543.45	542.47	541.48	540.49	539.50	538.52	537.53	536.54
6	588.18	554.65	549.23	547.94	546.66	545.37	544.08	542.80	541.51	540.23
7	591.10	559.03	553.52	552.30	551.08	549.86	548.63	547.41	546.19	544.97
8	593.56	562.65	556.84	555.42	553.99	552.57	551.14	549.72	548.29	546.87
9	595.64	565.70	559.65	558.05	556.45	554.85	553.24	551.64	550.04	548.44
10	596.77	568.30	562.06	560.31	558.55	556.79	555.03	553.27	551.51	549.76
11	597.49	570.54	564.15	562.26	560.36	558.47	556.57	554.68	552.78	550.88
12	598.12	572.50	565.98	563.96	561.95	559.93	557.92	555.90	553.89	551.87
13	598.68	574.21	567.59	565.47	563.35	561.22	559.10	556.98	554.86	552.74
14	599.18	575.72	569.01	566.80	564.58	562.37	560.16	557.94	555.73	553.51
15	599.63	577.05	570.27	567.98	565.69	563.40	561.10	558.81	556.52	554.23
16	600.02	578.25	571.40	569.04	566.68	564.32	561.96	559.60	557.23	554.87
17	600.38	579.31	572.41	569.98	567.56	565.14	562.71	560.29	557.87	555.45
18	600.70	580.20	573.31	570.83	568.35	565.88	563.40	560.92	558.44	555.96
19	600.99	580.80	574.12	571.59	569.07	566.54	564.02	561.49	558.96	556.44
20	601.24	581.31	574.85	572.28	569.71	567.14	564.57	562.00	559.44	556.87
21	601.48	581.76	575.51	572.90	570.30	567.69	565.08	562.47	559.86	557.25
22	601.69	582.17	576.11	573.47	570.82	568.18	565.54	562.89	560.25	557.61
23	601.88	582.55	576.65	573.98	571.30	568.63	565.95	563.28	560.60	557.93

### A.3 Exp.3: Lateral overlap weld bead thermal simulation

Table A.10 : Data surface deposition temperature ( $T_{dep}$ ) of Exp.3 at initial temperature ( $T_{init}$ ) = 300°C

Weld bead position (mm)	Number of layers									
	L1	L2	L3	L4	L5	L6	L7	L8	L9	L10
0	300.00	300.00	300.00	300.00	300.00	300.00	300.00	300.00	300.00	300.00
24	602.05	582.88	577.14	574.44	571.73	569.03	566.33	563.63	560.92	558.22
25	602.21	583.19	577.58	574.86	572.13	569.40	566.67	563.94	561.21	558.49
26	602.35	583.46	577.99	575.24	572.48	569.73	566.98	564.23	561.48	558.73
27	602.48	583.71	578.35	575.58	572.81	570.04	567.27	564.49	561.72	558.95
28	602.60	583.94	578.68	575.89	573.10	570.31	567.52	564.73	561.94	559.15
29	602.71	584.14	578.99	576.18	573.37	570.57	567.76	564.95	562.15	559.34
30	602.81	584.33	579.25	576.44	573.62	570.81	567.99	565.18	562.36	559.54
31	602.90	584.50	579.46	576.67	573.89	571.10	568.31	565.53	562.74	559.95
32	602.98	584.65	579.64	576.88	574.12	571.36	568.60	565.84	563.08	560.32
33	603.05	584.79	579.79	577.08	574.36	571.65	568.94	566.23	563.52	560.81
34	603.11	584.92	579.91	577.25	574.59	571.93	569.27	566.62	563.96	561.30
35	603.17	585.03	580.02	577.41	574.80	572.19	569.58	566.97	564.35	561.74
36	603.23	585.13	580.12	577.55	574.98	572.41	569.85	567.28	564.71	562.14
37	603.28	585.22	580.20	577.68	575.15	572.62	570.09	567.56	565.03	562.51
38	603.32	585.30	580.28	577.79	575.30	572.80	570.31	567.81	565.32	562.83
39	603.36	585.38	580.35	577.89	575.43	572.97	570.50	568.04	565.58	563.12
40	603.40	585.44	580.42	577.98	575.55	573.11	570.68	568.24	565.81	563.37
41	603.43	585.74	580.70	578.36	576.02	573.69	571.35	569.01	566.68	564.34
42	603.46	585.72	580.68	578.34	575.99	573.64	571.30	568.95	566.61	564.26
43	603.49	585.70	580.66	578.31	575.95	573.60	571.24	568.89	566.53	564.18
44	603.51	585.69	580.65	578.28	575.92	573.55	571.18	568.82	566.45	564.09

Appendix A The result of thermal simulation

Table A.10 : Data surface deposition temperature ( $T_{dep}$ ) of Exp.3 at initial temperature ( $T_{init}$ ) = 300°C

Weld bead position (mm)	Number of layers									
	L1	L2	L3	L4	L5	L6	L7	L8	L9	L10
0	300.00	300.00	300.00	300.00	300.00	300.00	300.00	300.00	300.00	300.00
45	603.53	585.67	580.63	578.25	575.87	573.50	571.12	568.74	566.37	563.99
46	603.55	585.65	580.61	578.22	575.83	573.44	571.05	568.67	566.28	563.89
47	603.56	585.63	580.58	578.18	575.78	573.38	570.98	568.58	566.18	563.78
48	603.57	585.60	580.56	578.15	575.73	573.32	570.91	568.49	566.08	563.67
49	603.58	585.58	580.54	578.11	575.68	573.26	570.83	568.40	565.97	563.55
50	603.59	585.55	580.51	578.07	575.63	573.19	570.75	568.31	565.87	563.42
51	603.60	585.53	580.49	578.03	575.58	573.12	570.66	568.21	565.75	563.30
52	603.61	585.50	580.46	577.99	575.52	573.05	570.58	568.11	565.63	563.16
53	603.61	585.48	580.43	577.95	575.46	572.97	570.49	568.00	565.51	563.03
54	603.61	585.45	580.40	577.90	575.40	572.90	570.39	567.89	565.39	562.89
55	603.61	585.42	580.38	577.86	575.34	572.82	570.30	567.78	565.26	562.74
56	603.62	585.39	580.35	577.81	575.27	572.74	570.20	567.67	565.13	562.59
57	603.61	585.36	580.32	577.76	575.21	572.66	570.10	567.55	565.00	562.44
58	603.61	585.33	580.28	577.71	575.14	572.57	570.00	567.43	564.86	562.29
59	603.61	585.30	580.25	577.66	575.08	572.49	569.90	567.31	564.72	562.13
60	603.61	585.27	580.22	577.61	575.01	572.40	569.79	567.19	564.58	561.97
61	603.60	585.24	580.19	577.56	574.94	572.31	569.69	567.06	564.44	561.81
62	603.60	585.21	580.16	577.51	574.87	572.23	569.58	566.94	564.30	561.65
63	603.59	585.18	580.13	577.46	574.80	572.14	569.48	566.82	564.16	561.49
64	603.58	585.15	580.10	577.42	574.74	572.06	569.38	566.70	564.02	561.34
65	603.58	585.12	580.07	577.37	574.67	571.97	569.28	566.58	563.88	561.19

### A.3 Exp.3: Lateral overlap weld bead thermal simulation

Table A.10 : Data surface deposition temperature ( $T_{dep}$ ) of Exp.3 at initial temperature ( $T_{init}$ ) = 300°C

Weld bead position (mm)	Number of layers									
	L1	L2	L3	L4	L5	L6	L7	L8	L9	L10
0	300.00	300.00	300.00	300.00	300.00	300.00	300.00	300.00	300.00	300.00
66	603.57	585.09	580.04	577.32	574.61	571.90	569.18	566.47	563.76	561.04
67	603.56	585.06	580.01	577.28	574.56	571.83	569.10	566.37	563.65	560.92
68	603.55	585.04	579.99	577.25	574.51	571.77	569.03	566.29	563.56	560.82
69	603.54	585.02	579.98	577.23	574.48	571.74	568.99	566.24	563.50	560.75
70	603.53	585.02	579.98	577.23	574.48	571.73	568.99	566.24	563.49	560.74
71	603.52	585.02	579.99	577.25	574.51	571.77	569.03	566.29	563.55	560.81
72	603.51	585.05	580.04	577.32	574.60	571.88	569.16	566.44	563.72	561.00
73	603.50	585.12	580.12	577.44	574.76	572.08	569.40	566.72	564.05	561.37
74	603.49	585.26	580.27	577.66	575.05	572.43	569.82	567.21	564.60	561.99
75	603.48	585.49	580.52	578.02	575.51	573.01	570.50	568.00	565.49	562.98
76	603.46	585.90	580.93	578.59	576.25	573.91	571.57	569.22	566.88	564.54
77	603.45	586.56	581.57	579.48	577.39	575.30	573.21	571.12	569.03	566.94
78	603.44	587.61	582.59	580.55	578.51	576.47	574.43	572.39	570.35	568.30
79	603.43	588.30	584.25	582.23	580.21	578.18	576.16	574.14	572.11	570.09
80	603.41	589.12	586.12	584.63	583.13	581.64	580.14	578.65	577.15	575.66

- Initial temperature ( $T_{init}$ ) of 400°C



Appendix A The result of thermal simulation

Table A.11 : Data surface deposition temperature ( $T_{dep}$ ) of Exp.3 at initial temperature ( $T_{init}$ ) = 400°C

Weld bead position (mm)	Number of layers									
	L1	L2	L3	L4	L5	L6	L7	L8	L9	L10
0	400.00	400.00	400.00	400.00	400.00	400.00	400.00	400.00	400.00	400.00
1	573.86	545.72	544.74	544.70	544.65	544.61	544.57	544.52	544.48	544.43
2	595.04	569.68	567.97	567.84	567.72	567.59	567.47	567.34	567.22	567.09
3	599.55	581.20	579.23	578.99	578.74	578.50	578.26	578.01	577.77	577.53
4	602.19	586.78	584.25	583.90	583.56	583.22	582.87	582.53	582.18	581.84
5	604.15	590.11	587.95	587.50	587.05	586.60	586.16	585.71	585.26	584.81
6	605.72	591.63	590.10	589.54	588.98	588.43	587.87	587.31	586.75	586.19
7	607.01	592.86	591.21	590.85	590.49	590.13	589.77	589.41	589.05	588.69
8	608.09	593.88	592.14	591.72	591.30	590.88	590.46	590.04	589.62	589.20
9	609.03	594.74	592.93	592.46	591.98	591.51	591.03	590.56	590.08	589.61
10	609.83	595.48	593.61	593.09	592.57	592.04	591.52	591.00	590.48	589.96
11	610.53	596.12	594.20	593.64	593.07	592.51	591.95	591.38	590.82	590.26
12	611.15	596.68	594.72	594.12	593.52	592.92	592.32	591.72	591.12	590.52
13	611.70	597.16	595.17	594.54	593.91	593.28	592.65	592.02	591.39	590.76
14	612.18	597.60	595.57	594.91	594.26	593.60	592.94	592.28	591.62	590.96
15	612.61	597.98	595.93	595.25	594.56	593.88	593.20	592.52	591.83	591.15
16	612.99	598.32	596.25	595.54	594.84	594.14	593.43	592.73	592.02	591.32
17	613.33	598.62	596.53	595.81	595.09	594.36	593.64	592.92	592.19	591.47
18	613.63	598.89	596.79	596.05	595.31	594.57	593.83	593.09	592.35	591.61
19	613.90	599.13	597.02	596.26	595.51	594.75	594.00	593.24	592.49	591.73
20	614.23	599.35	597.22	596.46	595.69	594.92	594.15	593.38	592.62	591.85
21	614.72	599.55	597.41	596.63	595.85	595.07	594.29	593.51	592.73	591.95

### A.3 Exp.3: Lateral overlap weld bead thermal simulation

Table A.11 : Data surface deposition temperature ( $T_{dep}$ ) of Exp.3 at initial temperature ( $T_{init}$ ) = 400°C

Weld bead position (mm)	Number of layers									
	L1	L2	L3	L4	L5	L6	L7	L8	L9	L10
0	400.00	400.00	400.00	400.00	400.00	400.00	400.00	400.00	400.00	400.00
22	615.17	599.72	597.57	596.78	595.99	595.20	594.41	593.62	592.84	592.05
23	615.57	599.88	597.72	596.92	596.13	595.33	594.53	593.73	592.93	592.13
24	615.93	600.02	597.86	597.05	596.24	595.44	594.63	593.82	593.02	592.21
25	616.26	600.15	597.98	597.17	596.35	595.54	594.72	593.91	593.09	592.28
26	616.56	600.27	598.09	597.27	596.45	595.63	594.80	593.98	593.16	592.34
27	616.82	600.37	598.19	597.36	596.53	595.71	594.88	594.05	593.23	592.40
28	617.06	600.46	598.28	597.44	596.61	595.78	594.95	594.12	593.28	592.45
29	617.28	600.55	598.36	597.52	596.68	595.85	595.01	594.17	593.34	592.50
30	617.47	600.62	598.43	597.59	596.75	595.90	595.06	594.22	593.38	592.54
31	617.65	600.69	598.49	597.65	596.80	595.96	595.11	594.27	593.42	592.58
32	617.80	600.75	598.55	597.70	596.85	596.00	595.16	594.31	593.46	592.61
33	617.95	600.80	598.60	597.75	596.90	596.05	595.19	594.34	593.49	592.64
34	618.07	600.85	598.64	597.79	596.94	596.08	595.23	594.38	593.52	592.67
35	618.18	600.89	598.68	597.83	596.97	596.11	595.26	594.40	593.55	592.69
36	618.28	600.92	598.72	597.86	597.00	596.14	595.29	594.43	593.57	592.71
37	618.37	600.95	598.75	597.89	597.03	596.17	595.31	594.45	593.59	592.73
38	618.45	600.98	598.77	597.91	597.05	596.19	595.33	594.47	593.61	592.74
39	618.52	601.00	598.80	597.93	597.07	596.21	595.34	594.48	593.62	592.76
40	618.58	601.02	598.81	597.95	597.09	596.22	595.36	594.49	593.63	592.77
41	618.63	600.95	598.74	597.87	597.00	596.13	595.26	594.39	593.52	592.65
42	618.67	600.94	598.72	597.85	596.98	596.12	595.25	594.38	593.51	592.64

Appendix A The result of thermal simulation

Table A.11 : Data surface deposition temperature ( $T_{dep}$ ) of Exp.3 at initial temperature ( $T_{init}$ ) = 400°C

Weld bead position (mm)	Number of layers									
	L1	L2	L3	L4	L5	L6	L7	L8	L9	L10
0	400.00	400.00	400.00	400.00	400.00	400.00	400.00	400.00	400.00	400.00
43	618.71	600.92	598.71	597.84	596.97	596.10	595.23	594.36	593.49	592.62
44	618.74	600.90	598.69	597.82	596.95	596.08	595.21	594.34	593.47	592.60
45	618.76	600.88	598.67	597.80	596.93	596.06	595.19	594.32	593.45	592.59
46	618.78	600.86	598.65	597.78	596.91	596.04	595.17	594.30	593.44	592.57
47	618.79	600.84	598.63	597.76	596.89	596.02	595.15	594.28	593.42	592.55
48	618.80	600.82	598.61	597.74	596.87	596.00	595.13	594.27	593.40	592.53
49	618.80	600.80	598.59	597.72	596.85	595.98	595.11	594.24	593.38	592.51
50	618.80	600.78	598.57	597.70	596.83	595.96	595.09	594.22	593.35	592.49
51	618.80	600.76	598.54	597.68	596.81	595.94	595.07	594.20	593.33	592.46
52	618.79	600.73	598.52	597.65	596.79	595.92	595.05	594.18	593.31	592.44
53	618.78	600.71	598.50	597.63	596.76	595.89	595.02	594.16	593.29	592.42
54	618.77	600.69	598.48	597.61	596.74	595.87	595.00	594.13	593.26	592.39
55	618.75	600.67	598.45	597.58	596.72	595.85	594.98	594.11	593.24	592.37
56	618.73	600.64	598.43	597.56	596.69	595.82	594.95	594.08	593.21	592.34
57	618.71	600.62	598.41	597.54	596.67	595.80	594.93	594.06	593.19	592.32
58	618.68	600.60	598.38	597.51	596.64	595.77	594.90	594.03	593.16	592.29
59	618.66	600.57	598.36	597.49	596.62	595.75	594.88	594.01	593.14	592.27
60	618.63	600.55	598.33	597.46	596.59	595.72	594.85	593.98	593.11	592.24
61	618.60	600.52	598.31	597.44	596.57	595.70	594.83	593.95	593.08	592.21
62	618.57	600.50	598.28	597.41	596.54	595.67	594.80	593.93	593.06	592.19
63	618.53	600.48	598.26	597.39	596.52	595.64	594.77	593.90	593.03	592.16

### A.3 Exp.3: Lateral overlap weld bead thermal simulation

Table A.11 : Data surface deposition temperature ( $T_{dep}$ ) of Exp.3 at initial temperature ( $T_{init}$ ) = 400°C

Weld bead position (mm)	Number of layers									
	L1	L2	L3	L4	L5	L6	L7	L8	L9	L10
0	400.00	400.00	400.00	400.00	400.00	400.00	400.00	400.00	400.00	400.00
64	618.50	600.45	598.24	597.36	596.49	595.62	594.75	593.87	593.00	592.13
65	618.46	600.43	598.21	597.34	596.47	595.59	594.72	593.85	592.98	592.10
66	618.43	600.41	598.19	597.31	596.44	595.57	594.70	593.82	592.95	592.08
67	618.39	600.38	598.17	597.29	596.42	595.55	594.67	593.80	592.93	592.05
68	618.35	600.36	598.15	597.27	596.40	595.52	594.65	593.78	592.90	592.03
69	618.31	600.34	598.13	597.25	596.38	595.51	594.63	593.76	592.88	592.01
70	618.26	600.33	598.12	597.24	596.37	595.49	594.62	593.74	592.87	591.99
71	618.22	600.32	598.11	597.24	596.36	595.49	594.61	593.74	592.86	591.99
72	618.18	600.32	598.12	597.24	596.37	595.49	594.62	593.74	592.86	591.99
73	618.13	600.34	598.14	597.26	596.39	595.51	594.63	593.76	592.88	592.00
74	618.09	600.38	598.19	597.31	596.43	595.55	594.67	593.80	592.92	592.04
75	618.04	600.46	598.28	597.39	596.51	595.63	594.75	593.86	592.98	592.10
76	617.99	600.61	598.42	597.53	596.65	595.76	594.87	593.98	593.10	592.21
77	617.95	600.85	598.66	597.76	596.87	595.97	595.08	594.19	593.29	592.40
78	617.90	601.23	599.03	598.13	597.23	596.33	595.43	594.53	593.63	592.73
79	617.85	601.80	599.60	598.71	597.81	596.92	596.02	595.13	594.24	593.34
80	617.80	602.48	600.40	599.54	598.68	597.82	596.95	596.09	595.23	594.37

Table A.12 : Average surface temperature deposition ( $T_{dep}$ ) and standard deviation ( $\sigma$ ) of Exp.3: Lateral overlap weld bead

$T_{init}$	200°C		300°C		400°C	
Number of layers	$T_{dep}$	$\sigma$	$T_{dep}$	$\sigma$	$T_{dep}$	$\sigma$
L1	581.13	5.92	602.53	1.67	617.05	2.45
L2	540.22	7.30	583.32	3.87	600.09	1.24
L3	529.96	7.55	577.90	4.41	597.91	1.17
L4	525.73	7.21	575.37	4.26	597.09	1.09
L5	529.96	7.55	577.90	4.41	597.91	1.17
L6	534.19	7.89	580.43	4.55	598.74	1.25
L7	538.42	8.22	582.95	4.70	599.56	1.33
L8	542.65	8.56	585.48	4.86	600.38	1.41
L9	546.88	8.90	588.00	5.02	601.20	1.49
L10	551.11	9.24	590.53	5.19	602.03	1.57

## A.4 Exp.4: Vertical overlap weld bead thermal simulation

### A.4.1 Thermal simulation process of Exp.4

Figure A.4.1 (a) & (b) shows the results of the fifth layer (L5) and tenth layer (L10) of temperature analysis, at initial temperatures of 100°C, 200°C, 300°C, and 400°C, respectively. The results show a history of surface temperatures occurring during deposition. It can be seen that the L5 and L10 temperatures are in the end zone. The surface deposition temperature ( $T_{dep}$ ) rises rapidly due to the small area for heat transfer at the end of the weld.

### A.4.2 Thermal simulation of vertical overlap weld bead at $T_{init} = 100^\circ\text{C}$ , $200^\circ\text{C}$ and $300^\circ\text{C}$

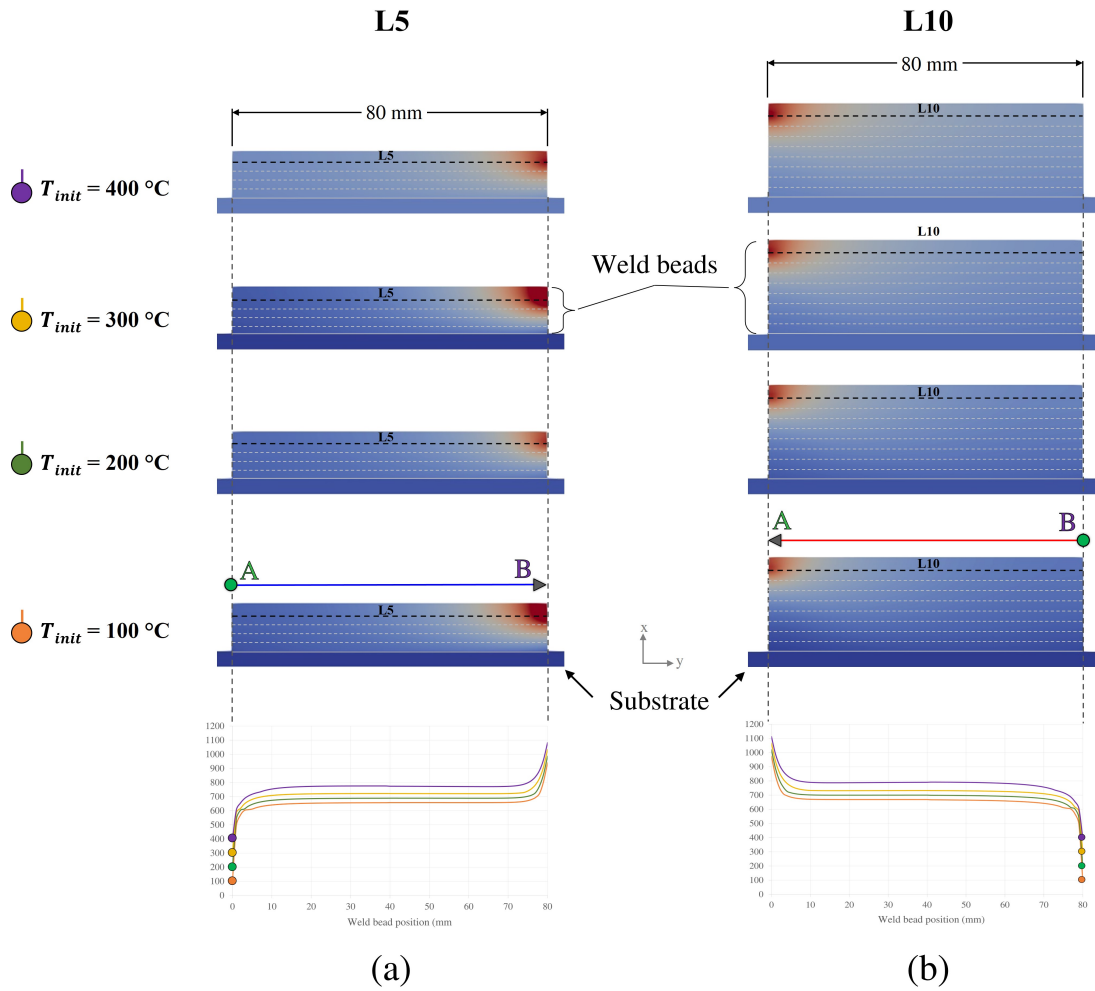


Figure A.4.1 : Thermal simulation of Exp.2: Vertical overlap weld bead, (a) Number of 5<sup>th</sup> layer (L5) and (b) Number of 10<sup>th</sup> layer

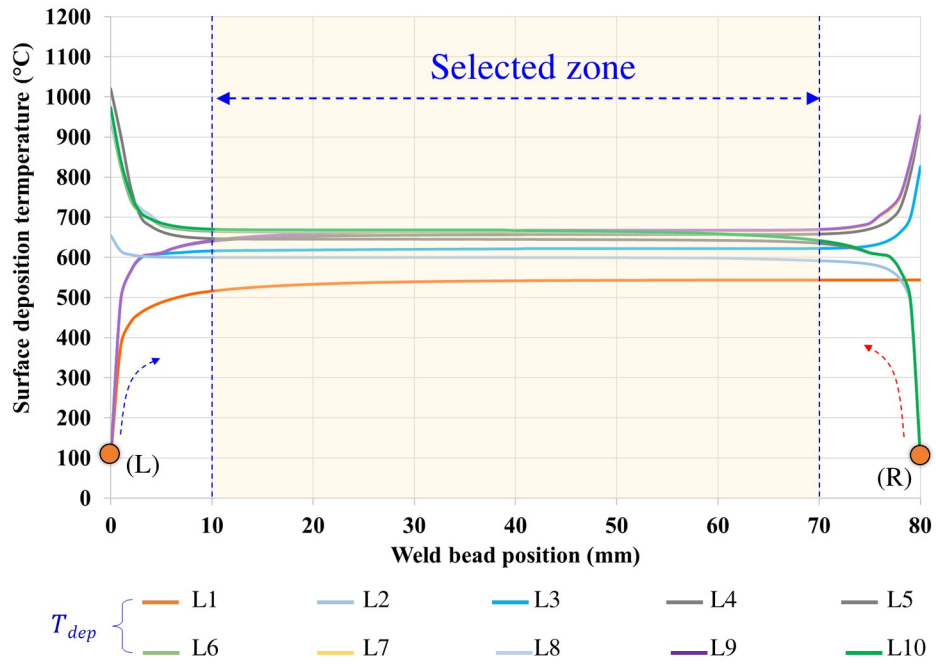


Figure A.4.2 : Thermal simulation result of Exp.4: Vertical overlap weld bead at initial temperature ( $T_{init}$ ) at 100°C

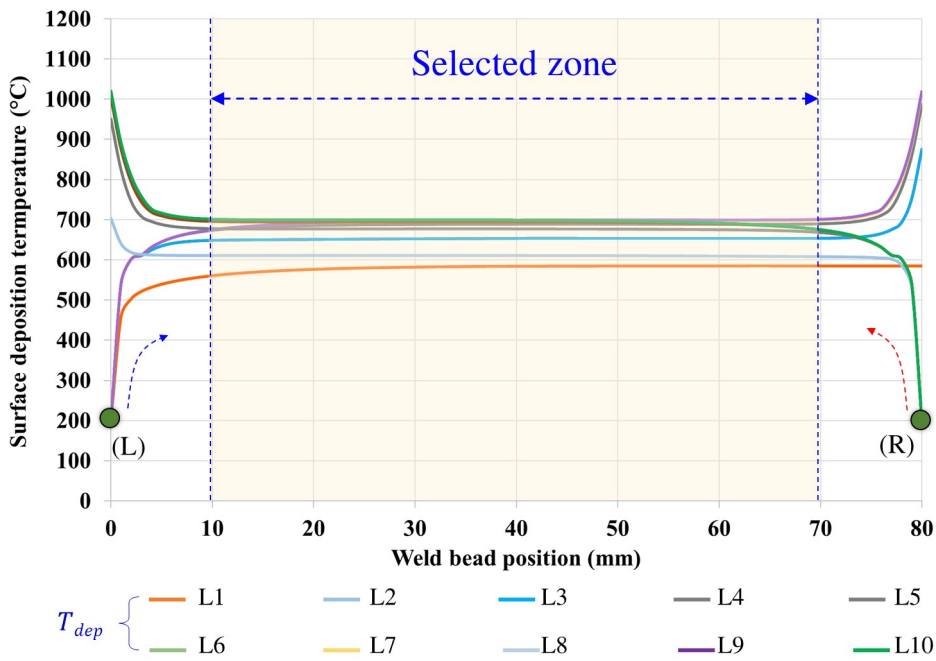


Figure A.4.3 : Thermal simulation result of Exp.4: Vertical overlap weld bead at initial temperature ( $T_{init}$ ) at 200°C

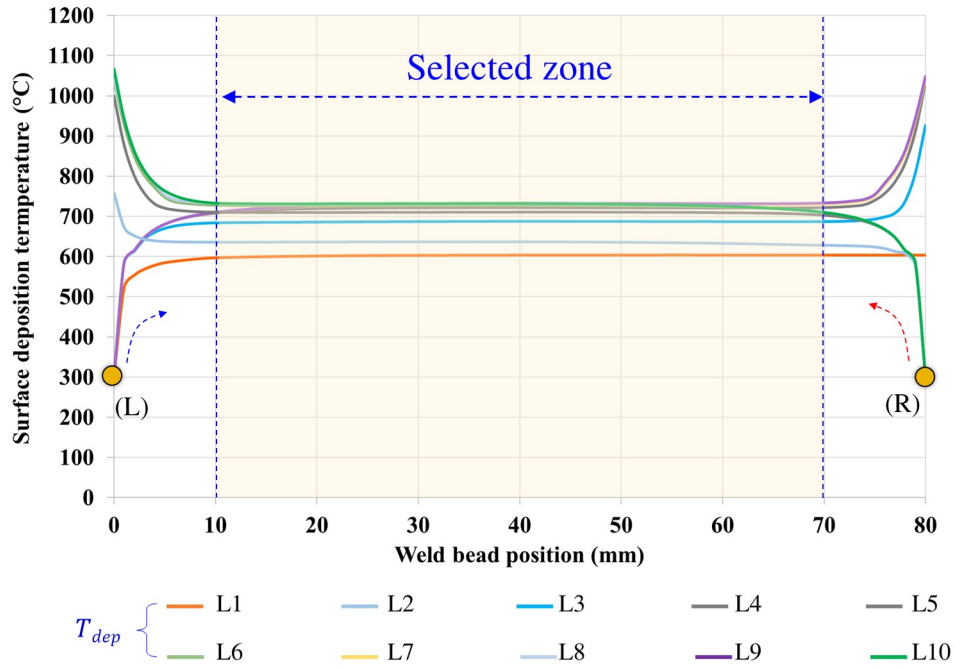


Figure A.4.4 : Thermal simulation result of Exp.4: Vertical overlap weld bead at initial temperature ( $T_{init}$ ) at 300°C

### A.4.3 Thermal simulation of vertical overlap weld bead data

- Initial temperature ( $T_{init}$ ) of 100°C

Table A.13 : Data surface deposition temperature ( $T_{dep}$ ) of Exp.4 at initial temperature ( $T_{init}$ ) = 100°C

Weld bead position (mm)	Number of layers									
	L1	L2	L3	L4	L5	L6	L7	L8	L9	L10
0	100.00	100.00	100.00	100.00	100.00	100.00	100.00	100.00	100.00	100.00
1	381.74	487.83	496.37	496.77	496.79	496.79	496.79	496.79	496.79	496.79
2	439.96	545.17	565.89	567.44	567.55	567.55	567.56	567.56	567.56	567.55
3	462.95	567.51	598.67	601.22	601.32	601.39	601.39	601.39	601.39	601.32
4	477.38	577.92	605.50	607.23	607.44	607.59	607.60	607.60	607.60	607.46
5	488.00	583.30	608.67	611.23	611.59	611.87	611.91	611.91	611.91	611.69



Appendix A The result of thermal simulation

Table A.13 : Data surface deposition temperature ( $T_{dep}$ ) of Exp.4 at initial temperature ( $T_{init}$ ) = 100°C

Weld bead position (mm)	Number of layers									
	L1	L2	L3	L4	L5	L6	L7	L8	L9	L10
0	100.00	100.00	100.00	100.00	100.00	100.00	100.00	100.00	100.00	100.00
6	496.35	586.46	610.66	619.30	621.21	621.66	621.73	621.73	621.73	621.51
7	503.18	588.45	611.89	625.52	628.24	628.92	629.02	629.03	629.03	628.75
8	508.92	589.86	613.82	629.94	633.52	634.45	634.62	634.63	634.63	634.29
9	513.07	590.96	615.15	633.12	637.57	638.80	639.04	639.06	639.06	638.66
10	516.25	591.89	615.95	635.45	640.74	642.28	642.61	642.65	642.65	642.21
11	519.01	592.74	616.45	637.18	643.28	645.14	645.57	645.63	645.64	645.17
12	521.43	593.52	616.78	638.48	645.34	647.52	648.06	648.14	648.15	647.69
13	523.57	594.26	617.02	639.49	647.03	649.52	650.18	650.29	650.31	649.84
14	525.46	594.96	617.21	640.28	648.43	651.22	652.00	652.15	652.18	651.72
15	527.15	595.63	617.39	640.91	649.59	652.67	653.58	653.77	653.81	653.36
16	528.66	596.26	617.56	641.42	650.57	653.91	654.95	655.19	655.24	654.82
17	530.01	596.85	617.73	641.85	651.39	654.98	656.15	656.44	656.50	656.11
18	531.23	597.40	617.90	642.20	652.10	655.91	657.21	657.54	657.62	657.27
19	532.33	597.92	618.08	642.51	652.70	656.73	658.14	658.53	658.63	658.30
20	533.31	598.40	618.27	642.77	653.22	657.43	658.96	659.40	659.52	659.24
21	534.21	598.62	618.45	643.01	653.68	658.06	659.69	660.19	660.33	660.08
22	535.02	598.74	618.64	643.22	654.07	658.60	660.34	660.89	661.06	660.85
23	535.75	598.85	618.82	643.41	654.42	659.09	660.92	661.53	661.71	661.54
24	536.43	598.96	619.00	643.58	654.72	659.51	661.44	662.10	662.31	662.17
25	537.04	599.06	619.17	643.74	654.99	659.89	661.90	662.61	662.84	662.75
26	537.60	599.15	619.34	643.89	655.23	660.23	662.32	663.08	663.33	663.28

*A.4 Exp.4: Vertical overlap weld bead thermal simulation*

Table A.13 : Data surface deposition temperature ( $T_{dep}$ ) of Exp.4 at initial temperature ( $T_{init}$ ) = 100°C

Weld bead position (mm)	Number of layers									
	L1	L2	L3	L4	L5	L6	L7	L8	L9	L10
0	100.00	100.00	100.00	100.00	100.00	100.00	100.00	100.00	100.00	100.00
27	538.11	599.23	619.50	644.03	655.44	660.53	662.69	663.50	663.78	663.76
28	538.58	599.31	619.66	644.16	655.64	660.80	663.03	663.88	664.18	664.20
29	539.01	599.38	619.81	644.27	655.81	661.04	663.33	664.22	664.55	664.60
30	539.40	599.44	619.95	644.39	655.96	661.26	663.60	664.54	664.89	664.97
31	539.76	599.51	620.09	644.49	656.10	661.45	663.85	664.82	665.19	665.31
32	540.09	599.56	620.22	644.59	656.23	661.63	664.07	665.08	665.47	665.62
33	540.40	599.61	620.34	644.68	656.35	661.78	664.27	665.31	665.73	665.91
34	540.68	599.66	620.45	644.76	656.45	661.93	664.45	665.53	665.96	666.17
35	540.94	599.70	620.56	644.85	656.55	662.05	664.61	665.72	666.17	666.41
36	541.18	599.75	620.66	644.92	656.64	662.17	664.76	665.90	666.37	666.63
37	541.40	599.78	620.75	644.99	656.72	662.27	664.90	666.06	666.54	666.83
38	541.60	599.82	620.84	645.06	656.79	662.37	665.02	666.20	666.70	667.02
39	541.79	599.85	620.92	645.12	656.86	662.46	665.13	666.33	666.85	667.19
40	541.96	599.88	620.99	645.18	656.92	662.63	665.49	666.72	667.25	667.34
41	542.12	600.15	621.72	645.23	657.46	663.17	666.03	667.44	668.12	668.75
42	542.26	600.15	621.73	645.28	657.46	663.17	666.04	667.45	668.13	668.77
43	542.40	600.16	621.74	645.33	657.47	663.18	666.04	667.46	668.14	668.79
44	542.52	600.16	621.75	645.37	657.47	663.18	666.05	667.47	668.15	668.81
45	542.64	600.16	621.76	645.41	657.48	663.19	666.05	667.47	668.16	668.82
46	542.74	600.17	621.77	645.45	657.48	663.19	666.05	667.48	668.16	668.84
47	542.84	600.17	621.77	645.48	657.48	663.19	666.06	667.48	668.17	668.85

Appendix A The result of thermal simulation

Table A.13 : Data surface deposition temperature ( $T_{dep}$ ) of Exp.4 at initial temperature ( $T_{init}$ ) = 100°C

Weld bead position (mm)	Number of layers									
	L1	L2	L3	L4	L5	L6	L7	L8	L9	L10
0	100.00	100.00	100.00	100.00	100.00	100.00	100.00	100.00	100.00	100.00
48	542.93	600.17	621.78	645.51	657.48	663.19	666.06	667.48	668.17	668.86
49	543.02	600.17	621.78	645.54	657.48	663.19	666.06	667.48	668.17	668.86
50	543.09	600.17	621.78	645.77	657.48	663.19	666.05	667.48	668.17	668.87
51	543.16	600.17	621.78	645.77	657.48	663.19	666.05	667.48	668.17	668.88
52	543.23	600.17	621.79	645.77	657.48	663.18	666.05	667.47	668.17	668.88
53	543.29	600.17	621.79	645.77	657.48	663.18	666.05	667.47	668.16	668.88
54	543.34	600.17	621.79	645.77	657.48	663.18	666.04	667.47	668.16	668.88
55	543.39	600.17	621.79	645.76	657.47	663.17	666.04	667.46	668.15	668.88
56	543.44	600.17	621.78	645.76	657.47	663.17	666.03	667.46	668.15	668.88
57	543.48	600.17	621.78	645.76	657.47	663.17	666.03	667.45	668.14	668.88
58	543.52	600.17	621.78	645.76	657.47	663.16	666.03	667.45	668.14	668.89
59	543.55	600.17	621.78	645.76	657.46	663.16	666.03	667.45	668.14	668.89
60	543.59	600.17	621.78	645.76	657.46	663.17	666.03	667.45	668.14	668.89
61	543.62	600.17	621.77	645.76	657.47	663.17	666.03	667.46	668.15	668.90
62	543.64	600.17	621.77	645.76	657.47	663.18	666.05	667.47	668.16	668.92
63	543.67	600.17	621.77	645.78	657.49	663.20	666.08	667.50	668.19	668.95
64	543.69	600.17	621.78	645.80	657.51	663.24	666.12	667.55	668.24	669.00
65	543.71	600.17	621.78	645.85	657.55	663.30	666.20	667.63	668.32	669.07
66	543.72	600.17	621.80	645.92	657.62	663.40	666.31	667.75	668.45	669.19
67	543.74	600.17	621.83	646.05	657.74	663.56	666.50	667.95	668.65	669.37
68	543.75	600.17	621.88	646.26	657.92	663.81	666.79	668.25	668.96	669.65

*A.4 Exp.4: Vertical overlap weld bead thermal simulation*

---

Table A.13 : Data surface deposition temperature ( $T_{dep}$ ) of Exp.4 at initial temperature ( $T_{init}$ ) = 100°C

Weld bead position (mm)	Number of layers									
	L1	L2	L3	L4	L5	L6	L7	L8	L9	L10
0	100.00	100.00	100.00	100.00	100.00	100.00	100.00	100.00	100.00	100.00
69	543.76	600.18	621.98	646.61	658.23	664.20	667.23	668.71	669.43	670.09
70	543.77	600.19	622.15	647.19	658.71	664.82	667.91	669.42	670.16	670.76
71	543.78	600.21	622.45	648.15	659.49	665.77	668.96	670.51	671.26	671.79
72	543.79	600.26	622.97	649.77	660.75	667.27	670.58	672.17	672.95	673.40
73	543.80	600.34	623.90	652.46	662.78	669.61	673.08	674.74	675.55	675.89
74	543.80	600.51	625.55	656.97	666.07	673.30	676.98	678.72	679.57	679.79
75	543.81	600.86	628.54	664.59	671.40	679.16	683.09	684.93	685.83	685.90
76	543.81	601.59	633.99	677.59	680.10	694.94	702.41	704.37	705.71	695.60
77	543.81	603.18	643.98	699.77	694.47	710.50	718.52	722.24	724.07	711.15
78	543.81	606.88	662.49	772.43	724.07	741.15	749.66	753.66	755.62	755.92
79	543.81	615.81	698.96	903.01	807.76	825.26	833.96	838.19	840.28	841.59
80	543.81	654.98	826.00	1020.26	939.48	944.47	946.77	951.10	953.24	974.08

- Initial temperature ( $T_{init}$ ) of 200°C

Appendix A The result of thermal simulation

---

Table A.14 : Data surface deposition temperature ( $T_{dep}$ ) of Exp.4 at initial temperature ( $T_{init}$ ) = 200°C

Weld bead position (mm)	Number of layers									
	L1	L2	L3	L4	L5	L6	L7	L8	L9	L10
0	200.00	200.00	200.00	200.00	200.00	200.00	200.00	200.00	200.00	200.00
1	459.19	532.45	540.66	541.06	541.08	541.08	541.08	541.08	541.08	541.08
2	502.90	585.92	601.73	602.17	602.20	602.20	602.20	602.20	602.20	602.20
3	521.40	601.73	610.86	611.88	611.98	611.98	611.98	611.98	611.98	611.98
4	531.81	604.35	625.09	631.03	631.72	631.79	631.80	631.80	631.80	631.80
5	539.46	605.66	635.09	643.81	645.07	645.22	645.23	645.24	645.24	645.24
6	545.43	606.38	641.22	652.67	654.63	654.91	654.95	654.95	654.95	654.95
7	550.28	606.80	644.86	658.78	661.55	662.01	662.07	662.08	662.08	662.08
8	554.33	607.08	647.04	663.10	666.74	667.41	667.52	667.54	667.54	667.54
9	557.78	607.30	648.33	666.20	670.71	671.64	671.81	671.83	671.84	671.84
10	560.75	607.49	649.11	668.45	673.80	675.03	675.27	675.31	675.32	675.32
11	563.33	607.68	649.59	670.12	676.27	677.81	678.13	678.19	678.20	678.20
12	565.58	607.86	649.91	671.37	678.25	680.11	680.54	680.62	680.63	680.63
13	567.56	608.04	650.13	672.33	679.86	682.04	682.58	682.69	682.72	682.72
14	569.31	608.22	650.32	673.08	681.19	683.68	684.34	684.49	684.52	684.52
15	570.87	608.39	650.48	673.66	682.29	685.08	685.86	686.06	686.10	686.10
16	572.26	608.56	650.64	674.14	683.21	686.29	687.20	687.44	687.50	687.50
17	573.50	608.71	650.80	674.53	683.98	687.33	688.37	688.65	688.73	688.73
18	574.62	608.86	650.96	674.85	684.64	688.23	689.40	689.73	689.83	689.83
19	575.62	609.00	651.13	675.13	685.20	689.02	690.31	690.70	690.82	690.82
20	576.53	609.14	651.30	675.37	685.68	689.70	691.12	691.56	691.71	691.71
21	577.35	609.26	651.47	675.58	686.10	690.31	691.83	692.33	692.50	692.50

*A.4 Exp.4: Vertical overlap weld bead thermal simulation*

Table A.14 : Data surface deposition temperature ( $T_{dep}$ ) of Exp.4 at initial temperature ( $T_{init}$ ) = 200°C

Weld bead position (mm)	Number of layers									
	L1	L2	L3	L4	L5	L6	L7	L8	L9	L10
0	200.00	200.00	200.00	200.00	200.00	200.00	200.00	200.00	200.00	200.00
22	578.10	609.37	651.64	675.76	686.45	690.83	692.47	693.02	693.23	693.23
23	578.77	609.48	651.81	675.93	686.77	691.30	693.04	693.64	693.88	693.88
24	579.39	609.58	651.97	676.08	687.04	691.71	693.54	694.20	694.47	694.47
25	579.94	609.67	652.13	676.22	687.28	692.07	694.00	694.70	695.01	695.01
26	580.45	609.76	652.28	676.34	687.49	692.39	694.40	695.16	695.49	695.49
27	580.91	609.83	652.43	676.46	687.67	692.67	694.76	695.57	695.94	695.94
28	581.34	609.91	652.57	676.56	687.84	692.93	695.09	695.94	696.34	696.34
29	581.72	609.97	652.70	676.66	687.99	693.15	695.38	696.27	696.71	696.71
30	582.07	610.03	652.83	676.75	688.12	693.35	695.64	696.57	697.04	697.04
31	582.40	610.09	652.95	676.84	688.23	693.53	695.87	696.84	697.35	697.35
32	582.69	610.14	653.06	676.92	688.34	693.68	696.08	697.09	697.62	697.62
33	582.96	610.18	653.16	676.99	688.43	693.82	696.27	697.31	697.87	697.87
34	583.21	610.23	653.26	677.06	688.51	693.95	696.43	697.51	698.10	698.10
35	583.43	610.26	653.35	677.12	688.59	694.06	696.58	697.69	698.31	698.31
36	583.64	610.30	653.43	677.18	688.65	694.16	696.72	697.85	698.50	698.50
37	583.83	610.33	653.51	677.23	688.71	694.25	696.84	698.00	698.67	698.67
38	583.99	610.36	653.58	677.28	688.77	694.32	696.94	698.13	698.83	698.83
39	584.11	610.39	653.65	677.32	688.81	694.39	697.04	698.25	698.97	698.97
40	584.20	610.41	653.71	677.36	688.85	694.45	697.12	698.35	699.10	699.10
41	584.29	610.58	654.10	677.57	689.02	694.74	697.60	699.01	700.00	700.00
42	584.37	610.58	654.10	677.56	689.01	694.73	697.59	699.00	700.00	700.00

Appendix A The result of thermal simulation

Table A.14 : Data surface deposition temperature ( $T_{dep}$ ) of Exp.4 at initial temperature ( $T_{init}$ ) = 200°C

Weld bead position (mm)	Number of layers									
	L1	L2	L3	L4	L5	L6	L7	L8	L9	L10
0	200.00	200.00	200.00	200.00	200.00	200.00	200.00	200.00	200.00	200.00
43	584.44	610.58	654.09	677.55	689.00	694.71	697.58	698.99	699.99	699.99
44	584.50	610.58	654.09	677.54	688.99	694.70	697.56	698.98	699.99	699.99
45	584.56	610.57	654.08	677.53	688.98	694.69	697.55	698.97	699.98	699.98
46	584.62	610.57	654.07	677.52	688.96	694.67	697.54	698.96	699.97	699.97
47	584.67	610.57	654.06	677.50	688.95	694.66	697.52	698.94	699.95	699.95
48	584.71	610.56	654.04	677.49	688.93	694.64	697.50	698.93	699.94	699.94
49	584.75	610.56	654.03	677.48	688.91	694.62	697.49	698.91	699.92	699.92
50	584.78	610.56	654.02	677.46	688.90	694.60	697.47	698.89	699.91	699.91
51	584.82	610.55	654.00	677.44	688.88	694.58	697.45	698.87	699.89	699.89
52	584.84	610.55	653.99	677.43	688.86	694.56	697.43	698.85	699.87	699.87
53	584.87	610.54	653.97	677.41	688.84	694.54	697.41	698.83	699.85	699.85
54	584.89	610.54	653.96	677.39	688.82	694.52	697.39	698.81	699.83	699.83
55	584.91	610.53	653.94	677.37	688.80	694.50	697.37	698.79	699.80	699.80
56	584.92	610.53	653.92	677.36	688.78	694.48	697.35	698.77	699.78	699.78
57	584.94	610.52	653.90	677.34	688.76	694.46	697.32	698.75	699.76	699.76
58	584.95	610.52	653.89	677.32	688.74	694.44	697.30	698.73	699.74	699.74
59	584.96	610.51	653.87	677.30	688.72	694.42	697.29	698.71	699.72	699.72
60	584.97	610.50	653.85	677.28	688.71	694.41	697.27	698.69	699.70	699.70
61	584.97	610.50	653.83	677.27	688.69	694.40	697.26	698.68	699.69	699.69
62	584.98	610.49	653.82	677.25	688.68	694.39	697.25	698.68	699.68	699.68
63	584.98	610.49	653.80	677.24	688.68	694.39	697.26	698.68	699.69	699.69

*A.4 Exp.4: Vertical overlap weld bead thermal simulation*

Table A.14 : Data surface deposition temperature ( $T_{dep}$ ) of Exp.4 at initial temperature ( $T_{init}$ ) = 200°C

Weld bead position (mm)	Number of layers									
	L1	L2	L3	L4	L5	L6	L7	L8	L9	L10
0	200.00	200.00	200.00	200.00	200.00	200.00	200.00	200.00	200.00	200.00
64	584.98	610.48	653.79	677.24	688.69	694.41	697.28	698.71	699.72	699.72
65	584.98	610.47	653.78	677.25	688.72	694.45	697.33	698.76	699.78	699.78
66	584.98	610.47	653.78	677.28	688.78	694.53	697.42	698.86	699.88	699.88
67	584.97	610.47	653.80	677.34	688.88	694.66	697.57	699.02	700.05	700.05
68	584.97	610.46	653.84	677.46	689.06	694.88	697.82	699.28	700.32	700.32
69	584.97	610.47	653.92	677.66	689.35	695.24	698.21	699.70	700.75	700.75
70	584.96	610.47	654.08	678.00	689.84	695.81	698.84	700.35	701.42	701.42
71	584.95	610.49	654.37	678.58	690.61	696.72	699.81	701.36	702.46	702.46
72	584.94	610.53	654.89	679.54	691.87	698.15	701.34	702.94	704.07	704.07
73	584.94	610.61	655.81	681.14	693.90	700.42	703.73	705.39	706.57	706.57
74	584.93	610.78	657.47	683.81	697.18	704.01	707.48	709.22	710.46	710.46
75	584.92	611.12	660.44	688.29	702.47	709.71	713.38	715.23	716.55	716.55
76	584.90	611.84	665.81	695.84	711.10	718.85	722.78	724.75	726.87	726.87
77	584.89	613.40	675.66	708.61	729.66	744.50	751.96	755.69	758.37	758.37
78	584.88	618.38	693.69	745.76	777.88	793.90	801.92	805.92	808.80	808.80
79	584.87	640.00	752.63	824.41	858.99	876.07	884.58	888.82	891.89	891.89
80	584.85	702.76	875.44	950.67	986.34	1003.83	1012.53	1016.86	1020.03	1020.03

- Initial temperature ( $T_{init}$ ) of 300°C



Appendix A The result of thermal simulation

Table A.15 : Data surface deposition temperature ( $T_{dep}$ ) of Exp.4 at initial temperature ( $T_{init}$ ) = 300°C

Weld bead position (mm)	Number of layers									
	L1	L2	L3	L4	L5	L6	L7	L8	L9	L10
0	300.00	300.00	300.00	300.00	300.00	300.00	300.00	300.00	300.00	300.00
1	523.63	577.41	585.20	585.59	585.61	585.61	585.61	585.61	585.61	585.61
2	553.56	607.29	613.65	615.14	615.24	615.25	615.25	615.25	615.25	615.25
3	568.51	612.98	643.70	647.17	647.49	647.56	647.57	647.57	647.57	647.52
4	578.15	620.45	660.41	666.41	667.12	667.27	667.29	667.29	667.29	667.20
5	584.59	624.17	670.28	679.01	680.29	680.57	680.60	680.60	680.60	680.46
6	588.18	626.07	676.30	687.68	689.67	690.12	690.19	690.19	690.19	689.99
7	591.10	627.01	679.86	693.64	696.44	697.11	697.22	697.23	697.23	696.97
8	593.56	627.58	681.97	697.83	701.49	702.43	702.60	702.61	702.61	702.30
9	595.64	628.02	683.22	700.83	705.34	706.57	706.81	706.83	706.84	706.49
10	596.77	628.43	683.96	702.99	708.33	709.87	710.20	710.24	710.24	709.86
11	597.49	628.87	684.41	704.57	710.69	712.54	712.97	713.03	713.04	712.64
12	598.12	629.34	684.70	705.75	712.57	714.75	715.29	715.38	715.39	714.97
13	598.68	629.83	684.90	706.64	714.10	716.59	717.25	717.37	717.39	716.97
14	599.18	630.34	685.06	707.33	715.35	718.14	718.92	719.08	719.10	718.69
15	599.63	630.85	685.21	707.86	716.38	719.45	720.37	720.56	720.60	720.19
16	600.02	631.35	685.35	708.29	717.23	720.57	721.61	721.85	721.90	721.50
17	600.38	631.83	685.49	708.64	717.94	721.53	722.70	722.98	723.05	722.67
18	600.70	632.30	685.63	708.92	718.54	722.36	723.65	723.98	724.07	723.70
19	600.99	632.74	685.78	709.16	719.05	723.07	724.48	724.87	724.97	724.62
20	601.24	633.16	685.92	709.37	719.48	723.69	725.21	725.66	725.78	725.45
21	601.48	633.55	686.07	709.54	719.84	724.22	725.86	726.36	726.50	726.18

*A.4 Exp.4: Vertical overlap weld bead thermal simulation*

Table A.15 : Data surface deposition temperature ( $T_{dep}$ ) of Exp.4 at initial temperature ( $T_{init}$ ) = 300°C

Weld bead position (mm)	Number of layers									
	L1	L2	L3	L4	L5	L6	L7	L8	L9	L10
0	300.00	300.00	300.00	300.00	300.00	300.00	300.00	300.00	300.00	300.00
22	601.69	633.91	686.22	709.70	720.16	724.69	726.43	726.98	727.14	726.85
23	601.88	634.25	686.36	709.83	720.43	725.10	726.93	727.54	727.72	727.44
24	602.05	634.56	686.50	709.95	720.66	725.45	727.38	728.03	728.25	727.98
25	602.21	634.84	686.64	710.06	720.86	725.76	727.77	728.48	728.71	728.47
26	602.35	635.11	686.77	710.16	721.03	726.03	728.12	728.88	729.14	728.90
27	602.48	635.35	686.89	710.25	721.18	726.27	728.43	729.24	729.52	729.30
28	602.60	635.57	687.01	710.33	721.31	726.48	728.70	729.55	729.86	729.65
29	602.71	635.77	687.12	710.40	721.43	726.66	728.95	729.84	730.17	729.97
30	602.81	635.95	687.22	710.47	721.53	726.82	729.16	730.10	730.45	730.26
31	602.90	636.12	687.31	710.53	721.61	726.96	729.35	730.33	730.70	730.52
32	602.98	636.27	687.40	710.58	721.68	727.08	729.52	730.53	730.93	730.75
33	603.05	636.40	687.48	710.63	721.75	727.18	729.67	730.71	731.13	730.96
34	603.11	636.53	687.55	710.67	721.80	727.27	729.80	730.87	731.31	731.14
35	603.17	636.64	687.62	710.70	721.85	727.35	729.91	731.02	731.47	731.31
36	603.23	636.74	687.68	710.74	721.89	727.42	730.01	731.14	731.61	731.46
37	603.28	636.83	687.73	710.76	721.92	727.47	730.10	731.26	731.74	731.59
38	603.32	636.91	687.78	710.79	721.94	727.52	730.17	731.35	731.86	731.71
39	603.36	636.97	687.82	710.81	721.96	727.56	730.23	731.44	731.96	731.81
40	603.40	637.04	687.86	710.82	721.98	727.69	730.55	731.77	732.31	731.90
41	603.43	637.19	687.79	710.57	721.66	727.37	730.23	731.64	732.32	732.13
42	603.46	637.16	687.77	710.54	721.62	727.33	730.20	731.61	732.29	732.10

Appendix A The result of thermal simulation

Table A.15 : Data surface deposition temperature ( $T_{dep}$ ) of Exp.4 at initial temperature ( $T_{init}$ ) = 300°C

Weld bead position (mm)	Number of layers									
	L1	L2	L3	L4	L5	L6	L7	L8	L9	L10
0	300.00	300.00	300.00	300.00	300.00	300.00	300.00	300.00	300.00	300.00
43	603.49	637.14	687.74	710.51	721.59	727.30	730.16	731.58	732.26	732.06
44	603.51	637.11	687.71	710.47	721.55	727.26	730.13	731.55	732.23	732.02
45	603.53	637.08	687.68	710.44	721.51	727.23	730.09	731.51	732.20	731.98
46	603.55	637.05	687.65	710.40	721.48	727.19	730.05	731.47	732.16	731.94
47	603.56	637.02	687.61	710.37	721.44	727.15	730.01	731.44	732.13	731.90
48	603.57	636.99	687.58	710.33	721.40	727.11	729.97	731.40	732.09	731.85
49	603.58	636.96	687.54	710.30	721.36	727.07	729.93	731.36	732.05	731.81
50	603.59	636.92	687.51	710.26	721.32	727.03	729.89	731.32	732.01	731.76
51	603.60	636.89	687.47	710.22	721.28	726.98	729.85	731.27	731.97	731.71
52	603.61	636.85	687.44	710.18	721.24	726.94	729.81	731.23	731.92	731.66
53	603.61	636.81	687.40	710.14	721.20	726.90	729.76	731.19	731.88	731.61
54	603.61	636.77	687.36	710.10	721.16	726.86	729.72	731.14	731.84	731.56
55	603.61	636.74	687.32	710.06	721.11	726.81	729.68	731.10	731.79	731.51
56	603.62	636.70	687.28	710.02	721.07	726.77	729.63	731.06	731.75	731.45
57	603.61	636.66	687.24	709.98	721.03	726.73	729.59	731.01	731.70	731.40
58	603.61	636.62	687.20	709.94	720.99	726.69	729.55	730.97	731.66	731.35
59	603.61	636.58	687.16	709.90	720.95	726.65	729.51	730.93	731.62	731.30
60	603.61	636.54	687.12	709.86	720.91	726.61	729.47	730.89	731.58	731.25
61	603.60	636.50	687.08	709.82	720.87	726.58	729.44	730.86	731.55	731.21
62	603.60	636.45	687.05	709.79	720.84	726.55	729.42	730.84	731.53	731.18
63	603.59	636.41	687.01	709.76	720.82	726.54	729.41	730.83	731.53	731.16

*A.4 Exp.4: Vertical overlap weld bead thermal simulation*

Table A.15 : Data surface deposition temperature ( $T_{dep}$ ) of Exp.4 at initial temperature ( $T_{init}$ ) = 300°C

Weld bead position (mm)	Number of layers									
	L1	L2	L3	L4	L5	L6	L7	L8	L9	L10
0	300.00	300.00	300.00	300.00	300.00	300.00	300.00	300.00	300.00	300.00
64	603.58	636.37	686.98	709.74	720.81	726.54	729.42	730.85	731.54	731.16
65	603.58	636.33	686.95	709.73	720.82	726.57	729.46	730.89	731.59	731.19
66	603.57	636.29	686.93	709.74	720.85	726.63	729.55	730.99	731.68	731.27
67	603.56	636.26	686.92	709.78	720.94	726.76	729.70	731.15	731.85	731.42
68	603.55	636.23	686.95	709.88	721.10	726.99	729.96	731.43	732.14	731.67
69	603.54	636.21	687.01	710.06	721.38	727.36	730.39	731.87	732.59	732.08
70	603.53	636.20	687.15	710.39	721.85	727.96	731.05	732.56	733.30	732.74
71	603.52	636.23	687.42	710.95	722.62	728.91	732.09	733.64	734.39	734.69
72	603.51	636.31	687.93	711.90	723.87	730.39	733.70	735.29	736.07	737.97
73	603.50	636.50	688.83	713.48	725.88	732.71	736.18	737.84	738.65	743.07
74	603.49	636.91	690.46	716.13	729.15	736.39	740.06	741.80	742.65	751.00
75	603.48	637.77	693.39	720.56	739.98	747.74	751.66	753.51	754.41	763.41
76	603.46	639.58	698.69	731.33	757.58	772.42	779.88	781.85	783.18	782.83
77	603.45	643.53	708.30	757.43	786.05	802.07	810.09	813.82	815.64	813.37
78	603.44	652.48	737.95	801.44	832.66	849.73	858.24	862.24	864.20	862.16
79	603.43	673.38	807.75	877.55	911.16	928.65	937.35	941.59	943.67	942.62
80	603.41	758.52	926.36	999.43	1034.07	1039.07	1041.36	1045.69	1047.83	1066.36

- Initial temperature ( $T_{init}$ ) of 400°C

Appendix A The result of thermal simulation

---

Table A.16 : Data surface deposition temperature ( $T_{dep}$ ) of Exp.4 at initial temperature ( $T_{init}$ ) = 400°C

Weld bead position (mm)	Number of layers									
	L1	L2	L3	L4	L5	L6	L7	L8	L9	L10
0	400.00	400.00	400.00	400.00	400.00	400.00	400.00	400.00	400.00	400.00
1	573.86	604.32	606.60	606.72	606.72	606.72	606.72	606.72	606.72	606.72
2	595.04	631.77	651.57	653.09	653.20	653.21	653.21	653.21	653.21	653.20
3	599.55	650.19	681.01	684.50	684.84	684.91	684.91	684.91	684.91	684.86
4	602.19	658.24	697.39	703.39	704.12	704.27	704.29	704.29	704.29	704.20
5	604.15	662.05	707.06	715.74	717.04	717.32	717.35	717.35	717.35	717.21
6	605.72	664.02	712.95	724.21	726.22	726.67	726.74	726.74	726.74	726.54
7	607.01	665.02	716.42	730.00	733.11	733.79	733.89	733.90	733.90	734.05
8	608.09	665.63	718.47	735.66	741.94	742.88	743.04	743.06	743.06	743.35
9	609.03	666.09	719.67	740.97	748.66	749.89	750.13	750.16	750.16	750.65
10	609.83	666.51	720.37	744.82	753.87	755.41	755.74	755.78	755.79	756.51
11	610.53	666.94	720.79	747.66	757.97	759.83	760.26	760.32	760.33	761.31
12	611.15	667.40	721.04	749.77	761.23	763.40	763.95	764.03	764.04	765.31
13	611.70	667.87	721.22	751.37	763.84	766.33	766.99	767.11	767.13	768.70
14	612.18	668.36	721.35	752.60	765.96	768.75	769.54	769.69	769.72	771.60
15	612.61	668.84	721.46	753.55	767.69	770.77	771.68	771.87	771.91	774.10
16	612.99	669.31	721.57	754.29	769.11	772.45	773.49	773.73	773.78	776.28
17	613.33	669.76	721.68	754.89	770.28	773.87	775.04	775.32	775.39	778.19
18	613.63	670.19	721.79	755.37	771.25	775.07	776.36	776.69	776.78	779.86
19	613.90	670.60	721.91	755.76	772.06	776.08	777.49	777.88	777.98	781.34
20	614.23	670.98	722.02	756.08	772.73	776.94	778.47	778.91	779.03	782.64
21	614.72	671.34	722.14	756.35	773.29	777.67	779.31	779.81	779.95	783.80

*A.4 Exp.4: Vertical overlap weld bead thermal simulation*

Table A.16 : Data surface deposition temperature ( $T_{dep}$ ) of Exp.4 at initial temperature ( $T_{init}$ ) = 400°C

Weld bead position (mm)	Number of layers									
	L1	L2	L3	L4	L5	L6	L7	L8	L9	L10
0	400.00	400.00	400.00	400.00	400.00	400.00	400.00	400.00	400.00	400.00
22	615.17	671.66	722.25	756.58	773.76	778.30	780.04	780.59	780.75	784.83
23	615.57	671.96	722.36	756.77	774.16	778.83	780.66	781.27	781.46	785.74
24	615.93	672.24	722.47	756.93	774.49	779.28	781.21	781.86	782.07	786.55
25	616.26	672.49	722.57	757.07	774.76	779.67	781.68	782.38	782.62	787.26
26	616.56	672.72	722.67	757.19	774.99	779.99	782.08	782.84	783.09	787.90
27	616.82	672.92	722.76	757.28	775.18	780.27	782.43	783.23	783.51	788.46
28	617.06	673.11	722.84	757.37	775.33	780.50	782.72	783.57	783.88	788.96
29	617.28	673.27	722.92	757.43	775.46	780.69	782.98	783.87	784.20	789.40
30	617.47	673.42	722.98	757.49	775.56	780.85	783.19	784.13	784.48	789.79
31	617.65	673.55	723.04	757.53	775.63	780.98	783.38	784.35	784.72	790.12
32	617.80	673.67	723.10	757.56	775.69	781.09	783.53	784.54	784.93	790.42
33	617.95	673.77	723.14	757.58	775.73	781.17	783.65	784.69	785.11	790.67
34	618.07	673.86	723.18	757.59	775.75	781.23	783.75	784.83	785.26	790.89
35	618.18	673.94	723.21	757.59	775.76	781.27	783.83	784.93	785.39	791.07
36	618.28	674.00	723.24	757.58	775.76	781.29	783.89	785.02	785.49	791.23
37	618.37	674.06	723.26	757.56	775.75	781.30	783.93	785.09	785.57	791.35
38	618.45	674.10	723.27	757.54	775.72	781.30	783.95	785.13	785.64	791.46
39	618.52	674.14	723.28	757.51	775.69	781.29	783.96	785.17	785.68	791.54
40	618.58	674.17	723.29	757.47	775.65	781.36	784.22	785.44	785.98	791.59
41	618.63	673.68	722.59	755.80	773.81	779.53	782.39	783.80	784.48	790.24
42	618.67	673.62	722.53	755.69	773.69	779.41	782.27	783.68	784.36	790.10

Appendix A The result of thermal simulation

Table A.16 : Data surface deposition temperature ( $T_{dep}$ ) of Exp.4 at initial temperature ( $T_{init}$ ) = 400°C

Weld bead position (mm)	Number of layers									
	L1	L2	L3	L4	L5	L6	L7	L8	L9	L10
0	400.00	400.00	400.00	400.00	400.00	400.00	400.00	400.00	400.00	400.00
43	618.71	673.56	722.48	755.57	773.57	779.28	782.15	783.56	784.25	789.96
44	618.74	673.50	722.42	755.46	773.45	779.16	782.03	783.44	784.13	789.81
45	618.76	673.44	722.35	755.34	773.33	779.04	781.90	783.32	784.01	789.67
46	618.78	673.38	722.29	755.22	773.20	778.91	781.78	783.20	783.89	789.52
47	618.79	673.32	722.23	755.10	773.07	778.78	781.65	783.07	783.76	789.36
48	618.80	673.26	722.16	754.98	772.95	778.66	781.52	782.94	783.63	789.21
49	618.80	673.19	722.10	754.85	772.82	778.53	781.39	782.82	783.51	789.05
50	618.80	673.13	722.03	754.73	772.69	778.40	781.26	782.69	783.38	788.89
51	618.80	673.06	721.97	754.61	772.56	778.26	781.13	782.55	783.25	788.72
52	618.79	672.99	721.90	754.48	772.43	778.13	781.00	782.42	783.11	788.56
53	618.78	672.92	721.83	754.36	772.30	778.00	780.87	782.29	782.98	788.39
54	618.77	672.86	721.76	754.23	772.17	777.87	780.73	782.16	782.85	788.23
55	618.75	672.79	721.70	754.10	772.04	777.74	780.60	782.02	782.72	788.06
56	618.73	672.72	721.63	753.98	771.90	777.60	780.47	781.89	782.58	787.89
57	618.71	672.65	721.56	753.85	771.77	777.47	780.34	781.76	782.45	787.72
58	618.68	672.58	721.49	753.72	771.65	777.34	780.21	781.63	782.32	787.56
59	618.66	672.50	721.42	753.60	771.52	777.22	780.08	781.50	782.19	787.40
60	618.63	672.43	721.35	753.48	771.40	777.10	779.96	781.38	782.07	787.25
61	618.60	672.36	721.28	753.36	771.28	776.98	779.85	781.27	781.96	787.11
62	618.57	672.29	721.22	753.24	771.17	776.88	779.75	781.17	781.86	786.99
63	618.53	672.22	721.15	753.14	771.08	776.80	779.68	781.10	781.79	786.89

*A.4 Exp.4: Vertical overlap weld bead thermal simulation*

Table A.16 : Data surface deposition temperature ( $T_{dep}$ ) of Exp.4 at initial temperature ( $T_{init}$ ) = 400°C

Weld bead position (mm)	Number of layers									
	L1	L2	L3	L4	L5	L6	L7	L8	L9	L10
0	400.00	400.00	400.00	400.00	400.00	400.00	400.00	400.00	400.00	400.00
64	618.50	672.15	721.09	753.06	771.02	776.75	779.63	781.06	781.75	786.84
65	618.46	672.08	721.03	753.00	771.00	776.75	779.64	781.08	781.77	786.85
66	618.43	672.01	720.99	752.98	771.04	776.82	779.73	781.17	781.87	786.96
67	618.39	671.94	720.95	753.04	771.18	777.01	779.94	781.39	782.10	787.22
68	618.35	671.88	720.95	753.20	771.48	777.37	780.34	781.81	782.52	787.69
69	618.31	671.83	720.99	753.55	772.03	778.01	781.04	782.52	783.24	788.50
70	618.26	671.80	721.10	754.20	772.98	779.08	782.18	783.69	784.42	789.80
71	618.22	671.80	721.35	755.34	774.54	780.82	784.01	785.56	786.31	791.87
72	618.18	671.85	721.82	757.28	777.09	783.60	786.91	788.51	789.29	795.11
73	618.13	672.01	722.70	760.54	781.21	788.04	791.51	793.17	793.98	800.15
74	618.09	672.39	724.29	766.01	787.85	795.08	798.76	800.50	801.35	807.97
75	618.04	673.21	729.13	775.11	798.48	806.23	810.16	812.00	812.90	820.07
76	617.99	674.97	740.21	790.21	815.50	830.33	837.80	839.77	841.10	838.85
77	617.95	678.82	760.15	815.36	842.93	858.96	866.98	870.70	872.53	868.31
78	617.90	687.45	796.44	857.79	887.88	904.96	913.47	917.47	919.43	915.41
79	617.85	716.31	863.93	931.35	963.75	981.24	989.94	994.18	996.26	993.23
80	617.80	815.76	978.31	1048.84	1082.22	1087.21	1089.50	1093.84	1095.97	1112.56



Table A.17 : Average surface temperature deposition ( $T_{dep}$ ) and standard deviation ( $\sigma$ ) of Exp.4: Vertical overlap weld bead

$T_{init}$	100°C		200°C		300°C		400°C	
Number of layers	$T_{dep}$	$\sigma$	$T_{dep}$	$\sigma$	$T_{dep}$	$\sigma$	$T_{dep}$	$\sigma$
L1	538.80	6.79	581.13	5.97	602.53	1.69	617.05	2.47
L2	599.06	1.97	609.96	0.85	635.33	2.36	672.19	1.85
L3	620.37	1.76	652.92	1.39	686.87	0.94	722.03	0.79
L4	644.29	2.29	676.39	1.90	709.68	3.79	754.89	5.01
L5	655.36	3.75	687.21	3.28	720.21	2.74	772.08	4.12
L6	660.43	4.84	692.20	4.45	725.28	3.79	777.15	5.01
L7	662.77	5.58	694.50	5.22	727.62	4.50	779.49	5.61
L8	663.82	6.02	695.54	5.66	728.66	4.92	780.53	5.95
L9	664.28	6.25	696.01	5.88	729.13	5.13	781.00	6.12
L10	664.58	6.65	696.21	5.99	728.83	5.17	785.73	7.40

# Appendix B

## The result of experiment produce

### B.1 Design of experiment Exp.2: Single weld bead on cylinder substrate

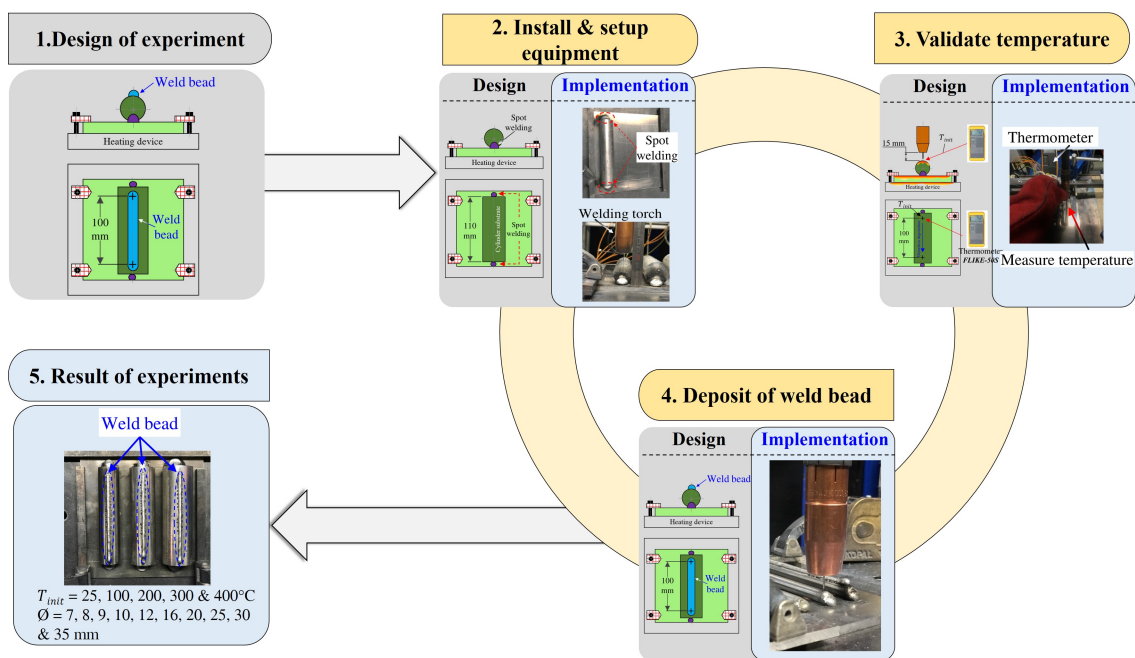


Figure B.1.1 : Design of experiment of single weld bead on cylinder substrate

### B.2 The result of Exp.2: Single weld bead on cylinder substrate at $T_{init} 25^{\circ}\text{C}$ , $100^{\circ}\text{C}$ , $200^{\circ}\text{C}$ , $300^{\circ}\text{C}$ and $400^{\circ}\text{C}$

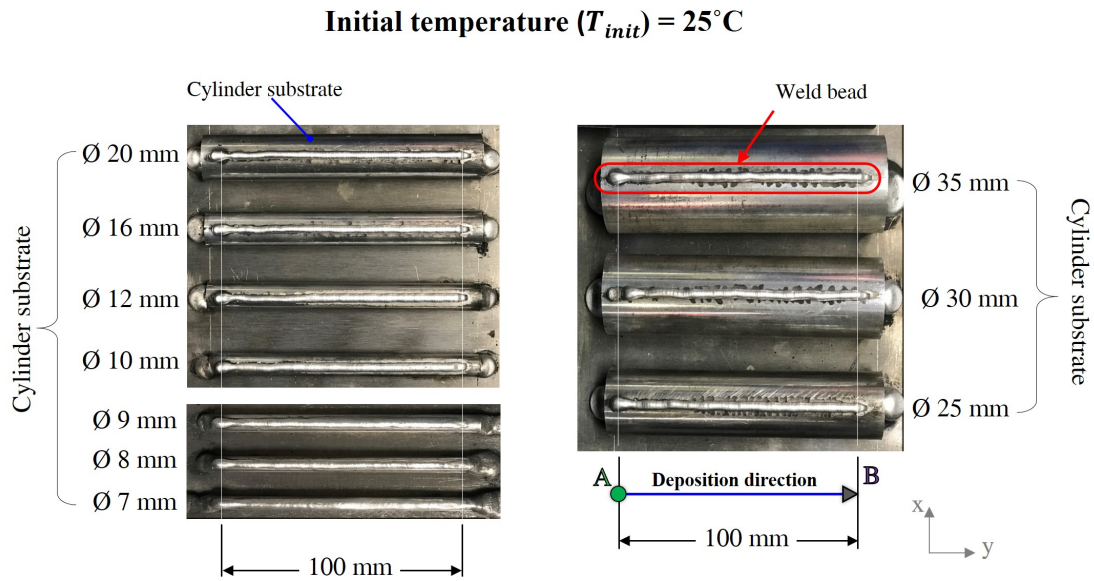


Figure B.2.1 : The result of Exp.3: single weld bead on cylinder substrate at  $T_{init}=25^{\circ}\text{C}$

Figure B.2.2 : The result of Exp.3: single weld bead on cylinder substrate at  $T_{init}=100^{\circ}\text{C}$

B.2 The result of Exp.2: Single weld bead on cylinder substrate at  $T_{init}$  25°C, 100°C, 200°C, 300°C and 400°C

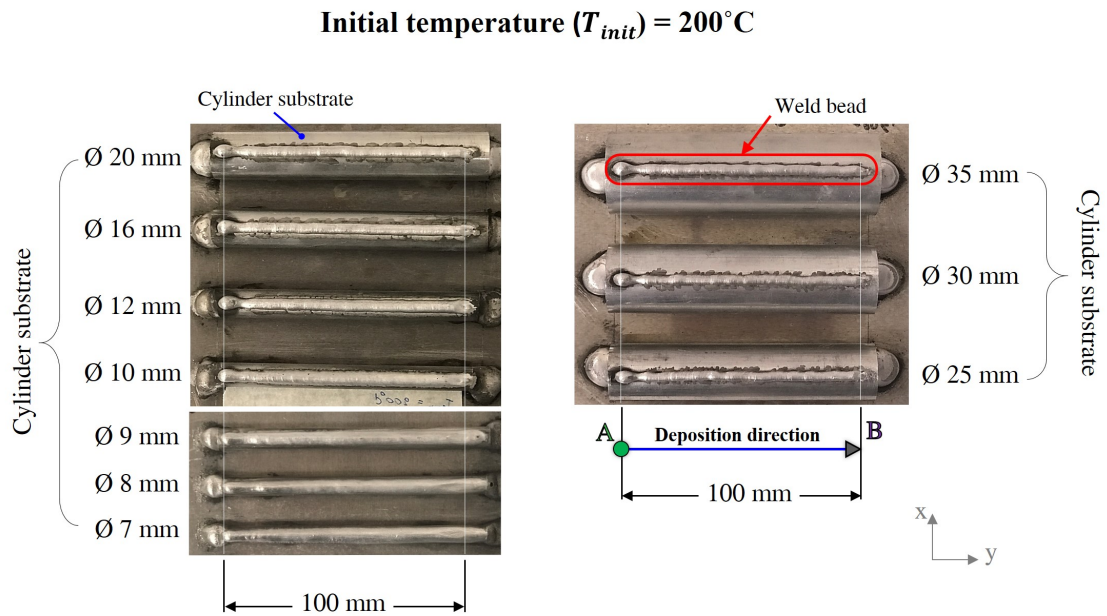


Figure B.2.3 : The result of Exp.3: single weld bead on cylinder substrate at  $T_{init}=200^{\circ}\text{C}$

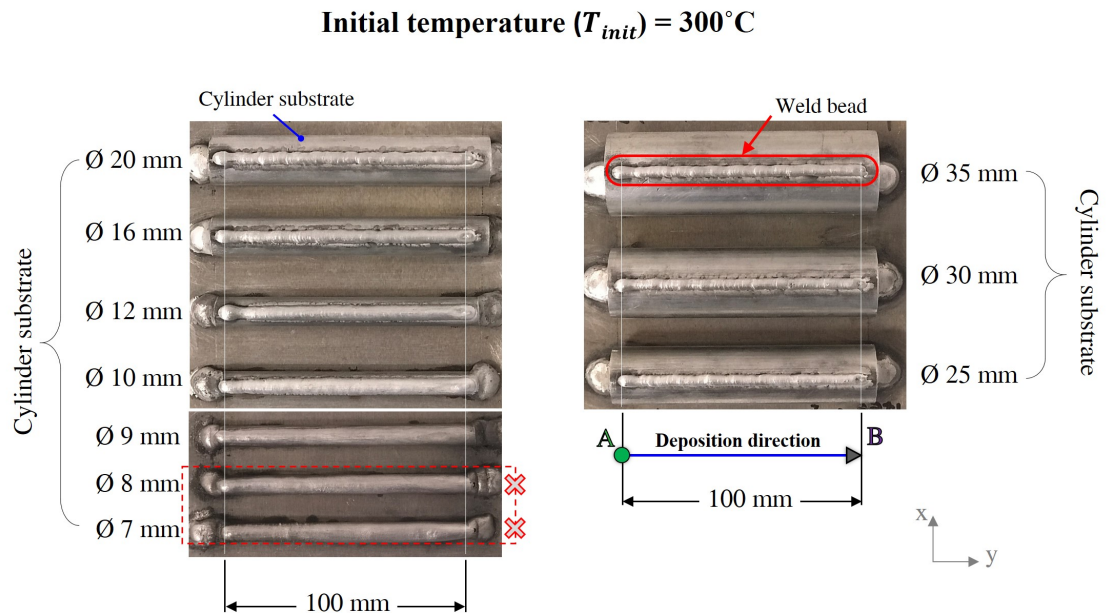


Figure B.2.4 : The result of Exp.3: single weld bead on cylinder substrate at  $T_{init}=300^{\circ}\text{C}$

### B.3 Design of experiment Exp.3: Lateral overlap weld beads

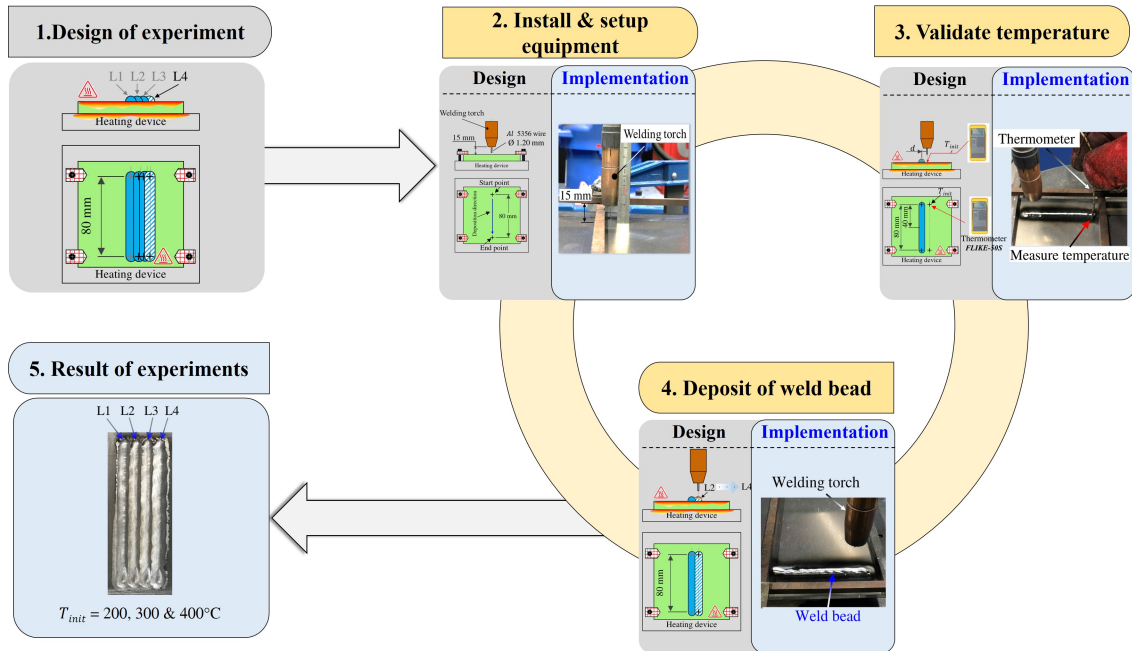


Figure B.3.1 : Design of experiment of lateral overlap weld bead

## B.4 Design of experiment Exp.4: Vertical overlap weld beads

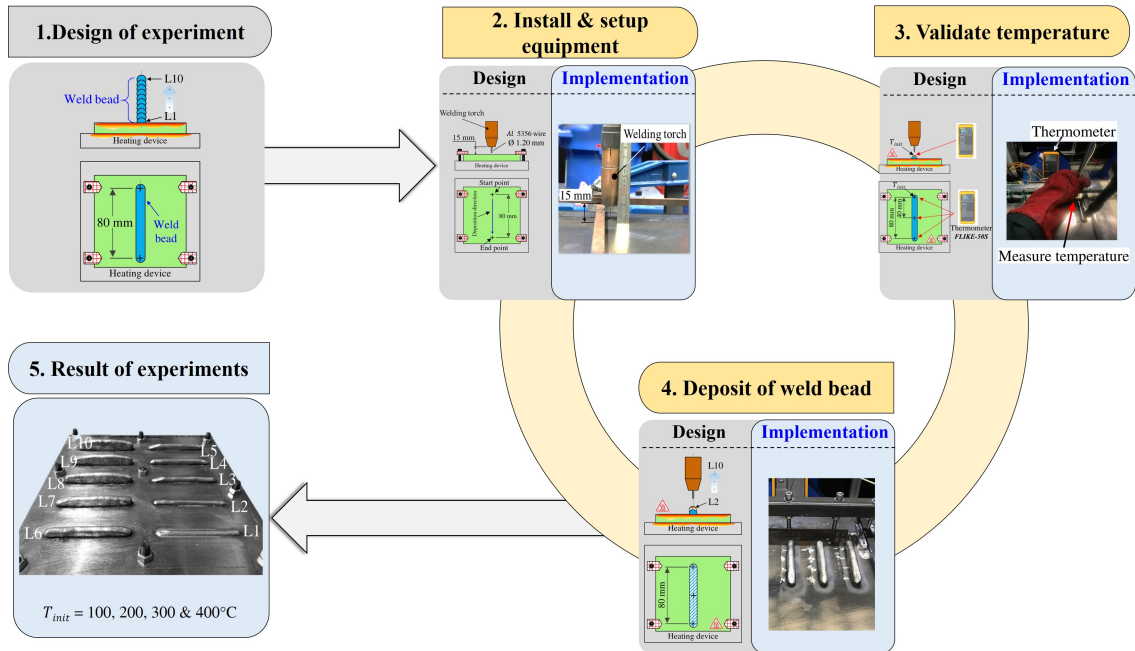


Figure B.4.1 : Design of experiment of vertical overlap weld bead

## B.5 The result of Exp.4: Vertical overlap weld beads at $T_{init}$ 100°C, 200°C and 300°C

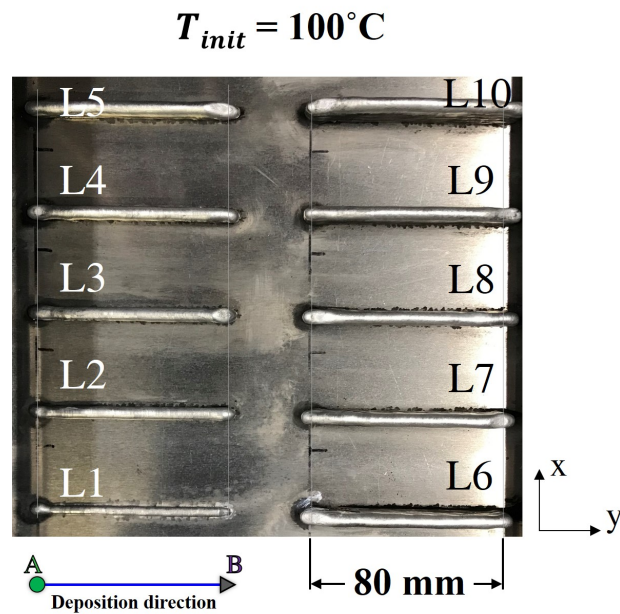


Figure B.5.1 : The result of Exp.4: Vertical overlap weld bead at  $T_{init} = 100^\circ\text{C}$

B.5 The result of Exp.4: Vertical overlap weld beads at  $T_{init}$  100°C, 200°C and 300°C

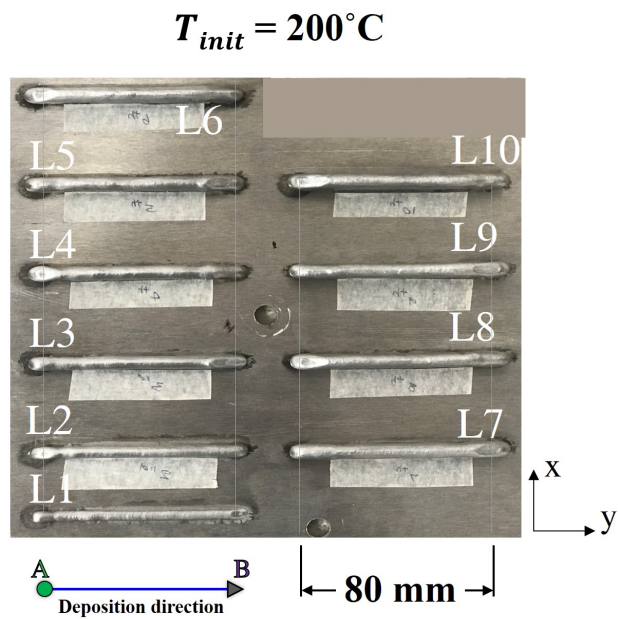


Figure B.5.2 : The result of Exp.4: Vertical overlap weld bead at  $T_{init} = 200^{\circ}\text{C}$

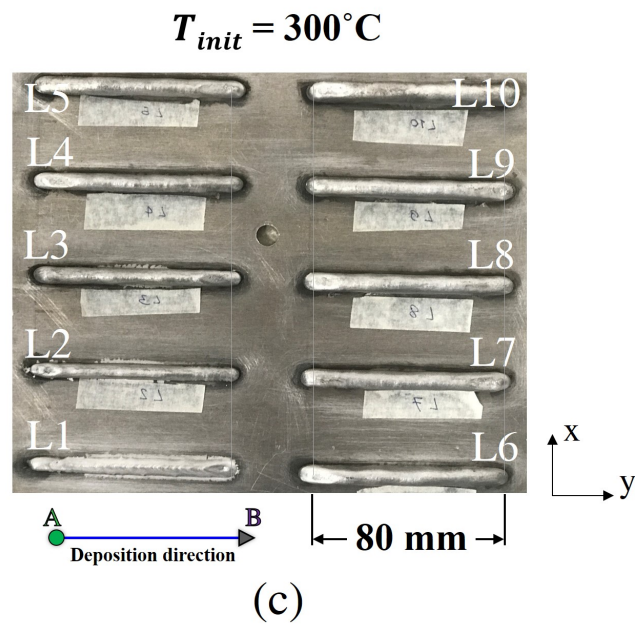


Figure B.5.3 : The result of Exp.4: Vertical overlap weld bead at  $T_{init} = 300^{\circ}\text{C}$





# Appendix C

## MLP Regression in Python

### C.1 Import library

We have imported all of the necessary modules, such as MLP Regressor, metrics, and data sets. Then, using Limited-memory Broyden–Fletcher–Goldfarb–Shanno (L-BFGS) algorithm or stochastic gradient descent, this model optimizes the  $R^2$  score [?] as show in Figure C.1.1.

```
1 import pandas as pd
2 from sklearn.metrics import mean_squared_error as mse
3 from sklearn.model_selection import train_test_split
4 from sklearn.neural_network import MLPRegressor
```

Figure C.1.1 : Import library in Python

### Setting up the data for MLP Regressor

We have imported the weld bead shape data set from storage, with the input data in X and the output in y. We have used train\_test\_split to split the data set into two parts such that 20% of the data is in testing and the training data is 80% as shown in Figure C.1.2.

```
7 df = pd.read_csv("cylinder.csv")
8
9 X = df[['temp', 'wfs', 'ts', 'subr']]
10 y = df[['r_h']]
11
12 X_train, X_test, y_train, y_test = train_test_split(X, y, test_size=0.2, random_state=123)
```

Figure C.1.2 : Setting up the data for MLP Regressor in Python

### Using MLP Regressor and calculating the scores

We created a model object and fitted the training data. Then we utilized the testing data to put the model to the test by predicting the model output for the testing data. We utilize the  $R^2$  score to calculate additional model scores by providing the expected and predicted values of the testing set output as shown in Figure C.1.3. The details are as follows:

#### Parameters:

- `atv` = activation function for the hidden layer.
- `random_state` = Determines random sample generation for weights and bias.
- `hidden_layer_size` = Number of hidden layer and number of neurons in hidden layers.
- `max_iter` = This number of iterations.
- `solver` = The weight optimization of solver.
- `tol` = Tolerance for optimization.
- `n_iter_no_change` = Maximum number of epochs.

#### Methods:

- `fit(X,y)` = Fit the model to data matrix X and output y.
- `predict(X)` = Predict using the multi-Layer perceptron model.
- `score(X,y[sample_weight])` = Return the coefficient of determination ( $R^2$ ) of the prediction.

```
14 atv = "relu" # 'relu' 'logistic' 'tanh'
15 i_range = list(range(1, 100))
16 N_epoch = 10
17 score_1 = []
18
19 print("Ativation Function : ", atv)
20 print("N_epoch : ", N_epoch)
21 def h1():
22     for i in i_range: # 'relu' 'logistic' 'tanh'
23         ann = MLPRegressor(activation=atv,
24                             random_state=123,
25                             hidden_layer_sizes=(i),
26                             max_iter=100000000,
27                             solver='adam',
28                             verbose=False, tol=0.00001,
29                             n_iter_no_change=N_epoch)
30         ann.fit(X_train, y_train)
31         pred_test = ann.predict(X_test)
32         score_test = ann.score(X_test, y_test)
33         score_1.append(score_test)
34         # print(i, " = ", '%.4f' % score_test)
35
36     s1_1 = pd.Series(i_range, name="Sample")
37     s1_2 = pd.Series(score_1, name="Score")
38
39     #Score r^2 & MSE :
40     df_1 = pd.concat([s1_1, s1_2], axis="columns")
41     print("N_hidden layer : 1")
42     print(df_1[df_1.Score == df_1.Score.max()])
43     print("MSE_1 : ", '%.4f' % mse(y_test, pred_test))
44     print("-"*50)
```

Figure C.1.3 : Using MLP Regressor and calculating the scores in Python

## C.2 The MLP regression results of training and testing set

Table C.1 : Comparison of experiment and predicted results

Data set	Index No.					Output					
		$T_{dep}$ (°C)	$WFS$ (m/min)	$TS$ (m/min)	$R_{sub}$ (mm)	$r$ (mm)	$r - pred$ (mm)	$Error$ (%)	$h$ (mm)	$h - pred$ (mm)	$Error$ (%)
Training set: 35 samples	1	597.66	5	0.6	4	2.52	2.63	4.25%	1.34	1.07	20.00%
	6	447.5	5	0.6	10	1.87	1.73	7.49%	2.09	2.06	1.46%
	24	587.48	5	0.6	6	2.7	3.05	12.94%	0.96	0.96	0.31%
	12	597.54	5	0.6	4.5	2.73	2.91	6.69%	1.04	0.96	7.31%
	37	576.54	5	0.6	17.5	2.51	2.65	5.45%	1.78	1.80	1.19%
	41	602.3	5	0.6	12.5	3.85	3.45	10.27%	1.23	1.16	5.42%
	29	530.89	5	0.6	17.5	2.18	2.36	8.10%	2.04	2.04	0.21%
	30	631.75	5	0.6	4.5	3.66	3.59	1.89%	0.31	0.71	128.88%
	31	610.49	5	0.6	5	3.8	3.46	9.02%	0.33	0.76	129.97%
	21	625.18	5	0.6	4	3.62	3.17	12.36%	0.44	0.87	97.10%
	7	436.21	5	0.6	12.5	1.82	1.69	7.13%	2.27	2.25	0.78%
	20	696.28	5	0.6	3.5	3.99	4.29	7.62%	0.93	0.45	51.92%
	43	601.14	5	0.6	17.5	3.38	3.32	1.75%	1.58	1.50	4.80%
	3	535.98	5	0.6	5	2.02	2.23	10.31%	1.63	1.33	18.11%
	39	607.83	5	0.6	8	4.25	3.73	12.14%	0.72	0.79	9.71%
	27	535.38	5	0.6	12.5	2.13	2.32	8.96%	1.81	1.74	3.72%
	16	491.51	5	0.6	10	2.08	2.01	3.38%	1.81	1.83	1.28%
	0	638.29	5	0.6	3.5	3.33	3.14	5.57%	0.79	0.88	11.20%
	4	515.07	5	0.6	6	2.02	2.11	4.36%	1.52	1.50	1.56%
	14	546.61	5	0.6	6	2.44	2.31	5.38%	1.15	1.33	16.01%
	40	603.98	5	0.6	10	3.6	3.56	1.10%	1.08	0.98	9.57%
	25	555.4	5	0.6	8	2.52	2.39	5.15%	1.39	1.40	0.50%
	15	510.72	5	0.6	8	2.22	2.11	5.13%	1.55	1.63	4.94%
	36	577.44	5	0.6	15	2.56	2.62	2.36%	1.72	1.66	3.40%
	35	580.64	5	0.6	12.5	2.69	2.69	0.13%	1.54	1.49	3.55%
	9	427.98	5	0.6	17.5	1.76	1.70	3.28%	2.47	2.56	3.83%
	32	604.71	5	0.6	6	3.15	3.66	16.20%	0.71	0.71	0.44%
	33	594.04	5	0.6	8	2.92	3.25	11.13%	1.13	0.99	11.95%

Table C.1 : Comparison of experiment and predicted results

Data set	Index No.					Output					
		$T_{dep}$ (°C)	$WFS$ (m/min)	$TS$ (m/min)	$R_{sub}$ (mm)	$r$ (mm)	$r - pred$ (mm)	$Error$ (%)	$h$ (mm)	$h - pred$ (mm)	$Error$ (%)
	22	609.75	5	0.6	4.5	2.99	3.15	5.51%	0.85	0.87	2.73%
	19	427.98	5	0.6	17.5	1.79	1.70	4.90%	2.42	2.56	5.98%
	17	482.68	5	0.6	12.5	1.9	1.99	4.51%	2.1	2.01	4.12%
	38	620.89	5	0.6	6	4.99	4.23	15.15%	0.31	0.47	50.45%
	34	585.51	5	0.6	10	2.69	2.91	8.01%	1.39	1.25	9.99%
	28	531.9	5	0.6	15	2.16	2.33	7.91%	1.94	1.90	2.29%
	2	576.45	5	0.6	4.5	2.49	2.49	0.18%	1.34	1.12	16.35%
Testing set: 9 samples	8	429.88	5	0.6	15	1.79	1.68	6.02%	2.37	2.42	2.10%
	11	607.03	5	0.6	4	2.77	2.81	1.55%	0.88	1.00	13.89%
	26	541.59	5	0.6	10	2.31	2.33	0.79%	1.65	1.58	4.49%
	42	601.38	5	0.6	15	3.65	3.38	7.52%	1.44	1.34	7.03%
	18	477.75	5	0.6	15	1.95	1.99	1.87%	2.14	2.17	1.58%
	13	566.81	5	0.6	5	2.56	2.42	5.30%	0.76	1.18	54.78%
	23	598.04	5	0.6	5	3.02	3.21	6.31%	0.80	0.85	6.44%
	10	662.23	5	0.6	3.5	3.25	3.62	11.36%	0.50	0.70	40.08%
5	468.43	5	0.6	8	1.92	1.84	4.31%	1.86	1.84	0.87%	
<b>Avg. error (%)</b>								6.38%			17.55%

## C.3 Case study validation

### C.3.1 Thermal simulation of case study

Table C.2 : Average surface temperature deposition ( $T_{dep}$ ) of validation part

Direction	L → R		R → L	
Number of layer	$T_{dep}$ (°C)	Number of layer	$T_{dep}$ (°C)	

Table C.2 : Average surface temperature deposition ( $T_{dep}$ ) of validation part

Direction	L -> R		R-> L
Number of layer	$T_{dep}$ (°C)	Number of layer	$T_{dep}$ (°C)
L1	468.71	L2	611.29
L3	607.32	L4	667.70
L5	638.08	L6	733.34
L7	673.81	L8	788.80
L9	709.13	L10	836.23
L11	749.29	L12	875.06
L13	788.40	L14	906.18
L15	819.61	L16	930.91
L17	844.35	L18	950.50
L19	863.92	L20	965.97
L21	879.37	L22	978.21
L23	891.60	L24	987.89
L25	901.30	L26	995.59
L27	909.03	L28	1001.73
L29	915.21	L30	1006.66
L31	920.17	L32	1010.63
L33	924.19	L34	1013.84
L35	927.44	L36	1016.45
L37	930.10	L38	1018.59
L39	932.27	L40	1020.34
L41	934.06	L42	1021.78
L43	935.54	L44	1022.98
L45	936.76	L46	1023.97

Table C.2 : Average surface temperature deposition ( $T_{dep}$ ) of validation part

Direction	L → R		R → L	
Number of layer	$T_{dep}$ (°C)	Number of layer	$T_{dep}$ (°C)	
L47	937.78	L48	1024.80	
L49	938.63	L50	1025.49	
L51	939.34	L52	1026.07	
L53	939.95	L54	1026.58	
L55	940.47	L56	1027.01	
L57	940.95	L58	1027.40	
L59	941.41	L60	1027.77	

### C.3.2 Prediction weld bead shape of case study

Table C.3 : Cause study validation result

No.	Input				Prediction output	
	$T_{dep}$ (°C)	$WFS$ (m/min)	$TS$ (m/min)	$Rsub$ (mm)	$r$ (mm)	$h$ (mm)
L1	503.19	5	0.60	flat	1.77	3.17
L2	611.29	5	0.60	1.77	2.44	1.12
L3	607.32	5	0.60	2.44	2.44	1.14
L4	667.70	5	0.60	2.44	3.12	0.89
L5	638.08	5	0.60	3.12	2.92	0.96
L6	733.34	5	0.60	2.92	4.69	0.30
L7	673.81	5	0.60	4.69	4.53	0.36
L8	788.80	5	0.60	4.53	6.72	-0.47
L9	709.13	5	0.60	6.72	6.40	-0.35
L10	836.23	5	0.60	6.40	8.74	-1.23
L11	749.29	5	0.60	8.74	8.36	-1.09
L12	875.06	5	0.60	8.36	10.64	-1.94
L13	788.40	5	0.60	10.64	10.09	-1.72



Table C.3 : Cause study validation result

No.	Input				Prediction output	
	$T_{dep}$ (C°)	$WFS$ (m/min)	$TS$ (m/min)	$Rsub$ (mm)	$r$ (mm)	$h$ (mm)
L14	906.18	5	0.60	10.09	12.25	-2.55
L15	819.61	5	0.60	12.25	11.16	-2.08
L16	930.91	5	0.60	11.16	13.36	-2.97
L17	844.35	5	0.60	13.36	12.02	-2.38
L18	950.50	5	0.60	12.02	14.24	-3.30
L19	863.92	5	0.60	14.24	12.70	-2.61
L20	965.97	5	0.60	12.70	14.94	-3.56
L21	879.37	5	0.60	14.94	13.23	-2.80
L22	978.21	5	0.60	13.23	15.48	-3.77
L23	891.60	5	0.60	15.48	13.66	-2.94
L24	987.89	5	0.60	13.66	15.92	-3.93
L25	901.30	5	0.60	15.92	13.99	-3.06
L26	995.59	5	0.60	13.99	16.27	-4.06
L27	909.03	5	0.60	16.27	14.26	-3.15
L28	1001.73	5	0.60	14.26	16.54	-4.17
L29	915.21	5	0.60	16.54	14.47	-3.23
L30	1006.66	5	0.60	14.47	16.76	-4.25
L31	920.17	5	0.60	16.76	14.65	-3.29
L32	1010.63	5	0.60	14.65	16.95	-4.32
L33	924.19	5	0.60	16.95	14.78	-3.33
L34	1013.84	5	0.60	14.78	17.08	-4.37
L35	927.44	5	0.60	17.08	14.90	-3.37
L36	1016.45	5	0.60	14.90	17.20	-4.42
L37	930.10	5	0.60	17.20	14.99	-3.41
L38	1018.59	5	0.60	14.99	17.30	-4.45
L39	932.27	5	0.60	17.30	15.06	-3.43
L40	1020.34	5	0.60	15.06	17.37	-4.48
L41	934.06	5	0.60	17.37	15.13	-3.45
L42	1021.78	5	0.60	15.13	17.44	-4.51
L43	935.54	5	0.60	17.44	15.18	-3.47

Table C.3 : Cause study validation result

No.	Input				Prediction output	
	$T_{dep}$ (C°)	$WFS$ (m/min)	$TS$ (m/min)	$R_{sub}$ (mm)	$r$ (mm)	$h$ (mm)
L44	1022.98	5	0.60	15.18	17.50	-4.52
L45	936.76	5	0.60	17.50	15.22	-3.48
L46	1023.97	5	0.60	15.22	17.54	-4.54
L47	937.78	5	0.60	17.54	15.25	-3.50
L48	1024.80	5	0.60	15.25	17.57	-4.55
L49	938.63	5	0.60	17.57	14.93	-3.35
L50	1025.49	5	0.60	14.93	17.40	-4.49
L51	939.34	5	0.60	17.40	15.31	-3.53
L52	1026.07	5	0.60	15.31	17.63	-4.58
L53	939.95	5	0.60	17.63	15.33	-3.52
L54	1026.58	5	0.60	15.33	17.65	-4.58
L55	940.47	5	0.60	17.65	15.35	-3.53
L56	1027.01	5	0.60	15.35	17.67	-4.59
L57	940.95	5	0.60	17.67	15.36	-3.54
L58	1027.40	5	0.60	15.36	17.69	-4.60
L59	941.41	5	0.60	17.69	15.38	-3.54
L60	1027.77	5	0.60	15.38	17.71	-4.60



